An integrated thermal-hydraulic system CFD model of a prismatic block HTR core using Flownex

SNP Khoza

orcid.org 0000-0001-6382-7708

Thesis accepted in fulfilment of the requirements for the degree *Doctor of Philosophy in Nuclear Engineering* at the North-West University

Promoter: Prof CG du Toit

Co-promoter: Prof PG Rousseau

Graduation: October 2019

Student number: 21294097

Declaration

I declare that the work I am submitting for assessment is an original report of my own research and has not been submitted for any other qualification. All information which has been taken from various journal articles, text books or other sources has been referenced accordingly. All collaborative contributions have been indicated and acknowledged.

Acknowledgements

I would like to convey my gratitude to my supervisors, Prof. C.G. Du Toit and Prof. P.G. Rousseau. Thank you for affording me the opportunity and also for the unwavering support and encouragement.

I would like to thank my family for their continued support. I would also like to thank the following people who have also assisted me in several ways:

- The North-West University (Potchefstroom Campus), the Department of Science and Technology (DST) and National Research Foundation (NRF) for their financial support.
- My colleagues at Potchefstroom Campus and staff members at the Nuclear Engineering group.
- M-Tech Industrial (Pty) Ltd for providing the Flownex® software and licence and their constant help and support.
- The staff at Korea Atomic Energy Research Institute (KAERI) nuclear hydrogen production and demonstration (NHDD) department. A special thank you to Dr Sung Nam Lee for providing relevant CORONA simulations and material properties.

This work is based on the research supported by the South African Research Chairs Initiative of the Department of Science and Technology and National Research Foundation of South Africa (Grant No. 61059), as well as supported by the Nuclear R&D Program of the NRF of Korea grant funded by the Korean government (Grant code: NRF-2012M2A8A2025679). Any opinion, finding and conclusion or recommendation expressed in this material is that of the author and the NRF does not accept any liability in this regard.

Abstract

The active core of a prismatic high temperature reactor (HTR) consists of standard fuel, reserve shutdown and control blocks which must be maintained within a safe operating envelope. The fuel blocks are coupled to the fluid behaviour by heat transfer and neutronic interactions. The evaluation of the heat transfer and fluid behaviour for prismatic HTRs is complex and have many facets.

The primary objective of this study is the philosophical development of a thermal-hydraulic Flownex network based model for a prismatic block-type HTR that can reasonably predict the temperature distribution for a standard fuel block. The application of the methodology is illustrated through Flownex models of segments and assemblies of the standard fuel block in steady state and transient conditions.

Verification of the $1/6^{th}$ three-dimensional (3-D) representation of the fuel bock model were done with the two-dimensional (2-D) previously developed Flownex and STAR-CCM+ integrated prismatic block models. The results were in good agreement. Validation of steady state models was also done by comparing temperature distribution results for various cases with those obtained using KAERI's Core Reliable Optimization and thermo-fluid Network Analysis (CORONA) code, which is a hybrid between 3-D CFD and two-dimensional (1-D) fluid system, developed for prismatic HTRs. These cases include a single fuel rod cell, a $1/6^{th}$ of a prismatic fuel block, a $1/6^{th}$ fuel block assembly, a standard fuel block, a fluid flow model and a three-fuel block assembly. Flownex results and CORONA results were found to be in good agreement. A coolant channel blockage incident was also investigated in a $1/6^{th}$ fuel block assembly and also on a single standard fuel block to see the effect of blocked coolant channels in the tangential heat transfer. In the case of blocked coolant channels, Flownex tends to under-predict the fuel compact temperatures and it becomes more evident as the number of blocked coolant channels increases.

Key terms: Thermal-hydraulic analysis, high temperature reactor, prismatic fuel block, heat transfer, unit cell

Table of Contents

List of Tables

List of Figures

Abbreviations

This list contains acronyms and abbreviations used in this document.

Table 1: List of acronyms

Acronym/ Abbreviation	Definition
1-D/2-D or 3-D	One/ two or three dimensional
AERE	Atomic Energy Research Establishment
AVR	Arbeitsgemeinschaft VersuchsReaktor
BISO	Bi-ISOtropic
CB	Core Barrel
CFD	Computational Fluid Dynamics
CO_2	Carbon Dioxide
CORONA	Core Reliable Optimization and thermo-fluid Network Analysis
CV	Control Volume
DLOFC	Depressurised Loss of Forced Cooling
DNS	Direct Numerical Simulation
EURATOM	European Atomic Energy Community
FEM	Finite Element Method
FVM	Finite Volume Method
GA	General Atomics
GAMMA+	Gas Mixture Multi-component Analysis code
GCR	Gas Cooled Reactor
GIF	Generation IV International Forum
GT-MHR	Gas Turbine Modular Helium Reactor
GUI	Graphical User Interface
HEU	High Enriched Uranium
HTGR	High Temperature Gas-cooled Reactor
HTR	High Temperature Reactor
HTTR	High Temperature Test Reactor
HTR-PM	High Temperature gas-cooled Reactor-Pebble-bed Module project
iPyC	Inner Pyrolytic Carbon
IPCM	Implicit Pressure Correction Method
JAERI	Japan Atomic Energy Research Institute
KAERI	Korea Atomic Energy Research Institute
KTA	Kerntechnische Ausschuss
LBP	Lumped Burnable Poison
LES	Large Eddy Simulation
LEU	Low Enriched Uranium
LMTD	Logarithmic mean temperature difference

MHTGR	Modular High-Temperature Gas-Cooled Reactor
MINATOM	Russian Federation Ministry of Atomic Energy
MW_{th}	MegaWatt thermal
MW_e	MegaWatt electrical
NHDD	Nuclear Hydrogen Development and Demonstration project
NGNP	Next Generation Nuclear Plant
oPyC	Outer Pyrolytic Carbon
PBMR	Pebble Bed Modular Reactor
PIRT	Phenomena Identification and Ranking Table
PLOFC	Pressurised Loss of Forced Cooling
PMR	Prismatic Modular Reactor
RCCS	Reactor Cavity Cooling System
RPV	Reactor Pressure Vessel
RSC	Reserve Shutdown Control
SiC	Silicon Carbide
SIMPLE	Semi-Implicit Method for Pressure-Linked Equations
THTR	German Thorium Hochtemperature Reaktor
TRISO	TRi-structural ISOtropic fuel particle
VHTR	Very High Temperature Reactor
UCO	Uranium Oxycarbide
UO_2	Uranium Dioxide
UK	United Kingdom
USA	United States of America

Nomenclature

Table 2: List of symbols

Symbol	Description
A	Area [m^2]
A_1	Upstream cross-sectional area [m^2]
A_2	Downstream cross-sectional area [m^2]
A_m	Average area [m^2]
A_{fs}	Equivalent surface area of fuel rods [m^2]
A_s	Equivalent surface area [m^2]
A_{sw}	Coolant channels surface area [m^2]
C	Circumference [m]
C_p	Heat capacity at constant pressure [kJ/K]
c_p	Specific heat capacity at constant pressure [kJ/kg.K]
D	Diameter [m]
D_H	Hydraulic diameter [m]
D_m	Mass diffusion coefficient i.e. mass diffusivity [m^2/s]
E	Energy [kJ]
f	Friction factor
F	Geometric view factor
F_{12}	Geometric view factor from surface 1 to surface 2
g	Gravitational acceleration [m/s^2]
h	Convection heat transfer coefficient [$W/m^2.K$]
	Specific enthalpy [kJ/kg]
h_0	Specific stagnation enthalpy = $h_o = h + \frac{1}{2}V^2$ [kJ/kg]
k	Thermal conductivity [W/m.K]
l	Characteristic length [m]
	Length of heat transfer path [m]
L	Length [m]

L_{fs}	Radial distance from the fuel rod surface to the graphite block node [m]
L_{sw}	Radial distance from the graphite block node to the coolant channel wall [m]
$\dot{m}$	Mass flow rate [kg/s]
$\dot{m}_0$	Initial value for mass flow rate at steady state [kg/s]
N_1	Upstream node
N_2	Downstream node
p	Static pressure [kPa]
p_0	Total/ stagnation pressure [kPa] = $p + \frac{1}{2}\rho V^2 + \rho g z$
P_{0_r}	Total pressure drop over an orifice in a pipe
q	Heat flux [kW/m^2]
Q	Heat transfer [kJ]
$\dot{Q}$	Rate of heat transfer [kW]
$\dot{Q_H}$	Net rate of heat transfer into the system [kW]
Q_{cond}	Rate of convection heat transfer [kW]
Q_{conv}	Rate of conduction heat transfer [kW]
Q_{rad}	Rate of radiation heat transfer [kW]
$\dot{q}$	Specific rate of heat transfer [kW/kg]
q'''	Rate of heat generation per unit volume [kW/m^3]
r	Radial coordinate
	Radius [m]
R	Specific gas constant [kJ/kgK]
	Thermal resistance [K/kW]
S	Conduction shape factor
S_{fs}	Conduction shape factor for the heat transfer from the helium gap edge to the graphite block node
S_{sw}	Conduction shape factor for the heat transfer from the graphite block node to the coolant channel wall node
T	Static temperature [°C]
T_0	Total/stagnation temperature [°C]

T_f	fuel rod surface temperature [°C]
T_s	Mass averaged graphite block temperature [°C]
	Surface temperature [°C]
T_{surr}	Surface absolute temperature of a larger (black surface) [°C]
T_w	Coolant channel wall surface temperature [°C]
T_∞	Temperature of fluid far from the surface [°C]
t	Time [s]
t_0	Reactor operating time [s]
u	Specific internal energy [kJ/kg]
V	Volume [m^3]
	Flow velocity [m/s]
	Mean velocity based on pipe diameter [m/s]
~~V~~	conduction heat transfer element volume [m^3]
v	Velocity [m/s]
$\dot{v}$	Volume flow rate [m^3/s]
W	Work [kJ]
w	Width [m]
$\dot{W}$	Power, i.e. rate of work done by the system [kW]
x	X-coordinate of three-dimensional Cartesian coordinate system. Length in the direction of flow
y	Y-coordinate of three-dimensional Cartesian coordinate system.
z	Elevation above datum line [m]
	Z-coordinate of three-dimensional Cartesian coordinate system.
$\sum K_S$	sum of the loss coefficients of the secondary loss components such as bends, valves and junctions
$\sum K_R$	loss coefficient of a sharp edged orifice present in the pipe
Greek symbols	**Description**
α	Thermal diffusivity = $\frac{k}{\rho c_p}$ [m^2/s]
	Solid fraction

β	Linear thermal expansion coefficient [K^{-1}]
δ	Gap width [mm]
ε	Surface roughness [m]
	Emissivity
	Solid fraction
η	Efficiency
γ	Ratio of specific heat capacities
К	Forward/ reverse losses
Л	Cross flow loss coefficient [m^{-4}]
μ	Static fluid viscosity [kg/m.s]
ν	Specific volume [m^3/s]
φ	Heat flux [kW/m^2]
ϕ	Azimuthal direction
θ	Absolute temperature [K]
	Tangential direction
ρ	Density [kg/m^3]
ν	Kinematic viscosity i.e. momentum diffusivity = $\frac{\mu}{\rho}$ [m^2/s]
σ	Stefan-Boltzmann constant = $5.670x10^{-8}$ [W/m^2K^{-4}]
Non-dimensional numbers	**Description**
f	Darcy-Weisbach friction factor= $\frac{D_H}{L}\frac{\Delta p_o}{\frac{1}{2}\rho v^2} = 4f_F$
M	Mach number = $\frac{v}{c}$
Nu	Nusselt number = $\frac{hD_H}{k}$
Pr	Prandtl number = $\frac{c_{p\mu}}{k}$
Ra	Raleigh number = $Gr.Pr$
Re	Reynolds number = $\frac{\rho v D_H}{\mu}$
Subscripts	**Description**
bg	Bypass gap

cf	Cross flow
CA	Conduction area
cc	Coolant channel
cht	Convective heat transfer
CP	Coated particle
CV	Control volume
e	Exit
eq	Equivalent
FD	Fully developed
fr	Fuel rod
g	Graphite
Gr	Groehn
h	Height
i	Inlet
	Inner
Ka	Kaburaki
o	Outlet
	Outer
p	Perpendicular
rep	Representative
s	Surface
sr	Side reflector
T	Total
UC	Unit cell
w	Wall

1 INTRODUCTION

A number of countries participating in the Generation IV International Forum (GIF) are currently involved in the development of the six Generation IV nuclear reactor technologies (Generation IV International Forum, 2015). The GIF was set up to carry out research and development needed to establish the feasibility and performance capabilities of the next generation nuclear systems. The GIF also promotes the fourth generation of advanced reactors with enhanced safety features, superior proliferation resistance attributes, efficient fuel resource utilization and improved economics (International Atomic Energy Agency, 2010). The identification and selection of the six nuclear technologies for further development are based on the requirements of providing sustainable energy generation that is clean, safe, reliable, has life-cycle-cost advantage over other energy sources, while being resistant to diversion of materials for weapons proliferation and secure from terrorist attacks.

This has motivated the creation of the Generation IV Nuclear Energy Systems program in which ten countries have agreed on a framework for international cooperation in research for advanced reactors. Six designs have been selected for continued evaluation with the objective of deployment by 2030. Among the six fourth-generation nuclear concepts is the very high temperature reactor (VHTR) technology which offers gas outlet temperatures of 900 to 1000 °C with net thermal efficiencies higher than 45% (International Atomic Energy Agency, 2010). The VHTR is a thermal neutron spectrum system with a helium-cooled and graphite moderated core (Walter, et al., 2004).

1.1 The history of gas-cooled reactors

The origins of the gas-cooled power reactor dates back to 1946 seeking to make the best type of reactor for plutonium production. The choice was between a water-cooled graphite moderated reactor and a graphite moderated reactor cooled by gas under pressure, both with natural uranium. The great disadvantage of the water cooled version was the hazard arising from the increased reactivity following an accidental interruption of the cooling water supply. The reactivity increase is caused by the positive void reactivity coefficient. The gas-cooled reactor was then deemed a safer option (Jensen & Nonbol, 1998).

Gas-cooled reactor design concepts have been evolving since the 1940s and started going commercial for electricity production in 1960 with the United Kingdom's (UK) Magnox at Berkeley nuclear power station (Jensen & Nonbol, 1998). The Magnox reactor was carbon

dioxide (CO_2) cooled and graphite moderated. The fuel used was natural uranium in metallic form, clad in magnesium alloy (magnox). The reactor internals consisted of a large graphite block core with a square array of fuel channels into which the fuel elements were placed. This graphite block functioned as a moderator and reflector. The Magnox was limited to practical operating fuel temperatures of 660 ℃ and maximum coolant temperatures of 400 ℃ to avoid fuel surface deformation and melting of the cladding (Nonbol, 1996). The thermal efficiency was still limited to about 20% (International Atomic Energy Agency, 2010).

Several Magnox reactors were built around the UK and as they evolved, they approached the design of the Advanced Gas-cooled Reactor (AGR) in Great Britain. The difference was in the type of fuel. The AGR fuel consists of slightly enriched uranium oxide (UO_2) cylindrical pellets in stainless steel cladding with a central hole. These are contained within stainless-steel cladding tubes, each of which is about 900 mm long. A fuel element consists of 36 fuel pins surrounded by two concentric graphite sleeves (Nonbol, 1996). The AGRs were designed to operate at a higher temperature to increase thermal efficiency. Higher CO_2 pressures were used and the coolant operating temperature was thus raised to about 650 ℃ and an efficiency of 40% (McKeen, 2010). The AGR thus offered higher burn-up and higher efficiency. Dungeness B was the first commercial AGR plant to be ordered. The reactor moderator is a 16-sided stack of graphite bricks designed to act as a moderator and to provide individual channels for fuel assemblies, control devices and coolant flow.

The second generation of gas-cooled reactors termed high temperature reactors (HTRs) used graphite as a moderator and helium as a coolant. With this generation, the Dragon reactor prototype was introduced and it was operated from 1964-1976. Here, coated fuel particles of highly-enriched uranium-thorium carbide and helium inlet temperatures of 350 ℃ were used and helium outlet temperatures of 750 ℃ could be obtained at 1 MPa. While the initial efforts could be credited to the Atomic Energy Research Establishment (AERE) in the UK, Germany was also developing a pebble bed core design. The German efforts were realised with the successful operation of the Arbeitsgemeinschaft VersuchsReaktor (AVR) from 1967-1988 (International Atomic Energy Agency, 2010). The AVR had increased core gas outlet temperatures of up to 950 °C.

Peach Bottom Unit 1 rated at 40 MW_e, was the first high temperature gas-cooled reactor (HTGR) demonstration prototype operating from 1967- 1974 in the United States of America (USA) (International Atomic Energy Agency, 2010). This reactor utilised BISO-coated particles containing high enriched Uranium (HEU) and fertile Thorium fuel materials in

carbide compounds dispersed in a graphite moderator in fuel compact form. The enhanced safety of the HTGR fuel is based on its coated fuel particle design consisting of uranium oxide/carbide particles coated with layers of pyrolytic carbon and silicon carbide. The Peach Bottom reactor produced 115 MW_{th} and 40 MW_e power with a helium coolant temperature of 377 °C inlet and 750°C outlet at 2.5 MPa pressure (International Atomic Energy Agency, 2010). Early operation experience prompted significant coated fuel particle design changes with the introduction of the buffer layer to the coated particle.

HTRs can have two design concepts; the prismatic core design and the pebble bed core design. While these design concepts were emerging, the German Thorium Hochtemperature Reaktor (THTR-300) represented the pebble bed concept and the USA's Fort St. Vrain represented the prismatic block concept (Methnani & Kupitz, 2004). The Fort St. Vrain reactor operated between 1976 and 1989, its core operated at 842 MW_{th} with 405 ℃ inlet and 785 ℃ outlet helium temperatures at 4.5 MPa pressure. The hexagonal block fuel element was designed at General Atomics (GA) in 1965, for the Fort St. Vrain nuclear generating station. The goal of the fuel element design was to utilize a simple geometry that could be adapted to larger reactor cores. The hexagonal blocks allowed for the stacking of fuel elements into approximately cylindrical reactor core configurations while accommodating control rods into symmetric core positions. The hexagonal blocks can be arranged in roughly cylindrical patterns that minimizes neutron leakage at the outer edge of the reflector. The hexagonal blocks fit relatively closely together, and therefore limit helium coolant flow inside gaps between the blocks, i.e., bypass flow. The THTR operated in Germany between 1986 and 1989 with 750 MW_{th} and 300 MW_e power, with 270 ℃ inlet and 750 ℃ outlet helium coolant temperatures at 3.9 MPa pressure (International Atomic Energy Agency, 2010).

1.2 Recent development in gas-cooled reactors

Global interest has been growing in the recent years in modular variants of gas-cooled reactors due to their promising features of enhanced safety and improved economics. Some of the countries that showed interest include: the South African PBMR project, USA-Russia GT-MHR project, USA next generation nuclear power (NGNP) in Idaho, high temperature engineering test reactor (HTTR) in Japan, Korean HTGR plan, and Chinese high temperature gas-cooled reactor-pebble bed module (HTR-PM) demonstration project. Modular high temperature gas-cooled reactor (HTGR) designs are currently considered one of the leading reactor concepts considered for any future nuclear power plant deployment. Current HTR designs are therefore based on the considerable body of existing technology and plant operating

experience gained over the years. Part of that experience is derived from the design and operation of other plants such as AVR, THTR, Peach Bottom I and Fort St. Vrain. The Fort St. Vrain hexagonal block geometry, design, and past experience are the basis for the current and future prismatic HTGR designs (Generation IV International Forum, 2014). A number of countries are taking part in the ongoing research of the modular high temperature gas-cooled reactor (MHTGR) technology. A brief description of some of these projects is given in sections 1.2.1 to section 1.2.5.

1.2.1 HTR-10

China started developing a test reactor (HTR-10) in the late 80s with the objective of verifying and demonstrating the technical and safety features of the modular HTGR and to establish an experimental base for developing nuclear process heat applications. The Institute of Nuclear Energy Technology (INET) of Tsinghua University carried out the key technology development, conceptual design and feasibility study of the HTGR. The HTR-10 reached first criticality in 2000 (Sousa, et al., 2013). The HTR-10 is a pebble bed type high temperature gas-cooled reactor that uses spherical fuel elements containing coated fuel particles. The design parameters of the HTR-10 are shown in Table 3.

Table 3: HTR-10 main design parameters (Sousa, et al., 2013)

Parameter (unit)	Value
Reactor thermal power (MW_{th})	10
Primary helium pressure (MPa)	3.0
Core inlet/outlet temperature (°C)	250/700
Primary helium mass flow rate at full power (kg/s)	4.3
Power output (MW_e)	~2.6

1.2.2 HTR-PM600

The HTR-PM demonstration power plant was then designed by INET in China based on the technology and the experience with the HTR-10. The HTR-PM takes the HTR-10 as a prototype, and uses the German HTR-module and the USA's modular high-temperature gas-cooled reactor (MHTGR) as references. The HTR-PM is a modular pebble bed HTGR demonstration plant with two reactor modules connected to a steam turbine to form a 210 MW_e nuclear power plant. First concrete was poured in December 2012 and the first vessel was installed in March 2016. It is expected to start commercial operation in late 2019. Fuel elements

are 6 cm in diameter with a 7 g heavy metal loading each and an enrichment of nearly 8.8% (Zhang, et al., 2016). The design parameters of the HTR-PM are shown in Table 4.

Table 4: HTR-PM600 main design parameters (Zhang, et al., 2016)

Parameter (unit)	Value
Reactor thermal power (MW_{th})	250
Number of modules	2
Active core diameter/height (m)	3/11
Primary helium pressure (MPa)	7
Core helium inlet/outlet temperature (℃)	250/750
Power output (MW_e)	210

1.2.3 HTTR

The Japan Atomic Energy Research Institute (JAERI) also sought to establish and upgrade the technology base of the HTGR. They wanted to demonstrate establishment of HTR technology, HTR safety operation and inherent safety characteristics, nuclear heat utilization, irradiation of HTR fuel and materials in an HTR condition, and provision for testing equipment for basic research. The result was the high temperature engineering test reactor (HTTR) which is a prismatic block, graphite-moderated and helium gas cooled reactor. HTTR first criticality was achieved in 1998 and full operation at an outlet coolant temperature of 850 ℃ reached in 2001. The coolant outlet temperature was then increased to 950 ℃ and a thermal output of 30 MW_{th} in 2004 (International Atomic Energy Agency, November, 2003; Takizuka, 2005). Japan's nuclear energy came under review after the Fukushima accident and currently only 42 of its reactors are operable. 17 reactors are currently in the process of restart approval (World Nuclear Association, 2018).

An HTTR standard fuel block is hexagonal with 36 cm across flats and 58 cm high. The fuel is pin-in-block type consisting of fuel rods and a hexagonal graphite block. The fuel consists of Tri-structural ISOtropic (TRISO) coated particles of low enriched UO_2 whose average enrichment is about 6%. The particles are dispersed in the graphite matrix and sintered so as to form annular fuel compacts. The fuel particles are contained in annular fuel compacts which are inserted into the fuel or coolant channels or holes. The details of the HTTR fuel elements are shown in Figure 1. The main design parameters of the HTTR are shown in Table 5. Thirty fuel assemblies and seven control assemblies are arrayed in the active core arranged cylindrically to form an annular core. The HTTR's annular fuel rods are inserted in vertical bore holes in the hexagonal blocks. For this reactor pin-in-block type fuel rods are inserted into

the coolant channels of the graphite blocks. The coolant flows through the annular gap between the fuel rods and the fuel rod bore holes.

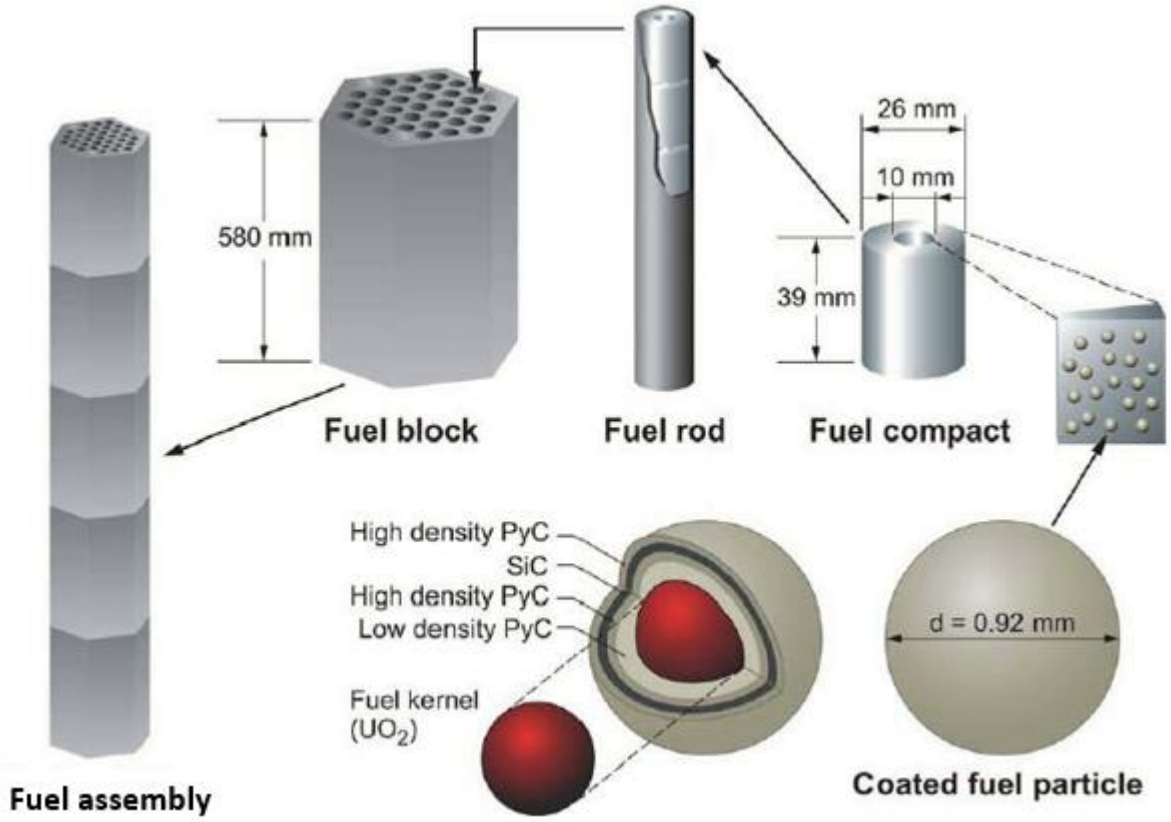

Figure 1: Configuration of the HTTR fuel element (Ortensi, et al., 2010)

Table 5: HTTR main design parameters (Takizuka, 2005)

Parameter (unit)	Value
Reactor thermal power (MW_{th})	30
Core helium inlet/outlet temperature (°C)	395/850-950
Active core diameter/height (m)	2.3/2.9
Primary helium pressure (MPa)	4
Power density (MW/m^3)	2.5

The HTTR and HTR-10 experimental reactors support the advanced reactor concept development for VHTR and provide important information for the demonstration and analysis of safety and operational features of VHTRs (Generation IV International Forum, 2014).

1.2.4 GT-MHR

In the mid-1990s, the Gas Turbine-Modular helium Reactor (GT-MHR) design was initiated between General Atomics (GA) of the USA and Russian Federation Ministry of Atomic Energy (MINATOM). In this design, a gas cooled modular helium reactor is coupled with a Brayton

cycle gas turbine to provide a high efficiency energy conversion of 47.7% (General Atomics, 1996). Each plant consists of four reactor modules. The active core consists of an assembly of hexagonal graphite fuel blocks containing blind holes for fuel compacts and full length channels for helium coolant flow. The fuel blocks are stacked ten blocks high and arranged in three annular rings forming the active fuel region. The hexagonal graphite fuel elements are 793 mm long and 360 mm across sides. The fuel for the GT-MHR is in the form of TRISO-coated particles embedded in a carbonaceous matrix and then formed into cylindrical fuel compacts. These compacts are 12.45 mm in diameter and 49.3 mm long. Fifteen fuel compacts are then stacked into fuel holes except for the dowel hole where 14 fuel compacts are stacked (General Atomics, 1996). Design parameters for the GT-MHR are shown in Table 6.

Table 6: GT-MHR main design parameters (General Atomics, 1996)

Parameter (unit)	Value
Reactor thermal power (MWth)	600
Active core diameter/height (m)	4.83/7.93
Primary helium pressure (MPa)	7
Core helium inlet/outlet temperature (°C)	490/850
Power output (MW_e)	286

1.2.5 PBMR

From the experience of the AVR and the German HTR-Modul, South Africa started designing the successor of the pebble bed HTGRs with the PBMR in 1994, originally with the aim to commission a 400 MW_{th} demonstration reactor. Various reactor design concepts evolved from the German HTR-Modul until a revised strategy was adopted by PBMR (Pty.) Ltd in 2009, supporting the development of a 200 MW_{th} reactor (delivering 80 MW_e) for both electricity and process heat applications (PBMR, 2010). The PBMR is also a helium cooled, graphite moderated high temperature reactor. A cylindrical core is surrounded by an outer reflector and other graphite structures at the top and bottom. Modular pebble bed reactors employ fuel elements similar to those used in the AVR. It uses particles of enriched UO_2 coated fuel particles encased in graphite to form fuel pebbles as shown in Figure 2.

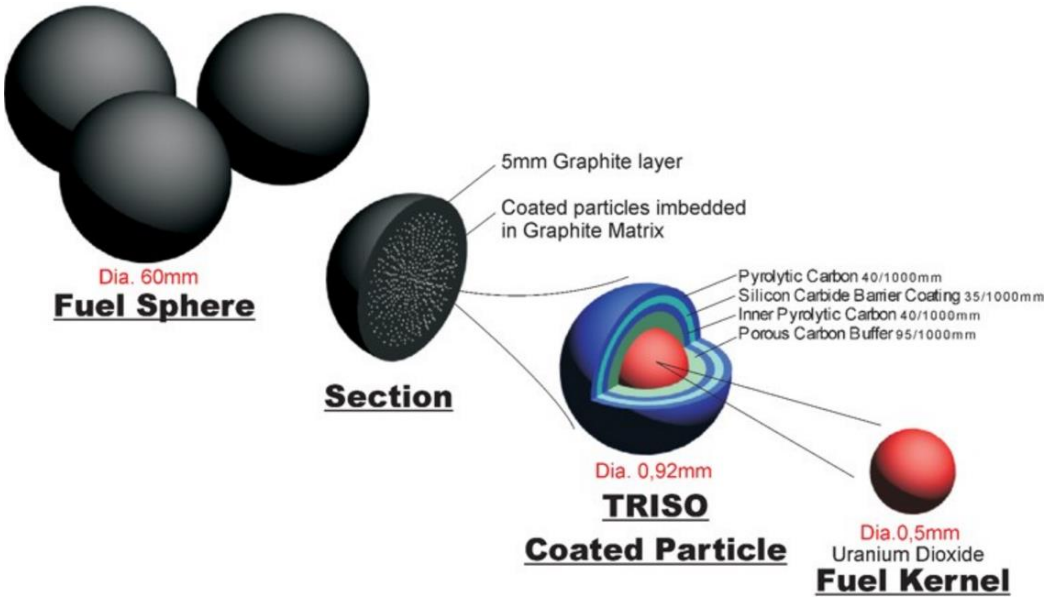

Figure 2: Fuel element design for PBMR (Greyvenstein, et al., 2004)

An important difference of pebble bed reactors compared to the prismatic reactor is the capability to do on-line refuelling. Design parameters for the PBMR are shown in Table 7.

Table 7: PBMR main design parameters (Matzner, 2004)

Parameter (unit)	Value		
Reactor thermal power (MW_{th})	200	268	400
Active core diameter/height (m)	3.5/9.4	3.5/8.5	3.7/11
Primary helium pressure (MPa)	7	7	9
Core helium inlet/outlet temperature (°C)	200/700	500/900	500/900
Power output (MW_e)	80	110	165

1.3 Very high-temperature gas-cooled reactors

The VHTR is a next step in the evolutionary development of high-temperature gas-cooled reactors and forms part of the Generation IV development concepts. VHTRs are graphite moderated and helium cooled reactors with a thermal neutron spectrum (Generation IV International Forum, 2015). The high outlet temperatures of the VHTR allows for use nuclear power for processes such as coal gasification, coal liquefaction, hydrogen production, research and test reactors, synthetic fuels, etc. A VHTR core can consist of a pebble bed such as the Chinese HTR-10 or HTR-PM and the PBMR or it may be prismatic blocks such as the Japanese HTTR and General Atomics' earlier GTMHR design and others in Russia, or VHTRs are descendants of HTRs developed in the 1980s and 1990s. They are characterised by a fully ceramic coated fuel particle fuel, the use of graphite as neutron moderators and helium as a coolant, self-acting decay heat removal capability and resulting in inherent safety features and

process heat application capability. The USA, European Atomic Energy Community (EURATOM), France, Japan, China, South Korea and Switzerland originally signed on to the system arrangement for the VHTR under the Framework Agreement.

A prismatic VHTR is a candidate design for national research programs such as the next generation nuclear plant (NGNP) project of the USA and the nuclear hydrogen production and demonstration (NHDD) project of South Korea. The reference prismatic modular reactor (PMR) power level is 600 MW_{th} and 286 MW_e. The Korea Atomic Energy Research Institute (KAERI) has been developing a pre-conceptual design of a prismatic VHTR. The design specification of the Korean VHTR design requires 490 ℃ and 950 ℃ for inlet and outlet coolant temperatures, respectively, at 7 MPa during normal operation. The full PMR200 core has 66 hexagonally shaped fuel assemblies (42 standard fuel assemblies, and 24 control fuel assemblies). Each fuel assembly consists of six fuel blocks stacked in a vertical orientation. The height of a fuel block is 79.3 cm and the distance from the centre of the block to one of its corners is 20.78 cm and the height of an active core is 4.758 m (Lee, et al., 2016 (b)). Figure 3 shows a schematic of a PMR200 reactor.

The reactor core is of annular design with an array of hexagonal fuel elements. The core is surrounded on the outside by rings of replaceable reflector elements and on the inside by the central reflector. A plan view of the reactor internals is shown in Figure 3 and Figure 4.

All HTR designs use coated particle fuel which can be in a form of spherical pebbles or hexagonal fuel blocks which contain cylindrical fuel compacts inserted in fuel holes. In the prismatic VHTR, coated fuel particles named TRISO are bonded together with a carbonaceous matrix into rod-shaped fuel compacts, which are stacked in the fuel holes of hexagonal graphite blocks. In the pebble bed type, on the other hand, the TRISO which contain uranium oxide (UO_2) or uranium oxycarbide (UCO) fuel kernel particles are surrounded by a coating of a carbonaceous material and the coated particles are pressed together into a spherical shape (Tak, et al., 2008). The multiple coating layers around the fuel kernel include porous carbon buffer, pyrolytic carbon and silicon carbide. The coated particles are mixed with a carbonaceous matrix and bonded into cylindrical fuel compacts, as shown in Figure 5. (Travis & El-Genk, 2013; Strydom, et al., 2015). The fuel compacts are stacked in a graphite sleeve to form fuel rods. Each fuel rod contains 10-15 fuel compacts except for the six stacks under each of the four dowels which contain one less fuel compact. Normal operating temperatures do not exceed about 1250 °C and worst case accident temperatures are maintained below 1600 °C (Tak, et al., 2012; MacDonald, 2003).

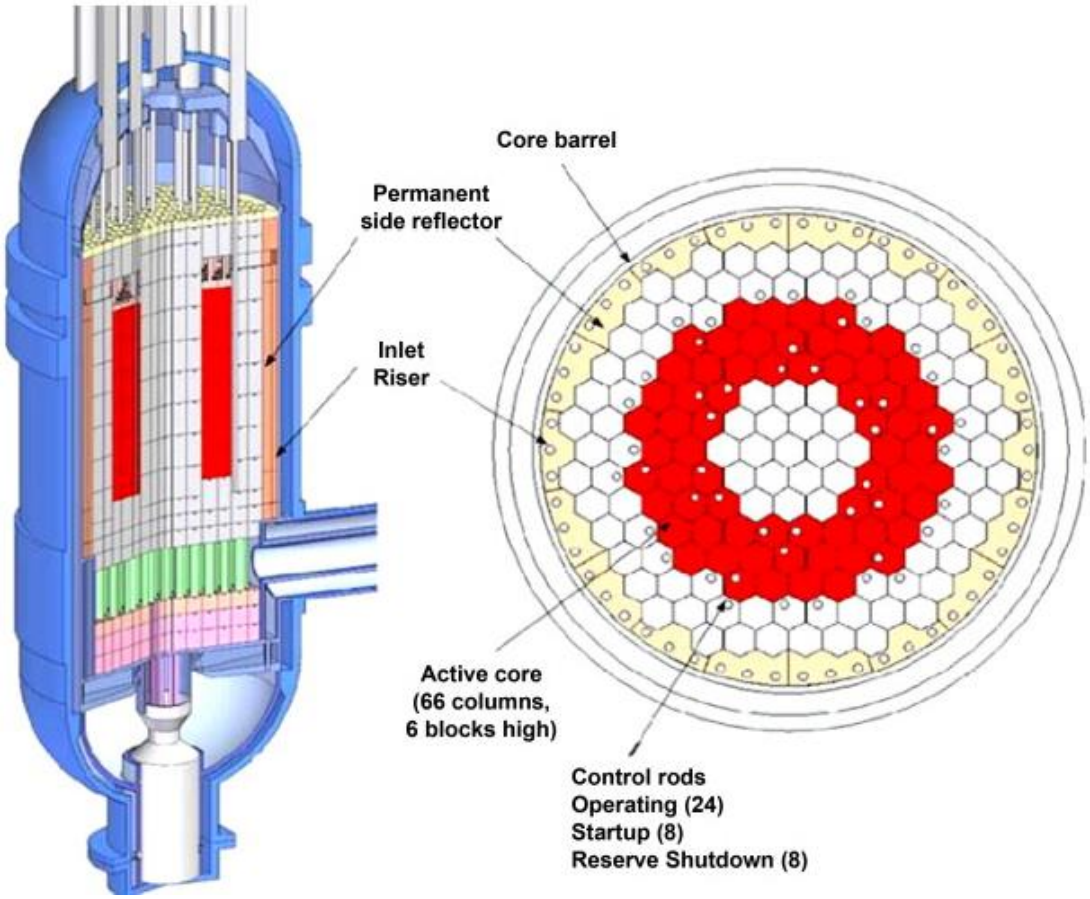

Figure 3: Configuration of the NHDD PMR200 (Yoon, et al., 2012)

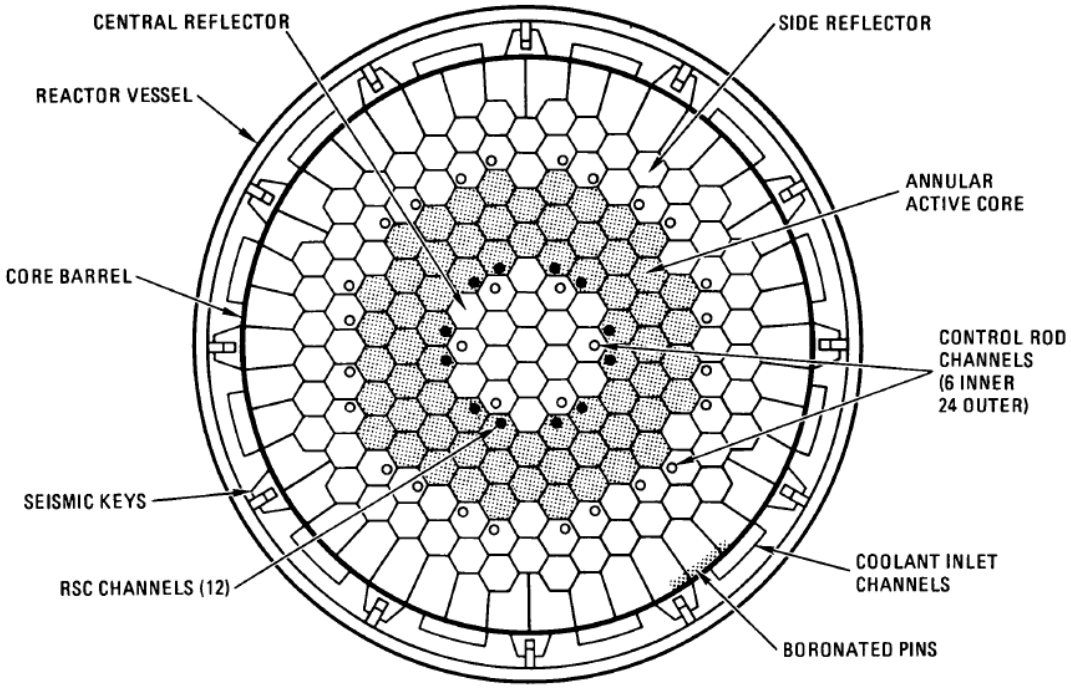

Figure 4: Example of a high temperature reactor cross-section (General Atomics, 1992)

Table 8: Design parameters of the NHDD PMR200 core (Kim & Lim, 2011)

Parameter (unit)	Value
Core thermal power (MW_{th})	200
Core inlet pressure (MPa)	7
Inlet helium temperature (°C)	490
Outlet helium temperature (°C)	950
Number of fuel block layers	6
Number of fuel block in a layer	66
Fuel block height (m)	0.793
Active core height (m)	4.758
Power density (W/cm^3)	5.68
Total coolant flow rate (kg/s)	83.73

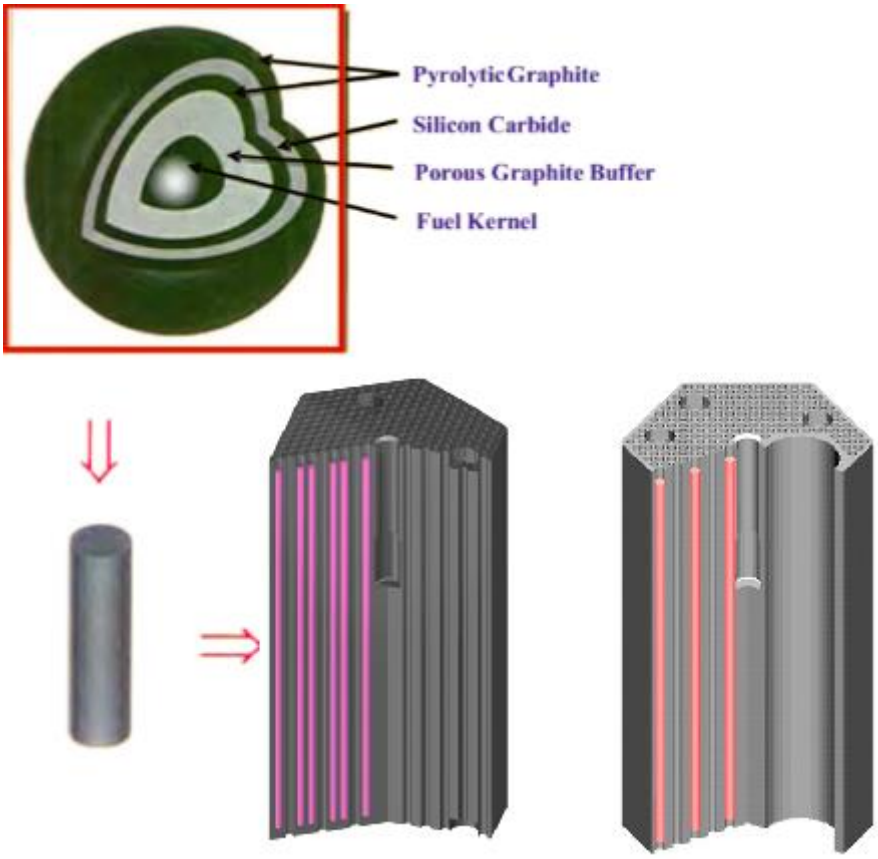

Figure 5: Fuel block components (Sato, et al., 2010)

The fuel rods are inserted into fuel holes drilled in the graphite fuel blocks. The geometric dimensions of the standard fuel block adopted in this work are those of the PMR200 (200 MW_{th}) reactor core based on the design concept of a gas turbine-modular helium reactor (GT-MHR) (Tak, et al., 2012). There are three types of hexagonal graphite blocks which contain fuel:

standard fuel block shown in Figure 6 and control rod and reserve shutdown control (RSC) fuel blocks shown in Figure 7 which contain control rod channels. The hexagonal fuel blocks contain blind holes for fuel and full length channels for helium coolant flow. Each fuel block is 79.3 cm in height and the height of the active core for the PMR200 is 7.93 m. Graphite reflector blocks are placed at both the top and bottom of the active core. The hexagonal blocks are doweled together to align the coolant holes and to form an assembly of stacked blocks.

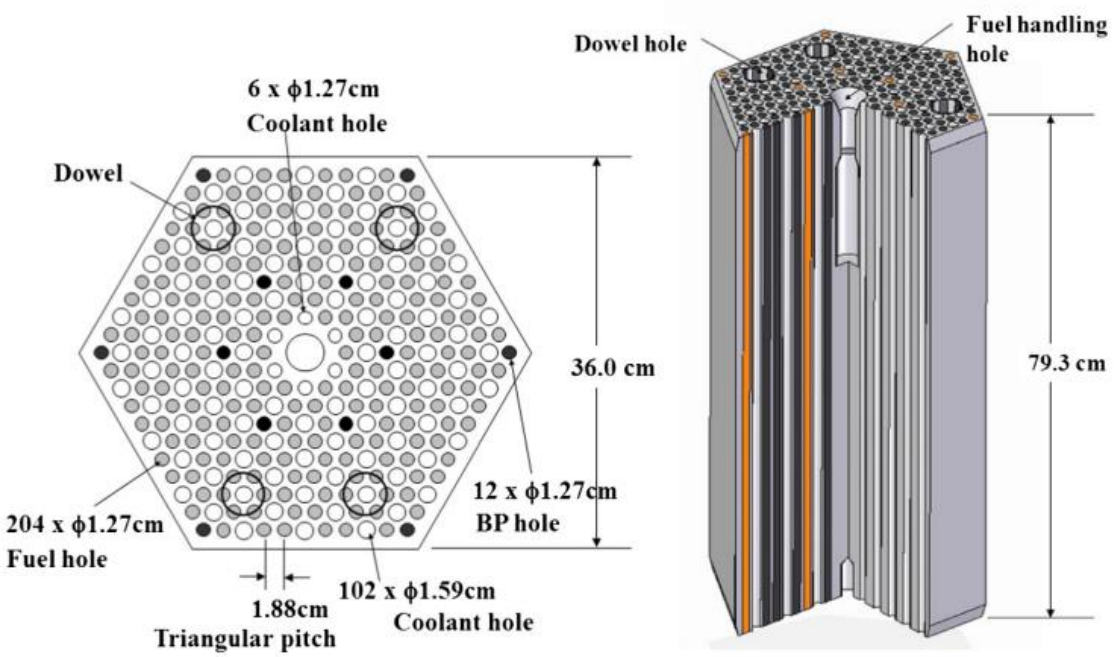

Figure 6: Standard HTR fuel block (Tak, et al., 2012)

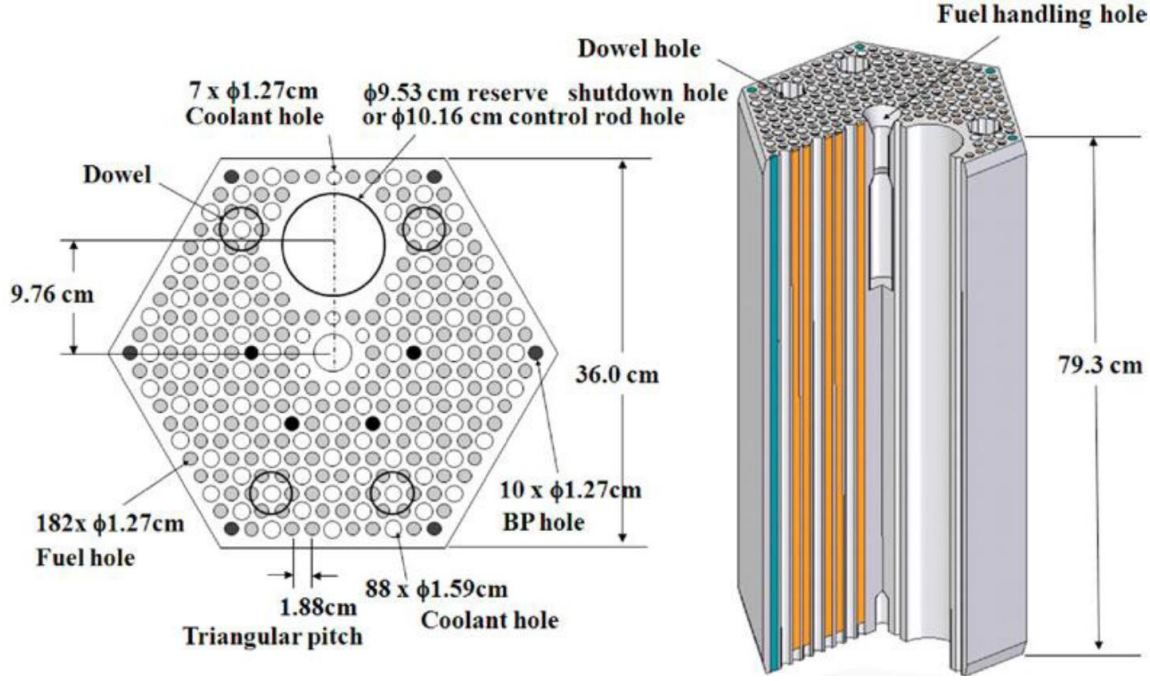

Figure 7: PMR200 control or reserve shutdown fuel block (Tak, et al., 2012)

1.4 Problem statement

The active core of a prismatic block HTR consists of fuelled graphite blocks in an annular region around the central reflector. A standard fuel block contains fuel rods and coolant channels while a control fuel blocks contain a control rod hole and reserve shutdown fuel blocks contain a hole for the reserved shutdown rod. Thermal-hydraulic analysis in high temperature prismatic block reactors involves determining the temperature distribution in the fuel blocks due to coupled heat conduction, convection and radiation. Accurate prediction of the fuel temperatures has thus far been done using fine mesh computational fluid dynamics (CFD) methods. This, however, comes with a huge computational effort and expense.

A more cost-effective way to predict core temperatures would be to employ a system code such as the Gas Mixture Multi-component Analysis (GAMMA+) code developed at KAERI (Lim, 2005). The problem with employing system codes is that they are designed for system transients and therefore have very coarse meshes. KAERI has developed a Core Reliable Optimization and thermo-fluid Network Analysis (CORONA) that addresses the insufficiencies between the CFD and system codes by using a coarser mesh than CFD codes but finer than general system codes (Tak, et al., 2012).

In the proposed study, an approach that seeks to achieve a balance between the methodologies discussed above is being developed. A thermo-fluid analysis Flownex model for a prismatic block type HTR that can reasonably predict the temperature distribution in the core where the coarseness of the mesh will lie in-between the mesh densities employed by GAMMA+ code and CORONA will be developed. The idea of the thermal-hydraulic analysis of high temperature gas-cooled reactors is not new, however the modelling of a prismatic block type core has been a challenge. The need therefore exists to create a thermo-fluid analysis Flownex model for a prismatic block type HTR that can reasonably predict the temperature distribution.

This thesis work therefore discusses the philosophy of modelling an HTR standard fuel block and assembly in Flownex.

1.5 Research aim

The main aims of this study include:

- The philosophical development of a thermal-hydraulic Flownex network model for a prismatic standard fuel block.

- A detailed study of the appropriate discretization required to model the heat transfer within a prismatic fuel block.
- To show how the fidelity of thermal-hydraulic in-core calculations using a system CFD code is affected.
- To propose methods to increase the speed of simplified reactor models, intended for use in system CFD codes while avoiding excessive grid refinement as it increases the calculation time and computing requirements.
- The use of a one dimensional (1-D) pipe network approach to model the three dimensional (3-D) fluid flow in the coolant channels, bypass and cross flow gaps.
- Development of a Flownex thermal-fluid network for an HTR prismatic block assembly.
- Providing guidelines for creating system CFD Flownex model for an HTR block component.
- Validation and verification of Flownex steady state models using similar CORONA models.
- Transient analysis of a fuel block assembly model.

Models developed in Flownex include:

- Thermal-fluid analysis of heat transfer within a fuel rod.
- Thermal-fluid analysis of heat transfer within an HTR coated fuel particle.
- Thermal-fluid analysis of heat transfer within a $1/6^{th}$ of an HTR prismatic fuel block.
- Thermal-fluid analysis of heat transfer within an HTR prismatic fuel block.
- Thermal-fluid model for a $1/6^{th}$ of an HTR prismatic fuel block assembly.
- Thermal-fluid model for a HTR prismatic fuel block assembly.
- Thermal-fluid model for a three-fuel block assembly.
- Prismatic graphite block.

In Flownex, the basic unit cell will not contain only coolant or fuel but part of the graphite and the associated fuel elements and coolant channels. The fuel and coolant channels will be modelled by defining representative coolant channels, fuel rods and coated particle layers associated with each unit cell. Flownex can therefore be used to model temperatures at coated particle level all the way through each standard fuel block. Flownex is capable of executing both steady state and transient analyses and these analyses will be done on several core components.

Verification of the Flownex models and or test cases was done using the CORONA code. Flownex models were validated by comparing the fuel and coolant temperature profile ranges with those obtained using CORONA. It should be noted that the assumptions made to simplify the detail of the geometry of the prismatic block within the two codes may differ and the distinctions will be stated explicitly throughout the report.

Only the standard fuel block and assembly were discussed and modelled in detail in Flownex for this study and not the whole core. Where fuel block assembly models were developed, models do not include variable gap size that is a result of shrinkage and expansion of the blocks due to thermal effects and irradiation by neutron flux. The models also do not include radiation heat transfer between adjacent fuel blocks. Modelling of neutronic parameters and feedback from neutronics do not form part of this study. This study on focuses on the thermal-hydraulic simulations and does not include coupling with neutronics.

1.6 Thesis layout

A short description of the chapters that follow is given below:

Chapter 2: An overview of the literature study that was conducted. The history of the development and application of the unit cell approach to thermal-fluid analyses within a prismatic fuel block is discussed. The application of CFD technology to thermal-fluid analyses of prismatic bock HTRs and its limitations to whole core analysis is also summarized.

Chapter 3: Several ways in which reactors can be modelled in Flownex are introduced. The detail of the theoretical background and modelling philosophy used in this study is then given, as well as solving of the 3-D heat equation for the solids and adopting a 1-D fluid assumption to model fluid flow in order to overcome the difficulties presented by implementing CFD methods and system calculations.

Chapter 4: This chapter gives the theory and guideline for the development of Flownex models for the prismatic block HTRs.

Chapter 5: In this chapter the Flownex model development is illustrated, which includes the assumptions, parameters and boundaries implemented in modelling an HTR prismatic block in Flownex. The assumptions, parameters and boundary conditions used in CORONA are also given.

Chapter 6: Validation and verification of Flownex models is done. Descriptions and results of each of the models is given. Several test cases for Flownex models were developed and the results are compared with the corresponding results obtained by CORONA for verification.

Chapter 7: Summary and conclusions of this study are given and recommendations for further study are made in this chapter.

2 LITERATURE REVIEW

Thermal-hydraulic analyses in high temperature prismatic block reactors involve determining the temperature distribution in the fuel blocks due to heat conduction, convection and radiation. It also includes the heat transfer between the fuel compacts, graphite block, coolant channels, coolant leakage flows and mixing in the lower plenum. The limiting factor on the reactor core heat generation rate is based on how much energy can safely be removed by the coolant.

Prediction of the steady state temperature distribution is influenced by, among others; core flow distribution, thermo-physical properties of the materials and the heat flow path from the UO_2/UCO fuel kernel to coated fuel particle surface to graphite to final heat sink heat transfer. Power is generated in fuel kernels within coated particles which are embedded in the graphite matrix in the fuel rods. The heat transfer takes place from the fuel kernels through the respective coating layers and from the fuel rod surface through the helium gap to the surrounding graphite in the hexagonal block, as helium in the gap is assumed to be stagnant. There is also radiation between the fuel rod surface and the fuel rod sleeve through the helium gap and also between the fuel rod sleeve and the graphite block. The heat generated in the fuel rod is finally transferred from the graphite block through convection to the helium in the coolant channels.

Reactor core thermal-hydraulic analyses can be divided into two principal categories namely conduction through the core and reactor fluid flow. The main idea of whole core analysis efficient methods is to solve a 3-D solid heat conduction equation combined with 1-D fluid flow equations (Huning, 2014). System models can simulate the full reactor from a 1-D implicit approach to explicit three-dimensional models that simulate selected small detail of the reactor unit. There has been a number of approaches to analyse heat transfer and flow paths that vary from either a unit cell method, network approach or a combination thereof to CFD. In the literature there are therefore a number of contributions that address a selected aspect in 3-D detail; contributions that employ various combinations of explicit 3-D detail, implicit 3-D detail, implicit 1-D approximations and systems or network approaches to systems approaches that can address a full reactor unit.

2.1 Thermal modelling of high temperature reactors

A reactor can be represented by a lumped model, a discretized sub-network of 1-D models, or a 3-D CFD model (Du Toit & Rousseau, 2012). Commercially available CFD codes include ANSYS CFX and FLUENT (ANSYS Inc., 2018) and STAR-CCM+ (Chung, 2002). Explicit

3-D models can provide very detailed local results but they cannot be used to simulate the whole reactor due to computational resources and time challenges. Systems approach on the other hand is capable of simulating a full reactor unit but cannot provide detailed results.

A widely adopted modelling technique for simplification of prismatic block-type HTR models for heat transfer analyses is the unit cell model (Tak, et al., 2008). The unit cell method recognises a repeated pattern or arrangement of unit cells within the fuel block and uses these cells as a basic unit for models (MacDonald, 2003; Tak, et al., 2008; Tak, et al., 2012; Tak, et al., 2014; Huning, 2014). A number of analysis approaches have been using the unit cell method to model conduction in the active core. In some applications of the basic unit cell method, different regions were modelled homogenously and therefore no explicit fuel and graphite temperatures were computed (MacDonald, 2003). According to Tak et al. (2008) the simplified models employed for evaluation of temperature profiles within HTR's fuel assemblies, cannot consider heat transfer within a fuel assembly as well as coolant bypass between the assemblies. This is because the traditional unit cell method models those regions within the fuel block that contain a triangular geometry and then assumes symmetry of the unit cell within the block, as shown in Figure 8 (b). Thus the heat generated in each unit cell is removed by the coolant channel/s in that unit cell. The limitation of this approach is that there is no consideration of heat transfer between the adjacent cells and within the fuel block or assembly.

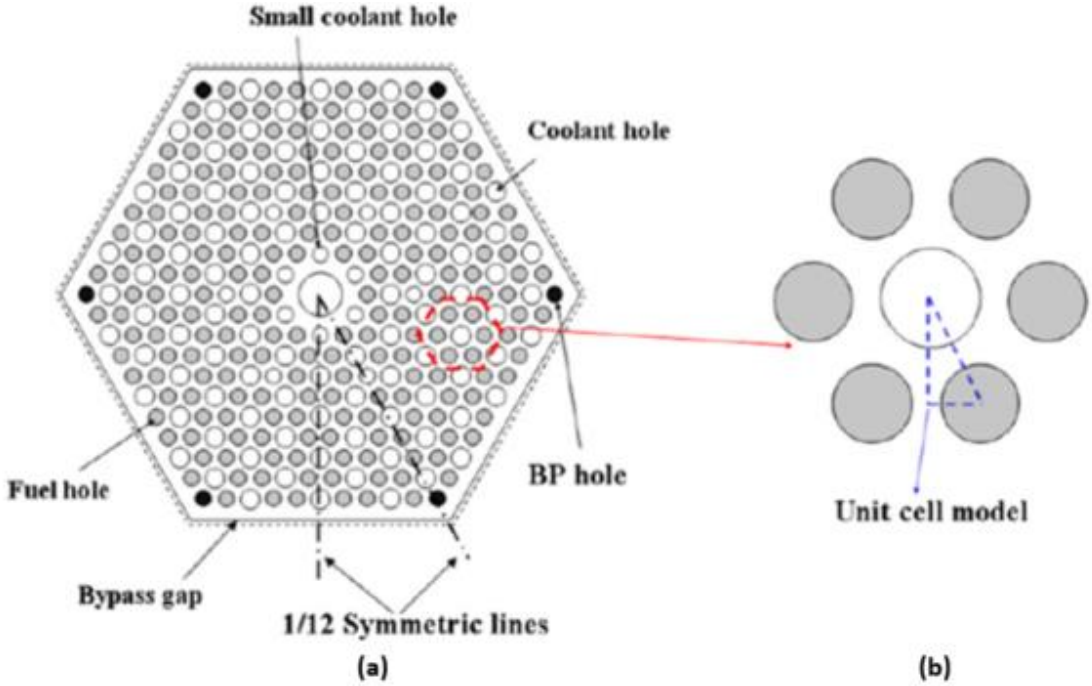

Figure 8: Symmetric lines for the 1/12th fuel assembly model and the unit cell model (Tak, et al., 2008)

2.1.1 CFD Approach

2.1.1.1 Fully 3-D CFD Approach

CFD entails the solution of the differential equations for the conservation of mass (also known as the continuity equation), momentum (also known as the Navier-Stokes equation), and energy equations (also known as the first law of thermodynamics) on a per unit volume basis (Olivier, 2005).

CFD codes are commonly used to analyse the flow behaviour in regions of a system where complex flow patterns are expected or present. Therefore, the CFD codes are usually used to analyse either two-dimensional (2-D) or 3-D flow behaviour. The great appeal of the CFD codes is their reliance on first principles to describe the fluid behaviour and their capability to calculate the behaviour in the regions of a system where complex flow patterns are expected or present (Schultz, 2008). Due to their reliance on fine mesh discretization to model the region of interest; consequently, even with modern fast computers, the region of a system that can be modelled is generally limited as defined by practical computing times and memory requirements. Thus, CFD codes are rarely used to model the behaviour of an entire system and instead are focused on the behaviour of a region of a system or component. The strength of CFD codes is therefore their capability to analyse the presence of localized hot spots and thermal gradients. The most limiting factor for using CFD codes is their computational requirements and the size of the problem that requires analysis (Schultz, 2008).

Some of the work done on CFD analyses carried out for a $1/6^{th}$, $1/12^{th}$ and a ½ of the prismatic core has been discussed in a study by Tak et al. (2008). To overcome the limitations of the basic triangular unit cell method in the prediction of the temperature distribution within the fuel block, Tak et al. (2008) used the $1/12^{th}$ fuel assembly of a PMR600 with 1 mm bypass gap, marked by symmetry lines in Figure 8 (a). This type of unit cell ensures that the central and peripheral regions of the fuel block are included and thereby overcome the limitations of the traditional unit cell method in Figure 8 (b). In Tak et al. (2008), a 3-D CFD analysis was carried out on a typical fuel assembly of a prismatic VHTR shown in Figure 9. This way, the bypass gap between adjacent blocks could be modelled. The effect of bypass gap size was then studied for 1, 3 and 5 mm bypass gaps.

The results obtained for the average coolant temperature indicated that the unit cell model reasonably predicted the temperature with a difference of 3 °C compared to the more detailed 3-D CFD analysis results. However, for the maximum fuel temperatures the unit cell model

was 20 ℃ lower than those obtained from the 3-D CFD analysis simulation. This was due to the inability of the unit cell model to consider heat transfer at the central and peripheral regions of the block as well as the bypass flow between neighbouring fuel assemblies. The bypass flow rate was observed to increase with gap size and that the flow fractions for the 3 and 5 mm bypass gap size are 5.4% and 12.1%, respectively. Results also showed that the larger size of the bypass gap results in a larger temperature change between the unit cell model and the model proposed in Tak et al. (2008). The conclusion was that triangular unit cell methods can be safely applied to cases with low bypass flow. For cases with large bypass flow fractions, temperature gradients within the assembly block are not adequately calculated and thus the maximum fuel temperatures are under predicted. For the bypass gap size of 5 mm, the unit cell model under-predicts the maximum fuel temperature by 79 ℃.

It was concluded in Tak et al. (2008) that the unit cell approach can be a reasonable approximation for real situations, if the bypass flow between the fuel assemblies is small and the radial power profile within the assembly is uniform. It was also found that the unit cell model significantly under-predicts the maximum fuel temperature when the bypass gap is large.

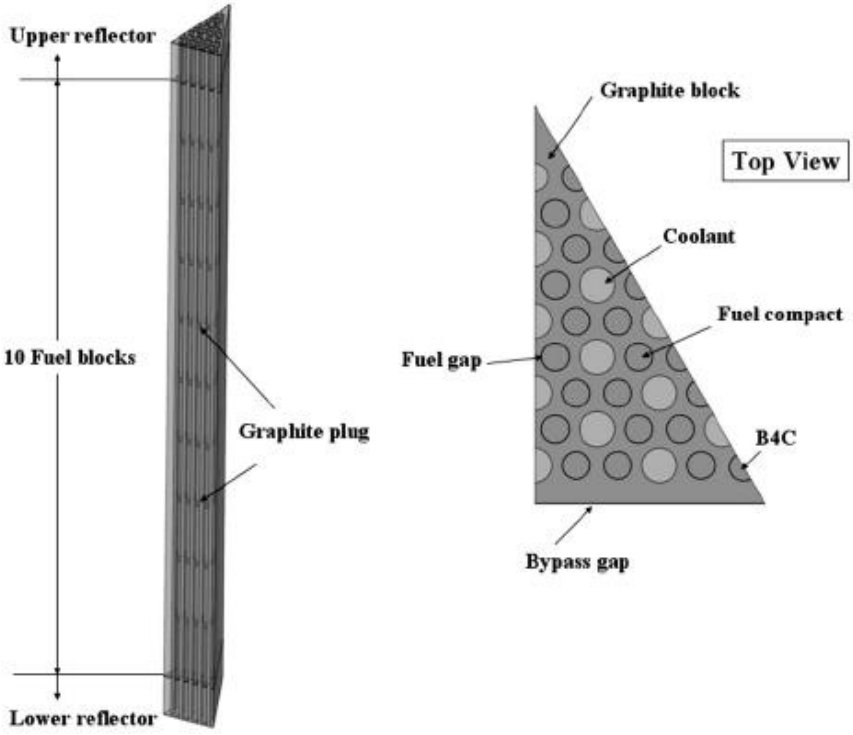

Figure 9: 1/12th Fuel assembly model for CFD analysis (Tak, et al., 2008)

CFD analysis was performed by (Sato, et al., 2010) on a 1/12th on a whole core length assembly of a 600 MW_{th} GT-MHR reactor. The assembly included the bypass gap to study the impact of

the bypass gap on flow and heat transfer in the core. The 1/12th model is made up of a section of the top reflector, an assembly of 10 fuel blocks, bottom reflector and half of the bypass gap.

A comparative study of gap widths of 0, 3 and 5 mm was done for the 1/12th assembly with a uniform heat generation of 27.88 MW/m^3 and the mass flow kept constant. The effect of gap size on one edge of the 1/12th section is shown in Figure 10. The temperatures in Figure 11 were taken along edge AB of the 1/12th assembly (Figure 10) where there are five coolant channels but no fuel pins.

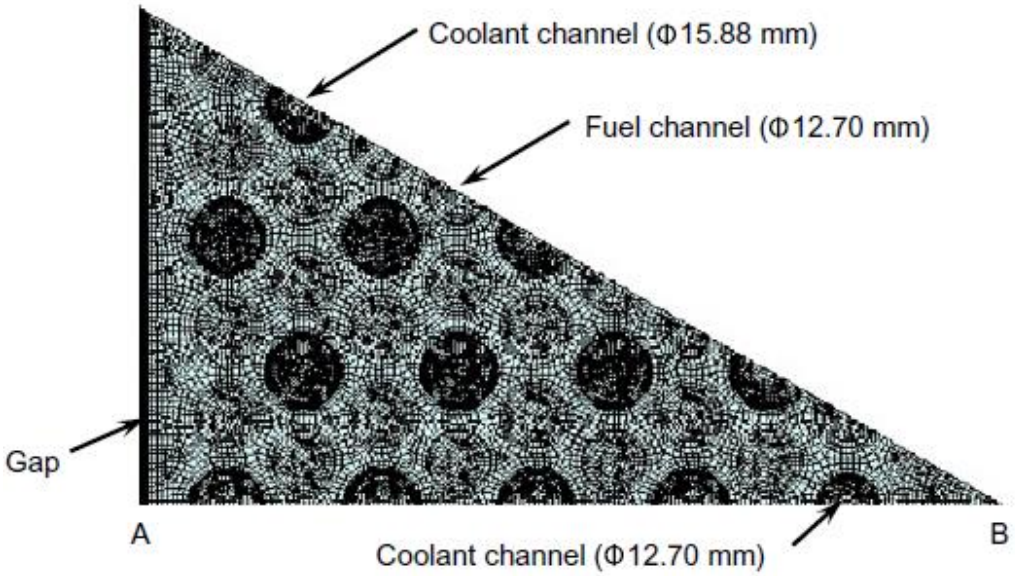

Figure 10: 1/12th meshed assembly (Sato, et al., 2010)

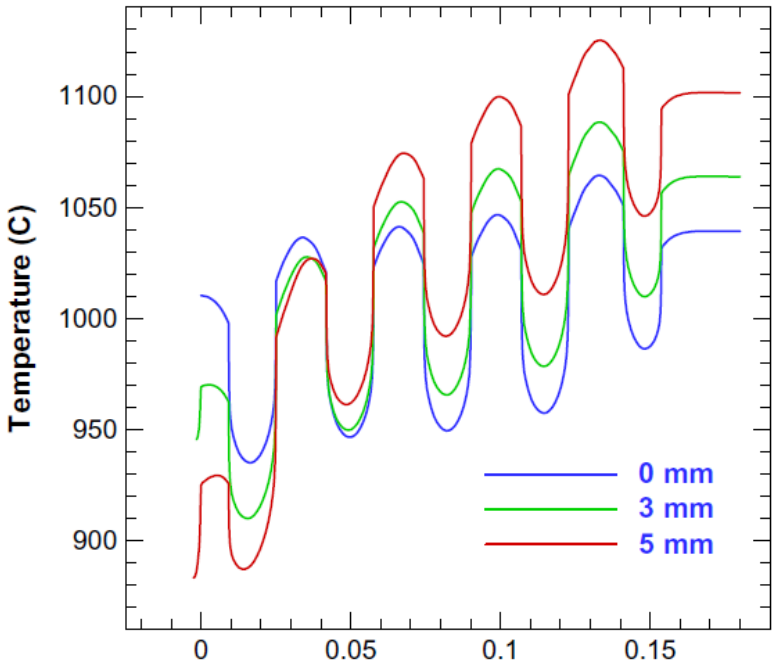

Figure 11: Temperature along the edge of the 1/12th for the fuel hot spot plane for various gap-widths (Sato, et al., 2010)

Results showed that the maximum graphite temperature differences were 65, 125 and 200 °C for the 0, 3 and 5 mm gaps, respectively. The maximum fuel and coolant channel outlet temperatures were also significantly increased with increasing gap size.

A similar study was done in Johnson and Sato (2012) where a $1/12^{th}$ of a GT-MHR (350 MW_{th} prismatic reactor) fuel assembly using the commercial CFD package FLUENT. The heat generation rate was set to 25.14 MW/m^3 for all the fuel channels. Figure 12 demonstrates that the effect of increasing gap width, while maintaining the same total mass flow rate, causes increased maximum fuel temperature while providing significant cooling to the near-gap region. The maximum outlet coolant temperature variation is increased by the presence of gap flow and also by an increase in total heat generation (Johnson & Sato, 2012).

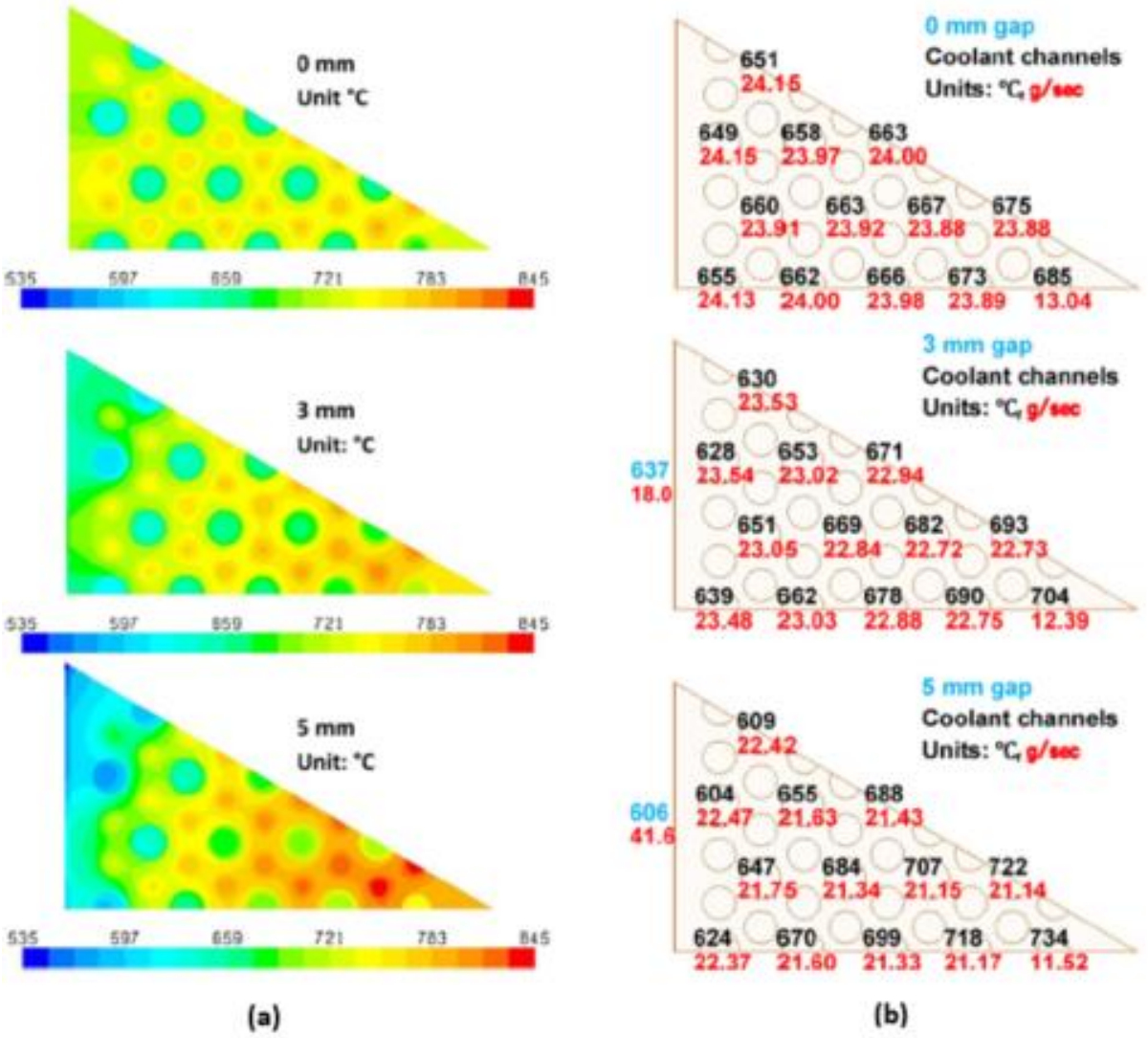

Figure 12: Temperature contours, coolant outlet, bypass gap and mass flow rates for the 0, 3 and 5 mm gap cases (Johnson & Sato, 2012)

As can be seen in Figure 12 (a), the maximum fuel temperature increases significantly as the gap width increases, from 785 ℃ to 808 ℃ to 841 ℃. It can also be seen that the temperature of the graphite near the gap decreases significantly, causing a larger overall temperature gradient across the block with increasing gap width. Figure 12 (b) shows the coolant and gap outlet temperatures and mass flow rates for the three gap width cases for each coolant channel and the gap.

Yoon et al. (2012) investigated the effects of fixed and variable bypass gaps and fixed cross gaps on the flow distribution in a physical and a computational model of a prismatic block VHTR core. The model core consisted of a transitional layer and four core layers. The core comprised five fuel blocks and two reflector blocks. The CFD code CFX was employed for the computational analysis of the flow. The flow in the bypass gaps, cross gaps and coolant channels were modelled in explicit 3-D detail. The variable bypass gaps sizes emulated the non-uniform dimensional changes that the fuel blocks undergo due to the variation in the neutron fluence and the temperatures throughout the core. The agreement between the experimental results and the results predicted by CFX was good.

In Yoon & Strydom (2014), a CFD study of a typical hexagonal 350 MW_{th} General Atomics Modular High Temperature Gas Cooled Reactor (MHTGR) was done. In this study, a comparison between the homogeneous model depicted in Figure 13 (a) and heterogeneous fuel model depicted in Figure 13 (b) were done. In the homogeneous fuel model, the fuel region was modelled as a volume-averaged homogeneous mixture consisting of H-451 graphite and TRISO fuel kernels.

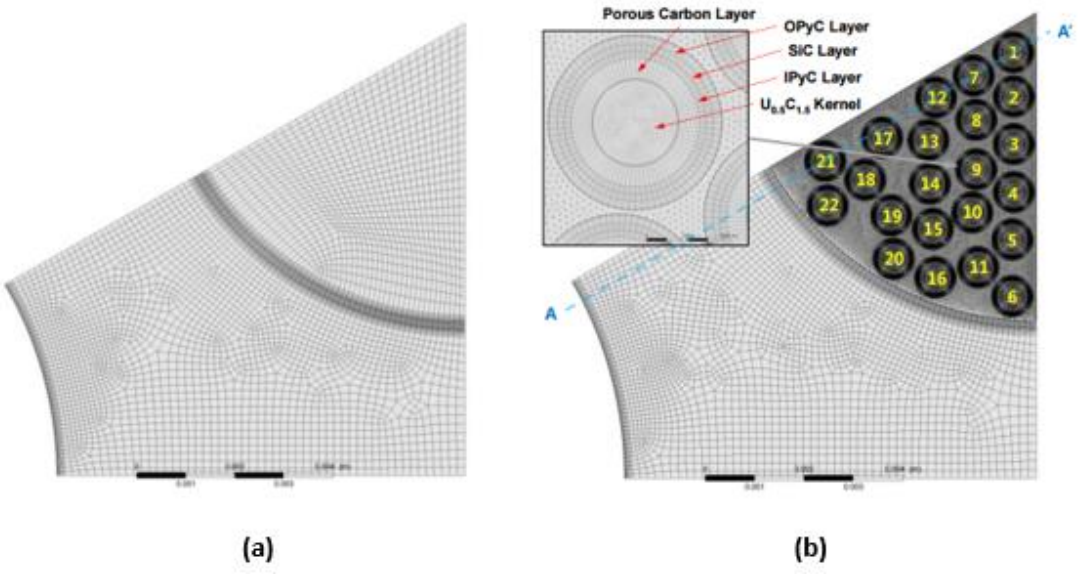

Figure 13: Unit-cell models of MHTGR-350 fuel (Yoon & Strydom, 2014)

A typical hexagonal MHTGR-350 unit cell consists of a helium coolant channel, six fuel compacts and a matrix graphite region. The helium gaps around the fuel compacts are also included in the fuel model. In the heterogeneous fuel model, shown in Figure 13 (b), UCO, inner and outer pyrolytic carbon (iPyC/oPyC) and silicon carbide (SiC) layers of the TRISO fuel particles were explicitly modelled. Heat transfer across the gap between the fuel compact and H-451 graphite region was modelled assuming heat conduction through stagnant helium and radiation heat transfer using an emissivity value of 0.85 for H-451 graphite. The major difference in the results was that the graphite region in the heterogeneous fuel compact shows a larger difference between the volume-averaged and maximum temperatures. The temperatures of the TRISO particles in the heterogeneous model were higher than those at the same location in the homogeneous model. Thus, the homogeneous model underestimates the peak fuel temperatures (Yoon & Strydom, 2014).

2.1.1.2 Coupled 3-D/1-D approach

Stainsby et al. (2009) studied the fuel-element internal flow and heat transfer models for a prismatic HTR. This study was conducted to develop and validate a suitable numerical model that can handle the conduction heat transfer from the surface of a fuel compact to its surrounding coolant channels, both in steady state and transient conditions. Also to be able to determine the effective thermal conductivity of a fuel block to be able to predict how heat is redistributed within a fuel element block.

Research conducted by Tak, et al. (2012; 2014) and Huning (2014) revealed similar methods for accurate and efficient determination of steady state thermal hydraulic parameters for prismatic high temperature gas reactors. This was achieved by discretization of the fuel assembly into unit cells containing a fuel compact or burnable poison, a coolant channel and the graphite region. The computational grids are then defined using a combination of the pre-generated basic unit mesh cells and thus the fuel and coolant channels were explicitly modelled. These methods consider various shapes of the unit cells as well as the heat transfer between unit cells. Computational grids were then used to model the heat transfer through the hexagonal blocks and a 1-D formulation to model the flow through the coolant channels.

A method was developed by Tak, et al. (2012) using the unit cell approach for grid generation. In this method unit cells that embody the shapes of the fuel, coolant, reflectors and those areas that are on the edges of the fuel blocks are employed instead of the traditional triangular unit cells. These unit cell representations and their use in the construction of a computational grid

for standard fuel block are shown in Figure 14. This makes it easier to fairly accurately retrace the complex geometry of the hexagonal blocks using unit cells. A combination of basic unit cells can therefore be used to model reactor internal structures.

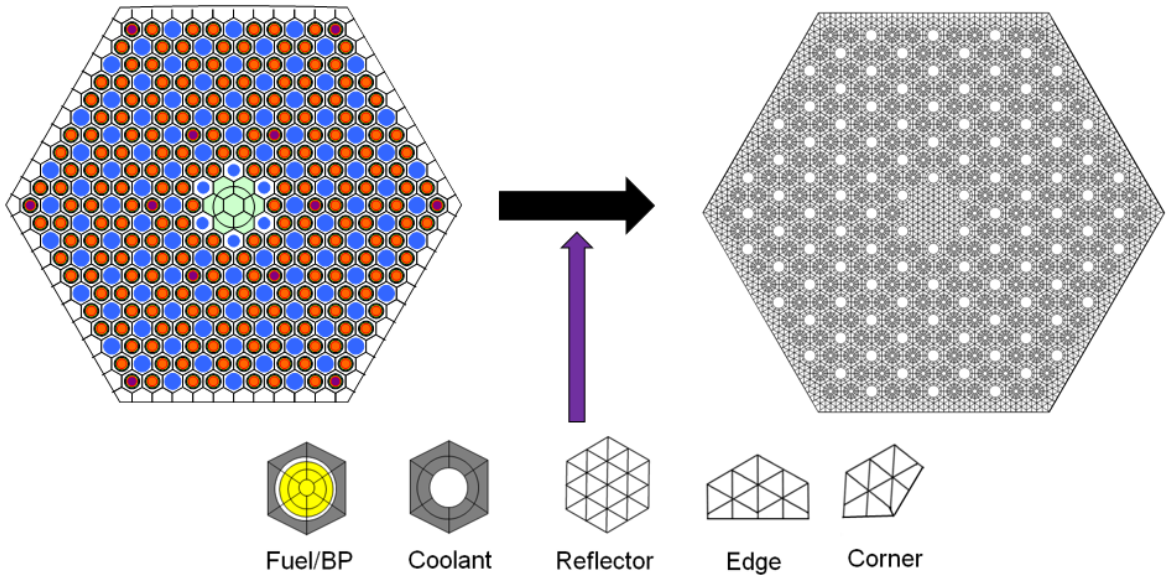

Figure 14: Basic unit cell types and examples of computational grids (Tak, et al., 2012)

This method was used in the efficient modelling of detailed geometries and materials of prismatic fuel and reflector blocks. The main advantage of using the Tak, et al. (2012) approach compared to the traditional triangular unit cell approach is that heat transfer between unit cells can now be modelled.

In a study conducted by Huning (2014) to determine core temperature and fluid flow distributions during steady state conditions for the prismatic HTGR (GT-MHR and MHTGR) the unit cell method was redeveloped to adequately predict the axial and radial heat conduction within each assembly block. Core heat transfer was approximated by discretizing each assembly into unit cells, calculating the associated heat rates, and then integrating the energy balance over a time step. The unit cells were formed by discretizing each prismatic fuel block into fuel pin or coolant channel unit cells. Different unit cells containing fuel compacts and coolant channels are shown in Figure 15 and Figure 16. Each fuel pin within the fuel assembly is then discretized in cylindrical coordinates. For a unit cell that contains a coolant channel, the assembly temperature was assumed to be the boundary condition for fluid transfer calculations. For the unit cell containing a fuel pin, the boundary condition was assumed to be the temperature of the surrounding graphite and this was used for heat conduction and radiation calculations. The average temperature location for each cell is based on the graphite centre of mass of the unit cell. The main benefit of this method is its ability for whole core analyses that

explicitly determine bypass flow and account for graphite conduction within the standard fuel block. Coolant flow was approximated by modelling each coolant and bypass channel as a segmented 1-D channel, and using correlations for the friction factor and Nusselt number (Nu) to compute the heat transfer rates. Three flow paths were modelled namely the coolant channels, the gap around the central handling hole and the bypass gaps. Each channel was modelled as 1-D flow in the axial direction.

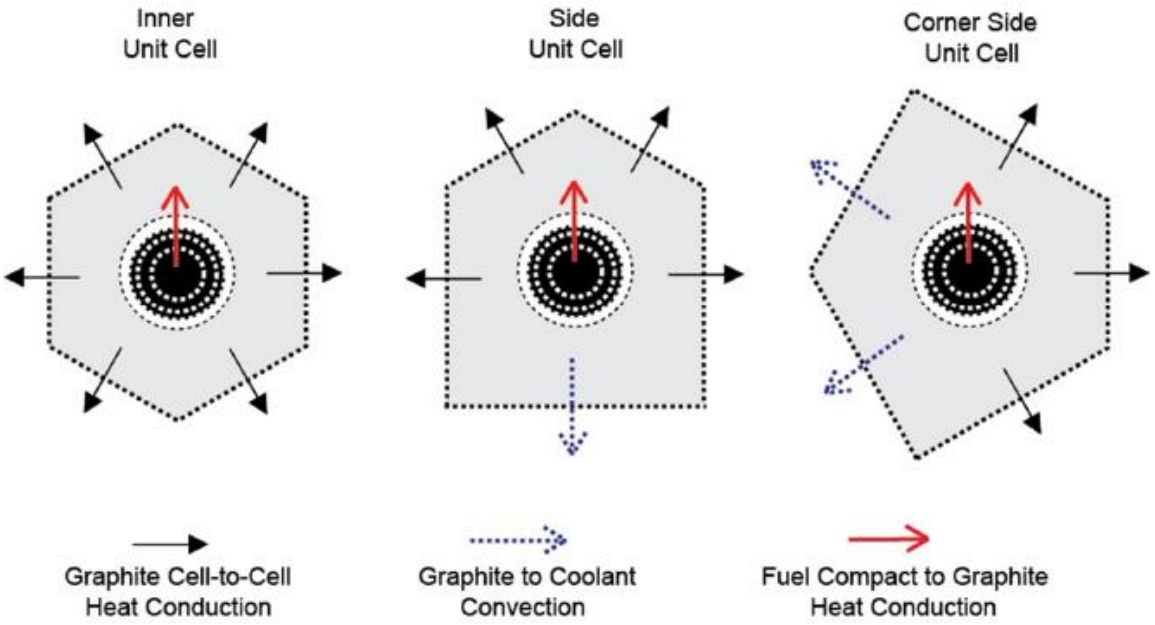

Figure 15: Different unit cells containing a fuel compact (Huning, 2014)

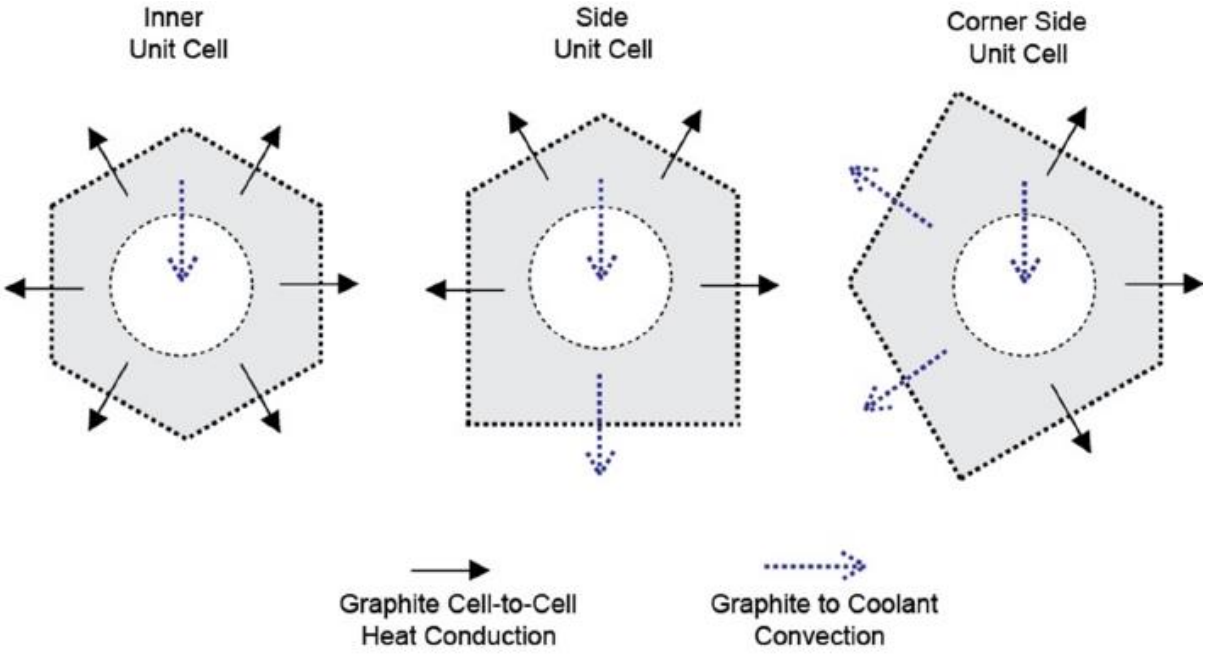

Figure 16: Different unit cells containing a coolant channel (Huning, 2014)

The effect of bypass gap size has been studied in the past (Sato, et al., 2010; Tak, et al., 2008; Travis & El-Genk, 2013). In all these cases, a uniform bypass gap size was assumed. In reality, the bypass gap varies according to the fuel cycle as the graphite blocks change due to fast neutron induced shrinkage and thermal expansion. Lee et al. (2016 (b)) analysed fuel temperatures in computational grids employing variable gap sizes in order to obtain an accurate hot spot fuel temperature. Seven fuel assemblies as shown in Figure 17 with constant gap size were modelled with CORONA and the results compared with those obtained using CFD commercial code CFX. To reduce the number of computational cells, only three fuel blocks were stacked to form an assembly in the Lee et al. (2016 (b)) model, with a 2 mm bypass gap. The temperature distribution of the hot spot plane obtained from the results of the CORONA simulations at the bottom of the seven fuel block assemblies with a 2 mm bypass gap size is shown in Figure 18.

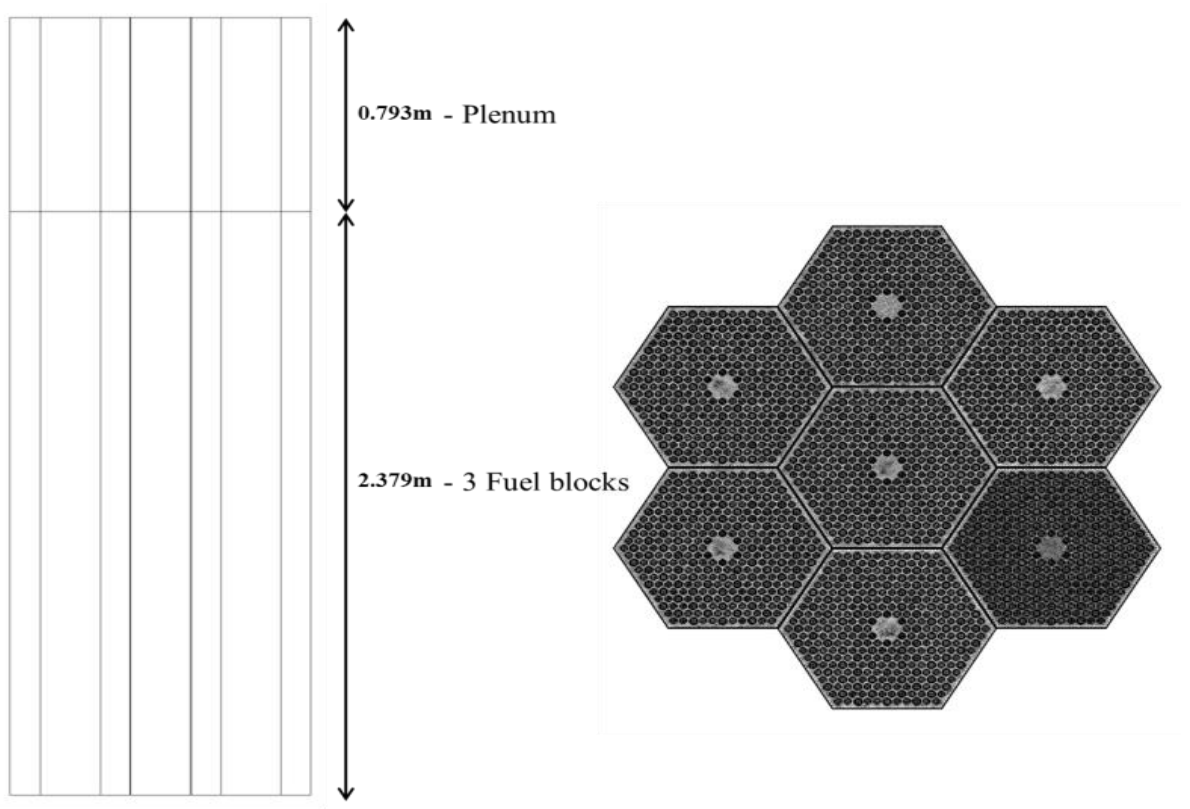

Figure 17: CORONA 7 assemblies (Lee, et al., 2016 (b))

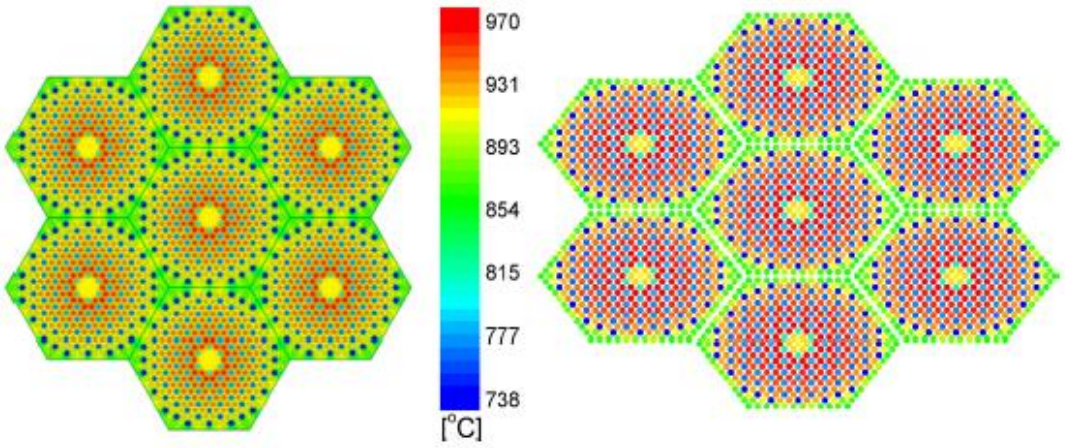

Figure 18: Temperature distributions on the hot spot plane in the seven fuel-unit assembly with a 2 mm bypass gap (Lee, et al., 2016 (b))

2.1.1.3 Distributed resistance or porous medium approach during loss of coolant transients

In Clifford (2013), heterogeneous unit cells were defined in the fuel, RSC, control rods, upper and lower reflector, flow distribution and core restraint elements. The heat conduction was modelled using a multiscale approach. For each of these unit cells, a shape function and geometric correction factors to calculate the effective thermal conductivity were determined. Heat transfer to the fluid was modelled using volumetric heat sources in the solid and fluid energy equations. The heat transfer coefficient was calculated using the Petukhov and Popov correlation for heat transfer in tubes (Krieth & Bohn, 2000):

$$\mathrm{Nu} = \frac{(\mathrm{f}/8)\mathrm{RePr}}{1.07+12.7\sqrt{(\frac{\mathrm{f}}{8})}(\mathrm{Pr}^{\frac{2}{3}}-1)} \tag{2-1}$$

Valid for $10^4 < \mathrm{Re} < 5 \times 10^6$ and $0.5 < \mathrm{Pr} < 1000$.

Purpose:

To study the event in which a loss of forced cooling occurs while the system remains pressurized.

Assumptions and simplifications:

- Two sets of cells are overlaid in the model because of the coupling of solid and fluid parts.

Methodology:

The graphite of the fuel blocks was represented by a separate set of mesh cells in OpenFOAM. Models for the fluid and solid components were created separately as shown in Figure 19. The models overlap in the fuel elements and upper and lower reflectors which are treated as porous

media (Clifford, 2013). Heat transfer between solid and fluid components in the fuel elements is modelled using volumetric heat sources in the solid and fluid energy equations. The solid and fluid meshes are identical in this region of the model, allowing a direct mapping of values between the two meshes. The solid-fluid heat transfer and the pressure drop were prescribed via coefficients. The radiation across the gaps was explicitly modelled. The bypass gap size was kept constant at 2 mm. The overlapping fluid and solids meshes were coupled through the heat flux between the fluid and solid. The vertical coolant channels in the reactor core are treated as a porous medium.

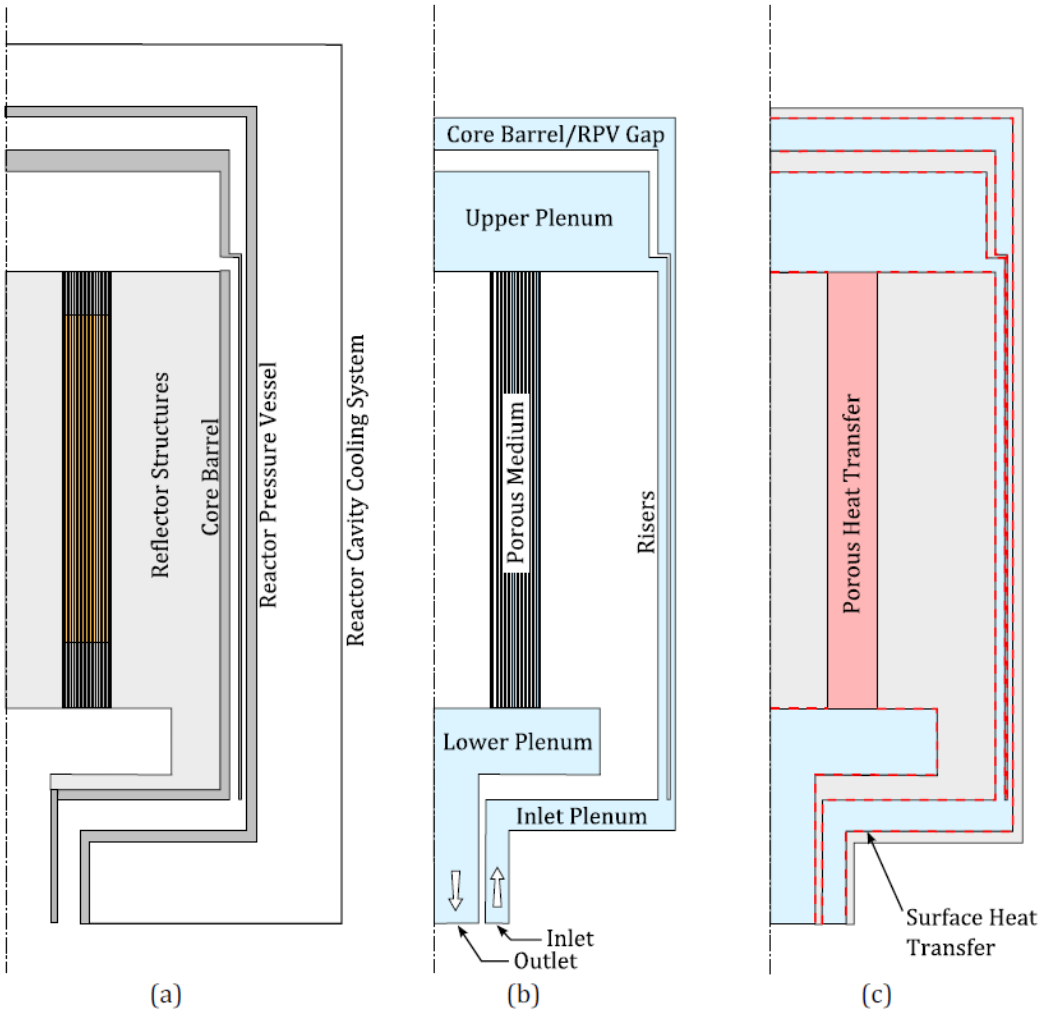

Figure 19: Basic layout of the solid, fluid components and heat transfer surfaces for the MHTGR 350 MW (Clifford, 2013)

Limitations:

- The gaps between the blocks are modelled explicitly since a porous media model would not be precise enough for resolving the natural convection during the PLOFC.
- A significant challenge for using the porous medium approach to simulate PLOFC is that solving the convection field in the transient regime requires very small time steps

whereas the total time of the transient is driven by the decay heat curve and the core graphite thermal inertia.

The limitation for the explicit 3-D approach is that it cannot be used to model an entire reactor unit. Although the implicit 3-D and systems approaches can be used to simulate a full reactor unit they cannot be used to resolve fine local detail. It is interesting to note that there are no contributions outlining the use of a LES or DNS approach to model the flow in prismatic block reactors.

2.1.2 System CFD

System CFD is a collection of models that account for different levels of complexity in a system. One component can be a 1-D network while other components may be presented as a lumped component. A 1-D CFD simulation (also called system level CFD) is a particular type of CFD simulation that focuses on the entire system rather than on the details of the flow inside a specific component of that system. Flownex solves fundamental governing equations of mass, momentum and energy but handles associated phenomena such as frictional losses by using necessary closure relations or correlations. Overall conservation of mass, momentum and energy must be ensured.

In 1-D CFD simulations a physical system is modelled using a network of different components each of which models a specific component of the system such as a pump, valve, pipe or bend.

In Flownex most of the formulations used for components are derived from the fundamental equations with the simplifying assumptions where necessary and empirical correlations where required. Each component is therefore characterized by geometrical and performance data. For these reasons the 1-D CFD software package used must include a comprehensive library of pre-defined components, performance data and materials used for creating and characterizing the network.

1-D CFD simulations can be:

- Steady state, in order to study the performance of a system in equilibrium, or
- Transient, in order to study the response of the system to a particular event.

Additionally thermal phenomena can be considered in order to study heat transfer processes inside the system or between the system and the external environment.

1-D CFD and 3-D CFD systems are not used in a mutually exclusive manner. On the contrary they should be considered as complementary systems where particular components in the 1-D network can be characterized using data coming from 3-D CFD simulations, and 1-D CFD simulations can be used to identify boundary conditions for 3-D CFD simulations.

Typical physical aspects to be covered in a 1-D CFD system are:

- Pressure drop calculations in each component and in the entire system,
- Flow balancing and sizing of the entire system,
- Water hammer effect (pressure surge) in transient incompressible analyses,
- Compressibility, Joule-Thomson effect and wave propagation in compressible transient analyses, and
- Heat transfer in the system and between the system and its surroundings.

2.1.2.1 GAMMA+

GAMMA+ (Lim, 2015) models the reactor core using a coarse computational grid of one to seven cells per fuel block as shown in Figure 20.

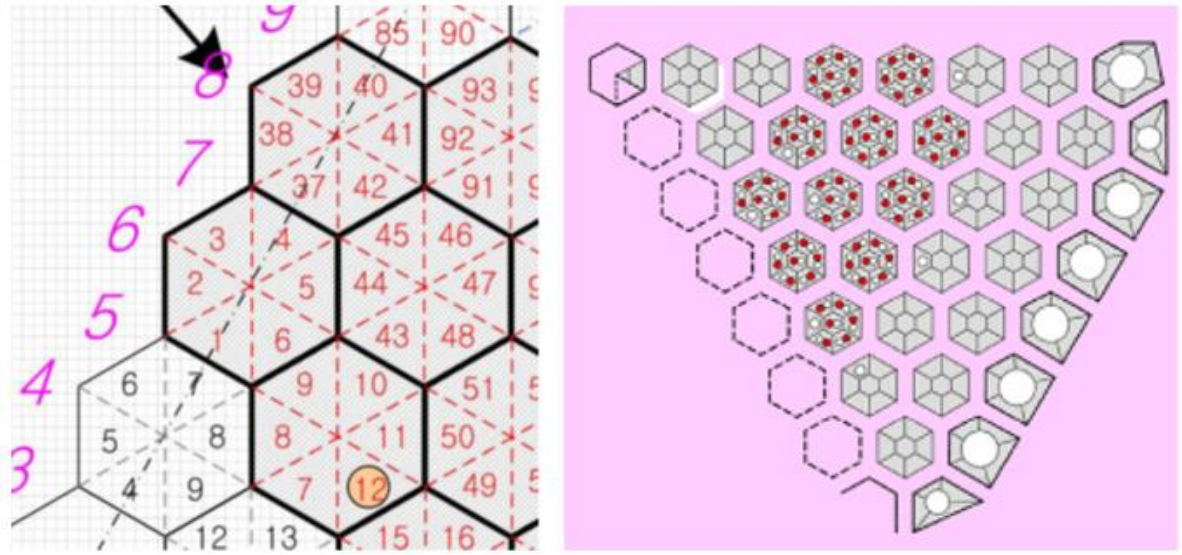

Figure 20: Discretization and generated mesh for GAMMA, (Lee, et al., 2016 (b)) & (Kim & Lim, 2011)

The full solid fluid models for the reactor are shown in Figure 21 and Figure 22.

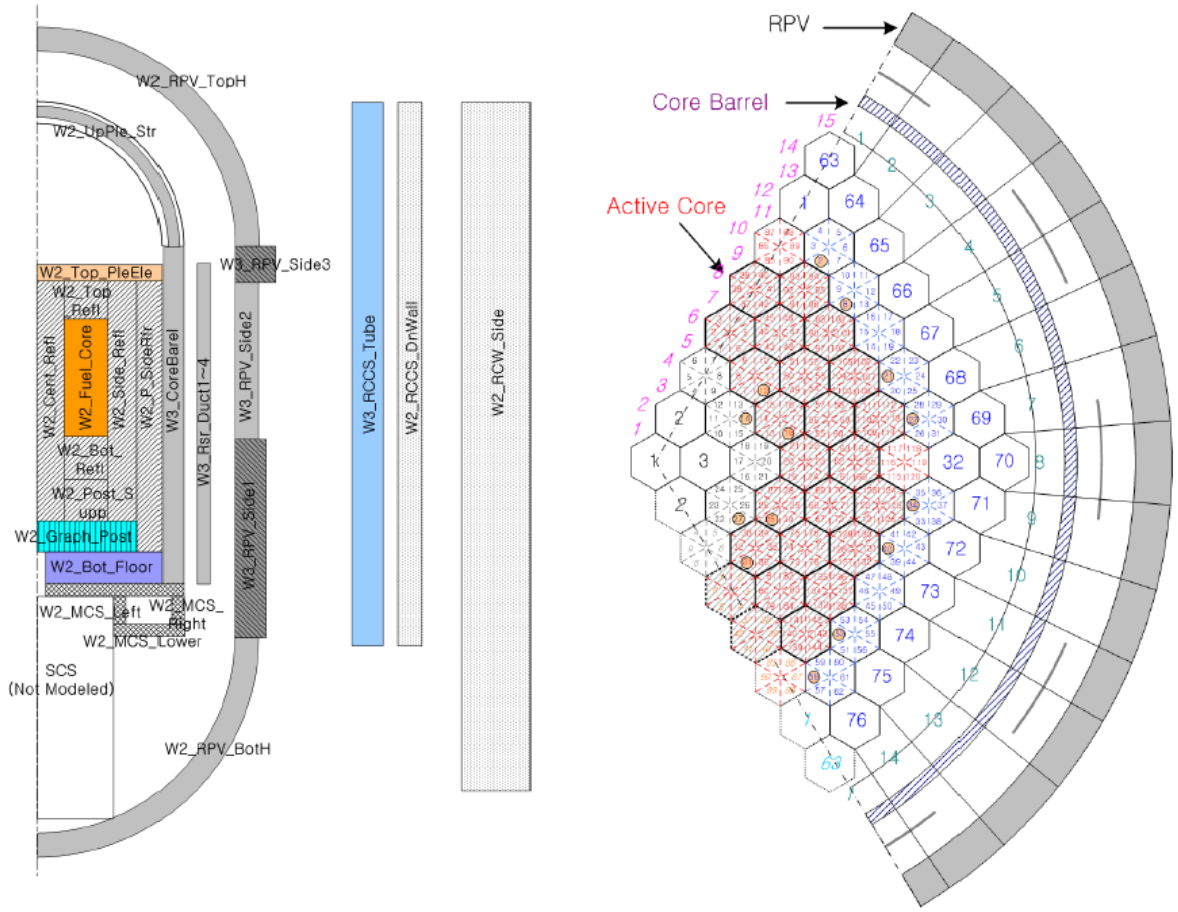

Figure 21: MHTGR GAMMA+ solid model (Tak & Lim, 2014)

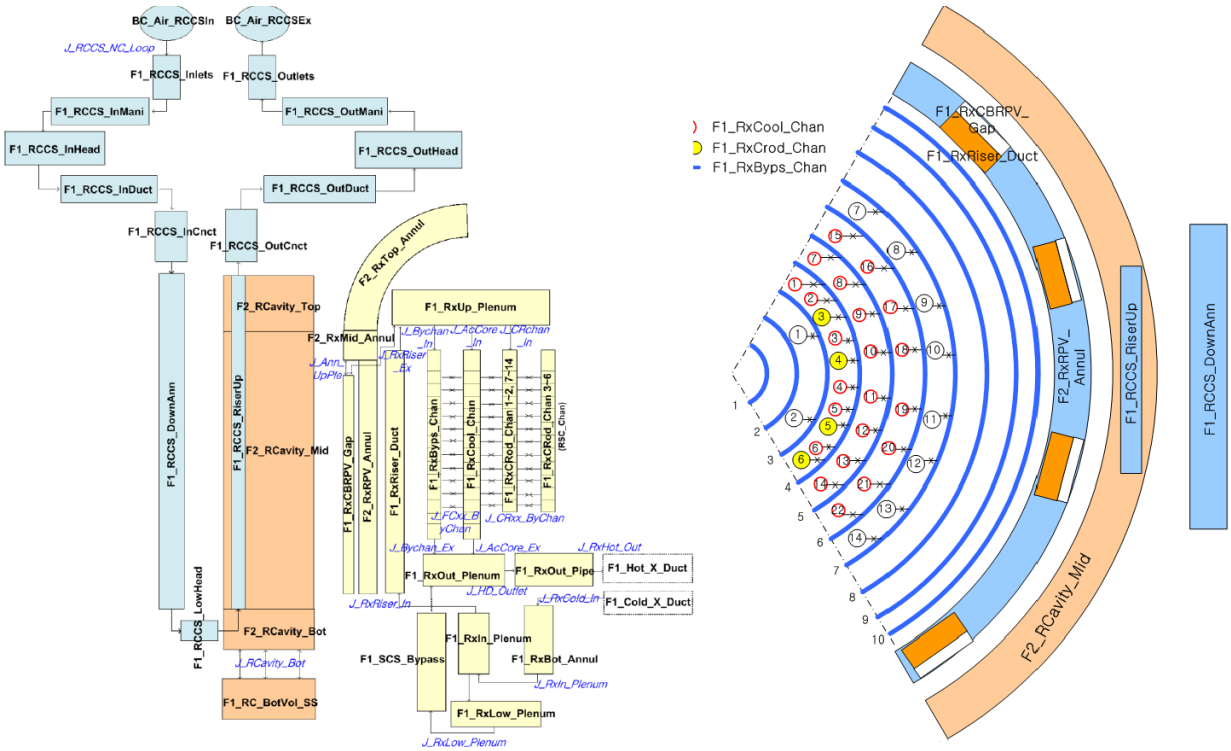

Figure 22: MHTGR GAMMA+ fluid model (Tak & Lim, 2014)

The sizes of the bypass gaps in prismatic block VHTR cores change during the core cycles due to irradiation and thermal expansion. Kim and Lim (2011) used the 1-D / 2-D / 3-D finite volume based system code GAMMA+ to evaluate the effect of these changes in the bypass gaps on the core hot spot. A $1/6^{th}$ of the PMR200 core consisting of eight layers of blocks was considered. A fuel assembly comprise a lower and an upper reflector block and six fuel blocks. Each fuel block was discretized into six trapezium shaped and one hexagonal shaped control volumes. A representative fuel rod (compact) and a representative coolant were associated with each fuel block control volume. The vertical and lateral flow in the bypass gaps and the flow in the cross gaps were accounted for. They evaluated the coolant outlet temperature, maximum fuel kernel temperature, bypass flow fractions and the flow fractions through the control rod and reserved shutdown channels as a function of cross gap and bypass gap sizes. They concluded that the local distributions of the neutron fluence and temperature should be considered in the core hot spot analysis due to their influence on the gap sizes.

2.1.2.2 Network approach

Another approach used to solve heat transfer problems is the network approach. Elements, nodes and boundary conditions define a network and form the basic building blocks to simulate a network. The network approach is derived from energy, mass and momentum balance equations and makes use of a finite volume approach which leads to finite difference equations after integration (where applicable). The advantage of the network approach is the capability of easily solving and simulating very complex problems and capability of solving and simulating coupled heat transfer fluid flow problems (Van der Merwe, 2003).

The underlying philosophy of the system computational fluid dynamics methodology is that for the analysis of large thermal-fluid systems it must be possible to link models of various levels of abstraction and varying degrees of complexity together to simulate the complete integrated system. The level of abstraction and the degree of complexity of the models are determined by the nature of the simulation, i.e., a first order analysis or a detailed analysis, and the detail and character of the information required. In systems CFD approach, the models of the components can be of varying degrees of complexity. These can range from simple lumped parameter models to complex fully three-dimensional CFD models (Du Toit & Rousseau, 2012).

2.1.2.3 Flownet simulation of an HTR using point kinetics neutronics and decay heat generation model and sphere heat conduction model

The PBMR core allows the maximum power to be delivered to the Brayton cycle given that the normal operating fuel temperature should not exceed ~1130 ℃ with a coolant outlet temperature of 900 ℃. Further, the maximum fuel temperature for the design basis depressurised loss of cooling with heat removal through passive means to the reactor cavity cooling system should not exceed 1500 ℃ in a best estimate calculation. These two requirements, together with the obvious one of being able to control and shut down the reactor, to a large extent dictate the shape of the reactor core. For passive removal of the decay heat after a loss of coolant event, the core needs to be long and slender to provide the required radiation surface on the pressure vessel (Koster, et al., 2003).

The point kinetics method is most-often used to solve short-term problems in a nuclear reactor encountered when there is an action that caused the reactor to be perturbed. This is based on the assumption that the shape of the spatial neutron flux of the reactor changes negligibly during a transient even though the amplitude may be strongly time-dependent. The reactor is assumed to act as a point (Lamarsh & Baratta , 2001). The global reactor behaviour is simulated dynamically, as a single point having certain weighted average properties that may be assumed to be constants over time (Rousseau & Greyvenstein , 2002 (a)).

Purpose:

To simulate the integrated system performance, focusing on the detail of the power conversion unit, while still ensuring acceptable calculation times.

Need:

A simplified reactor model that could supply sufficiently accurate values of pressure drop and heat transfer across the reactor.

Assumptions and simplifications:

- The calculation of the heat generated within the fuel sphere was based on a point kinetics neutronics and heat generation model.
- All the spheres contained in a single core cross-section have exactly the same temperature distribution and internal heat generation per unit volume.

Methodology:

System CFD modelling of the PBMR reactor in Flownet started with a fully integrated but simplified reactor model supplying sufficiently accurate values of pressure drop and heat transfer across the reactor (Rousseau & Greyvenstein , 2002 (a)). In this work, the reactor was divided into a number of layers along its height and each reactor section was then characterized by a single representative sphere. The combined effect of radial and axial contact conduction and radiant heat transfer between the surfaces of spheres in the different reactor sections were taken into account via an effective thermal conductivity.

Each sphere was divided into a number of discrete onion ring shaped control volumes each represented by a single node. The node on the surface of the sphere represents the surface temperature of all the spheres in that section of the reactor that is exposed to the coolant.

Limitations:

- Provides as output a single value of power generation for the reactor as a whole. Therefore, in order to apply this in the heat conduction model for each representative fuel sphere in each layer, the total heat generation is first distributed among the layers according to the prescribed normalised power distribution profile.
- The assumptions made exclude the use of such a heat generation model for detailed reactor design calculations.
- The point kinetic simplification is valid when the reactor is sufficiently small so that it is well-coupled and the space and time variables are essentially separable.

2.1.2.4 Prismatic HTTR

Purpose: To model heat and momentum transfer in the HTTR by reducing a complex 3-D geometry of an HTTR into a simplified axi-symmetric (2-D) geometry.

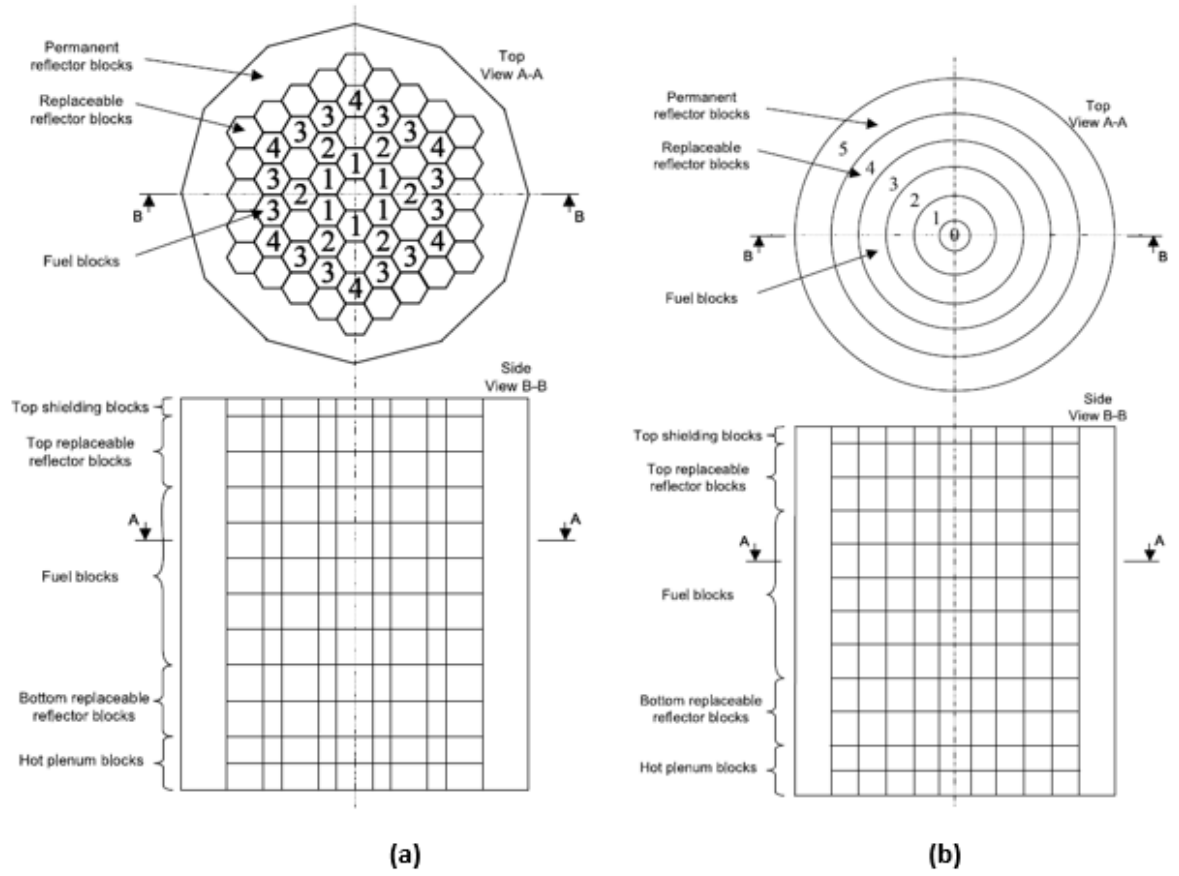

Figure 23: Schematic layout of an axi-symmetric core (Rousseau & Greyvenstein, 2002 (b))

Need: The thermal-fluid network software package Flownet developed at the North-West University had been previously used to model the heat transfer in the PBMR as discussed in section 2.1.2.3.

Assumptions and simplifications:

- A uniform temperature is assumed within each control volume at any given time step.
- Each control volume is therefore represented by a single thermal mass node.
- Each of the nodes representing the fuel assembly blocks also represents the surface temperature of the flow passages inside the fuel assembly block containing the fuel rods.
- The effect of radiation between the fuel rod and fuel assembly block surface, as well as heat losses on the outside surfaces of the core, were neglected.
- Heat losses on the outside surfaces of the core were ignored.

Methodology:

Rousseau & Greyvenstein (2002 (b)) introduced a simplification of the HTTR model, which has a prismatic core. In this approach, the geometry of the HTTR core shown in Figure 23 (a) was reduced to a simplified 2-D ring geometry as shown in Figure 23 (b). This method was

implemented by Van der Merwe (2005) to simulate heat and momentum transfer in the HTTR. The thermal mass of the original HTTR core geometry was maintained in the axi-symmetric core by making sure the rings have the cross-same area and height as the layer of blocks they represent. Each of the rings can then be discretized in the axial direction so that a control volume is represented by a single thermal mass node connected via a thermal resistance to the adjacent thermal mass nodes. The solid elements had the same thermal mass as the control volume they represent. The thermal masses were adjusted to account for porosity of the blocks containing the flow channels.

The reactor was modelled by means of a specially developed HTTR element in Flownet Nuclear. This model encompassed all the core internals starting from the channel entry at the upper reflector through to the hot plenum beneath the core. The Flownet model shown in Figure 24 did not include the effect of radiation heat transfer but this was done using XNET to model radiation heat transfer between the fuel rods and the fuel blocks (Van der Merwe, 2003). The graphite blocks that have the same flow path were grouped together. The fuel assembly blocks and the surface temperature of the flow passages in the fuel block containing fuel rods were represented by a single node. Thus the fuel blocks were represented by a single row of conduction elements and nodes. The graphite sleeve and fuel compact were discretized into a number of layers each represented by a single thermal mass node.

The height of the axi-symmetric rings is the same as that of the original hexagonal core elements, therefore the flow paths have the same lengths. The flow was also discretized in the axial direction and the pressure losses were calculated using the Darcy-Weisbach formulation.

Limitations:

- Single node representing a fuel block.

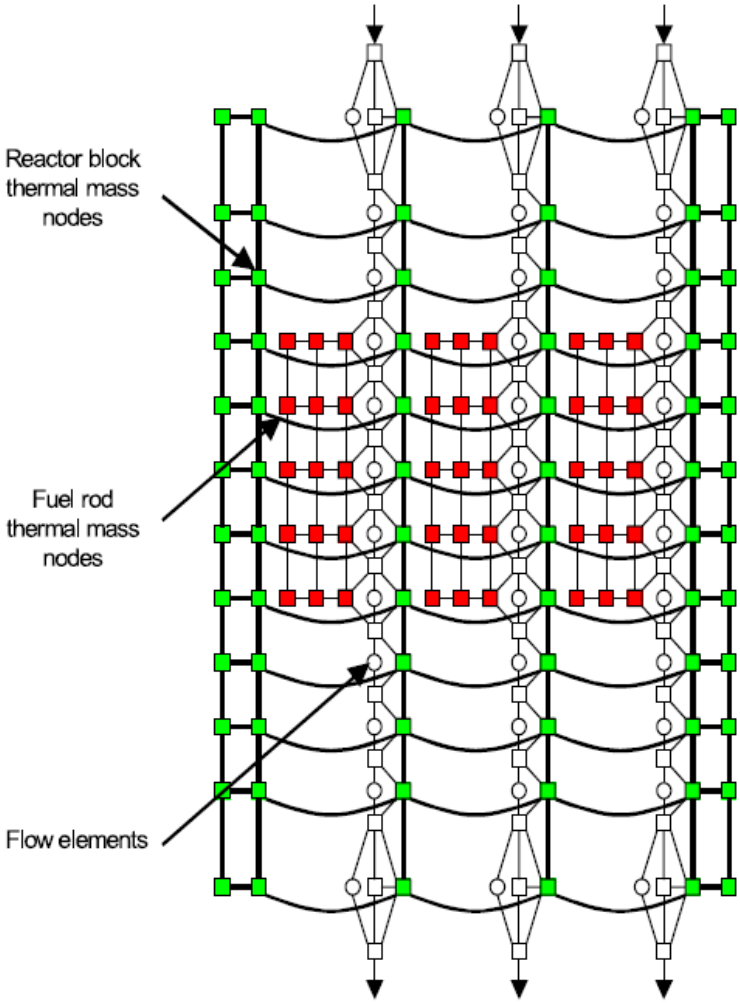

Figure 24: HTTR sub-network (Rousseau & Greyvenstein, 2002 (b))

2.1.2.5 Network approach applied to a prismatic fuel block

In a network approach a collection of nodes, boundary, 1-D conduction and convection heat transfer and pipe elements are used to model heat transfer and fluid flow.

Purpose:

To develop a system CFD model for the heat transfer and flow within an HTR prismatic fuel block

Need:

Simplified thermal-fluid network models have been developed for the PBMR and the HTTR using Flownet/Flownex, as stated in sections 2.1.2.3 and 2.1.2.4 but a detailed network model for a prismatic block-type HTR still had to be developed. The fuel blocks used in this model were based on the PMR200 adopted from the design concept of a gas turbine-modular helium reactor (GT-MHR) (Tak, et al., 2012). These fuel blocks are different from the HTTR fuel blocks in that the channels for helium coolant flow have no direct contact with the fuel channels

whereas in the HTTR the coolant flows through the annular gap between the fuel rods and the fuel rod bore holes.

Assumptions and simplifications:

- Fuel and coolant channels are implicitly modelled by defining representative channels associated with the unit cells in each control volume.
- Lumped burnable poison within the blocked not included in the model.
- The effect of radiation between the fuel rod and fuel assembly block surface as well as heat losses on the outside surfaces of the core were neglected.
- Helium coolant assumed to be incompressible.
- All coolant channels modelled the size of a standard coolant channel.
- The heat transfer was dominant in the radial direction which was modelled using conduction heat transfer elements.
- The heat transfer in the tangential direction was modelled by employing cross-conduction elements.

Methodology:

In Sambureni (2015) the fuel block was divided into six segments and a model of one $1/6^{th}$ of prismatic fuel block was created in Flownex. The one $1/6^{th}$ block segment was discretized radially and tangentially to form control volumes.

Figure 25 shows the arrangement of fuel rods and coolant channels within a control volume. The fuel rods are represented by the solid red circles and the coolant channels by the open blue circles. A typical prismatic block coolant channel (represented by C7 in Figure 25) is surrounded by six fuel rods (represented by F7, F8, F10, F11, F13 and F14). Figure 25 (b) shows the chosen unit cell b which depicts a representative conduction path in a typical prismatic fuel block. The unit cell is formed by the indicated symmetry planes, fuel rod surface and coolant channel surface.

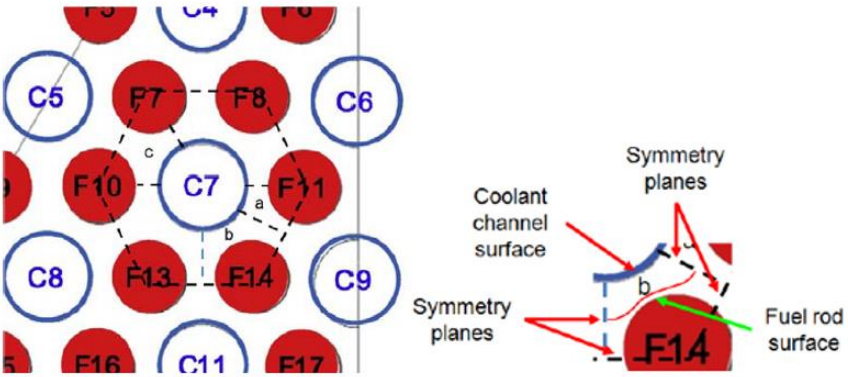

Figure 25: Fuel rods and coolant channels arrangement (Sambureni, 2015)

To determine the mass averaged graphite block temperature, a CFD (STAR-CCM+) simulation was done on unit cell b in a study by Sambureni (2015). This mass averaged graphite block temperature was used to determine the conduction shape factor for the heat transfer from the fuel rod surface to the graphite block node using equation (2-2):

$$Q = S_{fs}k(T_f - T_s) \tag{2-2}$$

Where:

S_{fs}= conduction shape factor for the heat transfer from the helium gap edge node to the graphite block node

T_f = temperature of the fuel rod surface, and

T_s= mass averaged temperature of the graphite block.

Similarly, the conduction shape factor for the heat transfer from the graphite block to the coolant channel wall was determined by employing equation (2-3):

$$Q = S_{sw}k(T_s - T_w) \tag{2-3}$$

Where:

S_{sw}= conduction shape factor for the heat transfer from the graphite block node to the coolant channel wall node and T_w = surface temperature of the coolant channel wall.

In Flownex the conduction shape factor for the heat transfer from the helium gap edge node to the graphite block node (S_{fs}) and the conduction shape factor for the heat transfer from the graphite block node to the coolant channel wall node (S_{sw}) can be expressed by implementing equations (2-4) and (2-5):

$$S_{fs} = \frac{A_{fs}}{L_{fs}} \tag{2-4}$$

$$\text{and } S_{sw} = \frac{A_{sw}}{L_{sw}} \tag{2-5}$$

Where L_{fs} is the radial distance from the fuel rod surface to the graphite block node and L_{sw} is the radial distance from the graphite block node to the coolant channel wall. A_{fs} is the equivalent surface area of the fuel rods and A_{sw} is the equivalent surface area of the coolant channels. Equations (2-4) and (2-5) are used to obtain the relevant areas that must be specified in Flownex. The calculated shape factor was used to characterize the heat conduction from the fuel rods to the graphite and from the graphite to the coolant channels.

The distance from the fuel rod surface to the graphite node, L_{fs} was calculated as 1.6309 mm and the distance from the graphite node the coolant channel wall L_{sw} as 2.8691 mm. The fuel and coolant channels were implicitly modelled by defining representative channels associated with the unit cells in each control volume. A uniform volume heat source is applied at the fuel nodes. Figure 26 shows the heat transfer and flow network for $1/6^{th}$ of a prismatic block. The heat transfer was modelled as dominant in the radial direction which was modelled using conduction heat transfer elements. The heat transfer in the tangential direction was modelled by employing cross-conduction elements. The heat that is conducted from the fuel surface via the graphite to the coolant wall is transferred to the coolant through convection. The convection elements were connected to the coolant wall node. The Dittus-Boelter correlation was employed to obtain the Nusselt number for the calculation of convection heat transfer between the graphite wall and the coolant.

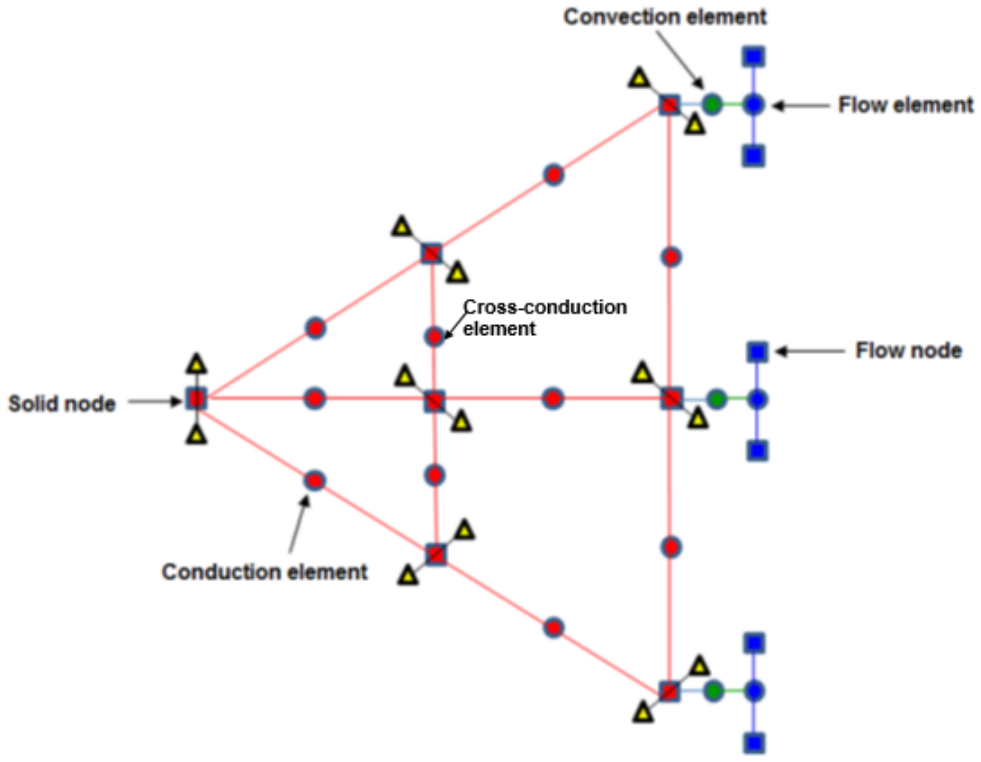

Figure 26: Schematic of heat transfer and flow network (Sambureni, 2015)

Limitations:

- The model did not include discretization in the axial direction and also did not include discretization in the fuel rod and the coated fuel particles.
- The heat generated in the fuel was uniformly distributed in the nodes within the control volume.

2.2 Coolant flow

The helium coolant enters the reactor from the outer annulus of the coaxial duct, the cold inlet duct which is the outer shell of the hot duct, cools down the bottom plate and flows up the riser coolant channels to the top of the core. The coolant is then delivered into the upper core inlet plenum. From the inlet plenum, the coolant is then distributed to numerous coolant channels running vertically through the core.

2.2.1 Flow paths

Helium coolant entering the top of the core can travel down various flow paths. It can flow through the small sized (around the fuel handling hole) and large coolant channels. It can also flow through gaps between fuel blocks in the active core and reflector blocks and also through the control rod channels.

2.2.1.1 Coolant channels

Coolant channels form the primary coolant flow path in the core to provide the heat transport path for the heat generated by the fission energy in the fuel. The coolant is therefore heated as it flows down through the active core. Coolant channels extend from the plenum element at the top of the core then to the top of the reflector elements above the active core, through the active core to the bottom reflector blocks. The flow then continues to the bottom transition reflector block and the flow distribution block where mixing with the flows from neighbouring fuel columns occurs in the core support block layer and exits into the core outlet plenum.

Approximately 89% of the circulating helium flow passes through the upper plenum and traverses the active core through the coolant channels in the fuel elements (General Atomics, 1992).

2.2.1.2 Bypass and cross flow gaps

Bypass flow is defined as the coolant that escapes and runs through the interstitial passages between the graphite fuel blocks instead of travelling through the designated coolant channels. These gaps are formed as a result of thermal expansion and fast neutron damage and the gap sizes vary with time.

Another coolant leakage path is formed by horizontal gaps between stacked graphite blocks. They form leakage paths to/from primary coolant flow path. This leakage path is termed cross flow and is driven by the lateral pressure gradient.

Bypass and cross flow gaps between fuel blocks may exist due to the following factors or a combination thereof (Kim & Lim, 2011):

- Manufacturing and installation tolerances,
- Thermal expansion of fuel blocks,
- Thermal expansion of the metallic core support structure, and
- Irradiation shrinkage and swelling.

Kaburaki and Takizuka (1987) carried out an experiment designed to study the effect of leakage flows on the main coolant channel flows in a full scale fuel block assembly with a cross flow gap shown in Figure 27. Four hexagonal blocks were stacked to form an assembly and was surrounded by a steel shroud to simulate a 1 mm wide bypass gap. A 1 mm cross flow gap was created in the middle of the assembly. Results of the static pressure distribution in a coolant channel for a case of a parallel cross flow gap is shown in Figure 28. This experiment was selected to validate the 1-D fluid flow network model implemented in Flownex.

About 11% of the coolant bypasses the core in the coolant channels in the gaps between columns in the core and reflector and the control rod channels. Heat transfer to the primary coolant flow is ensured by control of the core bypass flow and by maintaining the core coolant passage geometry (General Atomics, 1992). Flow leakage reduces the effective flow rate in the coolant channels and thus raises the fuel temperature. Prediction of the bypass flow is therefore an important thermal fluids phenomenon.

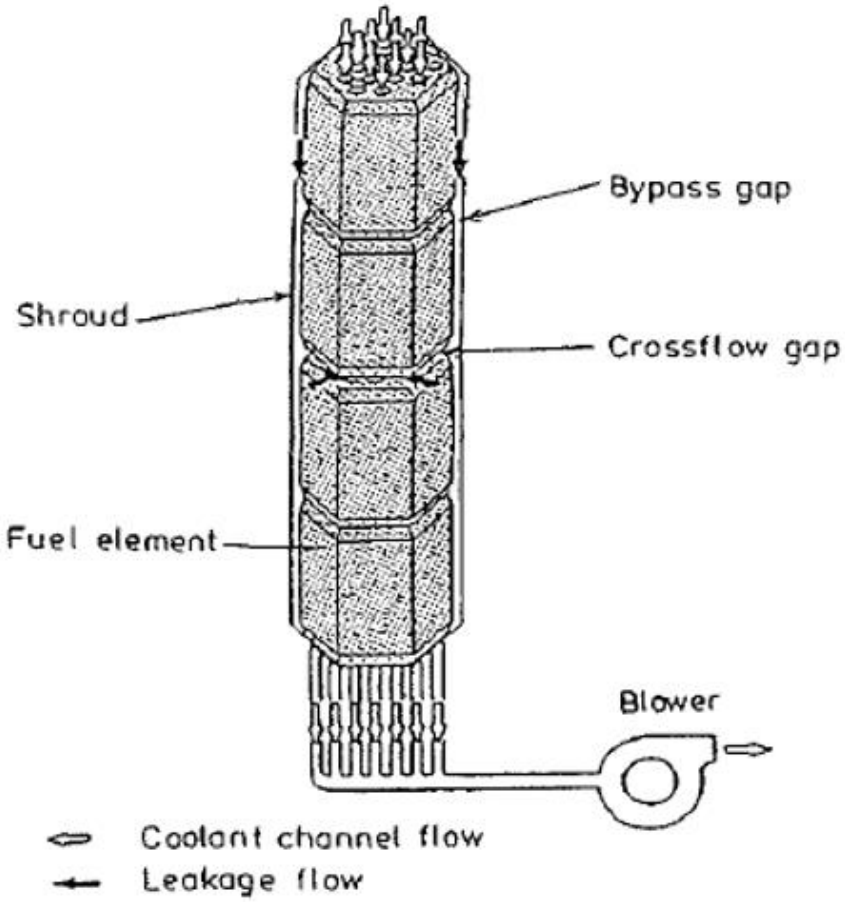

Figure 27: Fuel assembly flow distribution experiment (Kaburaki & Takizuka, 1987)

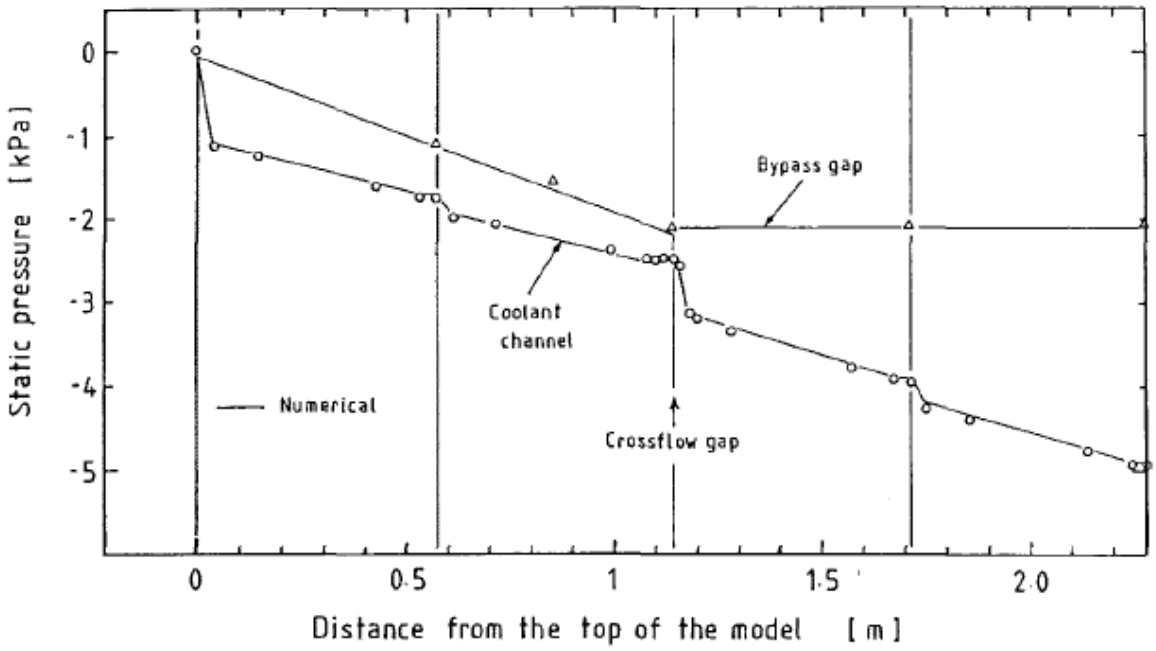

Figure 28: Static pressure distribution in a coolant channel (Kaburaki & Takizuka, 1987)

2.2.2 Coolant channel blockage

One of the common postulated accident scenarios in nuclear reactors is fuel block coolant channel blockage accident. Blockages may be caused by debris generated in the core resulting from local graphite failure due to neutron irradiation. Special attention has to be paid to the fuel temperature in the case of coolant channel blockage accidents since the fuel temperature may significantly rise and exceed the design limit owing to the local loss of forced convection (Lee, et al., 2014).

Cioni et al. (2006) performed a study to investigate a transient due to partial flow area blocking in an HTR core with thermal power of 600 MW_{th}. The helium enters the core at 500 ℃ and exits at 850 ℃ at a flow rate of 316 kg/s. The aim was to study the effect of partial flow area blocking of the helium channels in a standard fuel assembly on the fuel and graphite maximum temperatures. They employed the CFD code Trio_U which uses an explicit 3-D approach to model the fuel compacts and conduction in the graphite and fuel and an implicit 1-D approach to model the thermal-flow in each coolant channel and the bypass gap. Both the graphite and the fuel were modelled using the graphite physical properties.

They considered two configurations, namely a single central fuel assembly that has plugged coolant channels and is surrounded by six other unblocked fuel assemblies as shown in Figure 29, and the second case was a single fuel assembly with plugged coolant channel surrounded by five fuel assemblies and a reflector assembly. There were 24 blocked coolant channels in the central fuel assembly, for each configuration (marked by the black spots in Figure 29). In these configurations, each assembly consists of ten fuel blocks. The study was done on a standard HTGR fuel block assembly to determine the temperature distribution in the fuel block assembly, and more precisely to focus on the maximum temperature in the graphite and the fuel, that must not exceed 1600 ℃. Results of the study showed that the maximum temperature of the fuel reached 1920 ℃ and 1925 ℃ for the two considered configurations, respectively. These temperatures were reached 3 m before the outlet. Although the maximum fuel temperatures were found to exceed the maximum allowable limit of 1600 ℃, it was also noted that that the effect of blocked channels on the temperature is restricted to the region of the blockage. The temperature increase is limited to the blocked fuel assembly and does not spread to the surrounding fuel assemblies.

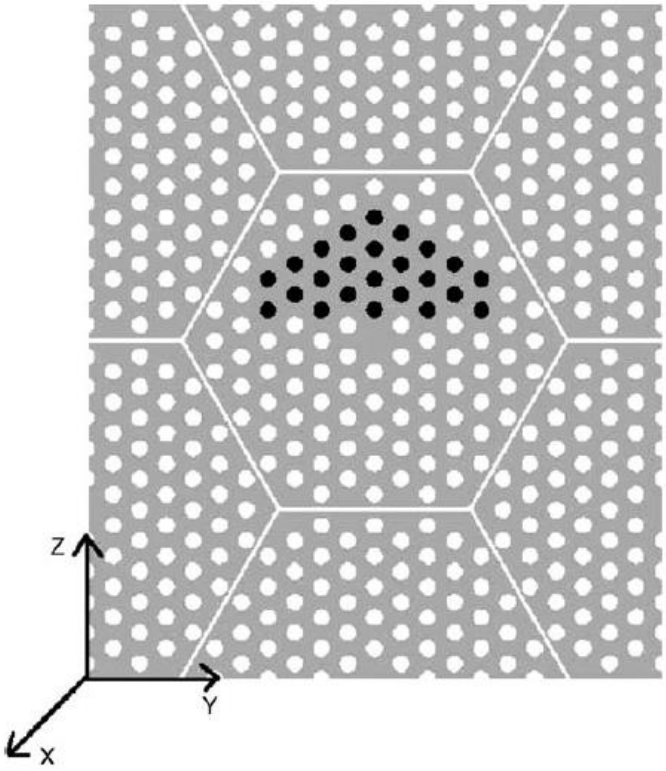

Figure 29: Plugged coolant channels in a central fuel assembly block (Cioni, et al., 2006)

Lee et.al (2014) also investigated the thermal response of the PMR200 core to a coolant channel blockage accident. In Lee et.al (2014), a few coolant channel blockage scenarios were considered. Firstly, a coolant channel blockage accident was investigated by blocking several coolant channels in a $1/12^{th}$ fuel block assembly consisting of six vertically stacked fuel blocks. This was done by blocking one, two and three coolant channels at a time. Secondly, a $1/6^{th}$ PMR200 core model was analysed for a single coolant channel blockage placed at different locations. From this analysis it was discovered that the impact of blockage is limited only to the area near the blocked channel. For the single coolant channel blockage case, the maximum fuel temperature increase from normal operation was found to be 58 ℃ and the fuel temperatures were lower than the design limit. Thirdly, they investigated the effect of simultaneous blocking of several coolant channels in two selected standard fuel type assemblies on adjacent assemblies. One of the two selected standard fuel type assemblies is at the centre of the core and the other at the outer edge of the core adjacent to the reflector blocks. The cases considered were for six, seven, twelve and eighteen blocked channels. It was shown that the fuel temperature significantly rises as the number of blocked channels increases.

2.2.3 Challenges with modelling flow

A full 3-D thermal-hydraulic analysis of the annular core would require parallelized computation due to 3-D computational CFD of helium flow in the coolant channels and coupling to 3-D heat conduction equations in the surrounding graphite and fuel compacts. Thus in most thermal-hydraulic analyses, the 3-D CFD coolant flow simulation is simplified by using 1-D approximation. These calculations employ representative turbulent convection heat transfer correlation (Travis & El-Genk, 2013). In the McEligot et al. (1965) work, low Reynolds number gas flow experimental data were used to develop a heat transfer correlation based on the Nusselt number power law or the modified Dittus-Boelter formulation. The heat transfer coefficient between the coolant and graphite moderator was obtained using modified Dittus-Boelter correlations:

$$\mathrm{Nu} = 0.021\mathrm{Re}^{0.8}\mathrm{Pr}^{0.4} \tag{2-6}$$

for turbulent flow which occurs inside the coolant channel and $\mathrm{Nu}_{\infty} = 4.364$ for laminar flow (through bypass and cross flow paths) (McEligot, et al., 2006).

The experimental data used for developing this correlation were based on air, helium and nitrogen gas flow at inlet Reynolds number from 1500 to 45000 and maximum wall to bulk temperature ratio of around four.

Travis and El-Genk (2013) also developed a turbulent convection heat transfer correlation based on 3-D simulation of the helium flow in the central coolant channel of the fuel module shown in Figure 30. The idea was to reduce the computational time and requirements for a full-core thermal-hydraulic analysis. The correlation would determine the local heat transfer coefficient along the heated channel length including the entrance mixing length. The numerical results used to develop the present turbulent convection heat transfer correlation were obtained by coupling the 3-D conduction in the graphite and fuel compacts to a 3-D CFD simulation of the helium flow in the central flow channel of the hexagonal module.

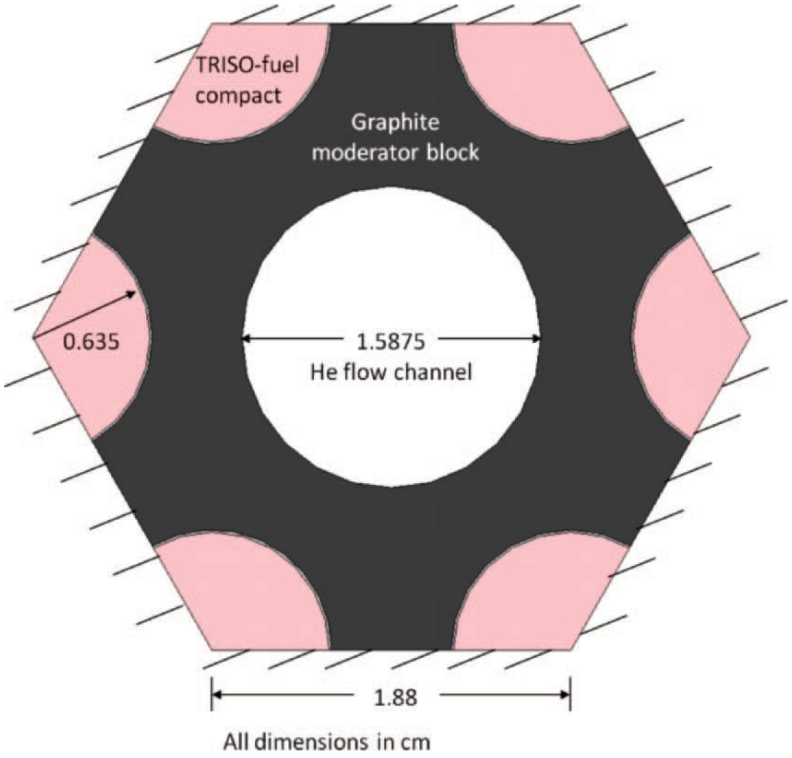

Figure 30: An HTGR single channel fuel module (Travis & El-Genk, 2013)

The 3-D thermal-hydraulic numerical analysis of the module was performed using the STAR-CCM+ to incorporate different meshing schemes that include tetrahedral, hexahedral, and trimmed square prisms that are capable of automatic surface wrapping/conforming to produce a user-set number of prism layers to refine meshing elements near boundaries or common interfaces.

The developed correlation for fully developed turbulent convection is given by equation (2-7).

$$\mathrm{Nu_{FD}} = 0.11\mathrm{Re_b^{0.646}Pr_b^{0.4}} \tag{2-7}$$

It was compared to those given by McEligot et al. (1965) and to the results of the full 3-D thermal-hydraulics numerical analysis of the single channel fuel module. The results were found to be within ±2% of the calculated values in the 3-D thermal-hydraulics numerical analysis for $2.2 \times 10^4 \leq \mathrm{Re_b^{0.646}} \leq 5.8 \times 10^4$ and $0.64 \leq \mathrm{Pr} \leq 0.68$.

A correlation for the local values of Nu for turbulent convection of helium flow along the length of the heated section of the coolant channels was also developed and is given in equation (2-8).

$$\mathrm{Nu} = 0.11\mathrm{Re_b^{0.646}Pr_b^{0.4}}\left[1 + 0.57\mathrm{e}^{-0.20z/D}\right] \tag{2-8}$$

Equation (2-8) accounts for the effect of entrance mixing and is valid for $2.2 \times 10^4 \leq \mathrm{Re} \leq 5.8 \times 10^4$ and $0.64 \leq \mathrm{Pr} \leq 0.68$.

The initial assumption is that the bypass and cross flow gap size in the fresh fuel is uniform. It has been observed though that as the fuel ages during normal operation and depending on the position in the core, the gaps tend to become non-uniform. This is as a result of blocks experiencing size changes due to thermal expansion which reduces the gap size and irradiation of graphite which tends to shrink the graphite thereby increasing the gap size. Most studies done assumed uniform bypass flow. Some studies did take into account the varying gap size, as mentioned earlier.

The coolant that escapes the coolant channels into bypass gaps does not cool the fuel. During normal operation, the flow from the channels is locally at a higher temperature than the flow from the leakage paths. These two flows combine at the outlet plenum, there is a resultant highly turbulent flow forming at the wakes of the graphite core supporting structures.

Possibly the most recent and comprehensive developments in modelling the heat transfer and fluid flow in prismatic HTGRs are given in a series of reports by (Stainsby, et al., 2009). These reports consider the heat conduction within the coated particles, fuel elements and across the reactor core. They further consider fluid flow within the coolant channels as well as leakage flows between adjacent fuel elements using a one-dimensional systems code approach. In all cases, their models are verified against detailed finite-element solutions.

Clifford et al. (2013) considered the heat conduction in prismatic block reactor. They used a formal multi-scale expansion homogenization method to obtain effective unit cell thermodynamic parameters from the fine scale which could be used to construct an implicit coarse grid formulation on the macro-scale. These methods were incorporated in the OpenFOAM finite volume framework. The fine scale solution could be reconstructed from results. The methodology was applied to miniature HTGR consisting of three mini fuel blocks and a cylindrical reflector. The coolant channels were treated as a porous medium within the fuel elements. The pressure drop within the coolant channels was modelled using standard correlations for fully developed turbulent pipe flows. Clifford (2013) states that because of the small cross-sectional area of bypass flow gaps, this presents another challenge when explicitly modelling using CFD techniques. This may result in a significant increase in computational time because of highly refined meshes. Consequently, the flow in the leakage gaps has been neglected in Clifford (2013).

2.3 Summary of literature review and way forward

The literature reviewed above has demonstrated that the various methods have been used by researchers in the past to model heat transfer in the prismatic fuel blocks. Some of these methods such as 3-D CFD could only be applied to a section of the prismatic block or assembly to avoid the computational effort required to carry out whole-core analysis.

It was shown through several studies that the unit cell approach can be a reasonable approximation for the modelling of complex geometries but should take into account bypass flow between adjacent blocks. Depending on the approach selected, the use of homogeneous instead of heterogeneous fuel models in the reactor safety analysis would be considered non-conservative as the homogeneous model underestimates the peak temperature of the fuel. More recently the unit cell method is being implemented using pre-generated mesh cells around the fuel and coolant channels to generate computer grids.

A philosophy on a network based model built on a previous study by Sambureni (2015) on a prismatic fuel block will be presented in detail in the following chapters. The point of departure from the earlier work would be the primary direction of discretization of a standard fuel block and the extensive detail in the modelling of the interior of a fuel block.

3 THEORETICAL BACKGROUND

This chapter starts with a short description of several generations of Flownex models that have been used in the past for thermal-fluid analyses in high temperature reactors that preceded this work presented in this thesis. The governing equations used by Flownex are presented. From this, heat transfer modes and their application to the thermal-fluid analysis of the HTR core are outlined. Heat transfer to or from a control volume can take place through three different processes namely conduction, convection and radiation. An approach to HTR core modelling using the Flownex system CFD code is discussed. The Implicit Pressure Correction Method (IPCM) solution algorithm which is utilised in Flownex is also discussed.

3.1 Hierarchy of Flownex models

The complexity associated with the thermal-flow design of the cycle requires the use of a variety of analysis techniques and simulation tools. These range from simple one-dimensional models that do not capture all the significant physical phenomena to large-scale three-dimensional CFD codes that, for practical reasons, cannot simulate the entire plant as a single integrated mode (Walter, et al., 2004). The complexity of the models can range from a simple lumped model to complex fully 3-D CFD models (Du Toit & Rousseau, 2012). In this section various modelling strategies that can be implemented in Flownex to model thermal-fluid systems are discussed. The focus of the work done in Flownex has been to develop models for PBMR. Not much work has been done in developing models for the prismatic block reactors except for the HTTR but much can be learned from the PBMR models. Similar models to the ones discussed in this section could be developed for prismatic block reactors.

3.1.1 Lumped model

The lumped model which consists of only one axial increment is used when one is interested in the fluid flow and pressure drop in the reactor. The total mass of the solids is lumped for solid heat transfer. The lumped model would consist of correlations to give the pressure drop over the reactor as a function of mass flow rate and the heat added to the flow by the reactor (Du Toit & Rousseau, 2012).

The Darcy-Weisbach correlation is used for pipe geometry of the coolant channels, calculating the pressure drop, while the Dittus-Boelter correlation or a fixed heat transfer coefficient is used in the convection heat transfer between solid and fluid nodes. For the solid conduction along the flow channel direction, area is reduced with a permeability-factor, while a lumped

flow resistance can be used to account for the transverse conduction heat flow paths. In this way, geometrical detail is taken into account without adding complexity to the solution.

Maximum fuel temperature is calculated with a single representative sphere, having the heat generation, conduction resistances and internal node masses equivalent to the sum of all spheres in a control volume. Gas flow pressure drop for a pebble bed is calculated with the Kerntechnische Ausschuss (KTA) correlation which is based on the Carman equation, while the convection heat transfer coefficient is calculated with the correlation by Kugeler and Schulten (Greyvenstein & Van Antwerpen, 2004).

The thermal mass and heat generation are dispersed throughout the core. In a pebble bed, the reactor thermal mass can be taken into account by a 1-D model assuming a uniform flow profile throughout the pebble bed. All thermal mass in the axial zone can be lumped in order to get a first order approximation for coolant temperature response. The lumped model can be used to model steady state or transient with or without the surface temperature (Van Antwerpen, 2007).

3.1.2 Axial model

The axial model is similar to the lumped model, except that is consists of a number of axial increments which amongst others allows the specification of an axial power profile. It can be used to model steady state or transient and with or without the surface temperature.

Rousseau and Greyvenstein (2002 (a)) developed a 1-D reactor model for the originally proposed cylindrical configuration for the PBMR reactor. In the model the reactor was divided into a selected number of layers in the axial direction. The heat generated in the reactor was determined using a point kinetics neutronics model, whilst the pressure drop over each layer was determined using the Kerntechnische Ausschuss (KTA Nuclear Safety Standards Commission) pressure drop correlation (Nuclear Safety Standards Commission (KTA), 1981).

3.1.3 Axi-symmetric model

The axi-symmetric model was created to provide quick results of the main flow and heat transfer phenomena in the core only. This was done by Rousseau and Greyvenstein (2002 (a)) for the HTTR. The model is based on a discretized 2-D axi-symetric network, which consists of any number of control volumes in the axial and/or radial directions. This model can be used for steady state or transient analyses and can have a radial or axial power profile with or without surface temperature. Discretization can be zone-based or block-based.

The model includes the convective heat transfer between the gas and the surface of a representative sphere in each of the control volumes (Walter, et al., 2004).

Each of the core control volumes contains a representative pebble for which the heat conduction is modelled in a one-dimensional spherical frame of reference together with the convection heat transfer between the gas and the surface of the sphere. This allows for the calculation of the temperature distribution within the pebbles in any region of the core. The nuclear power generated in the core is distributed with the fuel matrix region only in the form of a source term in the heat conduction equation.

Limitations:

- This model only allows for the simulation of the core itself, excluding all core structures, and is based on a core layout with a homogeneous graphite pebble region at the centre and a homogeneous fuel pebble region in the annulus without a solid central reflector column.
- Also, it does not allow for the addition or extraction of leak flows from the inner or outer perimeter of the core and the gas inlet and outlet is assumed to be from voids at the very top and the very bottom of the core.
- The ability to take into account variations in porosity throughout the core.
- The ability to specify normalized radial power distribution profiles within the different axial layers in the core.
- The ability to account for heat generation that may occur in any of the core structures

3.1.4 3-D model

The 3-D model is an extension of the 2-D axi-symmetric model. This model can be used for steady state or transient analyses and one can specify a radial, axial or tangential power profile with surface temperature. Discretization can be zone-based or block-based.

3.1.5 Block-based model

The block-based model for the prismatic block of a PMR200 was created by Sambureni (2015) to model a basic control volume with a representative coolant channel and fuel rod. It can be used to model fuel, control and reflector blocks. One can also model bypass and cross flow gaps between adjacent blocks in the core. There are several variations of block-based modelling:

- A block can be divided into six triangles as was done in GAMMA+. In this approach, there is one representative coolant channel, fuel rod and node per triangle. The heat is uniformly distributed across the fuel block.
- There can be different nodes for the graphite, fuel and coolant channel zones.
- The block can be divided into control volumes. In this case the heat may be non-uniformly distributed over the volume of the fuel block.

The control volume based approach serves the purpose to facilitate the discretization of complex geometries, taking detail effects into account (Greyvenstein & Van Antwerpen, 2004).

What the control volume based network approach has in common with classical CFD control volume approach is that momentum conservation is solved at control volume interfaces (elements) while mass and energy conservation are solved at nodes. In contrast to the control volumes used in classical CFD, the control volumes in this approach are of a much larger scale, incorporating empirical correlations or analytical models to take smaller-scale detail into account such as flow channels through a solid or conduction shape factors, without losing the simplicity of the large-scale control volumes (Greyvenstein & Van Antwerpen, 2004).

3.2 Governing equations

The governing equations of mass, momentum and energy conservation as implemented in Flownex are discussed.

3.2.1 Conservation of mass

Considering the control volume shown in Figure 31.

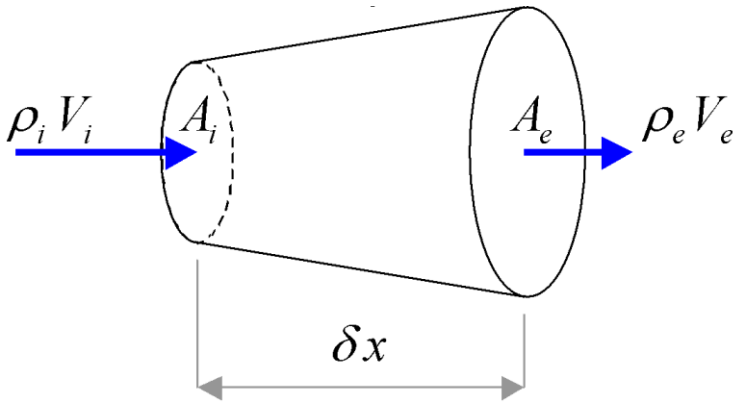

Figure 31: One- dimensional control volume (M-Tech Industrial, 2016 (b))

The general equation of mass conservation can be written in a one-dimensional coordinate system in the form expressed in in equation (3-1) (M-Tech Industrial, 2016 (b)):

$$\frac{\partial \rho}{\partial t} + \frac{\partial}{\partial x}(\rho V) = 0 \quad (3\text{-}1)$$

where:

V = the flow velocity in the x direction

ρ = the density of the fluid

For steady state eq. (3-1) reduces to:

$$\frac{\partial}{\partial x}(\rho V) = 0$$

For the control volume in Figure 31 the equation can be presented in discretized form as in equation (3-2).

$$\rho_e V_e A_e - \rho_i V_i A_i = 0 \quad (3\text{-}2)$$

Subscripts i and e refer to the inlet and outlet of the control volume respectively.

3.2.2 Conservation of momentum

The momentum conservation equation for one-dimensional flow in a pipe is obtained in non-conservative form as:

$$\rho \frac{\partial V}{\partial t} + \rho V \frac{\partial V}{\partial x} = -\frac{\partial p}{\partial x} - \rho g \frac{\partial z}{\partial x} - \frac{f \rho |V| V}{2D} \quad (3\text{-}3)$$

Where f = friction factor calculated as a function of Reynolds number for pipe flow

ρ = the density of the fluid

p = static pressure

g = acceleration due to gravity

D = pipe diameter

z = elevation

3.2.2.1 Incompressible flow

For incompressible flow, the convection term in the equation (3-3) is written in terms of the kinetic energy. This term, together with the pressure gradient term are then grouped into a total pressure term.

$$\rho \frac{\partial V}{\partial t} + \frac{\partial p_o}{\partial x} + \rho g \frac{\partial z}{\partial x} + \frac{f \rho |V| V}{2D} = 0 \quad (3\text{-}4)$$

For steady flow the equation reduces to:

$$\frac{\partial p_o}{\partial x} = -\rho g \frac{\partial z}{\partial x} - \frac{f \rho |V| V}{2D} \quad (3\text{-}5)$$

Where p_o = total/ stagnation pressure = $p + \frac{1}{2}\rho V^2$

3.2.2.2 Compressible flow

For compressible flow the equation for conservation of momentum is expressed as in equation (3-6).

$$\frac{p}{p_0}\frac{\partial p_o}{\partial x} + \frac{\rho V^2}{2T_o}\frac{\partial T_0}{\partial x} = -\rho g\frac{\partial z}{\partial x} - \frac{f\rho|V|V}{2D} \quad (3\text{-}6)$$

where:

T_0= stagnation (total) temperature

And p_0= stagnation (total) pressure

3.2.3 Conservation of energy

The energy equation for one-dimensional flow is expressed in terms of the specific stagnation enthalpy h_0 as:

$$\frac{\partial(\rho(h_0+gz)-p)}{\partial t} + \frac{\partial(\rho V(h_0+gz))}{\partial x} = \dot{Q}_H - \dot{W} \quad (3\text{-}7)$$

Written in terms of stagnation temperature, the steady flow equation can be written as:

$$\frac{\partial(\rho V c_p T_0)}{\partial x} + \rho g V\frac{\partial z}{\partial x} = \dot{Q}_H - \dot{W} \quad (3\text{-}8)$$

Where c_p = specific heat capacity

$\dot{Q}_H$ = net rate of heat transfer into the system

$\dot{W}$ = rate of work done by the system

3.2.3.1 Heat transfer modes

3.2.3.1.1 Conduction heat transfer

Conduction is the mode of heat transfer where a temperature difference is present in a solid material or fluid when there is no bulk motion present (M-Tech Industrial, 2016 (b)). The rate of heat conduction through a medium depends on the geometry and material composition of the medium and the temperature across the medium (Cengel, et al., 2008). The rate of heat conduction through a solid material or a fluid can then be expressed using Fourier's law of heat conduction given in equation (3-9).

$$q_{cond} = -k\nabla T \quad (3\text{-}9)$$

Equation (3-9) can be used in its differential form in one dimension, in the x-direction, as expressed in equation (3-10).

$$q_{cond,x} = -k\frac{dT}{dx} \quad (3\text{-}10)$$

When equation (3-10) is applied to a control volume with nodes 1 and 2, it yields equation (3-11).

$$\dot{Q}_{cond} = kA\frac{T_1 - T_2}{\Delta x} - kA\frac{\Delta T}{\Delta x} \quad (3\text{-}11)$$

Where:

$\frac{dT}{dx}$ = temperature gradient

$q_{cond,x}$= local heat flux density

$\dot{Q}_{cond}$ = heat flow rate by conduction

k = thermal conductivity of the material

A = the cross-sectional area normal to the direction of heat flow

3.2.3.1.2 Convection heat transfer

Convection is the transfer of energy between a solid surface and the adjacent fluid that is in motion, and it involves the combined effects of conduction and fluid motion (Cengel, et al., 2008). The convection heat transfer coefficient determines the amount of heat transferred from the surface to the fluid or vice versa. The heat transfer coefficient is often a complex function of the surface geometry and boundary layer (M-Tech Industrial, 2016 (b)). The rate of convection heat transfer is expressed in equation (3-12).

$$\dot{Q}_{conv} = hA_s(T_s - T_\infty) \quad (3\text{-}12)$$

Where:

h = convection heat transfer coefficient

A_s = the surface area through which convection heat transfer takes place

T_s = surface temperature

T_∞ = temperature of the fluid sufficiently far from the surface

3.2.3.1.3 Radiation heat transfer

Radiation is the transfer of energy due to the emission of electromagnetic waves (or photons) as a result of the changes in the electronic configurations of the atoms or molecules (Cengel, et al., 2008). The radiation heat transfer between a two surfaces enclosure is calculated by equation (3-13).

$$\left(k\frac{\partial T}{\partial n}\right)A = \dot{Q} = \frac{\sigma\left(T_{S1}^4 - T_{S1}^4\right)}{\frac{1-\varepsilon_1}{\varepsilon_1 A_1} + \frac{1}{A_1 F_{12}} + \frac{1-\varepsilon_2}{\varepsilon_2 A_2}} \quad (3\text{-}13)$$

Where:

σ = Stefan-Boltzmann constant (5.670×10^{-8} W/m^2·K^4)

ε_1 and ε_2 = the upstream and downstream surface emissivity, and

F_{12} = form view factor

3.3 Solution algorithms for pressure-velocity coupling

Every velocity component appears in each momentum equation, and the velocity field must also satisfy the continuity equation. If the pressure gradient is known, the process of obtaining discretized equations for velocities from the momentum equations is exactly the same as that for any other scalar. If the flow is compressible the continuity equation may be used as the transport equation for density and the energy equation is the transport equation for temperature. The pressure may then be obtained from density and temperature by using the equation of state in equation (3-14).

$$p = p(\rho, T) \tag{3-14}$$

Problems associated with the non-linearities in the equation set and the pressure-velocity linkage can be resolved by adopting an iterative solution strategy such as the Semi-Implicit Method for Pressure-Linked Equations (SIMPLE) algorithm of Patankar and Spalding (1972). The system CFD approach is based on staggered grid discretization. This discretization has the advantage of excellent coupling between pressure and velocity as mass, pressure and temperature are calculated at control volume centres while velocity is calculated at volume faces (Greyvenstein, et al., 2004).

3.3.1 Staggered grid

The staggered mesh is the simplest strategy for incompressible flow calculations if velocities and pressures are both defined at the nodes of an ordinary control volume a highly non-uniform pressure field can act like a uniform field in the discretized momentum equations. A remedy for this problem is to use a staggered grid for velocity components. The idea of the staggered grid is to evaluate scalar variables such as pressure, temperature and density at ordinary nodal points, but to calculate the velocity components on staggered grids centred around the cell faces (Versteeg & Malalasekera, 2007). Therefore, for the staggered grid approach, velocities are computed at cell faces and pressures are computed at cell centres.

3.3.2 SIMPLE algorithm

The SIMPLE is a segregated method used in CFD to solve the Navier-Stokes equations (Greyvenstein & Laurie, 1994). The original algorithm is essentially a guess-and-correct procedure for the calculation of pressure on the staggered grid (Versteeg & Malalasekera,

2007). Greyvenstein & Laurie (1994) adapted this algorithm to solve steady state flows in pipe networks. Flownex therefore solves compressible and incompressible mass and momentum equations with an adaptation of the SIMPLE algorithm called the implicit pressure correction method (IPCM).

3.3.3 IPCM algorithm

Flownex solver employs a segregated solution algorithm in which the different governing equations and additional closure equations are solved sequentially. It is therefore based on the IPCM that solves the momentum equation at each element and the continuity and energy equations at each node in large arbitrary structured networks for both steady state and dynamic flow. The solver can deal with both fast and slow transients (Greyvenstein, 2002) (M-Tech Industrial, 2016 (b)).

3.4 Summary

In this chapter the fundamental mass, momentum and energy equations governing thermal-fluid analyses through the reactor were also discussed. Phenomena that are taken into account include convection heat transfer between all gas and solid structures and solid conduction, as well as radiation.

4 THEORY AND INSTRUCTION FOR MODEL DEVELOPMENT

The objective of this thesis work is a philosophical development of a thermal-hydraulic Flownex network model for a prismatic block-type HTR. This will be achieved by solving the governing equations of mass, momentum and energy with the equation of state for the heat transfer in the fuel blocks and 1-D pipe network approach to model fluid flow in coolant channels, bypass and cross flow gaps. In the proposed method, a conduction shape factor derived by Sambureni (2015) to account for the heat transfer from the fuel rods to the graphite and from the graphite to the coolant channels for a basic unit cell containing part of the graphite, fuel element and coolant channel was implemented.

In this chapter the principle of the modelling of the conduction path between the fuel kernel and the pipe elements representing the coolant channels will be explained. The implementation of this approach on an HTR fuel block will be discussed, paying particular attention to standard fuel blocks and flow paths of a PMR200 reactor.

4.1 Description of a PMR200 standard fuel block

The active core of a PMR200 consists of an array of hexagonal graphite fuel blocks. The PMR200 fuel design is based on the GT-MHR (Tak, et al., 2012). Fuel blocks are stacked to form a fuel assembly. As mentioned in section 1.3, there are three types of fuel blocks (standard fuel blocks, control and reserve shutdown blocks). Calculations for the standard fuel blocks only will be showed in this section.

Standard fuel blocks are made of H-451 graphite and are hexagonal in shape. The dimensions of one fuel block is 79.3 cm high and 360 cm across the flats as shown in Figure 32. Fuel and coolant holes run parallel through the length of the prism in a pattern with the number of fuel holes being twice the number of coolant holes. After careful study one can see that a typical coolant holes is associated with six one third fuel holes, i.e. 6 x 1/3 = 2.

The standard fuel block contains a continuous pattern of fuel and coolant holes except for a central handling hole surrounded by smaller coolant holes and the corner holes in which the fuel is replaced with lumped burnable poison (LBP) (General Atomics, 1992). The PMR200 standard fuel block has 204 blind holes for fuel compacts and 108 channels for a helium coolant flow. Twelve blind holes are assigned for the burnable poison rods with six placed at each corner of the hexagonal fuel block and six others in the interior of the block (Tak, et al., 2012).

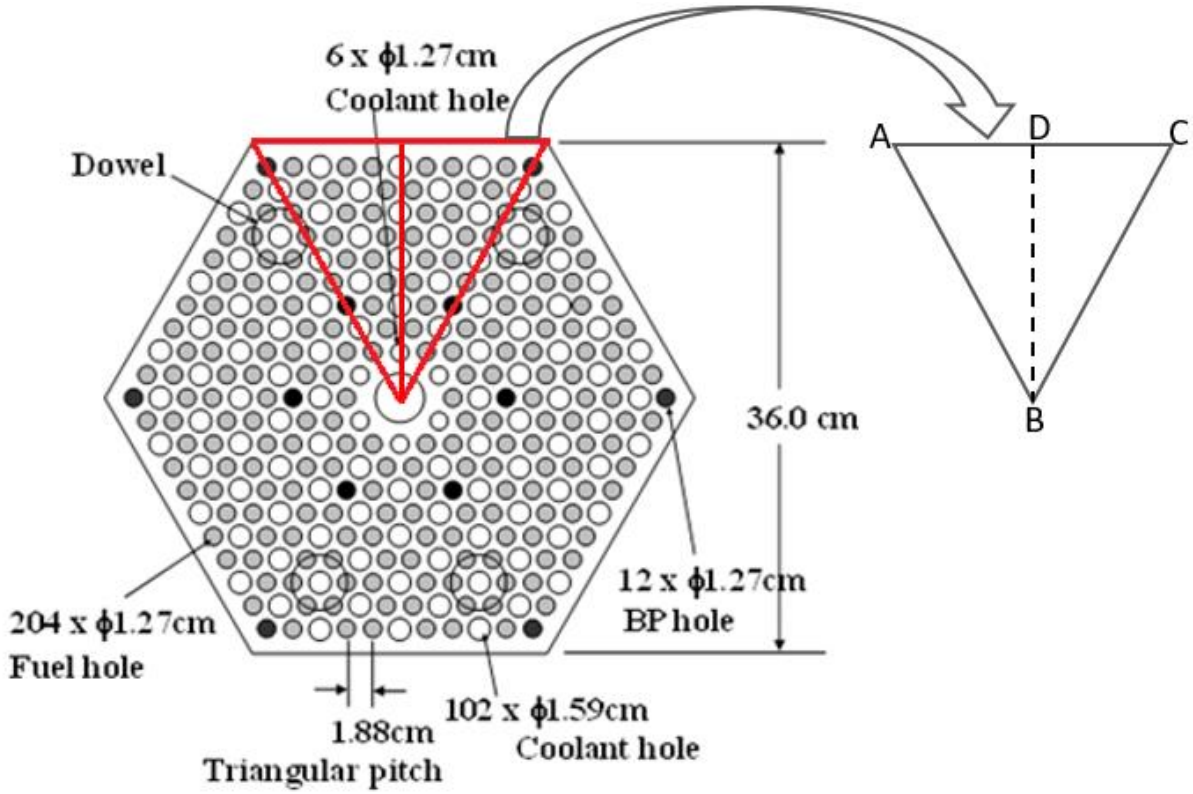

Figure 32: Standard fuel block dimensions (Tak, et al., 2014)

4.2 Modelling philosophy

4.2.1.1 Conduction in the coated fuel particles

In the PMR200, the heat in a fuel block is generated in the fuel kernels inside the TRISO coated fuel particle and conducted through the graphite block to the helium coolant. Each coated fuel particle in the fuel compact graphite matrix is discretized into five spherical volumes of specified radii. There is one node for the centre of the fuel kernel and one node for each of the coated fuel particle coating layers (i.e. buffer layer, inner pyrolytic carbon, silicon carbide and the outer pyrolytic carbon) and one associated with the coated fuel surface. The heat transfer within the coating layers is accounted for by conduction elements. In the case of a fuel kernel, the radius of the fuel kernel will be the conduction length. Discretization in this manner allows for the calculation of the temperature distribution within the coated fuel particles in any region of the fuel compact. As a first approximation, the surface temperature of the coated fuel particle is assumed to be the same as the temperature of the surrounding graphite matrix within the fuel rod.

4.2.1.2 Conduction in the fuel rod

The spherical TRISO coated fuel particles discussed in section 4.2.1.1 are bonded into a fuel compact. Fuel compacts are stacked in each of the fuel holes in the fuel block to form a fuel rod. The distribution of fuel kernels in the fuel rods will be estimated using the packing fraction. Fuel rods are cylindrical in geometry and will be discretized in the axial and radial directions. The fuel rod is discretized into four radial and three axial volumes. The radial discretization of the fuel rod is shown in Figure 33. A study of the effect of discretization on a single fuel compact unit cell with surrounding graphite was done and is reported in section 6.2. The results showed that the discretization of a fuel rod into four cylindrical volumes is sufficient for the purposes of this study.

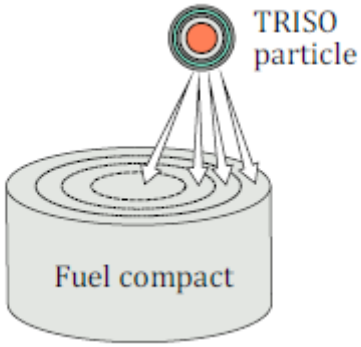

Figure 33: Radial coated fuel particle layers in a fuel compact/rod (Clifford, 2013)

The inner most node represents the temperature at the centre of the fuel rod and the outer most node represents the temperature at the surface of the helium gap. The helium in the gap between the fuel rod and the graphite is assumed to be stagnant, therefore heat transfer from the fuel edge through the helium gap to the surrounding graphite matrix in the fuel block will be modelled by a combination of conduction and radiation elements. The PMR200 fuel block has an initial radial gap of 0.125 mm thickness between the fuel compact and the fuel hole wall. The helium gap is assumed to stay uniform thereby ensuring complete separation of the fuel compact and graphite region. In reality, however, if the fuel compact swells at a larger rate than the graphite of the fuel block, the fuel gap would not be uniform or may close. This may introduce contact resistance between the fuel compact and graphite (Stainsby, et al., 2009).

The conduction element accounting for conduction through the fuel rod typically has mass associated with it that is distributed to the fuel rod nodes (or control volumes). Fuel rods nodes include all the nodes in the fuel rod, even those that are assumed to be on the surface of the fuel rod representing the outer control volume. However, massless conduction elements have also been implemented in the implicit solution algorithm, to ensure that where applicable the

correct thermal mass is associated with the relevant nodes during a transient (Greyvenstein & Van Antwerpen, 2004). In the proposed method, only the conduction elements accounting for conduction through the fuel rod in the axial direction will have mass associated with it that will be distributed to the fuel rod nodes. The graphite node ($T_{F,\ surface}$ in Figure 34) will give the surface temperature of the fuel rod and fuel rod centre temperature ($T_{F,\ centre}$ in Figure 34) will be given by the temperature of the solid node at the centre of the fuel rod.

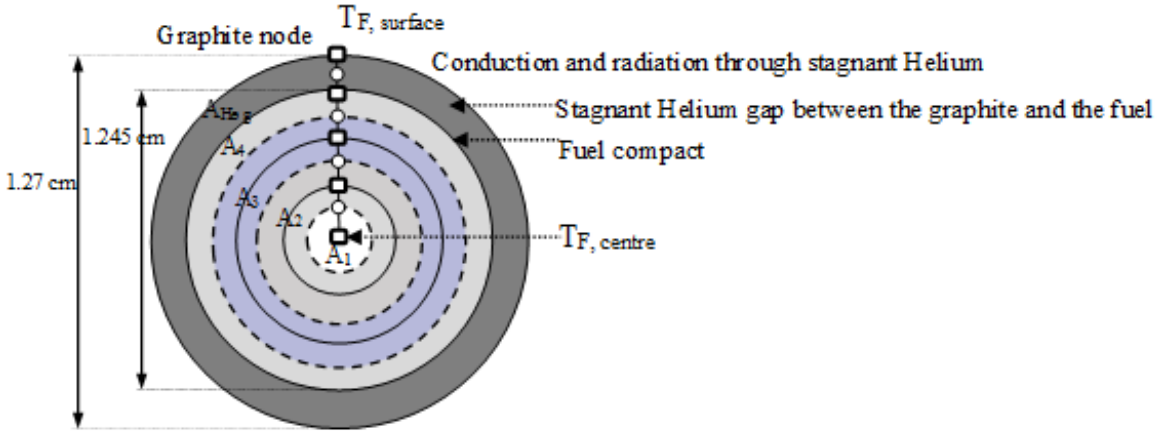

Figure 34: Radial discretization of the fuel rod

4.2.1.3 Conduction in the graphite block

In the proposed method, a basic unit cell containing a $1/6^{th}$ of the circumference of a coolant channel and a third of the circumference of a fuel rod was used to characterize the heat transfer the radial direction in the fuel block from the surface of the fuel rod hole to the coolant channel wall as explained in section 2.1.2.5.

The Flownex model for the heat transfer from the surface of the fuel rod hole to the coolant channel wall will consist of three solid nodes and two conduction elements. The first node will represent the surface of the fuel rod hole temperature, the second the graphite block temperature and the third the coolant channel wall temperature. The conduction elements will account for the heat transfer from the surface of the fuel rod hole to the graphite and from the graphite to the surface of the coolant channel wall respectively. The mass associated with graphite block node will be obtained from the conduction elements connecting the solid nodes in the axial direction. This approach can be applied to an arbitrarily chosen control volume of a standard fuel block as explained in section 4.3. The axial direction will be taken as the primary direction of conduction heat transfer and zero mass conduction heat transfer elements will be assumed for the radial and tangential direction. In cases where blocks contain coolant channels or control rods, thermal resistances will be adjusted to account for the porosity of the blocks. This can be

done by subtracting the void area from the actual solid area of the block and then using the solid fraction (shown in section 4.7) as input to Flownex.

4.2.1.4 Convection and leakage flow paths

Heat is transferred from the graphite block to the helium in the coolant channels through forced convection cooling. This cooling removes the heat generated in the reactor core during normal operating conditions. Cylindrical coolant channels run along the height of the block, therefore the discretization of the flow nodes will be in the axial direction. As shown in Figure 35, the coolant in the channels and bypass flow both flow vertically and cross flow is horizontal. Three convection and vertical pipe elements will be connected to the coolant channel wall nodes at the top, middle and bottom of the fuel block to model flow in the coolant channels and to account for the heat transfer from the block to the coolant. The helium that escapes the coolant channels and runs through bypass and cross flow gaps between the fuel blocks are also modelled with convection and pipe elements. The bypass gap will also be modelled by three vertical pipe elements that will be connected to three convection elements at the edges of the block for the top, middle and bottom nodes of the fuel block. Modelling of cross flow is discussed in section 4.13.1.

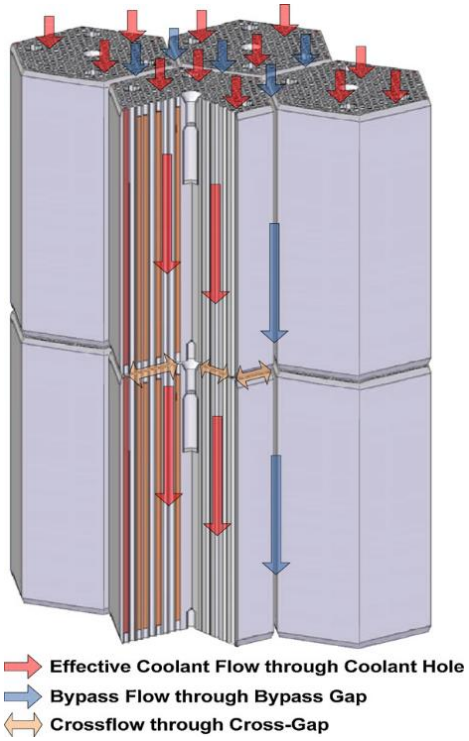

Figure 35: Flow paths in the prismatic VHTR core (Yoon, et al., 2012)

4.3 Discretization of a standard fuel block into control volumes

The hexagonal fuel block has a complex geometry and to simplify the calculations, a standard fuel block is first divided into six equal segments. Due to symmetry, one of the $1/6^{th}$ segments can be isolated (segment ABC in Figure 32 and then discretized into smaller control volumes. The $1/6^{th}$ segment is discretized in three directions (i.e. in the radial - along x, the tangential- along y and the vertical direction- along z). The grid size was varied in the radial and tangential directions but kept at three nodes in the vertical direction. There are thus three control volumes in the axial direction. Discretization of the fuel block in this manner radially and tangentially ensures that the regions at the edges of the fuel block are included in the model unlike in the traditional unit cell method described by Tak et al. (2008) in Figure 8 in section 2.1. The top and bottom control volumes are a quarter of the height of the fuel block and the middle axial control volume is half the height of the fuel block. Note that the grid independence study that was done is described in section 5.2.4.1.1 where it is shown that the 11×5 node model that was implemented in this study is sufficient. However a 3×3 node model is described in this section for illustrative purposes.

To explain the philosophy, a case where $1/6^{th}$ of a fuel block is discretized into a 3x3 grid as shown in Figure 36 is considered. The nodes, shown by rectangles in Figure 36, are equally spaced in the radial (along lines AE, AG and AI), tangential directions (along lines CK and EI) and along the z direction. It was assumed that the fuel rods and coolant channels are uniformly distributed over the fuel block and that all the coolant channels have the same diameter. In the actual fuel block, the fuel rods and coolant channels are not distributed over the entire area of the fuel block, as discussed in detail in Appendix C. To characterize the heat transfer through the representative fuel rods as well as representative coated fuel particles, it is required to make sure that the conduction length and areas are representative of the number of fuel kernels associated with each control volume. For each control volume, coated fuel particles, fuel rods and coolant channels are grouped together and modelled implicitly as representatives for each instance. It is possible to develop a Flownex model that accounts for the graphite (solid only) areas using appropriate CVs. However, it was assumed that the fuel rods and coolant channels are uniformly distributed over the fuel blocks.

The unit cell approach described in section 2.1.2.5 was firstly implemented in a case study of a $1/6^{th}$ of a fuel block discretized into a 3x3 grid as shown in Figure 36. The coolant channels associated with the number of unit cells within each control volume were grouped into a representative coolant channel. The representative coolant channel in each control volume

accounts for the total free flow area and hydraulic diameter within the specified control volume. Similarly, the fuel rods and coated fuel particles for each control volume were grouped into representative fuel rods and coated fuel particles, respectively.

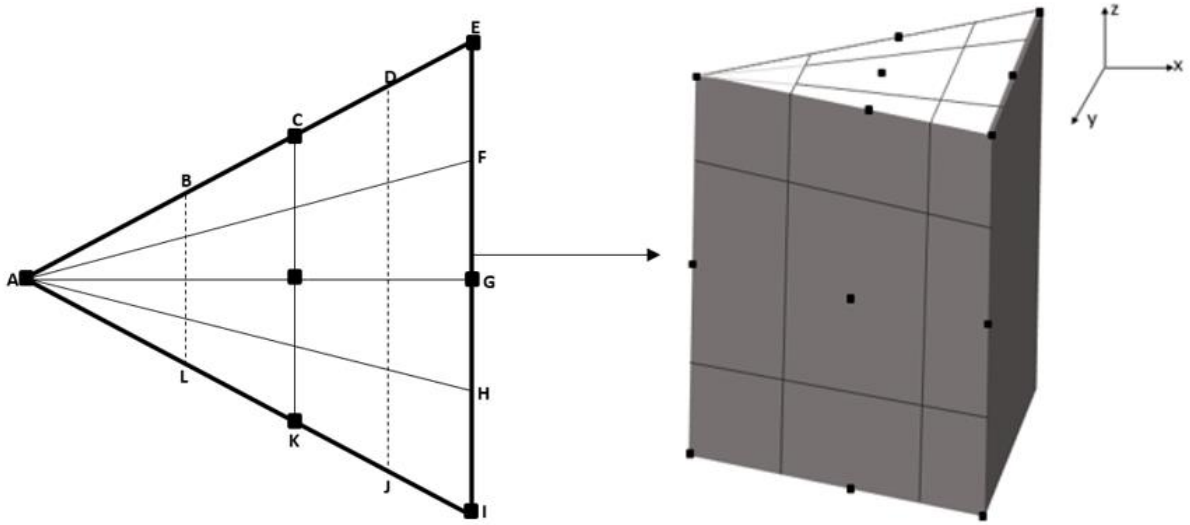

Figure 36: 1/6th of a fuel block discretized by a 3x3 grid

The cross-sectional area of the 1/6th segment of a fuel block can be calculated using equation (4-1).

$$A_{1/6} = 0.5 \times \frac{36}{2} \times \frac{18}{\cos 30^\circ} = 187 \text{ cm}^2 \quad (4\text{-}1)$$

Number of coolant channels in 1/6th segment of a fuel block can be calculated using equation (4-2).

$$N_{cc,1/6} = \frac{108}{6} = 18 \quad (4\text{-}2)$$

The ratio of the control volume area to the area of the 1/6th segment can be used to obtain the number of coolant channels in each CV as shown in equation (4-3).

$$N_{cc/CV} = \frac{A_{CV}}{A_{1/6}} \times 18 \quad (4\text{-}3)$$

Similarly, the number of fuel rods on 1/6th segment of a fuel block can be calculated by equation (4-4).

$$N_{fr,1/6} = \frac{204}{6} = 34 \quad (4\text{-}4)$$

The number of fuel rods in each CV can be calculated by equation (4-5).

$$N_{fr/CV} = \frac{A_{CV}}{A_{1/6}} \times 34 \quad (4\text{-}5)$$

4.4 Calculation of conduction element areas in a coated fuel particle

The radii for the coated fuel particle used in this study were adopted from Strydom et al. (2015) and are given in Table 46 in Appendix A. For a selected control volume, the number of coated fuel particles can be calculated if the fuel rod and coated fuel particle volumes are known. The volume of a single coated particle and that of a fuel kernel are calculated using equation (4-6).

$$V_{CP,kernel} = \frac{4}{3}\,\pi\left(r_{CP,kernel}\right)^3 \tag{4-6}$$

For each of the four radial layers in the fuel rod, the volume of each fuel rod layer per axial control volume can be calculated by equation (4-7).

$$V_{fr\ layer,i} = \pi\left(r_{o,layer,i}^2 - r_{i,layer,i}^2\right) \times h_{CV} \tag{4-7}$$

The number of coated fuel particles in a fuel rod radial layer per axial control volume using a packing fraction of 20% can be calculated using equation (4-8)

$$N_{CP,layer,i} = \frac{0.2 \times V_{fr\ layer,i}}{V_{CP}} \tag{4-8}$$

Volume occupied by fuel kernels in a fuel rod radial layer per axial control volume:

$$V_{kernel,layer\ i} = V_{kernel} \times N_{CP,layer,i} \tag{4-9}$$

Representative fuel kernel volume in a fuel rod radial layer per axial control volume:

$$V_{rep,kernel,layer\ i} = V_{kernel,layer\ i} \times N_{fr} \tag{4-10}$$

If the power of the assembly is given, then the power in each control volume is given by:

$$P_{CV} = \frac{P_{assembly}}{6 \times \text{number of blocks per assembly}} \times \frac{Area_{CV}}{Area_{\frac{1}{6}}} \tag{4-11}$$

The power applied to each representative fuel kernel per radial layer of the fuel rod per axial control volume is then:

$$P_{rep\ kernel/layer,i} = P_{CV} \times \frac{Vrep\ kernel,_i}{V_{T,rep\ kernel}} \tag{4-12}$$

where: $V_{T,rep\ kernel}$ is the total volume of the representative fuel kernels in the fuel rods in the control volume, i.e. the sum of the volumes of the representative fuel kernels in all the, i.e. four, fuel rod layers. For each control volume, the conduction areas for each coated particle layer (i.e. fuel kernel, buffer layer, etc.) are grouped into a representative conduction area for that coating layer but the actual coating layer radii are used for each of the associated conduction lengths.

The average conduction area of a coated fuel particle can be obtained using equation (4-13):

$$A_{CP\ layer} = N_{CP\ layer} \times 4\pi \left(\frac{r_i^2 + r_o^2}{2}\right) \quad (4\text{-}13)$$

4.5 Calculation of representative fuel rod areas

For each control volume, the conduction areas for each of the radial layers grouped into a representative conduction area for that fuel rod and the actual fuel rod radii are used for each of the associated conduction lengths.

Since there are three axial nodes, or control volumes, for the fuel rods there will be two conduction elements between these nodes and their representative conduction area per fuel rod radial layer will be calculated using equation (4-14).

$$A_{rep/fr\ layer,i} = N_{fr,layer,i} \times \pi(r_o^2 - r_i^2) \quad (4\text{-}14)$$

For the radial layer representative conduction lengths per axial control volume, the average conduction areas are calculated using equation (4-15).

$$A_{rep/fr\ layer,i} = N_{fr,layer,i} \times \pi \frac{(D_o + D_i)}{2} \times h_{CV} \quad (4\text{-}15)$$

4.6 Calculation of representative coolant channel areas and volumes

The area A_{cc} of a coolant channel is calculated by:

$$A_{cc} = \frac{\pi d_{cc}^2}{4} \quad (4\text{-}16)$$

If A_{cc} is the area of a coolant channel then the total area $A_{rep,cc}$ of the coolant channels in the CV is given by (equation 4-17).

$$A_{rep,cc} = \text{Number of Coolant channels}_{\_CV} \times \text{Area of a coolant channel}$$

$$A_{rep,cc} = N_{cc} \times A_{cc} \quad (4\text{-}17)$$

The volume of a single coolant channel and that of all the coolant channels in a control volume can be calculated by equations (4-18) and (4-19).

$$V_{cc} = A_{rep,cc} \times h_{CV} \quad (4\text{-}18)$$

$$V_{cc,T} = V_{cc} \times N_{cc} \quad (4\text{-}19)$$

4.7 Calculation of fuel to graphite conduction element areas

Between the fuel and the graphite, there are no perforations and therefore the value of the solid fraction is one. As was illustrated in Figure 25, the (cross-sectional) area of a unit cell, A_{UC}

contains 1/6th coolant channel and 1/3rd fuel rod. If A_{CV} is the cross-sectional area of a control volume, then the number of unit cells in a control volume is given by equation (4-20).

$$N_{UC} = \frac{A_{UC}}{A_{CV}} \tag{4-20}$$

If the cross-sectional area of a fuel rod is A_{fr} and $A_{fr,T}$ is the total area of the fuel rods in the CV, then we can also write:

$$N_{UC} = \frac{3 \times A_{fr,T}}{A_{fr}} = 3 \times N_{fr} \tag{4-21}$$

The total conduction area (CA) per unit axial length for the radial heat transfer from the surfaces of the fuel rod holes to the graphite in the CV A_{CA}^{fs} is expressed as:

$$A_{CA}^{fs} = 3 \times N_{fr} \times A_{fs} \tag{4-22}$$

The total conduction area $A_{CA,T}^{fs}$ for the radial heat transfer from the surface of the fuel rod hole to graphite for each of the axial control volume, is therefore given as:

$$A_{CA,T}^{fw} = A_{CA}^{fs} \times h_{CV} \tag{4-23}$$

4.8 Calculation of conduction element areas within the graphite

The (axial) conduction area within the graphite will be given by the cross-sectional area of the selected control volume. In Flownex, the perforations made by the coolant channels in the graphite are accounted for by using the solid fraction. The solid fraction α can be obtained by calculating the ratio of the area covered by solid to the total area of the control volume as shown in equation (4-26). In a control volume the area covered by solids (graphite in this case) $A_{s,CV}$ is obtained by subtracting the total area occupied by the coolant channels in the volume control volume from the total area of the control volume, $A_{T,CV}$.

$$\alpha = \frac{A_{s,CV}}{A_{T,CV}} \tag{4-24}$$

4.9 Calculation of graphite coolant conduction element areas

If the cross-sectional area of a coolant channel is A_{cc} and $A_{cc,T}$ is the total cross-sectional area of the coolant channels in the CV, then we can also write:

$$N_{UC} = \frac{6 \times A_{cc,T}}{A_{cc}} = 6 \times N_{cc} \tag{4-25}$$

The total conduction area per unit length A_{CA}^{sw} for the radial heat transfer from the surface of the graphite to the wall of the coolant channel in the CV is given by equation (4-26).

$$A_{CA}^{sw} = 6 \times N_{cc} \times A_{sw} \tag{4-26}$$

The total conduction area $A_{CA,T}^{sw}$ for the radial heat transfer from the graphite to the wall of the coolant channel for each of the axial control volume, is therefore given as:

$$A_{CA,T}^{sw} = A_{CA}^{sw} \times h_{CV} \tag{4-27}$$

4.10 Calculation of convection element areas

Since the coolant channels run along the (axial) height of the block, the discretization of the flow nodes is in the axial direction. These nodes are aligned with the interfaces between the solid nodes or control volumes. There are therefore three convection and pipe elements along the height of a fuel block. The total circumference of the coolant channels associated with a control volume is given as:

$$C_{cc,T} = \pi \times D_{cc} \times N_{cc} \tag{4-28}$$

The total coolant wall area associated with convection heat transfer is then obtained as:

$$A_{cht,T} = C_{cc,T} \times h_{CV} \tag{4-29}$$

4.11 Approximating lateral conduction between adjacent control volumes

In addition to the heat transfer within the control volumes, there is also heat transfer between adjacent control volumes that needs to be accounted for. For example, if one considers a 1/6th segment discretized into a 3 x 3 grid and select the central control volume (CV 2 in Figure 37), the conduction heat transfer between CV 2, CV 1, CV 3, CV 4 and CV 5 is indicated in Figure 37 (a) by red arrows into and out of CV 2. To model this phenomenon, conduction lengths and areas between the adjacent volumes need to be calculated.

The following calculations indicate how the conduction lengths for the 1/6th in Figure 37 (b) were calculated. As a first approximations the areas perpendicular to the conduction (lines connecting the nodes) were assumed to represent the conduction areas. Orthogonal lines are drawn between control volumes to estimate the conduction areas (Figure 37 (b)).

The perpendicular conduction length between CV 1 and CV 3, $L_{13,p}$ was calculated using equation (4-30).

$$L_{13,p} = L_{14,p} = L_{13} \sin 60° \tag{4-30}$$

where L_{13} is the conduction length between CV 1 and CV 3.

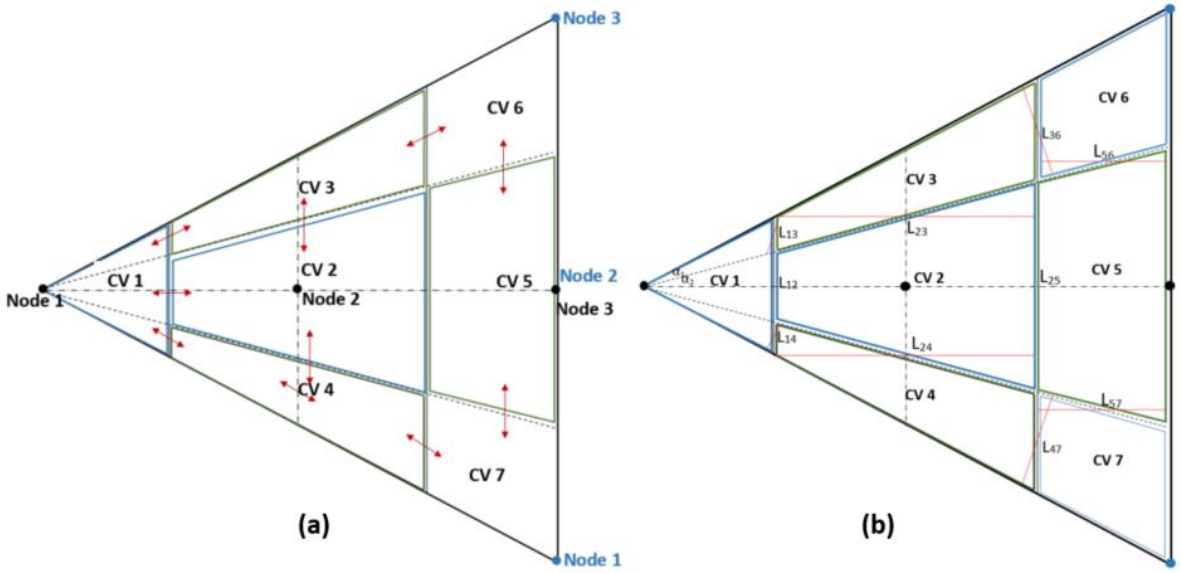

Figure 37: Lateral conduction approximation between adjacent control volumes

$$L_{23,p} = L_{24,p} = L_{23}\sin\ (90 - \alpha_2) \quad (4\text{-}31)$$

$$L_{56,p} = L_{57,p} = L_{56}\sin\ (90 - \alpha_2) \quad (4\text{-}32)$$

It is recommend that an appropriate conduction shape factor analysis be performed to determine the relevant values. The conduction components that account for the conduction heat transfer between adjacent CVs are massless conduction components.

Conduction area between CV 1 and CV 2 was calculated using equation (4-33).

$$A_{12} = L_{12} \times h_{cv} \quad (4\text{-}33).$$

Conduction areas between CV 1 and CV 3 or between CV 1 and CV 4 were calculated using equation (4-34).

$$A_{13} = A_{14} = L_{13} \times h_{cv} \quad (4\text{-}34)$$

Conduction areas between CV 2 and CV 3 or between CV 2 and CV 4 were calculated using equation (4-35).

$$A_{23} = A_{24} = L_{23} \times h_{cv} \quad (4\text{-}35)$$

Similarly, the conduction areas between CV 3 and CV 6 or between CV 4 and CV 7 were calculated using equation (4-36).

$$A_{36} = A_{47} = L_{36} \times h_{cv} \quad (4\text{-}36)$$

Conduction area between CV 2 and CV 5 was calculated using equation (4-37).

$$A_{25} = L_{25} \times h_{cv} \quad (4\text{-}37)$$

Conduction areas between CV 5 and CV 6 or between CV 5 and CV 7 were calculated using equation (4-38).

$$A_{56} = A_{57} = L_{56} \times h_{cv} \tag{4-38}$$

4.12 HTR Flownex block model

A full fuel block model is created by joining six 1/6th fuel block models. The interface between two adjacent segments is formed by the corresponding edges of the segments connecting the apexes with the bases of the segments. The corresponding nodes on the edges are essentially common nodes between the two adjacent segments. The conduction heat transfer between two corresponding nodes is modelled using a conduction component with an infinite conductivity, a very short length and the relevant area.

4.13 HTR Flownex block assembly model leakage paths

In this section the equations that were used for the approximation of the cross flow and bypass areas and circumferences are given.

4.13.1 Cross flow areas and circumference

Consider a cross flow area associated with a control volume represented by a trapezoidal volume shown in Figure 38.

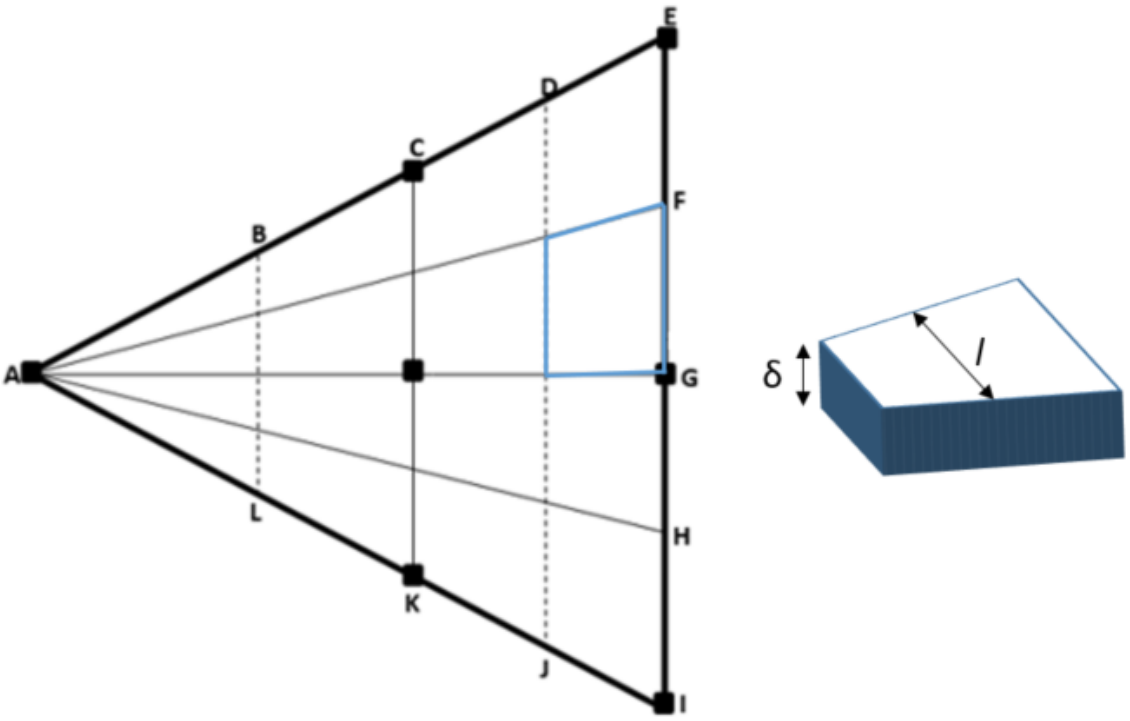

Figure 38: Cross flow gap schematic

The area for the cross flow is the calculated by equation (4-40), where l is the average width.

$$A_{cf} = l \times \delta \tag{4-39}$$

And the circumference is calculated by equation (4-39)

$$C_{cf} = 2 \times (l + \delta) \tag{4-40}$$

4.13.2 Bypass gap area and circumference

In the case of a bypass gap, if δ is the thickness of the bypass gap, the area of the bypass gap is given by equation (4-41).

$$A_{bg} = \delta \times w \tag{4-41}$$

The circumference of the bypass gap then is calculated by equation (4-42)

$$C_{bg} = (2 \times w) + (2 \times \delta) \tag{4-42}$$

Where w is the width of the side or base of a standard fuel block and δ is the thickness of the gap.

4.14 Control volume compound component

In Flownex one can define a fuel block CV as a compound component consisting of relevant nodes, conduction components, convection components and pipe component(s). The relevant inputs, outputs and connections to other control volume can be exposed. Within each control volume in each Flownex model, one can specify which inputs and /or outputs that can be exposed to be used for results acquisition or plotting. Since there are three nodes in the vertical direction, all three nodes were used for axial temperature distribution plots for each of the following outputs. As a minimum, in this project this is a list of common temperature outputs that can be exposed for Flownex models:

- Fuel kernel centre
- Fuel compact centre
- He gap
- Graphite block
- Representative coolant channel

4.15 Summary

In this chapter, the development of the philosophy for the modelling thermal-hydraulic Flownex network for a prismatic block-type HTR was outlined. As part of the discussion, the approach to modelling heat conduction within coated fuel particles, fuel rods, graphite and convection in the coolant channels was discussed. The concept of implicitly modelling of

coated fuel particles, fuel rods and coolants by using representative models was also discussed. The implementation of the conduction shape factor for the unit cell developed by Sambureni (2015) on the standard fuel block was demonstrated. As full fuel block assembly models will be built in Flownex, calculation of conduction areas within the fuel block and usage of infinite conductivity conduction elements and handling of bypass and cross flow areas was also shown.

5 MODEL DEVELOPMENT

5.1 Introduction

A thermal network consisting of a set of nodes, thermal resistances and boundary conditions will be set up. The flow network will be represented by a set of pipes and nodes. The temperatures obtained for nodes will represent the average mass temperature of a control volume. The thermal mass assigned to a node is computed from the volume contributed by the conduction elements and the specific heat and density of the material evaluated at the temperature of the node.

In this chapter, the modelling approach used in Flownex and CORONA will be reviewed and model layouts will be discussed. Since the purpose of this study is to build a thermal-hydraulic model of a prismatic block HTR using Flownex, the components used to build a Flownex model for the PMR200 will be discussed but mainly focusing more on the fuel block and fuel assemblies. If one does come to a point of developing a whole core model then the guidelines for developing the control rod and graphite block are given in this section.

5.2 Flownex

Flownex is a system CFD code (based on a one-dimensional thermal-fluid network methodology) for the analysis of thermal-fluid networks that is based on the numerical solution of the governing equations of fluid dynamics and heat transfer. Flownex solves the partial differential equations for mass, momentum and energy conservation to obtain the mass flow, pressure and temperature distributions throughout a network. Flownex solves the steady state and transient forms of the fundamental one dimensional conservation equations together with built-in fluid property relations and component characteristics representative of all the different types of components (M-Tech Industrial, 2016 (b)).

Flownex has been audited based on mostly nuclear standards and quality procedures and these are deemed to be the most stringent regulations. The South African National Nuclear Regulator found the verification and validation status of Flownex acceptable for use in support of design and safety case for the PBMR (M-Tech Industrial, 2017).

5.2.1 Different elements used in Flownex

Flownex is an integrated systems CFD code used for the design, simulation and optimization of complete thermal-fluid systems. The ability to model the complete integrated system gives

engineers the capability to quickly and accurately size components, do flow balancing and test different control methodologies in real time (M-Tech Industrial, 2016 (b)).

5.2.1.1 Pipe elements

The basic pipe element in Flownex can be used to model flow in pipes and ducting with non-constant cross-sectional area, as long as the flow area and the wetted perimeter are specified. It takes friction, inlet and outlet losses into account. The basic pipe element in Flownex has the following capabilities (M-Tech Industrial, 2017):

• It can model gas, liquid and two-phase flow.
• It can model both steady-state and transient flows.
• With regard to gas and two-phase flows it can solve up to a Mach number of one.
• The convective acceleration term in the pressure drop equation is retained in the calculations.
• Gravitational effects are taken into account.
• With regard to transient flows, the inertia terms are retained in the calculations

A pipe element has the capability to model pressure drop employing the Darcy-Weisbach equation (compressible and incompressible flows) and Hazen-Williams equation (incompressible flows). The pressure drop for the steady-state incompressible flow in a pipe with Darcy-Weisbach primary losses is given by equation (5-1).

$$\Delta p_o = \left(\frac{fl}{D} + \Sigma K_S + \Sigma K_R\right)\frac{\rho|V|V}{2} + \rho g \Delta z + \frac{1}{2}K\rho|V|V \qquad (5\text{-}1)$$

Where:

f = friction factor

l = length of pipe

D = inside diameter of pipe

ρ = density

V = mean velocity based on the pipe diameter

K = the forward or reverse losses

Δz = height difference between the inlet and outlet

ΣK_S = sum of the loss coefficients of the secondary loss components like bends, valves and junctions

ΣK_R = loss coefficient of a sharp edged orifice present in the pipe.

The total pressure drop for steady-state compressible flow is given by equation (5-2)

$$\Delta p_o = \left(\frac{fl}{D} + \Sigma K_S + \frac{\Delta T_0}{T_0}\right)\frac{p_0 \gamma M^2}{2} + \Delta p_{0_r} + \frac{p_0}{p}\left(\rho g \Delta z + \frac{1}{2}K\rho|V|V\right) \qquad (5\text{-}2)$$

where:

ΔT_0 = total temperature difference

T_0 = mean total temperature in element

p_0 = mean total pressure in element

γ = ratio of specific heats of the fluid

M = the mean Mach number in the pipe, and

Δp_{0_r} = total pressure drop over an orifice in the pipe

For models in this study, the Darcy-Weisbach pipe was used. In Flownex, the required input data for pipes includes: fluid data reference, length, inlet circumference and area, roughness and number of discretization increments.

5.2.1.2 Convection heat transfer elements

Convection heat transfer elements serve as the heat exchange link between a fluid and a solid surface. When a convection and conduction element are connected between a solid node and flow node as shown in Figure 39, heat transfer between a solid node and a flow node is encountered.

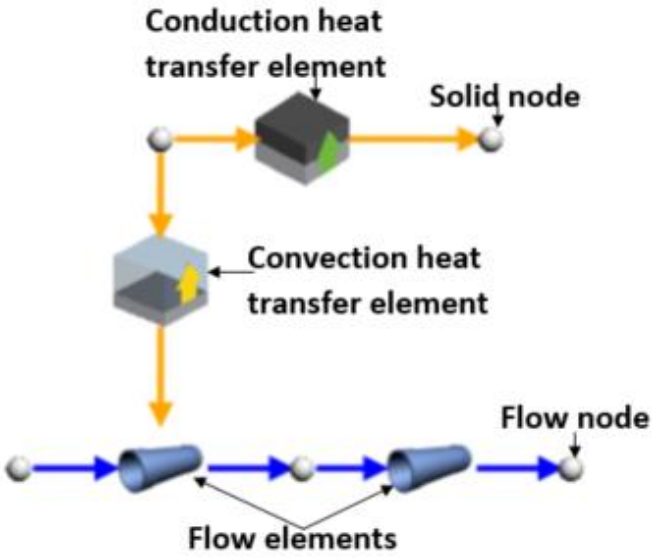

Figure 39: Schematic representation of a heat transfer link between a solid node and a flow element (M-Tech Industrial, 2017)

The required Flownex input data for convection elements includes heat transfer area and a convection coefficient option. In the heat transfer area specification, one can choose to specify an area or a shape. The heat transfer coefficient for the convection element is specified by the user or calculated using either the Dittus-Boelter, Gnielinski or user defined correlations (M-Tech Industrial, 2017). For convection elements connected to a pipe element, the logarithmic

mean temperature difference (LMTD) of the nodal temperatures associated with the pipe element is used.

5.2.1.3 Conduction heat transfer elements

Conduction heat transfer elements are used only for linear, one-dimensional heat transfer. Conduction heat transfer can be modelled using massless conduction heat transfer elements or conduction heat transfer elements that have mass associated with them. In the case where there is a mass associated with the heat transfer element, the user can choose whether the mass of the conduction element is calculated and added to the up- and downstream nodes or not. The option for nodal masses to be calculated needs to be selected if any transient inertia is to be taken into account. If there is mass associated with the conduction element and the option of calculating the nodal masses was not selected, then the mass associated with half the heat transfer length is lumped at the upstream node (N_1 in Figure 40) and the mass associated with the other half of the heat transfer length is lumped at the downstream (N_2 in Figure 40) (M-Tech Industrial, 2017). This is defined in equations (5-3) and (5-4).

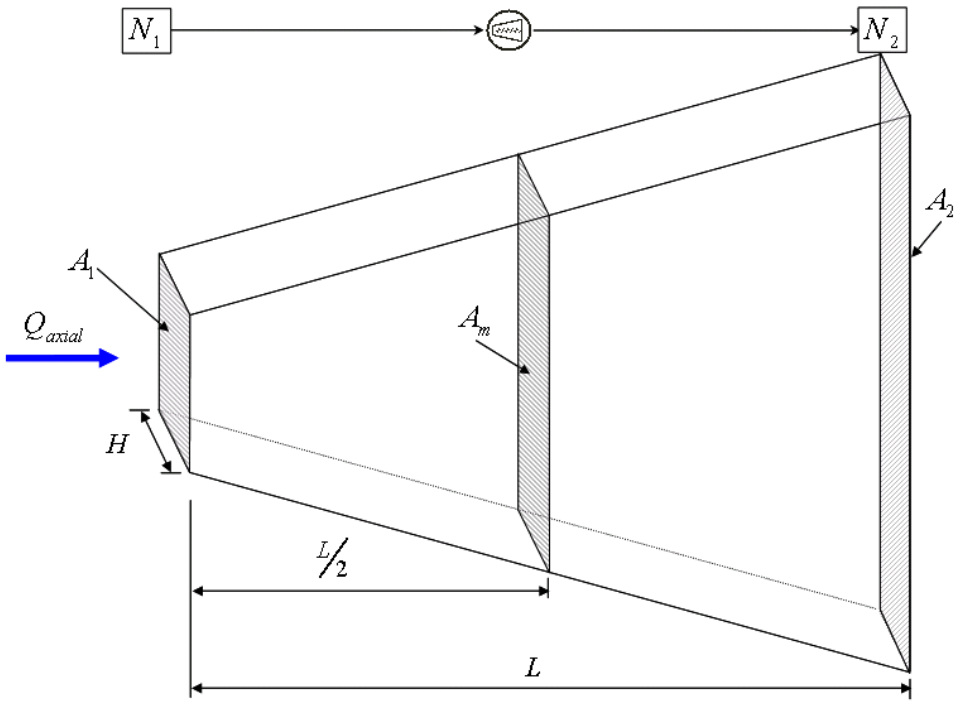

Figure 40: Typical Conduction heat transfer element layout (M-Tech Industrial, 2017)

$$m_{N1} = \rho V_1 = \rho \left(\frac{\varepsilon_1 A_1 + A_m}{2} \right) \frac{L}{2} \quad (5\text{-}3)$$

$$m_{N2} = \rho V_2 = \rho \left(\frac{\varepsilon_2 A_2 + A_m}{2} \right) \frac{L}{2} \quad (5\text{-}4)$$

Where:

$\forall_1$ and $\forall_2$ = up and downstream conduction heat transfer element volumes respectively

A_1 and A_2 = user specified up and downstream cross-sectional areas

A_m = the average area in between A_1 and A_2

ε_1 and ε_2 = the solid fraction of the up and downstream side, and

L = the length of the heat transfer path in the axial direction

5.2.1.4 Radiation heat transfer elements

The Surface Radiation element is used in Flownex to model radiation heat transfer between surfaces. The radiation can be between two solid nodes or between a solid node and a flow node or between two flow nodes (M-Tech Industrial, 2017). The radiation heat transfer between the surfaces in a two surface enclosure is calculated using equation (3-13).

5.2.1.5 Nodes and boundary conditions

A node can be used to denote an end point of an element or to represent a component (e.g. a tank or reservoir or reactor) in a system. There are two types of nodes namely; a solid node and a fluid node. A flow node is a type of node that is connected to a flow component, e.g. a pipe. The number of branching elements that can be connected to a node is unlimited.

A boundary condition component can be used to specify the boundary conditions of a network. When a system is modelled, the boundary conditions for the system can be specified at the relevant nodes through boundary condition elements. Boundary condition components can only be connected to a node component. The boundary condition at a node would then be the inlet and outlet condition for the adjacent element. There are several boundary conditions associated with a node that can be specified in various combinations for a node namely; pressure, temperature, height above datum level, quality (only valid when a two-phase fluid is used) and a mass source for a flow node. One can also specify a fixed heat transfer or a fixed temperature at a solid node.

5.2.2 Flownex Model Layout

A previous study by (Sambureni, 2015) done on a single prismatic block showed that Flownex (a system CFD code) can be used to build a network model of a prismatic block reactor. In the Sambureni (2015) study, however, the heat conduction was modelled only in the radial and tangential directions and discretization in the axial direction was not done. The heat generated in the fuel associated with a control volume was applied to the node within the control volume

that represented the interface between the fuel rods and the graphite, namely the wall of the representative fuel rod hole. A unit cell was used to calculate a conduction shape factor for heat transfer between the wall of the representative fuel rod hole and the representative coolant channel wall. The basic unit cell contains part of the graphite and the associated fuel elements and coolant channels.

In the current study, Flownex is used to predict the axial and transverse or radial and tangential temperature distributions within a single control volume of a hexagonal fuel block. The proposed model differs from the Flownet model (Van der Merwe, 2003; Rousseau & Greyvenstein, 2002 (b); Emslie, 2005) in that the prismatic fuel block is modelled in detail therefore employing multiple nodes to represent the fuel block, the fuel rods and the coated fuel particles. The discretization of the coated fuel particle is important because the temperature of the fuel kernel is a critical temperature in terms of fuel preservation. The current work describes the conceptual formulation of a model for the conduction path between the fuel rods and the coolant channels for a prismatic block using a unit cell as a foundation.

5.2.3 Assumptions and simplifications

In Flownex, a basic unit cell containing part of the graphite and the associated fuel elements and coolant channels was developed as explained in section 3.2.

- The effect of the dowel holes is negligible so symmetry can be assumed for $1/6^{th}$ or $1/12^{th}$ of a fuel block.
- Fuel rods and coolant channels are uniformly distributed throughout the cross-sectional surface perpendicular to the axial direction, i.e. the plan or top view of the fuel block.
- The fuel rods are the same height as the fuel blocks.
- The graphite plugs used to enclose stacks of fuel compacts are not modelled in Flownex.
- The fuel handling hole at the centre of the block is omitted.
- If the width of the bypass gap is defined as δ mm, the full width is associated with both of the adjacent blocks.
- Axial heat transfer and flow development in the reflector blocks is neglected as reflector blocks are not modelled in this work.
- Lumped burnable poison not modelled.

5.2.4 Components needed to build a core model

5.2.4.1 Standard fuel block

The approach to model a standard fuel block that was explained in sections 4.2 was used to create the Flownex network shown in Figure 41. Each of the $1/6^{th}$ segments is discretized into a number of control volumes to create grid models. Each control volume consists of a network of nodes, conduction and convection heat transfer elements and pipe elements and shown in Figure 41. These represent coated fuel particles layers, fuel rod/ compact radial layers, graphite block matrix and coolant channels. The network in Figure 41 represents an axial column of three CVs to form the full height of a fuel block and they are considered together to represent a typical Flownex fuel block control volume model.

Heat sources used were given in literature in the form of power per fuel block assembly or as a power density. A fuel block assembly, in the case of a PMR200 consists of six vertically stacked standard fuel blocks. Thus the thermal power for each standard fuel block can be determined from this value and can be further divided to obtain values for each control volume. The power per control volume is applied to each of the fuel kernel nodes or fuel rod nodes, depending on the model used.

The representative coated fuel particles are spherically discretized to contain one node for each layer. The centre node represents the centre of the coated fuel particle which is the fuel kernel. The other adjacent nodes represent each coating layer namely; porous PyC or buffer, inner pyrolytic carbon (iPyC), silicon carbide (SiC) and outer pyrolytic carbon (oPyC) layers. The conduction heat transfer elements represent conduction between these layers. Coated fuel particles are dispersed in the fuel rod graphite matrix and are modelled for each radial layer of the fuel rod. The outer three groups of four strings of coated particle nodes on the left in Figure 41 represent the coated fuel particle nodes for the three axial nodes. The coated fuel particle nodes have the fuel kernel centre temperature node on the left and the other nodes represent the buffer, iPyC, SiC and oPyC temperature nodes with conduction elements between them modelling conduction heat transfer. The network of coated particle nodes and conduction elements is then linked to the fuel road radial layer by the fuel rod centre temperature node. The fuel rod centre temperature node is mirrored for the coated particle and fuel rod network by using paste view which links the coated particle representative fuel rod centre temperature node to the actual corresponding node in the fuel rod. This nodes are then outer three groups of four strings of coated particle nodes and conductions components mean and how they are connected to the corresponding fuel rod nodes.

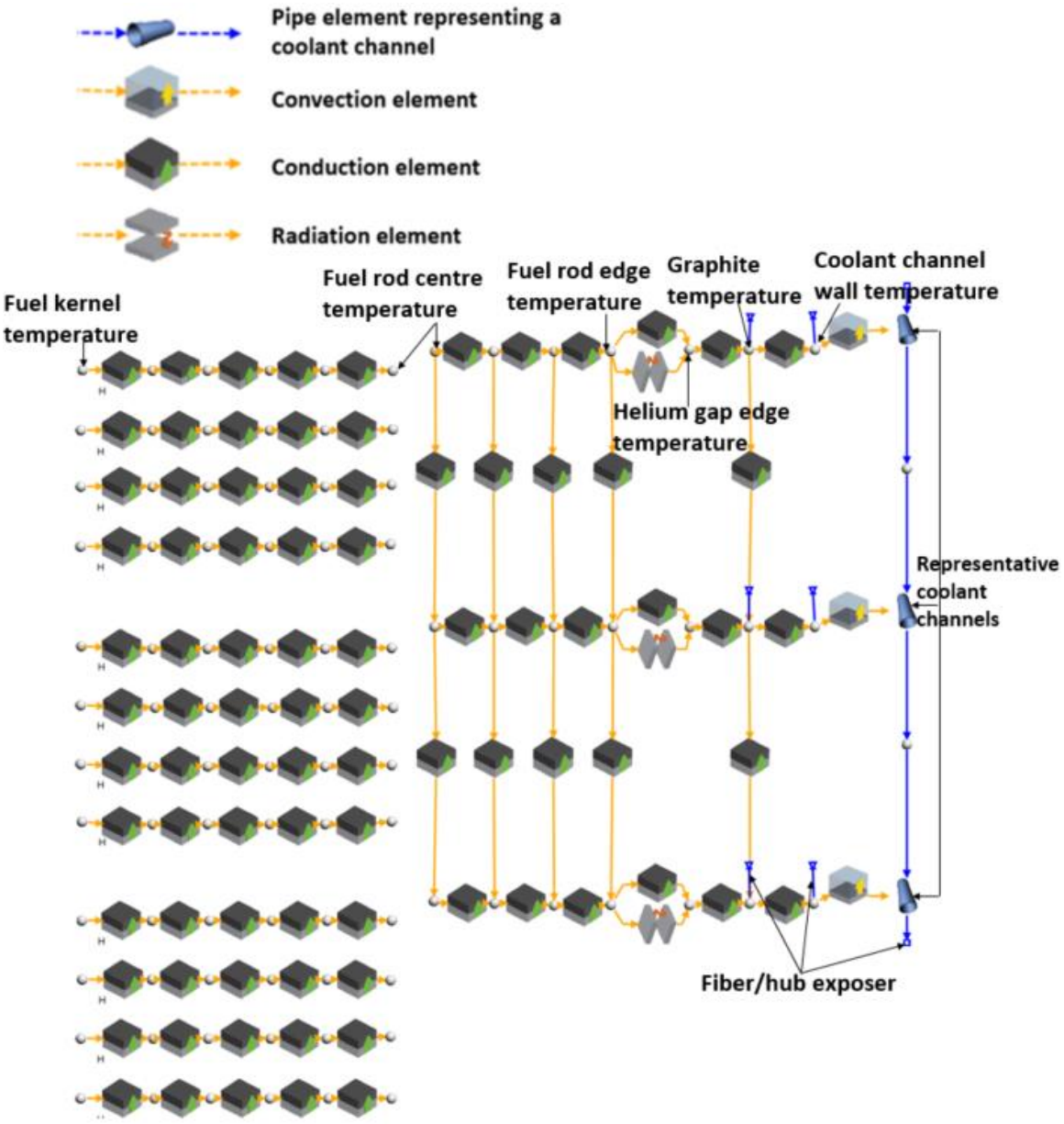

Figure 41: Typical fuel block Flownex control volume model

Each fuel rod then has a centre fuel rod temperature, two radial nodes within the matrix of the fuel rod and then a fuel rod surface temperature node. These nodes are connected by conduction heat transfer elements to model conduction within and to the edge of the fuel rod. The axial conduction components within the fuel rods (which are the primary fuel rod conduction components) that connect the three axial nodes for each radial layer of the fuel rod also constitute the volume or thermal mass of the fuel rods. The radial conduction components in the fuel rod and graphite have no mass associated with them.

The helium gap between the fuel rod and graphite block is modelled by conduction heat transfer and radiation elements for each axial node of the fuel block.

There are two conduction heat transfer elements on either side of the graphite node representing the conduction from the wall of the fuel rod hole to the graphite and conduction from the graphite to the coolant channel wall.

There is one node for the graphite block temperature for each fuel block axial element. This node gives the mass averaged temperature of the representative unit cell in the associated control volume.

The coolant channel wall nodes are then connected to representative coolant channel pipe components by convection elements stemming from each fuel block axial element.

Since the network shown in Figure 41 is the representation of a typical fuel block control volume it forms the basic building block that is used to create the computational grids or networks for fuel block models. The computational grid or network for the complete problem will therefore amongst others consist of a (large) collection of the basic CV building blocks joined together in the appropriate manner.

In order to de-clutter the models and reduce the load on the GUI, a compound component shown in Figure 42 was created to represent the control volume network in Figure 41. This was implemented in section 5.2.4.1.1. Hub exposers were added to the graphite and coolant wall temperature nodes at the top, middle and bottom of the control volume. This was done to allow for the connection of the nodes within compound components of different control volumes. A hub exposer allows connection to multiple nodes as a central control volume will need to be connected to all the other control volumes surrounding it. For the representative coolant channels, a fiber exposer was attached to the top and bottom representative coolant channels for each control volume.

For example if one were to connect a control volume within a compound component to an adjacent one, one would need to connect the graphite temperature hub for the top, middle and bottom axial nodes to the corresponding hub in the adjacent compound component. The coolant wall temperature nodes exposed fibers are used at the edge of the fuel block where for each control volume, the coolant wall temperature node fiber is connected to the convection element linking to the bypass gap pipe. The coolant wall temperature nodes fiber connection is also defined for the top, middle and bottom axial level nodes. To connect the flow channels, the

exposed fiber at the top of the control volume connects to the inlet boundary node if the control volume being simulated is at the top of the assembly or connects to the corresponding cross flow manifold node if the control volume is in a middle block in the assembly. The bottom exposed fiber connects to the outlet boundary node if the control volume being simulated is at the bottom of the assembly or connects to the corresponding cross flow manifold node if the control volume is in a middle block in the assembly. If only one block is being simulated then the top and bottom exposed fibers for the representative coolant channels will be connected to the inlet and outlet boundary nodes, respectively.

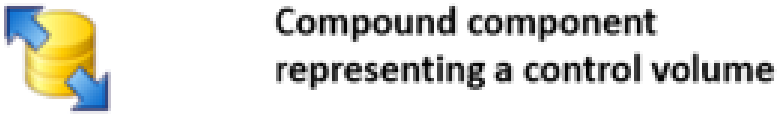

Figure 42: Flownex compound component representing a control volume network

5.2.4.1.1 1/6th of a standard fuel block

Using the heat transfer symmetry in the cross-section of the hexagonal fuel block, 1/6th of a fuel block was modelled in Flownex. In this study the basic unit cell concept was implemented in Flownex by first discretizing a 1/6th fuel block into a number of control volumes to create a grid as explained in section 4.3. The control volume model shown in Figure 41 was implemented in the grid that was created to form an nx5 node model. The n represents the discretization along the centreline in the radial direction. Five is the discretization in the tangential direction. For all the models, the axial discretization was kept constant at three nodes. In Figure 43 the Flownex model consisting of eleven radial increments (shown by the black numbers 1 to 11), five tangential increments (shown by the red numbers 1 to 5) and three axial increments (shown by the blue numbers 1 to 3) is shown. In this figure, one can see the implementation of the compound elements in the 11x5 grid. The compound components are interconnected to other tangentially and axially adjacent control volumes at each axial node. These connections between the control volumes within the block can be seen in Figure 43. To model the transfer of heat between two adjacent compound components (e.g. compound components numbered 6 and 7 in Figure 43) conduction elements were used. Since each compound component consists of three axial nodes (as shown in Figure 41), each of the three graphite axial nodes from compound component 6 would need to be connected to the corresponding graphite nodes in compound component 7 using exposed fibers explained in 5.2.4.1. The three conduction elements between compound component 6 and 7, represent the heat transfer between the top, middle and bottom graphite nodes.

The compound components at the outer edge of the 1/6th fuel block, shown by compound components 1 to 5 in red numbers in Figure 43 are linked to the bypass gap which is modelled by pipe elements. Fiber exposers at the top, middle and bottom of the graphite nodes are used to connect the convection elements to the pipe elements.

A grid dependence study was performed by varying the number of grid points in the radial and the tangential directions. The variation in the graphite temperatures along the centreline and outer edge were used as the measures. The inlet temperature was assumed to be 490 ℃ at a pressure of 7 MPa. The mass flow rate through the main coolant channels for the 1/6th fuel block was assumed to be 0.20117 kg/s and the power of 0.08656 MW with no bypass gap. The results are shown in Figure 44 and Figure 45, for the centreline and outer edge temperatures, respectively. It can be observed that as the number of nodes in the radial direction increase, convergence starts to show between the 11x5 and 13x5 grid models. Since there was only up to 0.026 ℃ change in the temperatures between the 11x5 and the 13x5 node grid, the graphite temperatures were observed not to change significantly between the two models. It was therefore concluded that the 11x5 node model to represent 1/6th of a fuel block is sufficient for the purposes of this study as further discretization will only result in very small changes in the temperatures.

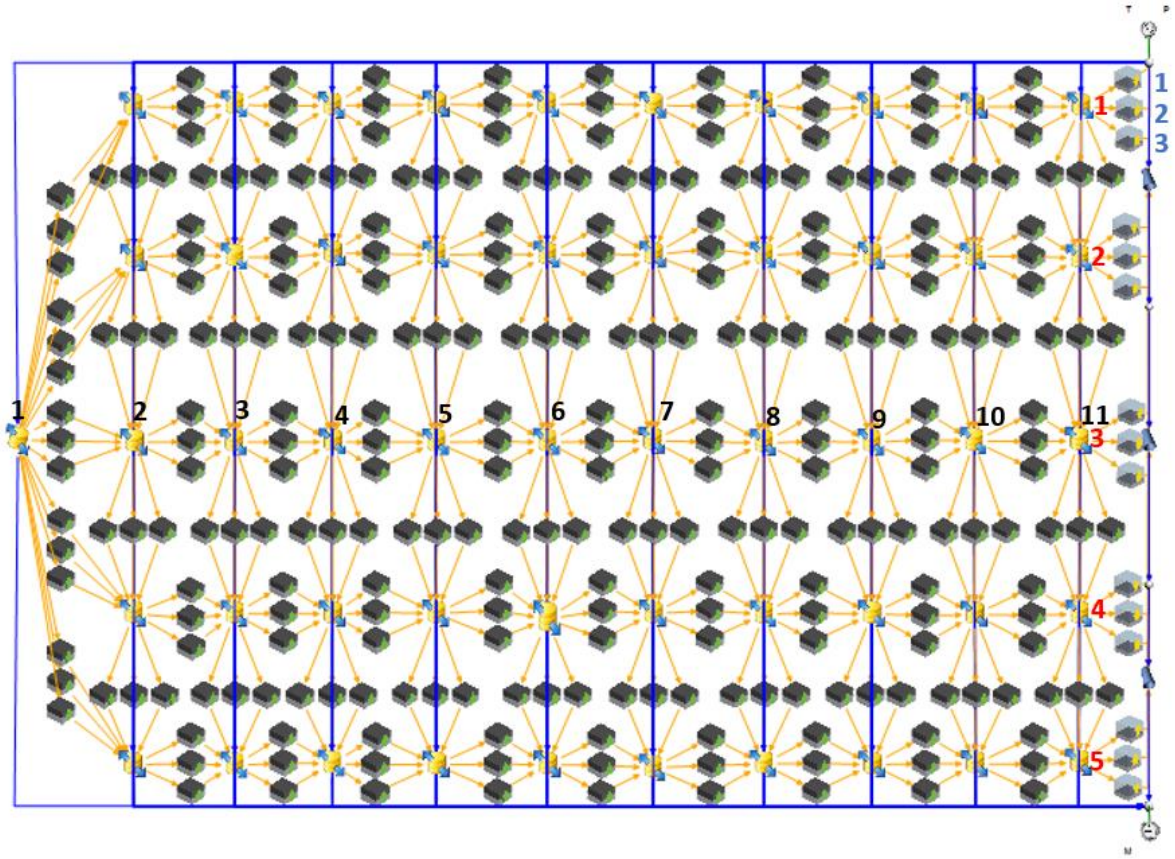

Figure 43: 11x5 node Flownex model of a 1/6th of a fuel block

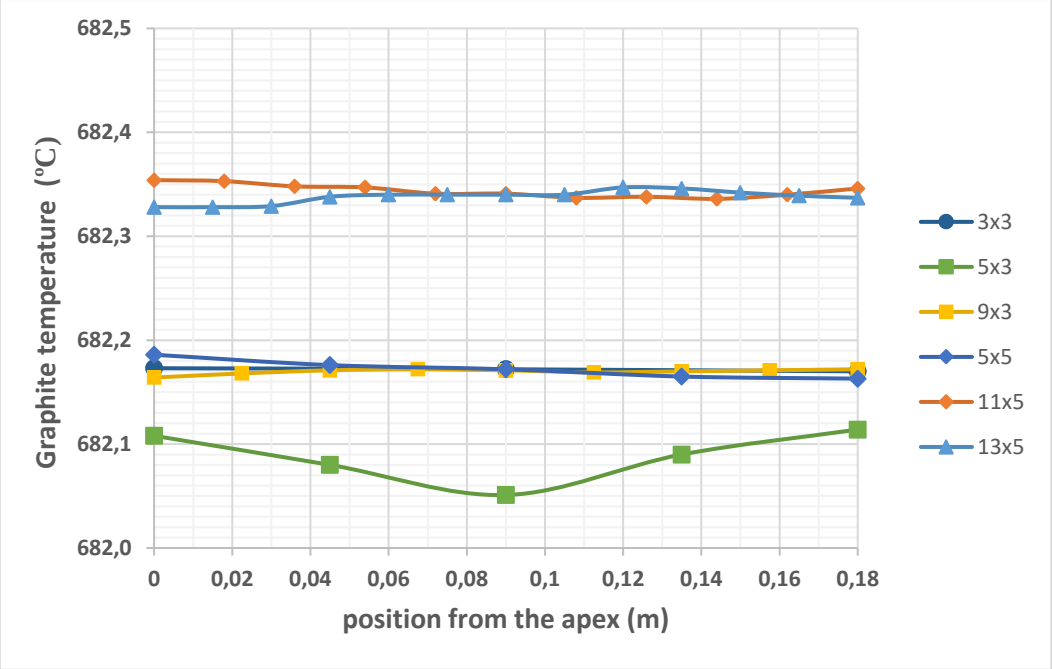

Figure 44: Centreline graphite temperatures for different node models for a 1/6th section of a fuel block

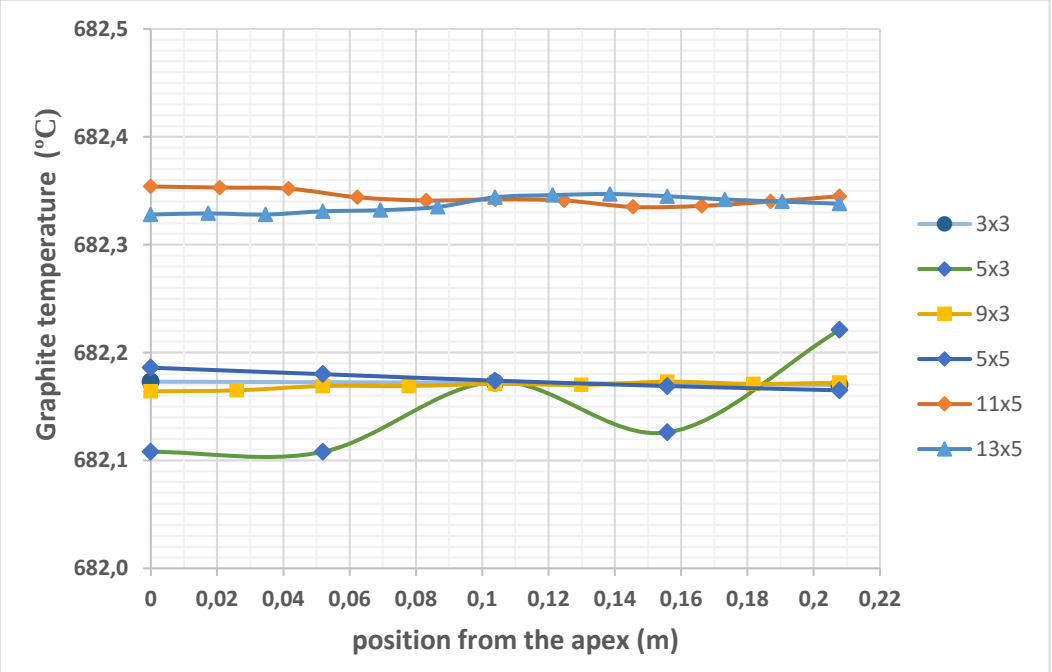

Figure 45: Outer edge graphite temperatures for different node models for a 1/6th section of a fuel block

5.2.4.1.2 Full fuel block

To build a fuel block model, six of the 1/6th fuel block models shown in Figure 43 are used. Firstly all the six the inlet and outlet boundary nodes and elements for the six segments are combined into one inlet/outlet node and boundary. Then the control volumes at the edges/interface between the 1/6th models were connected using infinite conductivity

conduction elements as shown in Figure 46 and discussed in section 4.12. Each control volume compound component has a coolant channel fiber exposed at the top and bottom for connection to a representative coolant channel inside the control volume. The fibers/coolant channel lines (indicated by blue lines in Figure 46) at the top of each control volume for all the six segments are all joined to the inlet boundary node and those from the bottom of all the control volumes linked to the outlet boundary node. The bypass gaps at the edge of each 1/6th segment are also connected to the inlet and outlet boundary nodes. The inlet and outlet boundary conditions are then updated to reflect those of a standard fuel block and not a 1/6th segment.

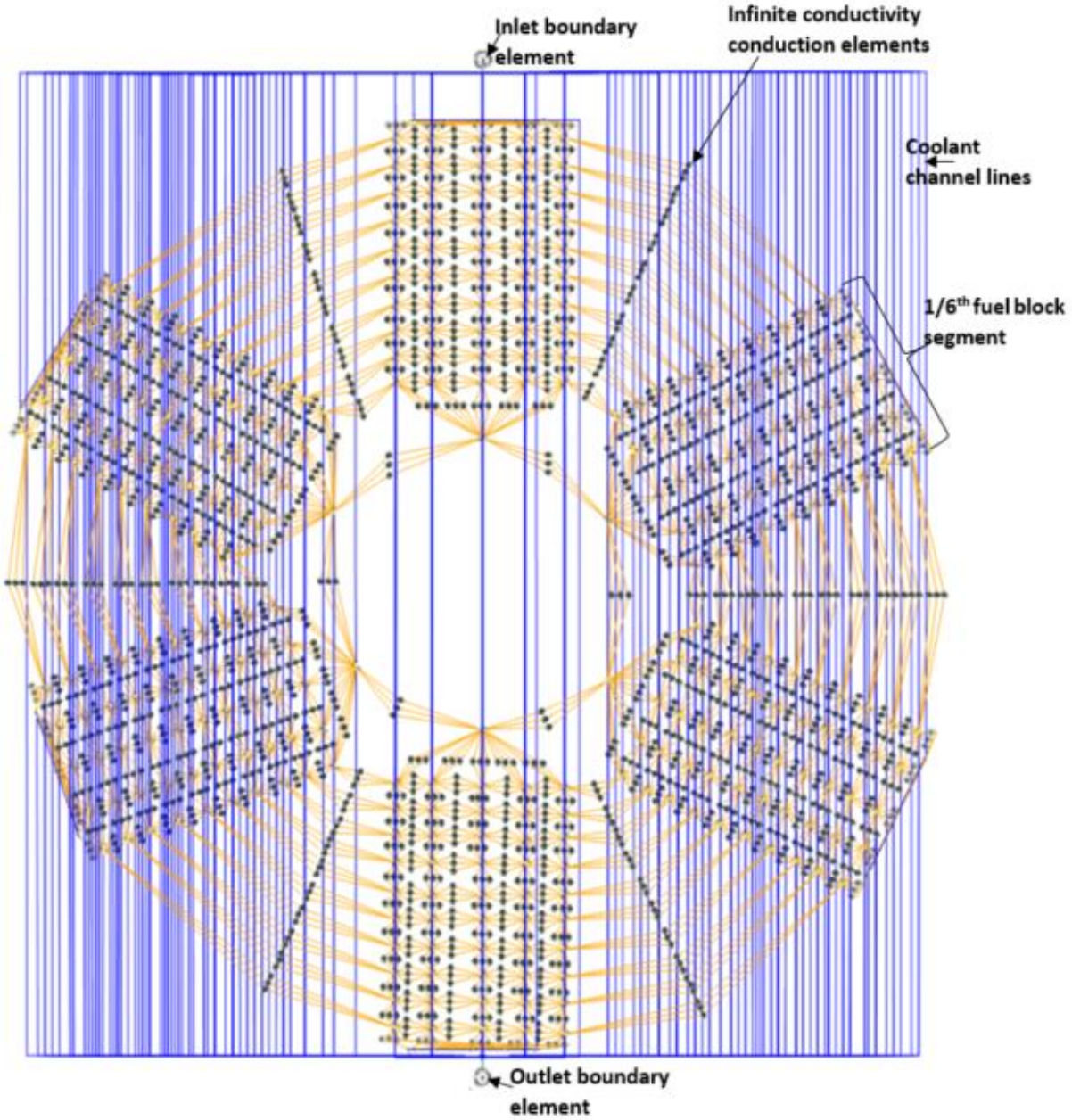

Figure 46: Flownex standard fuel block model

5.2.5 Fuel block Assembly

The active core of a PMR200 consists of hexagonal fuel blocks (introduced in section 5.2.4.1), vertically stacked to form a fuel block assembly (Tak, et al., 2008). In the construction of the Flownex model for the fuel block assembly, the fuel block model can be used as a building block. The cross flow gap between two stacked fuel blocks is modelled using pipe elements. The flow area through these pipe elements represents the cross flow area perpendicular to each control volume. These cross flow pipes are then connected to each other by nodes to form a cross flow manifold. In a fuel block assembly, there is a cross flow manifold between every two blocks and it represents the total cross flow area between the blocks. The manifold is also connected to the bypass gap at the edge of the block. In Flownex, the fuel assembly is then constructed by vertically linking the representative coolant channels in each of the control volumes of the fuel block segments to the cross flow manifold between the fuel blocks. The top most fuel block representative coolant channels are connected to the inlet boundary condition which specifies the inlet temperature and pressure. The middle blocks representative coolant channels are then connected to the cross flow manifold between the blocks whilst the bottom fuel block representative coolant channels are connected to the outlet boundary condition which specifies the mass flow rate.

5.2.5.1.1 1/6th Standard fuel block assembly

The 1/6th fuel block assembly model was developed by linking the respective control volumes for each of 1/6th fuel block models through the cross flow gap nodes as shown in Figure 47. Similarly, the inlet boundary condition which specifies the inlet temperature (at 490 °C) and pressure of 7 MPa is connected to the top of the fuel block assembly's representative coolant channels. The mass flow rate of 0.201167 kg/s was prescribed at the outlet boundary condition connected to the bottom fuel block.

5.2.5.1.1 Full Standard fuel block assembly

The whole standard fuel block assembly model was developed in a similar manner to the 1/6th fuel block assembly using the model shown in Figure 46. This model, however, only consisted of three standard fuel blocks due to the size of the model and the Windows screen memory limiting the Flownex graphical user interface (GUI) capability to display the larger models. It might be possible to overcome the problem by putting the models for the various layers on separate pages and then to use copies (views) of nodes on the pages to link the models. The other alternative would be to put a full fuel block into a compound but this might become very complex.

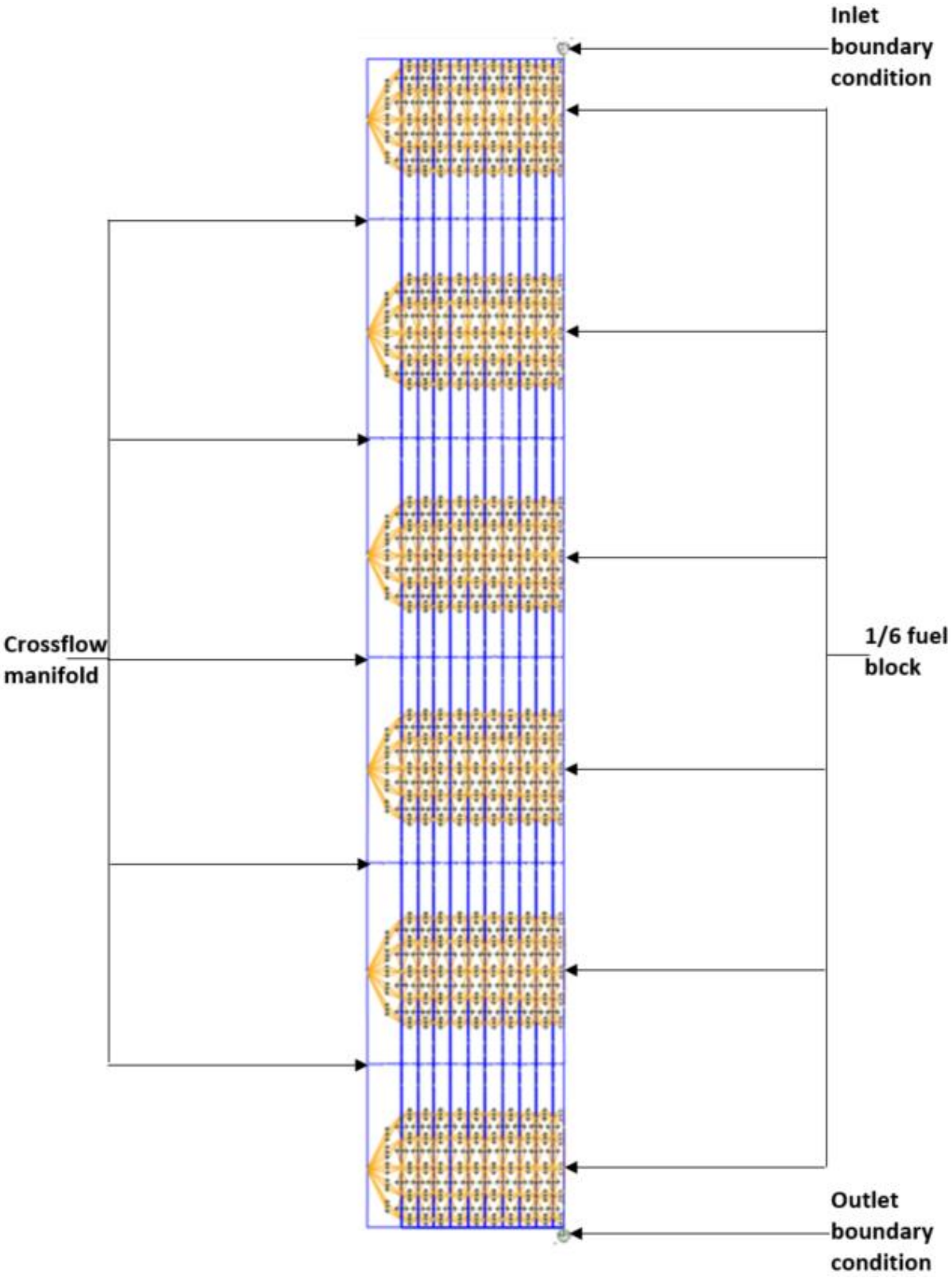

Figure 47: 11x5 node Flownex model of a 1/6th assembly with 6 blocks and cross flow

5.2.6 Control rod block

Selected fuel blocks contain channels for insertion of reserve shutdown material. The control rod and reserve shutdown control assemblies are located in penetrations in the top head of the reactor vessel. The reserve shutdown material channel is blind in the bottom-most fuel row in these selected elements. Boronated graphite pellets housed in hoppers above the core provide a reserve shutdown capability. Upon actuation, these pellets drop into channels in selected columns of the active core to provide reactor shutdown in the event that the control rods are inoperable, or if necessary, to provide additional shutdown margin over what may be provided by the control rods located in the hexagonal side reflector. (General Atomics, 1992).

Twelve reserve shutdown fuel elements differ in that they contain a 95.25 mm diameter channel for reserve shutdown material. This channel replaces 20 fuel and 12 coolant holes (General Atomics, 1992). The control fuel block has 186 fuel holes and 95 coolant channels and one control hole. They have the same array of coolant holes as the fuel element and the same holes for the insertion of reactivity control devices.

To build a control block model in Flownex, the model could be adapted from the $1/6^{th}$ fuel block model and to accommodate the fuel rod hole, the thermal conductivity can be adjusted. As explained in section 4.8, equation (4-24) is used to calculate the solid fraction in the graphite. In this case, to obtain the solid fraction, the area occupied by the coolant channels and by the control rod hole will be subtracted from the total area of the control volume to get the area occupied by the solid material. The control rod or reserve shutdown hole could also be modelled using pipe elements with zero mass flow and connected to the surrounding CVs via convection components. A model for a control and reserve shut down fuel blocks were not developed during the study.

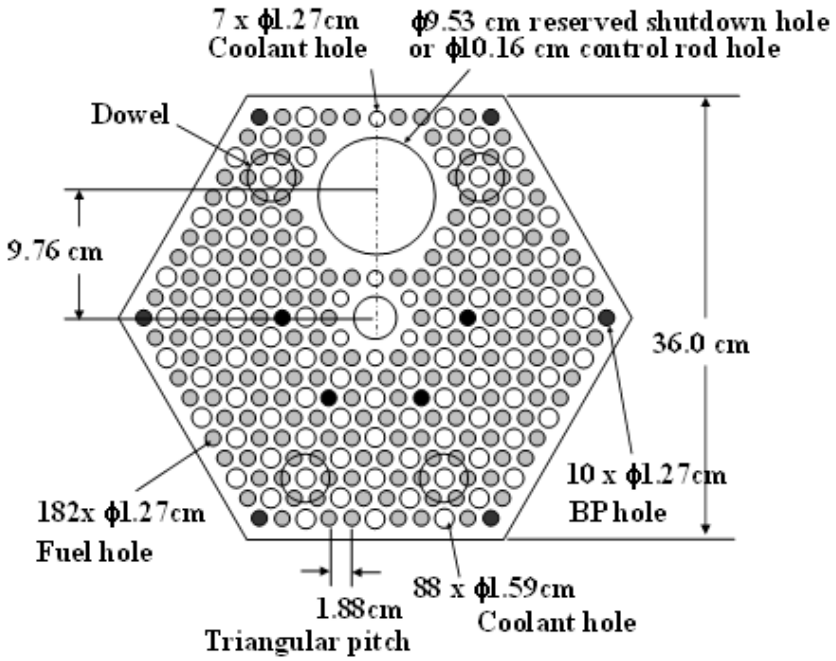

Figure 48: Control rod block dimensions (Tak, et al., 2012)

5.2.7 Graphite reflector block

The hexagonal H-451 graphite reflector blocks have a similar size, shape, and handling hole to the fuel elements (except that some are half-height or three-quarter height). Differences exist in the hexagonal reflectors, depending on their locations in the core, i.e., top, bottom, side, and central reflectors which are described below.

The reflector above the active core is composed of two layers, a layer of full-height elements over a layer of half-height elements. The top reflector elements channel coolant flow to the active core and provide for the insertion by gravity, of reserve shutdown material into the active core.

The bottom reflector under the active core is also composed of two layers, a layer of three-quarter height elements over a layer of half-height elements. The bottom reflector elements provide for the passage of coolant from the active core into the core support. In the standard columns, this is accomplished by collecting the coolant channel flows into six intermediate coolant holes 68 mm in diameter. The channel for the reserve shutdown material is blind and stops in the lower reflector (General Atomics, 1992).

To create a graphite reflector block model in Flownex, the model could be derived from the standard fuel block model and adapted by plugging the fuel holes with graphite to form a graphite block. The graphite block model was not developed during the study.

5.3 CORONA Model Layout

5.3.1 CORONA

CORONA was developed by KAERI for the whole-core thermo-fluid analysis of a prismatic gas cooled reactor. It is a system CFD code developed as one of the numerical codes by the NHDD department. CORONA is meant to bridge the gap between system codes, whose mesh is too coarse for detailed thermo-fluid analyses of a prismatic fuel block, and CFD. Through efficient grid generation and numerical methods, fast computation of whole-core thermal fluid analysis with reasonable accuracy can be achieved. CORONA therefore solves the three-dimensional heat conduction equation for a solid using the finite volume method similar to that in CFD calculations. It follows an approach similar to that adopted by system codes for the fluid flow by solving one-dimensional conservation equations (Tak, et al., 2014).

CORONA was tested against commercial CFD codes such as CFX that are believed to be able to solve a multi-dimensional heat conduction problem accurately. It has also been validated against experiments (particularly, the airflow experiment performed by (Kaburaki & Takizuka, 1987) for 1-D fluid flow (Tak, et al., 2014).

The 3-D solid heat conduction equation through a hexagonal fuel block with coolant channels and fuel compacts is given as (Tak, et al., 2012) (Tak, et al., 2014):

$$\frac{\partial}{\partial t}(\rho_s C_s T_s) + \nabla \cdot (-k_s \nabla T_s) = q_s''' \tag{5-5}$$

In CORONA, q_s''' is a heat source due to the fuel compact and it is zero in the graphite matrix. The helium gap between the fuel compact and graphite was treated as a solid area using an effective thermal conductivity to represent conduction and radiation heat transfer. The radiation heat transfer between fuel blocks was not considered. The maximum temperature of a fuel kernel is calculated with the resistance model (Lee, et al., 2016 (b)).

$$T_{kernel} = T_\infty + R \times q_{kernel}''' \tag{5-6}$$

The resistance (R) of the triso-coated fuel particle consists of the resistances due to the fuel kernel, buffer, iPyC, SiC and oPyC is given by equation (5-7):

$$R = R_{kernel} + R_{buffer} + R_{iPyC} + R_{SiC} + R_{oPyC} \tag{5-7}$$

The 1-D governing equations for continuity, momentum and energy as applied in CORONA are given in equation (5-8) to (5-10).

$$\frac{\partial \rho_f}{\partial t} + \frac{\partial(\rho_f w A)}{A\,\partial z} = 0 \tag{5-8}$$

$$\frac{\partial(\rho_f w)}{\partial t} + \frac{\partial(\rho_f w^2 A)}{A\,\partial z} + \frac{\partial p}{\partial z} + f\frac{\rho_f w|w|}{2D_H} = 0 \quad (5\text{-}9)$$

$$\frac{\partial(\rho_f C_f T_f - p)}{\partial t} + \frac{\partial(\rho_f w A C_f T_f)}{A\,\partial z} - q'''_{conv} = 0 \quad (5\text{-}10)$$

The coupling between the three-dimensional solid model and the one-dimensional fluid model uses typical Nusselt number correlations given by equations (5-11) and (5-12) for fully turbulent forced convection (Tak, et al., 2014) (Lee, et al., 2014) (McEligot, et al., 2006).

$$\text{Modified Dittus-Boelter } Nu = 0.021 \times Re^{0.8} Pr^{0.4} \quad (5\text{-}11)$$

$$\text{Gnielinski } Nu = \frac{(f/8)\times(Re-1000)\times Pr}{(1+12.7\times\sqrt{(\frac{f}{8})}\times(Pr^{\frac{2}{3}}-1)} \left(\frac{T_w}{T_b}\right)^{-0.45} \left(1 + \left(\frac{x}{D}\right)^{-\frac{2}{3}}\right) \quad (5\text{-}12)$$

where f is the Darcy friction factor.

The Nusselt number for laminar flow is assigned a value of 8.23 for a plate and 4.364 for a tube.

The heat transfer coefficient is evaluated by equation (5-13) (Tak, et al., 2012).

$$h = Nu\frac{k_f}{D_h} \quad (5\text{-}13)$$

The cross flow gap loss coefficient was obtained using existing correlations given in equations (5-14) (Kaburaki & Takizuka, 1987) and (5-15) (Groehn, 1982) (Lee, et al., 2016 (a)).

$$K_{Ka} = \frac{(\frac{C_1}{\delta Re} + C_2)}{\delta^2} \times A_{gap}^2 \quad (5\text{-}14)$$

$$K_{Gr} = (\frac{A_{gap}}{A_c})^2 \left[3.58(\frac{\delta}{D})^{-2.3} \times 6.33(\frac{A_{gap}}{\delta l})^{-1.68}\right] \quad (5\text{-}15)$$

Where A_{gap} is the cross flow gap area; A_c is the coolant channel area; and δ is the cross flow gap width.

5.3.2 CORONA assumptions and simplifications

CORONA uses a basic unit cell concept for generating computational grids using several types of basic unit cells shown in section 2.1.1.2 to model the heat transfer through the hexagonal blocks and a 1-D formulation to model the flow through the coolant channel.

5.4 Summary

In this chapter, the philosophy to model a prismatic block-type HTR employing a Flownex thermal-hydraulic network was implemented. The building blocks for the models and the simplifications made in the building of the models were discussed. The construction of a single control volume up to a complete a standard fuel block assembly was illustrated. The approach to building a graphite reflector block and a control rod block was also discussed.

6 VERIFICATION AND VALIDATION

6.1 Validation of the HTGR core Flownex model

In this chapter, a few selected validation and verification cases for the Flownex models will be presented. The verification cases include single fuel unit cell with surrounding graphite, 2-D integrated prismatic fuel block, 3-D integrated prismatic fuel block and fuel block assemblies. Several conditions were studied for their effect on temperature profiles within the standard fuel block. These include cross flow, bypass gap size and coolant channel blockage accident in a $1/6^{th}$ assembly and in a standard fuel block. A transient was also modelled to demonstrate Flownex capabilities.

6.2 Heat transfer in a single fuel unit cell with surrounding graphite

In this section, a grid independence test was performed on the basic fuel unit cell introduced by Tak et al. (2014) and implemented in CORONA in order to validate and verify the multi-dimensional heat conduction within the fuel and to the surrounding graphite. 1-D models of the single unit cell containing a fuel compact, helium gap and surrounding graphite region shown in Figure 49 were developed using Flownex and CORONA. In the compact, a uniform heat generation was assumed and the outside temperature of the surrounding graphite was fixed. The results of the simulations will be compared with the corresponding results obtained from the CORONA code of the same model to verify the Flownex results.

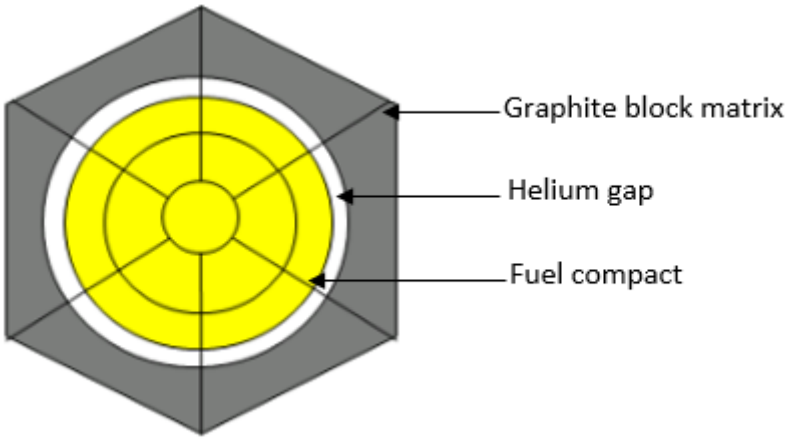

Figure 49: Fuel basic unit cell as defined in CORONA (Tak, et al., 2014)

The properties and boundary conditions for the fuel unit cell considered are shown in Table 9.

Table 9: Fuel unit cell properties and boundary conditions (Tak, et al., 2014)

Unit cell pitch (side of the hexagon) (cm)		1.0885188
Fuel compact radius (cm)		0.6225
Fuel hole radius (cm)		0.635
Fuel rod height (cm)		73.92
Thermal conductivity (W/mK)	Fuel	10
	Helium gap	0.4
	Graphite	30
Power density MW/m^3		28.76
Fixed outside temperature (°C)		1023.9

6.2.1 Approximation of the area of the surrounding graphite

To simplify the calculation, the area around the fuel compact could be estimated using one of the cases listed below:

Case 1: Hexagon Circumscribed About A Circle

Consider a hexagon circumscribed about a circle as shown in Figure 50. If R is the apothem of the triangle marked in Figure 50, then the adjacent angle would be 30º.

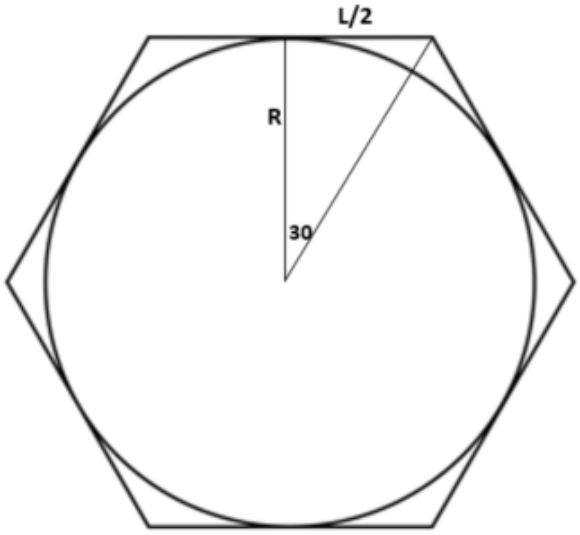

Figure 50: Hexagon Circumscribed About A Circle

$$\therefore R = \frac{w}{2\times\tan(30°)} = \frac{\sqrt{3}w}{2} = \frac{1.0885188\times\sqrt{3}}{2} = 0.942684933 \text{ cm} \quad (6\text{-}1)$$

So, the diameter of the circle in terms of the side length of the hexagon would be:

$$D = \sqrt{3}w$$

So the thickness/length of the graphite area is $L_{graphite} = 0.942 - 0.635 =$ 0.307684933 cm

Conduction area of graphite

$$A_{graphite1} = \frac{\pi h(d_o+d_i)}{2} = \pi \times 0.7392 \times \frac{((0.942\times2)+(0.635\times2))}{2} = 0.03663803\ m^2 \quad (6\text{-}2)$$

Case 2: Hexagon Inscribed In A Circle

If we now consider a hexagon inscribed in a circle as shown in Figure 51 and let R be the radius of a circle and the side of a hexagon.

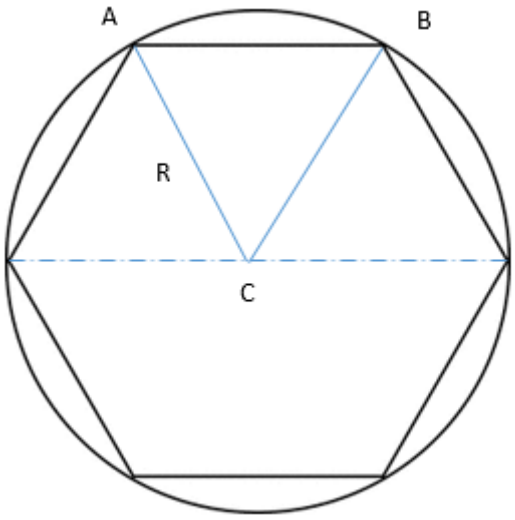

Figure 51: Hexagon Inscribed in a Circle

Since triangle ABC is an equilateral triangle, then the R is the same as the length of the side of the hexagon. R is given as, 1.0885188 cm and the radius of the fuel hole is 0.635 cm. So the thickness or length of the graphite area is $L_{graphite} = 1.0885188 - 0.635 = 0.4535188$ cm

Case 3: Area of a circle of equivalent area to the hexagon

In this case the area of the fuel unit cell hexagon in Figure 52 is approximated with an equivalent circle.

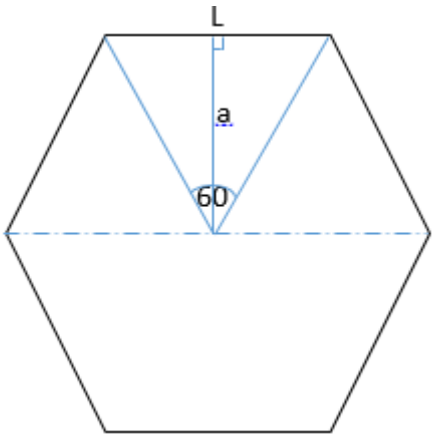

Figure 52: Hexagon

$$\text{Area of hexagon, } A_{hex} = 6 \times \left(\frac{1}{2} \times L \times a\right) \quad (6\text{-}3)$$

$$= 6 \times \left(\frac{1}{2} \times 1.0885188 \times \frac{1.0885188}{2 \times \tan(30°)}\right) = 3.078390817 \text{ cm}^2$$

$$\text{Area of equivalent circle: } A_{eq} = \pi R_{eq}{}^2 = 3.078390817 \text{ cm}^2$$

Therefore the radius of the equivalent circle is $R_{eq} = \sqrt{\frac{A_{eq}}{\pi}} = \sqrt{\frac{3.078390817}{\pi}} = 0.9898900$ cm. Thus the thickness or length of the graphite area is $L_{graphite} = 0.989890009 - 0.635 = 0.354890009$ cm, which is approximately the average of the first two scenarios. This is the value that was adopted for the length of the graphite area for all the fuel rod unit cell Flownex models.

6.2.2 Test cases for different fuel cell mesh sizes

The single fuel unit cell was modelled in Flownex for different mesh sizes that match the CORONA model. The different mesh sizes information is given in Table 10.

Table 10: Grid sizes of single fuel unit cell models

Region	Coarse mesh	Medium mesh	Fine mesh
Fuel	2	4	7
Helium gap	1	2	4
Graphite block	2	3	5

6.2.2.1 Flownex models

6.2.2.1.1 Coarse mesh

The coarse mesh model consists of two conduction elements in the fuel cell, one set of conduction and radiation elements in the helium gap and two in the graphite block region as shown in Figure 53.

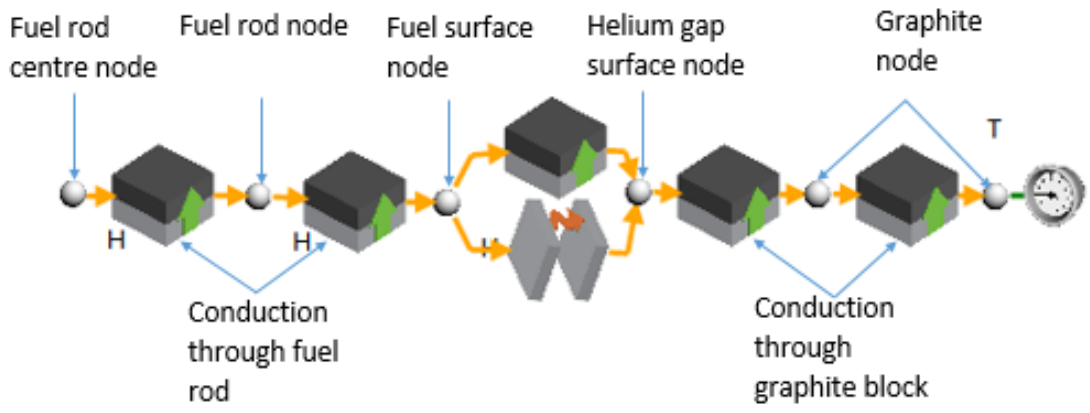

Figure 53: Flownex network for a fuel cell coarse mesh

6.2.2.1.2 Coarse to medium mesh implemented in Flownex

The coarse to medium mesh comprises of three conduction elements in the fuel rod, one set of conduction and radiation elements in the helium gap and two conduction elements in the graphite block region and is shown in Figure 54. This is the mesh size that was implemented in Flownex for the discretization of the fuel rod in the fuel block models.

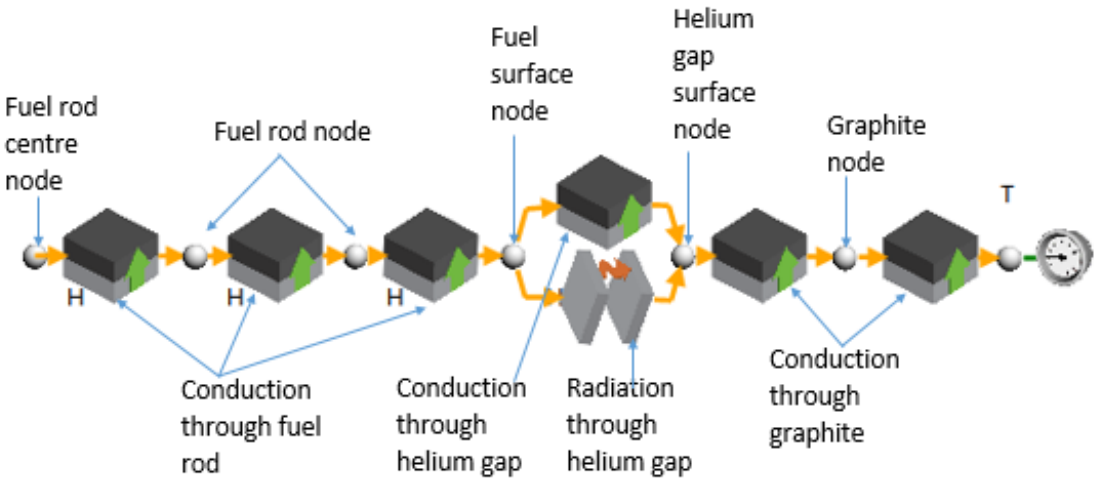

Figure 54: Flownex model for a fuel cell coarse to medium mesh

6.2.2.1.3 Medium mesh

The medium mesh contains four conduction elements in the fuel rod, two sets of conduction and radiation elements in the helium gap and three conduction elements in the graphite block region. The medium mesh Flownex model is shown in Figure 55.

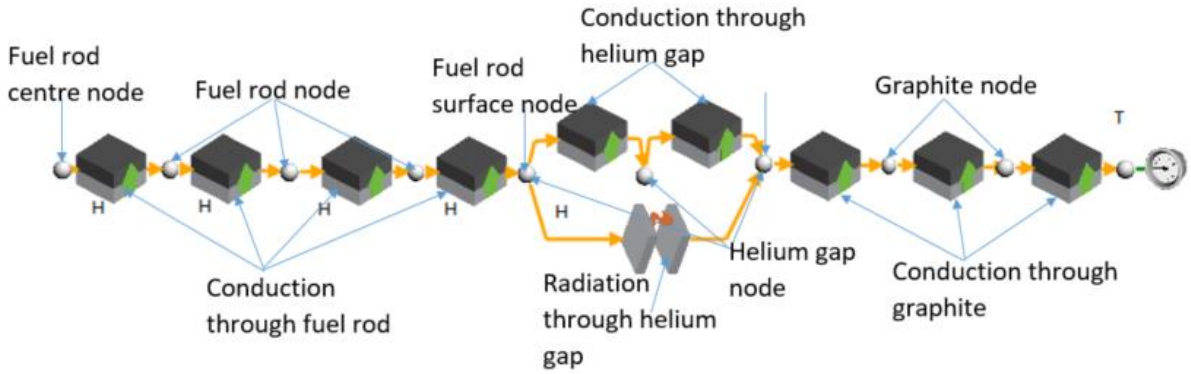

Figure 55: Flownex model for a fuel cell medium mesh

6.2.2.1.4 Fine mesh

The fine mesh model consists of seven conduction elements in the fuel rod, four sets of conduction and radiation elements in the Helium gap and five conduction elements in the graphite block region as shown in Figure 56.

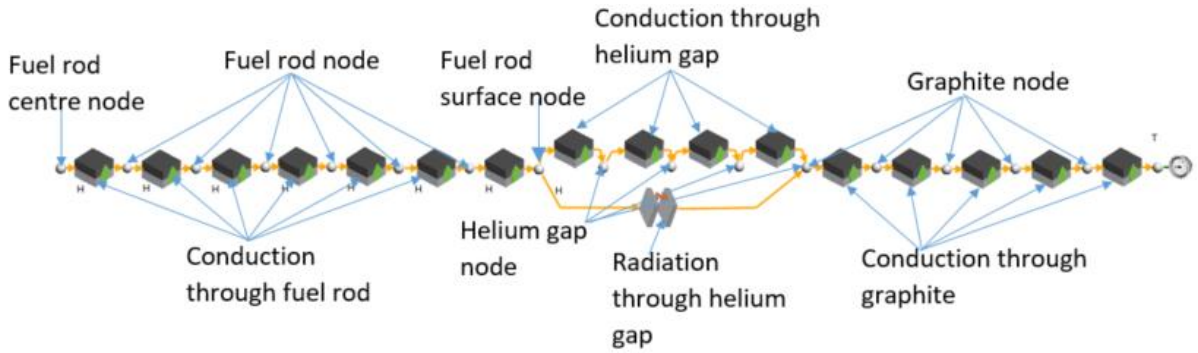

Figure 56: Flownex model for a fuel cell fine mesh

6.2.3 Results for different fuel cell mesh sizes

Figure 57 shows the Flownex predicted temperature distribution in the fuel unit cell for the different mesh sizes compared to CORONA results.

The temperature of the fuel cell is highest at the centre, decreases gradually through the radial length of the fuel unit cell and a sharp drop in the temperature across the helium gap. The coarse mesh model predicted a centre temperature of 1085 °C while the medium mesh predicted 1086 °C and the 1088 °C was predicted by the fine mesh model. The maximum difference in the centre temperatures was found to be 3 °C. The fine mesh model matches the CORONA results very closely. Since the temperatures do not differ by a maximum of 3 °C, it was decided that the coarse mesh is sufficient to implement in the Flownex models to reduce the number of elements used to build the network.

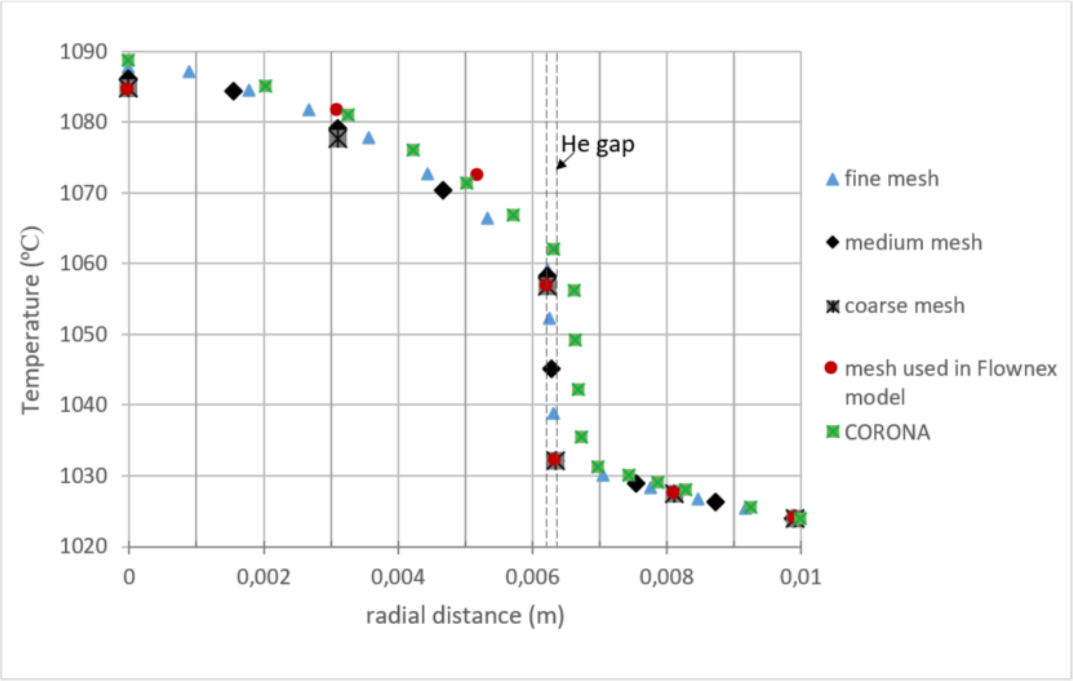

Figure 57: Flownex fuel rod temperatures for different mesh sizes compared to CORONA results

6.3 2-D Integrated prismatic block Flownex model

As a first approximation, a 2-D Flownex model of a 1/6th prismatic fuel block of a PMR200 was created by Sambureni (2015). In the 2-D Flownex model, the lumped burnable poisons and the fuel compacts were not modelled explicitly. The heat generated in the fuel was uniformly distributed in the nodes. The heat source was therefore applied at the node which lies on the surface of the fuel rod channel (interface between fuel rod and graphite). The heat transfer was modelled as dominant in the radial direction and the heat transfer in the tangential direction was modelled by employing cross-conduction elements. The total coolant mass flow rate of the helium through the fuel block was taken as 0.358 kg/s and the surface roughness of 20 µm was assumed for the coolant channels and the bypass gap (the gap between adjacent fuel blocks). This model was verified using a STAR-CCM+ model. The parameters used by Sambureni (2015) for the Flownex and STAR-CCM+ models are shown in Table 11 and Table 12. For both models, a boundary condition of 490 °C for the coolant inlet temperature and a pressure of 7 MPa was prescribed. In the case of the STAR-CCM+ model, the lumped burnable poison and fuel rods were assumed to be the same material properties as the graphite block.

Table 11: Parameters used to simulate 1/6th fuel block in Flownex (Sambureni, 2015)

Number of standard coolant channels	18
Number of fuel rods	35
Diameter of coolant channels (cm)	1.59
Area of coolant channel (cm^2)	1.99
Area of 1/6th segment (cm^2)	187.1
Height of a block (cm)	79.3
Total heat input (kW)	98
Bypass gap width (mm)	1
Mass flow rate (kg/s)	0.3588
Thermal conductivity (W/m.K)	52.7

Table 12: Parameters used to simulate 1/12th fuel block in STAR-CCM+ (Sambureni, 2015)

Number of standard coolant channels	8.5
Number of small coolant channels	0.5
Number of lumped burnable poison rods	0.5
Block height (cm)	79.3
Bypass gap width (mm)	0.5
Volumetric heat source (MW/m^3)	27.8

In the STAR-CCM+ model, a constant velocity was applied at the inlet to the bypass gap of 0.5 mm width and adjusted to give a mass flow of 0.002 kg/s. In this case the Reynolds number

still falls within laminar flow region. The Flownex model that matches the STAR-CCM+ bypass gap flow rate was achieved with a 1 mm bypass gap width.

In the present work, an improvement to the fuel block Flownex model was added by discretizing the block in the axial direction thereby creating a 3-D Flownex model. The axial direction was chosen as the primary direction for conduction heat transfer within the block. For direct comparison, the same modelling parameters as in Table 11 were used. Only the results of the 3-D Flownex model will be shown here for the purpose of comparison with the 2-D Flownex model. The details of the 3-D integrated block Flownex model will be discussed in section 6.4.

Figure 59 and Figure 60 show a comparison of results for temperature distribution for steady state simulations of the 2-D and 3-D $1/6^{th}$ prismatic fuel block Flownex models and the STAR-CCM+ model. Since there was no discretization (or only one increment) in the axial direction in the original 2-D Flownex model, the temperature distributions shown are representative temperatures of each control volume halfway through the height of the block. The 2-D Flownex results indicate the fuel surface, graphite and representative coolant channel temperatures which were obtained from the fuel nodes, graphite nodes and the pipe elements respectively. Also, the fuel compact temperature in the 2-D Flownex model, was taken at the interface between the fuel compact and the block graphite as the helium gap was not modelled.

The STAR-CCM+ results show a 3-D distribution of the temperature for the integrated $1/12^{th}$ fuel block model with a volumetric heat source of 27.8 MW/m^3. The results plotted were obtained from the middle line probe inserted halfway through the height of the fuel block. Figure 58 shows temperature contours for the $1/12^{th}$ block obtained from STAR-CCM+. The centreline plane of the $1/12^{th}$ model (which coincides with the centreline for the $1/6^{th}$ Flownex model) is shown by plane ABCD in Figure 58 and the outer edge shown by plane AFED.

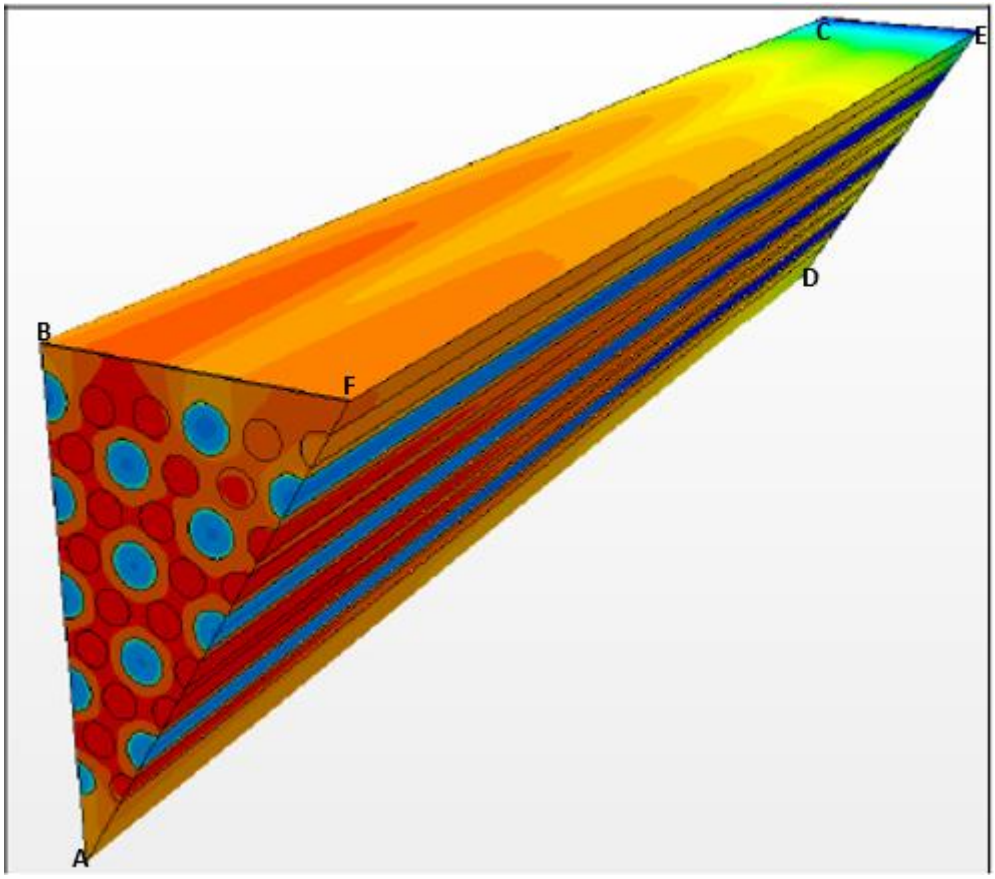

Figure 58: STAR-CCM+ temperature contours for a steady state solution for 1/12th fuel block model (Sambureni, 2015)

The level of discretization into control volumes of the 3-D Flownex model allows one to get the radial, tangential and axial temperature distribution results within the fuel block. The results shown for this model are for the representative, surface and centre temperatures of the representative fuel compact, graphite and coolant channel and were taken halfway through the height of the fuel block. In the 3-D Flownex model, it is possible to take the fuel compact temperature at the centre and at the surface of the fuel compact since the fuel rod was also discretized into radial layers.

Figure 59 shows a comparison between the results for temperature distributions for steady state simulations along the centreline of a 1/6th prismatic fuel block (along line BD in Figure 32) obtained by the 2-D and 3-D Flownex and the STAR-CCM+ models.

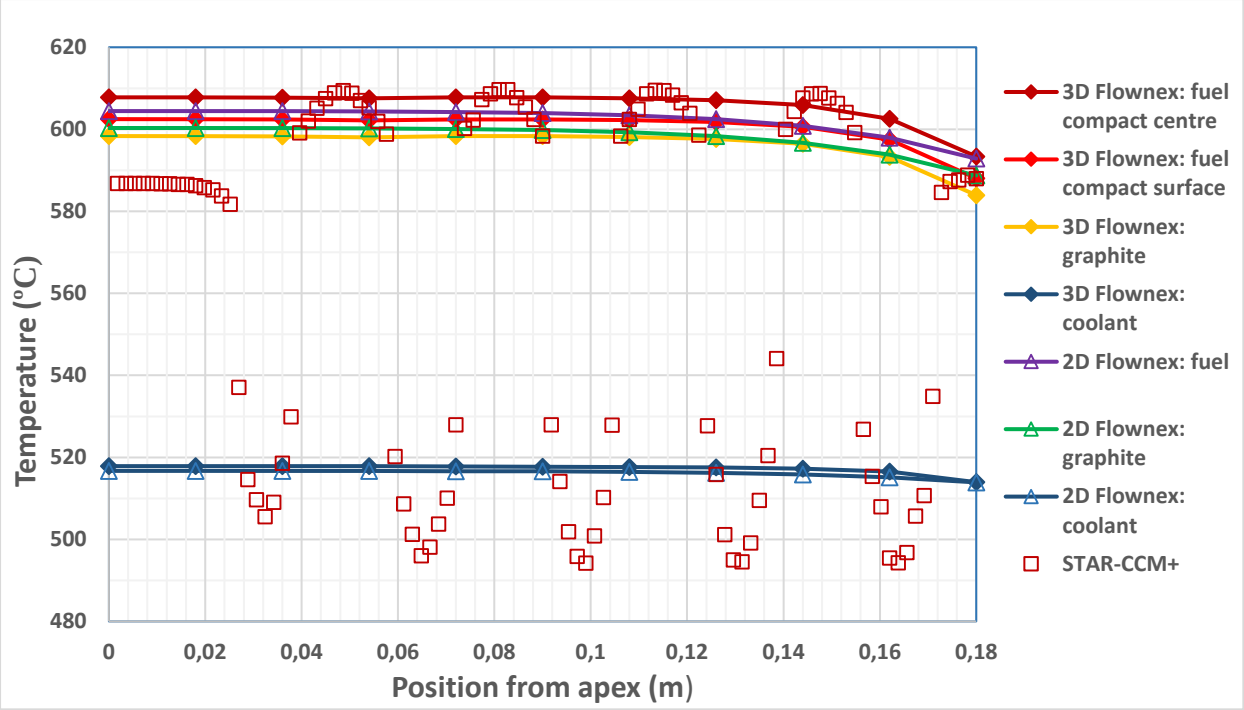

Figure 59: Temperature distributions along the centreline for STAR-CCM+ and Flownex for the integrated block

In the 2-D Flownex model, the fuel rod or compact was not modelled but rather the fuel temperature shown was that of the fuel surface. In this model, the average exit temperature of the helium was found to be 542.98 ℃.

The STAR-CCM+ results show peaks in temperature near each fuel rod and minimum temperatures near each coolant hole. The average exit temperature of the helium was found to be 542.94 ℃ for the STAR-CMM+ model. The four peaks correspond to the maximum temperatures of the four fuel regions close to line AB in Figure 58.

In the 3-D Flownex model, the highest temperature is that of the fuel compact centre. The heat is then transferred through conduction and to the matrix within the fuel compact. The temperature then drops further in the surrounding block graphite. The temperatures were seen to be fairly constant in the fuel in the radial direction up until a short distance from the outer edge of the fuel block where a slight temperature drop of the fuel temperatures can be observed due to the effect of the bypass gap. The average exit temperature of the helium was found to be 542.55 ℃ which closely matches the helium exit temperature obtained from the 2-D Flownex model and STAR-CCM+. The heat application was therefore implemented correctly in the 3-D integrated block Flownex model.

The maximum fuel surface temperature along the centreline was predicted to be 604.4 ℃ from the 2-D integrated block Flownex model, 602.5 ℃ for the 3-D integrated block Flownex model,

fuel centre temperature of 609.7 ℃ for the STAR-CCM+ and 607.8 ℃ for the 3-D integrated block Flownex model. It should be noted that the 2-D Flownex model results give the representative temperatures on the surface of the fuel rod whereas the STAR-CCM+ gives the temperature in the fuel. The 3-D integrated block Flownex model gives both the surface and centre temperature of the fuel compact.

Figure 60 shows a comparison between the results for temperature distributions for steady state simulations along the outer edge of a 1/6th prismatic fuel block (along line AB or BC in Figure 32), as obtained by the Flownex models and the STAR-CCM+ model.

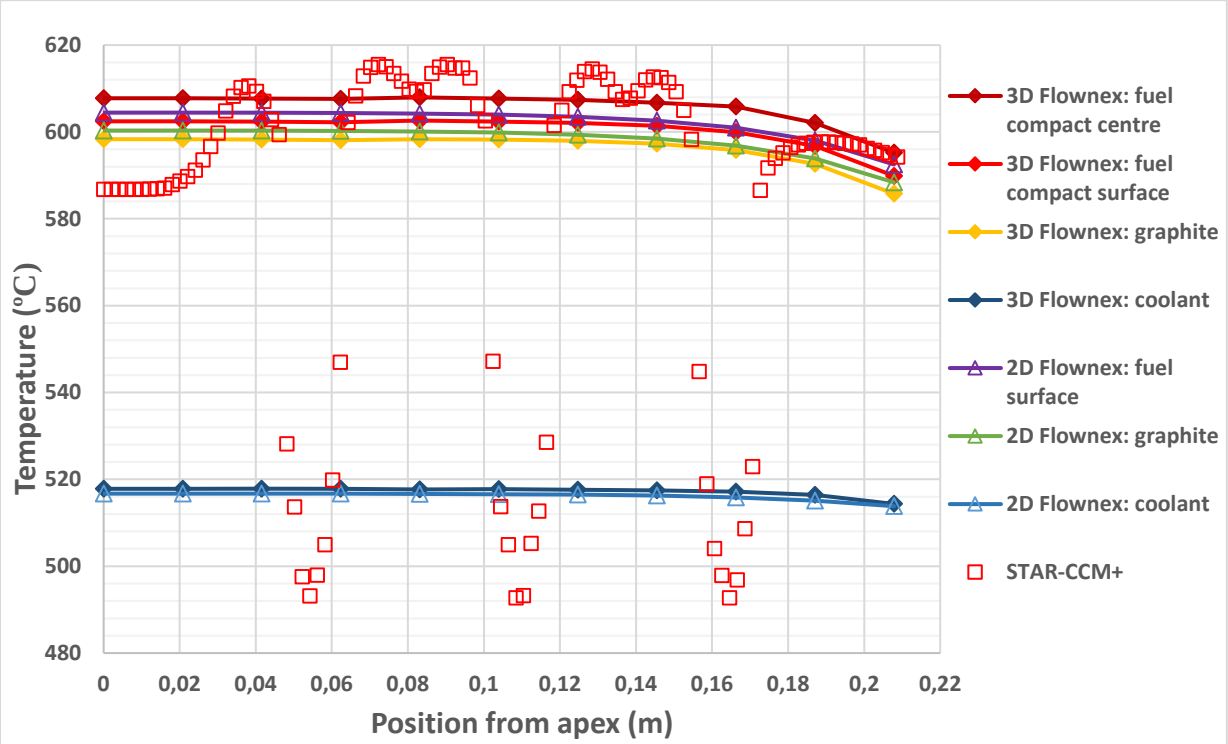

Figure 60: Temperature distributions along the outer margin for STAR-CCM+ and Flownex for the integrated block

The five peaks correspond to the maximum temperatures of the five fuel regions along line AF in Figure 58. The maximum fuel rod temperature along line AF in Figure 58 was predicted to be 615.49 ℃ for the STAR-CCM+ and 607.8 ℃ for the 3-D integrated block Flownex model while the maximum fuel surface temperature was found to be 604.4 ℃ for the 2-D integrated block Flownex model, and 602.45 ℃ for the 3-D integrated block Flownex model. The average radial coolant temperatures difference between the 2-D and 3-D Flownex model measured halfway through the height of the fuel block was 1 ℃ with the maximum being 1.4 ℃.

The 2-D and 3-D integrated block Flownex fuel surface temperature results are lower than the STAR-CCM+ fuel results because in the STAR-CCM+ model, the fuel was modelled explicitly

and not in a representative manner as in the Flownex models. The 3-D integrated block Flownex fuel centre temperatures are closer to the values predicted by STAR-CCM+. This shows that the 3-D integrated block Flownex model improves the accuracy of the predicted temperatures than the 2-D Flownex model.

6.4 3-D Integrated prismatic block Flownex model

In this section, a 3-D integrated block Flownex model of a $1/6^{th}$ section of the PMR200 fuel block was developed and the details of how the 3-D Flownex model differs from the 2-D Flownex model given in section 6.3 are given. The results for the $1/6^{th}$ model are shown in this section.

It has already been shown in a previous study by Sambureni (2015) that Flownex can be used to build a 2-D network model for an HTR prismatic standard fuel block. The temperature distributions calculated using this network model were discussed in section 6.3. In this model, however, the heat conduction was investigated only in the radial and tangential directions thereby making it a 2-D representation of a cross-section cut halfway through the height of the fuel block. The limitation of the 2-D model becomes evident when one wants to determine the axial temperature distribution in the fuel block or fuel assembly in order to evaluate the hot spot fuel temperature. In the HTR prismatic block type reactor the axial discretization becomes essential for this purpose. Also, in the 2-D model, the fuel was represented by one node (the fuel surface node) in each control volume. The heat generated in the fuel was uniformly distributed in the fuel surface nodes and the material for the fuel was assumed to be the same as that of the graphite block. This means that the radial temperature distribution within the fuel compact could not be determined and therefore the maximum fuel temperature at the centre of the fuel compact or fuel kernel could not be predicted using the Sambureni (2015) model.

In the present study, a conceptual formulation of a model for the conduction path between the fuel rods and the coolant channels as discussed in section 5.2.2 is presented. The fuel compacts and coolant channels were modelled implicitly by defining representative coolant channels, fuel compacts and coated fuel particle layers. The main benefit of this approach is that one can extract temperature profile for any representative section of the fuel block from the multiple nodes employed to represent the fuel block. Another advantage is that the axial direction was chosen as the primary direction for conduction heat transfer within the block. This allows for axial temperature distribution of any component or material of interest within the fuel block or assembly to be extracted.

6.4.1 Model inputs

For the 3-D Flownex model implementation, a 1/6th section of a typical PMR200 standard fuel block was used. The geometry and dimensions of the standard prismatic fuel block are shown in Figure 32 in section 4.1. The 3-D integrated block Flownex model shown in this section differs from that modelled in section 6.3 in that this model accounts for conduction within the fuel kernels in the fuel rod matrix. The model accounts for the helium gap between the fuel compact and the graphite and also has three nodes along the height of the block so the temperatures at the top, middle or bottom of the block can be extracted.

The input parameters and material properties used are given in Table 37 to Table 45 in Appendix A. The LBP rods are not modelled in Flownex. The heat generated by the fuel is uniformly distributed in the fuel kernel nodes and fuel compact nodes.

The total coolant mass flow rate into the fuel block assembly was given as 1.207 kg/s (Tak, et al., 2014), from which the 1/6th mass flow rate was calculated to be 0.20116 kg/s. A surface roughness of 20 μm (Tung et al., 2012) was assumed for the coolant channels and a bypass gap size of 2mm. The geometry of the PMR200 also includes a small coolant channel positioned near the fuel handling hole. In Flownex this coolant channel was modelled the same size as the standard coolant channel. A pressure of 7 MPa was prescribed at the inlet of the coolant channels and bypass gap. In the standard fuel block Flownex model that was discussed in Figure 41, section 5.2.4.1, the power for each control volume can be applied to either the fuel kernel nodes or fuel compact nodes. The fuel assembly thermal power of 3.116 MW was used in this model and was obtained from Tak et al. (2014). Thus the power allocated to a 1/6th of a fuel block was then 0.086 MW.

6.4.2 Model results

A steady state simulation of a 1/6th of a standard PMR200 fuel block was done using the Flownex control volume model introduced in Figure 41 as the basic building block for the control volumes. Since this is only one segment of fuel block simulated in isolation from other segments, only the heat transfer within the block can be modelled. Heat transfer was modelled in the tangential, radial and axial directions within the control volumes and between the adjacent control volumes.

When the coated fuel particles are not explicitly discretized in the model, their mass is assumed to be implicitly included in the mass of the fuel rod or compact. Therefore it is possible to apply the heat sources to the fuel kernel nodes or apply the heat source to the fuel rod nodes. Two

models were then developed in Flownex to investigate this assumption. In one model, the power was applied to fuel kernel nodes and in the other model it was applied to fuel rod nodes. The steady state fuel compact centre temperatures for both cases were then extracted and are shown in Table 13 and Table 14 for the 1/6th fuel block. The power application to the fuel compact nodes instead of representative fuel kernels was done in order to reduce the size of the network in the models but with the mass of the representative fuel kernels still implicitly included in the mass of the compacts.

Table 13: Comparison of centreline fuel temperatures of a 1/6th fuel block with representative coated fuel particle network and 1/6th fuel block without fuel particle network

Position from the apex (m)	1/6th with rep. coated fuel particle network Fuel compact centre temperature (°C)	1/6th without rep. coated fuel particle network Fuel compact centre temperature (°C)
0	757.583	757.583
0.0180	757.590	757.590
0.0360	757.564	757.564
0.0540	757.479	757.479
0.0720	757.278	757.278
0.0900	756.868	756.868
0.1080	756.012	756.012
0.1260	754.166	754.166
0.1440	749.906	749.906
0.1620	739.330	739.330
0.1800	710.902	710.902

As shown in Table 13 and Table 14, the results are in exact agreement. It was therefore concluded that the reduced order model would be used in succeeding models to reduce the load on the memory and GUI. The fuel kernel temperatures can be obtained using equations (5-5) and (5-6) and or the spherical fuel kernel temperatures equation given in Appendix B.

Table 14: Comparison of outer edge fuel temperatures of a 1/6th fuel block with representative coated fuel particle network and 1/6th fuel block without fuel particle network

Position from the apex (m)	1/6th with rep. coated fuel particle network Fuel compact centre temperature (℃)	1/6th without rep. coated fuel particle network Fuel compact centre temperature (℃)
0	757.583	757.583
0.020785	757.567	757.567
0.041569	757.516	757.516
0.062354	757.38	757.38
0.083138	757.097	757.097
0.103923	756.521	756.521
0.124708	755.342	755.342
0.145492	752.909	752.909
0.166277	747.854	747.854
0.187061	737.354	737.386
0.207846	716.625	716.625

Figure 61 shows the Flownex results for steady state temperature distribution along the centreline of a 1/6th prismatic fuel block represented by line BD in Figure 32. The temperatures reported here were taken at the bottom of the fuel block where the maximum temperatures occur.

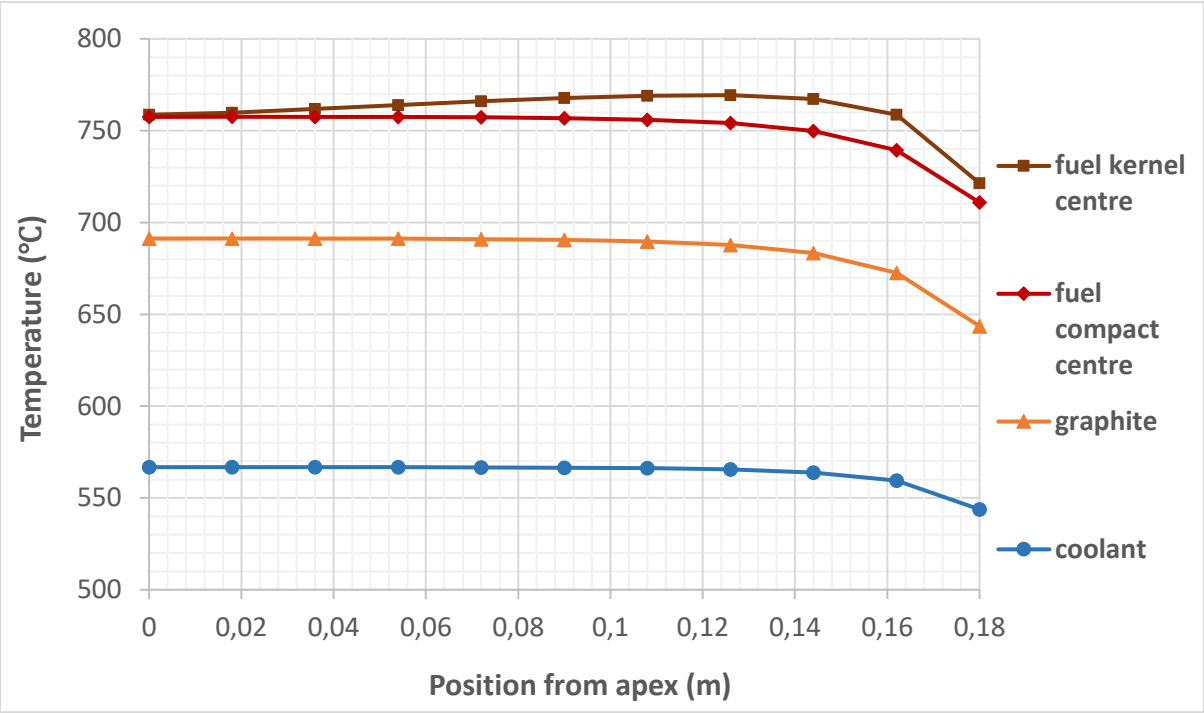

Figure 61: Maximum temperature distributions along the centreline of the prismatic 1/6th fuel block

Figure 62 shows steady state Flownex results for temperature distribution within the 1/6th fuel block for simulations along the outer edge of a 1/6th prismatic fuel block represented by lines BC and BD in Figure 32.

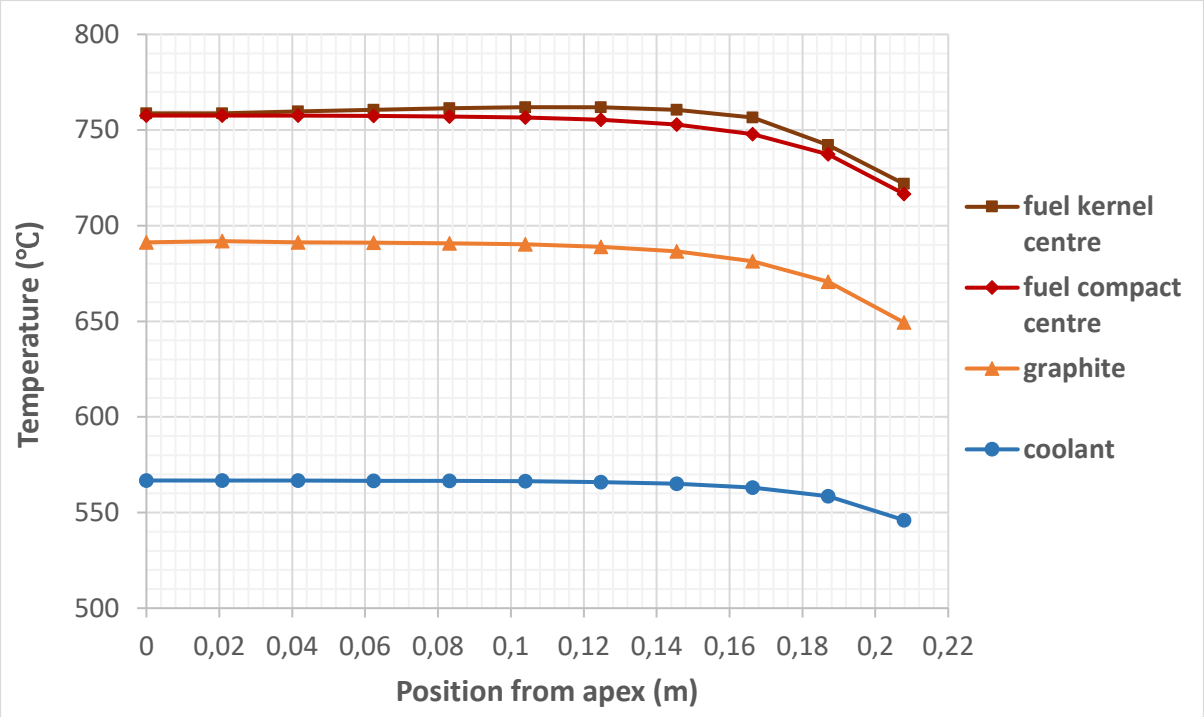

Figure 62: Maximum temperature distributions along the outer edge of the prismatic 1/6th fuel block

The temperatures in Figure 61 and Figure 62 differ from those shown in Figure 59 and Figure 60 in that in Figure 61 and Figure 62 the resistance through the fuel gap is accounted for and therefore these fuel temperatures are higher. The reflection of the fuel rod unit cell results obtained in section 6.2.3 where a drop in temperature at the gap was demonstrated. Also the temperatures in section 6.3 were taken halfway along the height of the fuel block as there was only one axial node. The maximum difference in temperatures between the 3-D integrated fuel block model in Figure 59 and that of Figure 61 was 150 °C for the fuel compact centre, 92.9 °C in the graphite and 48.9 °C for the coolant.

6.5 Heat transfer in a fuel block

In section 6.4, a 1/6th of a block was modelled in isolation but in the actual standard fuel block shown in section 5.2.4.1, the heat transfer between the adjacent segments in the tangential direction will have to be taken into consideration. From the 1/6th model description given in 5.2.4.1.2, a full fuel block model was created by joining the control volumes at the edges of the 1/6th models with infinite thermal conductivity conduction elements. This ensured that a low

thermal resistance was applied between the adjacent control volumes at the edges of each of the 1/6th as they essentially form one control volume. Table 15 shows the properties that were used in the full fuel block model.

Table 15: Thermo-fluid properties for a prismatic fuel block assembly

Parameter (unit)	Value
Inlet temperature (°C)	490
Operating pressure (MPa)	7
Fuel block power (MW)	0.519
Assembly mass flow rate (kg/s)	1.207
Bypass gap size (mm)	2
Coated particle packing fraction (%)	20

Figure 63 shows the radial temperature distribution for the fuel block taken along the centreline indicated by line BD in Figure 32. Figure 64 shows the radial temperature distribution for the fuel block taken along the edge indicated by line AB or BC in Figure 32.

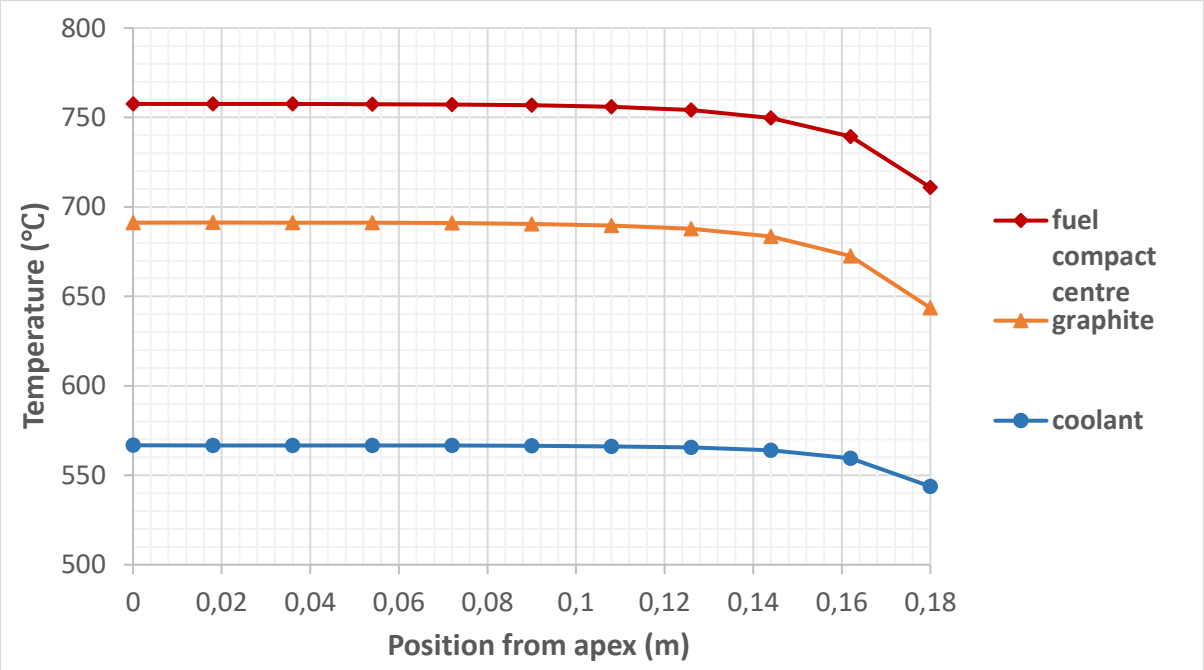

Figure 63: Radial temperature distribution along the centreline of a single fuel block

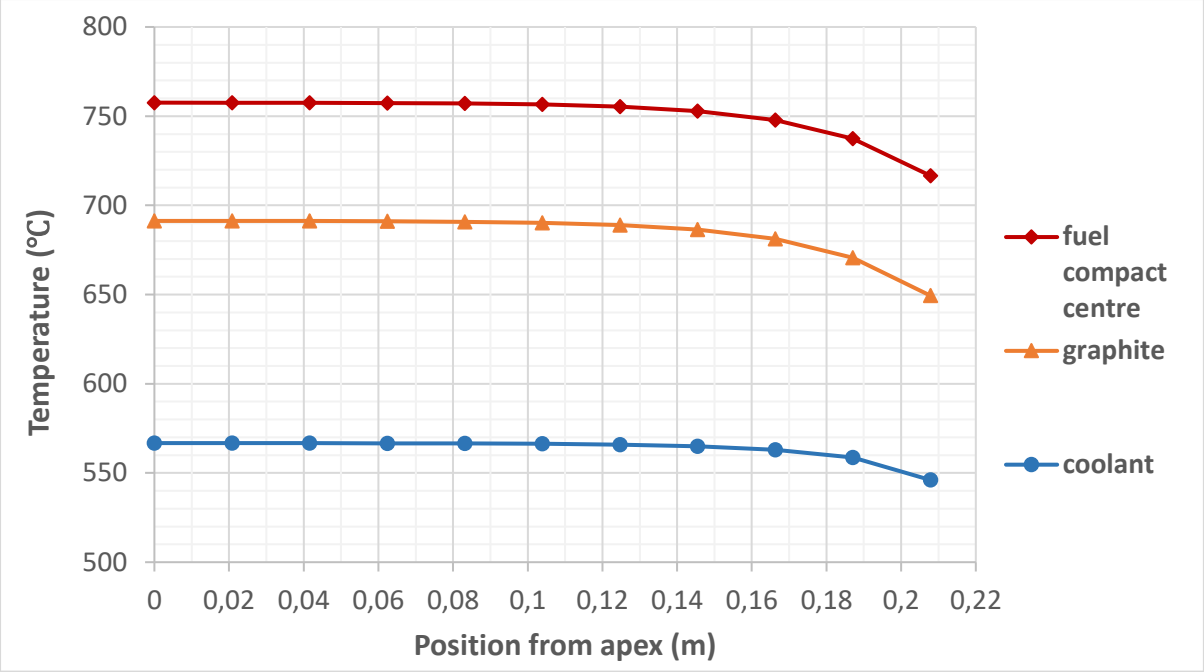

Figure 64: Radial temperature distribution along the outer edge of a single fuel block

Maximum fuel compact, graphite and coolant temperature along the outer edge were found to be 757.6, 691.3 and 566.7 ℃, respectively. The average helium exit temperature was found to be 572.915 ℃. These results were the same as the results in Figure 61 and Figure 62 and are further compared in Table 16 and Table 17. This shows that the 1/6th fuel block model used to build the fuel block model was implemented correctly.

The average helium exit temperature can be verified using equation (6-4).

$$T_{out} = T_{in} + \frac{Q}{\dot{m}c_p} \tag{6-4}$$

$$= 490 + \frac{3.116 \times 10^6}{6 \times 1.207 \times 5197.6}$$

$$= 572.79\ ℃$$

Table 16 and Table 17 show a comparison of centreline and edge fuel compact temperatures of the 1/6th fuel block model and the whole fuel block model.

Table 16: Comparison of centreline fuel temperatures between a 1/6th and a whole block model

Position from the apex (m)	1/6th fuel block model Fuel compact centre temperature (°C)	Whole fuel block model Fuel compact centre temperature (°C)
0	757.583	757.583
0.0180	757.59	757.59
0.0360	757.564	757.564
0.0540	757.479	757.479
0.0720	757.278	757.277
0.0900	756.868	756.868
0.1080	756.012	756.011
0.1260	754.166	754.165
0.1440	749.906	749.905
0.1620	739.33	739.329
0.1800	710.902	710.902

Table 17: Comparison of outer edge fuel temperatures between a 1/6th and a whole block model

Position from the apex (m)	1/6th fuel block model Fuel compact centre temperature (°C)	Whole fuel block model Fuel compact centre temperature (°C)
0	757.583	757.583
0.020785	757.567	757.567
0.041569	757.516	757.516
0.062354	757.380	757.380
0.083138	757.097	757.097
0.103923	756.521	756.520
0.124708	755.342	755.341
0.145492	752.909	752.907
0.166277	747.854	747.841
0.187061	737.354	737.384
0.207846	716.625	716.624

The two sets of results are in very good agreement which means that the 1/6th and whole block models produce the same results for the same conditions. The model of a 1/6th fuel block and its use in building the full bock model can therefore be considered to be verified. The method followed for building the full block model from the 1/6th fuel block is therefore valid.

6.6 Heat transfer in a fuel assembly

In this section Flownex and CORONA were used to simulate a standard PMR200 fuel block assembly. The intention was to model a standard fuel block assembly consisting of six vertically stacked fuel blocks using Flownex and CORONA. It was established during the model development stage that the number of Flownex elements required to build such a model would not be practically viable because of storage space, memory and graphic user interface

problems. It was therefore decided that a six block assembly model could be constructed by using a reduced order model. The fuel kernel elements were therefore removed in order to reduce the total number of elements in the model. As it has been demonstrated in Table 13 and Table 14, the removal of fuel kernel elements in the model will not compromise the accuracy of the fuel compact temperature distribution results. Using this general idea and that of symmetry in the fuel block, it was decided that only a $1/6^{th}$ of a reduced order six-block fuel assembly and a three-fuel block assembly models would be built in Flownex. These models are discussed in the next sections.

6.6.1 $1/6^{th}$ six-block fuel assembly

To model a $1/6^{th}$ fuel block assembly, six standard fuel blocks were stacked vertically with cross flow gaps between adjacent fuel blocks and a bypass gap at the edge of the blocks. The details of the construction of these models are given in section 5.2.4.1.1. Table 18 shows the parameters that were used in the $1/6^{th}$ assembly Flownex and the CORONA fuel block assembly models.

Table 18: Parameters used for Flownex $1/6^{th}$ assembly and CORONA assembly models

Parameter (unit)	Flownex $1/6^{th}$ assembly	CORONA assembly
Reactor Power (MW_{th})	200	200
assembly power (MW_{th})	0.5194	3.1164
assembly mass flow rate (kg/s)	0.2012	1.207
Inlet temperature (°C)	490	490
Operating pressure (MPa)	7	7
Active core height (m)	4.758	4.758
Packing fraction (%)	20	20
Number of stacked fuel blocks	6	6
Cross flow gap size (mm)	1	1
Bypass gap size (mm)	2	2

Table 19 and Table 20 show a comparison of centreline and edge fuel compact temperatures of the one $1/6^{th}$ fuel block model and a $1/6^{th}$ assembly model first fuel block.

Table 19: Comparison of centreline fuel temperatures between a 1/6th fuel block and a 1/6th assembly first fuel block

Position from the apex (m)	1/6th fuel block model	1/6th assembly 1st fuel block model
	Fuel compact centre temperature (°C)	Fuel compact centre temperature (°C)
0	757.583	757.59
0.0180	757.59	757.597
0.0360	757.564	757.571
0.0540	757.479	757.486
0.0720	757.278	757.285
0.0900	756.868	756.875
0.1080	756.012	756.018
0.1260	754.166	754.172
0.1440	749.906	749.912
0.1620	739.33	739.336
0.1800	710.902	710.907

Table 20: Comparison of outer edge fuel temperatures between a 1/6th fuel block and a 1/6th assembly first fuel block

Position from the apex (m)	1/6th fuel block model	1/6th assembly 1st fuel block model
	Fuel compact centre temperature (°C)	Fuel compact centre temperature (°C)
0	757.8583	757.583
0.020785	757.567	757.524
0.041569	757.516	757.524
0.062354	757.38	757.387
0.083138	757.097	757.104
0.103923	756.521	756.527
0.124708	755.342	755.349
0.145492	752.909	752.914
0.166277	747.854	747.848
0.187061	737.386	737.39
0.207846	716.625	716.63

The two sets of results are in exact agreement which means that 1/6th and 1/6th fuel block assembly models produce the same results for the same conditions. The model of a 1/6th fuel block and its use in building the 1/6th fuel block assembly model can therefore be considered to be verified. The construction of the 1/6th fuel block assembly model is therefore valid.

Figure 65 shows the steady state temperatures for the fuel compact and coolant along the centreline of a 1/6th of a hexagonal block, obtained from CORONA and Flownex. The temperatures shown are the highest temperature of the representative fuel compacts at the bottom of the assembly. The temperatures are observed to be the highest along the centreline of the 1/6th section and lowest at the edge of the assembly closest to the bypass gap. For the

Flownex model, the highest fuel compact temperature was found to be 1178.77 ºC and the average coolant outlet temperature to be 987.7 ºC. In CORONA, the highest fuel temperature was found to be 1179.3 ºC and the average coolant outlet temperature to be 986.3 ºC. The average helium exit temperature can be verified using equation (6-5).

$$T_{out} = T_{in} + \frac{Q}{\dot{m}c_p} \tag{6-5}$$

$$= 490 + \frac{3.1164 \times 10^6}{1.207 \times 5197.6}$$

$$= 986.76\ ℃$$

It should be noted that the fuel compact temperatures in Flownex are indicative of a representative fuel compact within a control volume whereas in CORONA the fuel compact temperature represents the average temperature of fuel compact and attached graphite in unit cell discussed in section 6.2.

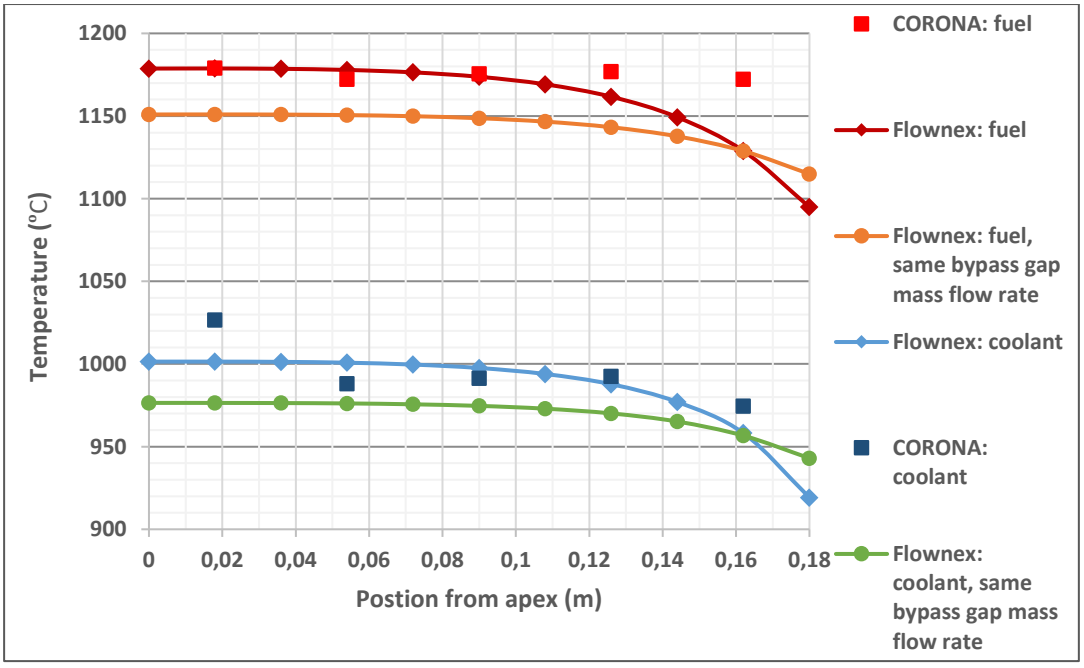

Figure 65: Comparison of Flownex and CORONA results along the centreline of a 1/6th of a block assembly

Figure 66 shows the steady state temperatures for the fuel compact and coolant along the outer margin of a 1/6th of a hexagonal block indicated by line AB and BC in Figure 32, obtained from CORONA and Flownex.

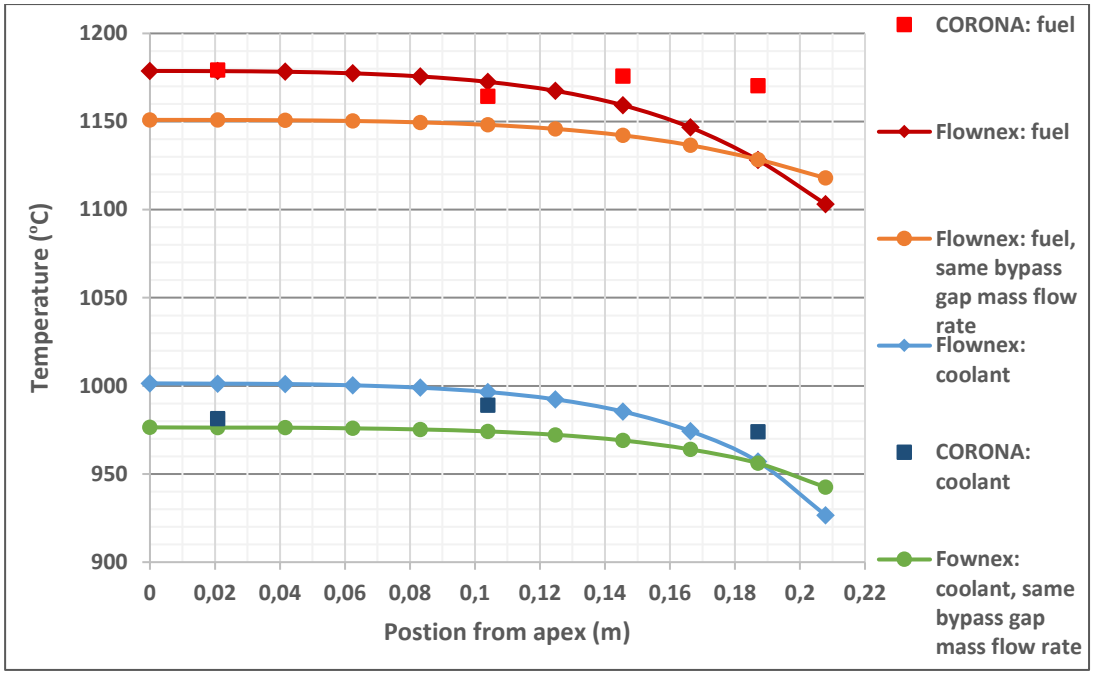

Figure 66: Comparison of Flownex and CORONA results along the outer margin of a 1/6th of a block assembly

The difference in the maximum fuel temperatures predicted by the two codes is about 0.53 ºC. This difference was deemed good given the coarseness of the Flownex mesh compared to CORONA. The average coolant outlet temperatures for the Flownex and CORONA models are in good agreement, with a 1.4 ºC difference. Although no direct comparison for temperature distribution can be made with the CORONA model because of the difference in the distribution of coolant channels and fuel rods, it was observed that the highest fuel temperature in both CORONA and Flownex occurs close to the centre of the block around the smallest coolant channel. It should be noted that all coolant channels were assumed to be same size in the Flownex model and because the coolant channels and fuel rods were grouped into a representative coolant channel and a representative fuel rod, respectively, for each control volume, there will not be distinct peaks at the position of the fuel rods or dips where coolant channels are positioned. CORONA, on the other hand, models each fuel rod and coolant channel explicitly.

Even through the Flownex and CORONA fuel compact and coolant temperatures match very well inside the fuel block, a drop in fuel compact and coolant temperatures can be observed towards the edge of the fuel block due to bypass gap cooling. This effect is not observed for the CORONA model. The difference in the Flownex and CORONA results is due to the fact that the mass flow rate obtained in the Flownex model (i.e. 0,0111777 kg/s) was more than that modelled in CORONA (i.e. 0.0043 kg/s). If the bypass gap flow rate is made to be the same

for both CORONA and Flownex, lower fuel compact and coolant temperatures are obtained. The maximum fuel temperature drop due to change in mass flow rate is about 29 ℃ at the apex of the 1/6th fuel block. Reducing the mass flow rate of the coolant through the bypass gap in the Flownex model improves the temperatures near the edge of the block. The lower the mass flow rate through the bypass gap, the lesser the cooling effect on the fuel.

It should be noted that CORONA heat input is over a smaller area than the in the Flownex model where the fuel rods were assumed to be evenly distributed over the area of the fuel block. Therefore in CORONA model, the volumetric heat source will be larger in fuel region and lower in the graphite or non-fuel region. In CORONA the heat source was only applied to the fuel region and not in the graphite. The Flownex model does not reflect the graphite around the edge of a fuel block.

6.6.2 Three-fuel block assembly

The details how the three-fuel block assembly model was built in Flownex are given in section 5.2.4.1.2. This simulation was done for a three-fuel block assembly to limit the number of elements used in Flownex. Table 21 shows thermo-fluid properties used as Flownex input for the fuel three-fuel block assembly.

Table 21: Thermo-fluid properties for a three-fuel block assembly

Parameter (unit)	Value
Inlet temperature (℃)	490
Operating pressure (MPa)	7
Assembly Power (MW)	1.0388
Assembly mass flow rate (kg/s)	1.207
Number of fuel blocks	3
Cross flow gap size (mm)	1
Bypass gap size (mm)	2
Coated particle packing fraction (%)	20

Since the model is this section only consists of three blocks, only the first three blocks of the 1/6th six fuel block assembly in section 6.6.1 can be used for comparison. In Table 22 and Table 23 the comparison was done between the bottom block of the three-block fuel assembly and the third fuel block of the 1/6th six fuel block assembly. The comparison was done for the centreline and outer edge fuel compact temperatures.

Table 22: Comparison of centreline fuel temperatures between a 1/6th assembly 3rd block and a three-fuel block assembly 3rd block model

Position from the apex (m)	1/6th assembly block model - 3rd block	Three -fuel block assembly model - 3rd block
	Fuel compact centre temperature (°C)	Fuel compact centre temperature (°C)
0	926.856	926.851
0.0180	926.88	926.875
0.0360	926.798	926.793
0.0540	926.512	926.507
0.0720	925.867	925.861
0.0900	924.633	924.628
0.1080	922.338	922.333
0.1260	918.076	918.072
0.1440	909.948	909.944
0.1620	893.955	893.952
0.1800	861.415	861.415

Table 23: Comparison of edge fuel temperatures between a 1/6th assembly 3rd block and a three-fuel block assembly 3rd block model

Position from the apex (m)	1/6th assembly block model - 3rd block	Three-fuel block assembly model - 3rd block
	Fuel compact centre temperature (°C)	Fuel compact centre temperature (°C)
0	926.856	926.851
0.020785	926.809	926.803
0.041569	926.649	926.644
0.062354	926.242	926.237
0.083138	925.419	925.414
0.103923	925.800	923.875
0.124708	921.087	921.082
0.145492	916.095	916.091
0.166277	907.313	907.903
0.187061	892.355	892.353
0.207846	868.659	868.658

The two sets of results are in good agreement which means that 1/6th assembly and whole block assembly models produce the same results for the same conditions. The building of the three-fuel block assembly and the 1/6th fuel block assembly was therefore done correctly.

Figure 67 shows the steady state results for axial temperature distribution in the centre of the hottest fuel compact for the three-fuel block assembly.

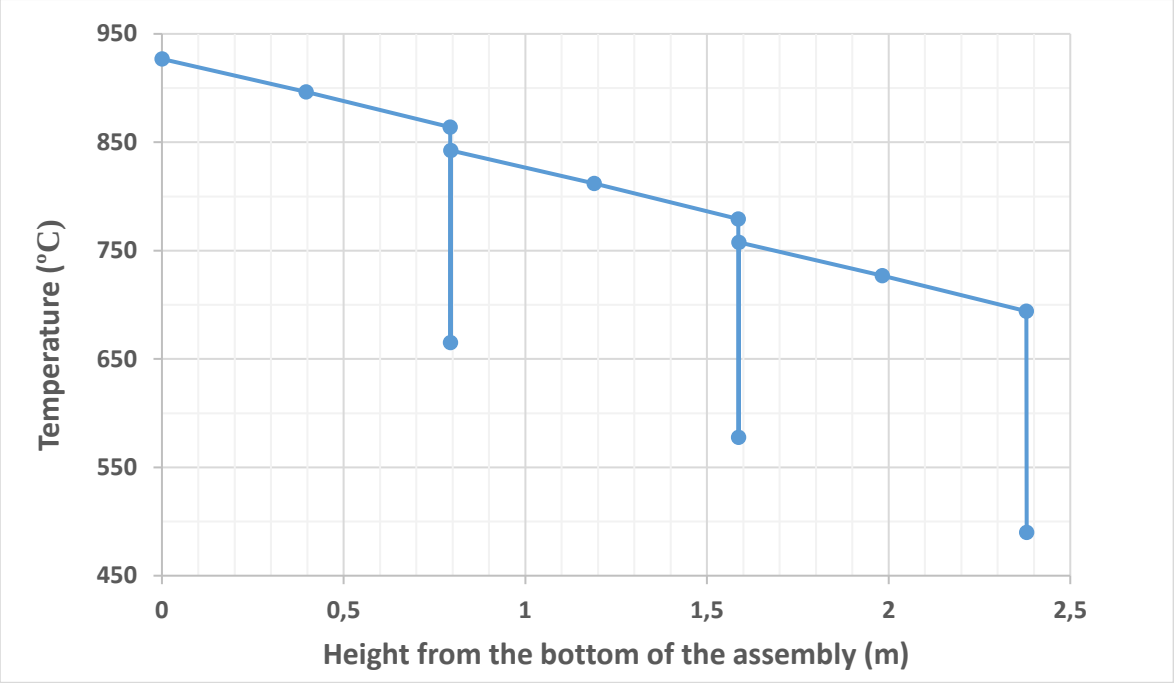

Figure 67: Flownex predicted axial temperature distribution at the centre of the hottest fuel compact in the three-fuel block fuel assembly

Table 24: Parameters used for Flownex three-fuel block assembly and CORONA assembly models

Parameter (unit)	Values
Reactor Power (MW_{th})	200
Assembly power (MW_{th})	3.116
Assembly mass flow rate (kg/s)	1.207
Inlet temperature (°C)	490
Operating pressure (MPa)	7
Packing fraction (%)	20
Number of stacked fuel blocks	3
Cross flow gap size (mm)	1
Bypass gap size (mm)	2

Figure 68 shows a comparison of axial temperature distribution for the three-fuel block assembly modelled in Flownex and CORONA. The parameters used for the model are given in Table 24. The predicted temperatures were extracted at the centre of the hottest fuel compact in the assembly. In the Flownex model, it was assumed that the fuel compact/rods are the same length as the fuel blocks and that the graphite plug and seat were not modelled. The CORONA model has a finer grid (six axial elements per fuel block) than the Flownex grid which uses three axial elements per block.

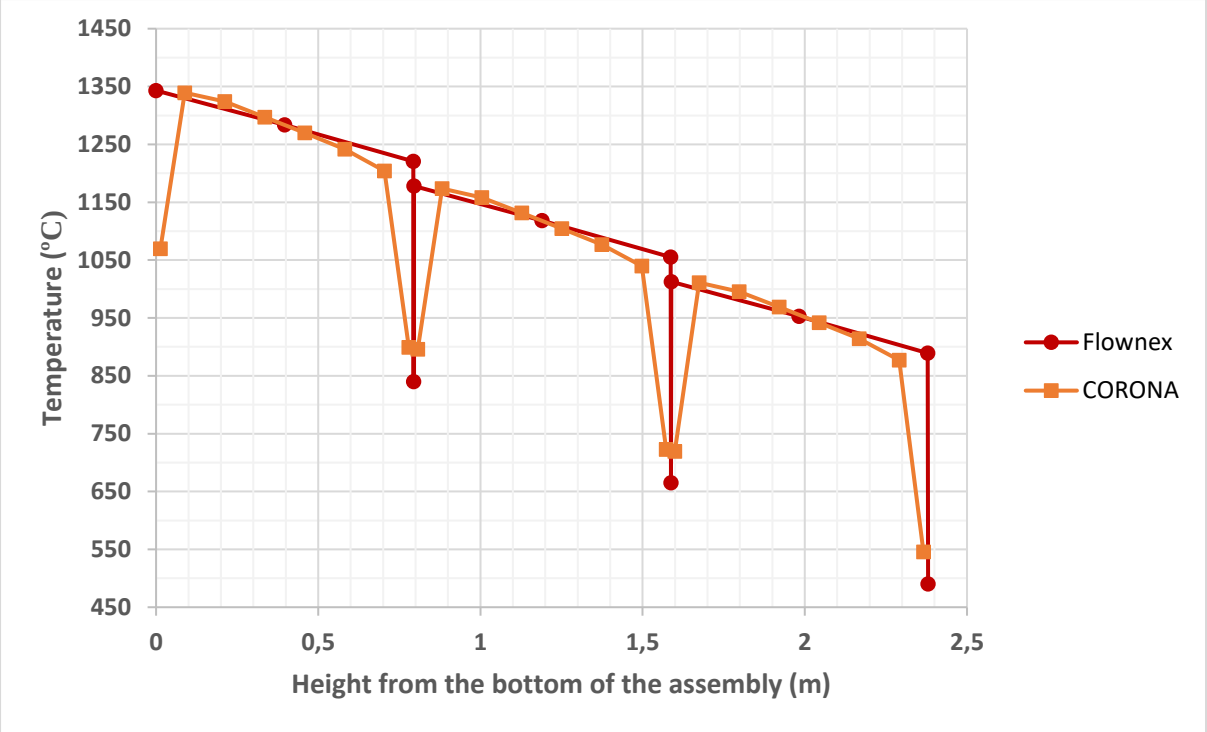

Figure 68: Comparison of Flownex predicted axial temperature distribution at the centre of the hottest fuel compact in the three-fuel block assembly with CORONA

In CORONA, the non-continuous regions between blocks are as a result of non-fuel zones i.e. graphite plug and seat. The results show that Flownex overestimates the axial temperature in the centre of the hottest fuel compact with the maximum being 1343.1 °C whilst the CORONA value for the hottest fuel compact at the bottom of the assembly was 1339.3 °C. The results from the two codes were found to be in good agreement. The slight differences can be attributed to the fact that the CORONA model has more axial nodes per fuel block (i.e. six) compared to Flownex which has three axial nodes. CORONA is therefore assumed to predict the fuel temperatures slightly more accurately. In CORONA, the fuel and graphite regions and the coolant channels were explicitly modelled, even though the flow was approximated with 1-D simulations. Flownex on the other hand modelled the fuel, graphite and coolant channels fully implicitly.

6.6.3 Effect of cross flow on flow distribution in a fuel block assembly

The cross flow leakage flow experiment carried out by Kaburaki and Takizuka (1987) on a full scale fuel block assembly with a cross flow gap as detailed in section 2.2.1.2 was used a basis for this section. A simulation based on this to test the performance of the three-fuel block assembly model built in Flownex was done. In the Flownex model this was done at a pressure of 7 MPa, an inlet pressure of 490 °C, at 3.116 MW, a mass flow rate of 1.207 kg/s and 2 mm bypass gap.

Figure 69 shows static pressure distribution in the coolant channel and the bypass gap for the three-fuel block assembly with a parallel cross flow gap of 1 mm and a 2 mm bypass gap modelled in Flownex.

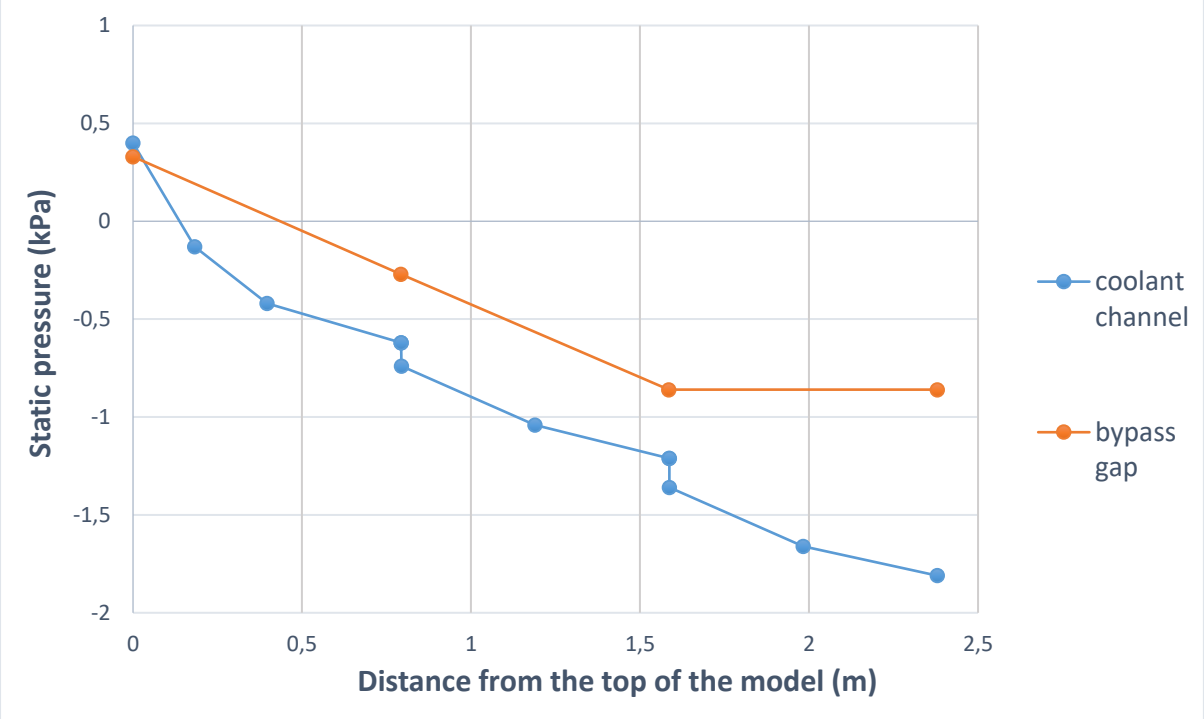

Figure 69: Static pressure distribution for coolant channel in an assembly with parallel cross flow gap

The coolant channel static pressure distribution results in Figure 69 can be compared with the results shown in Figure 70 obtained by Tak et al. (2014) for the validation of CORONA using the Kaburaki and Takizuka (1987) experiments.

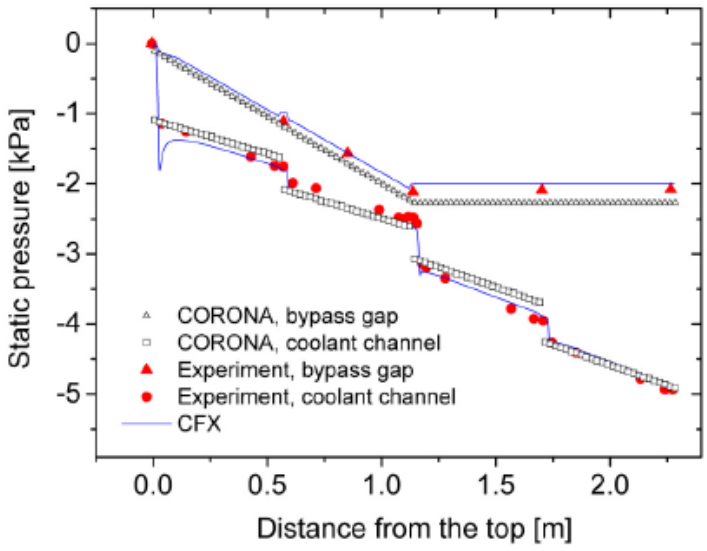

Figure 70: Result of validation of CORONA Using the Kaburaki and Takizuka Experiment (Tak, et al., 2014)

It should be noted that in the model used to produce the results shown in Figure 69 the three standard fuel blocks of 793 mm each discussed in section 5.2.4.1 were simulated in the model whereas in . The Takizuka and Kaburaki (1987) experiment shown in Figure 27, modelled four blocks of 570 mm each with the bottom of the bypass gap completely sealed. The bypass gap in the experiment was taken as 1 mm. Also in the experiment there were twelve coolant channels, 20 mm in diameter. The results in Figure 69 and Figure 70 are not directly comparable due to the modelling parameters being different. In the results shown in Figure 69 and Figure 70, as was found by Kaburaki and Takizuki (1987) discussed in section 2.2.1.2, a sudden drop in the pressure can be observed in the coolant flow channel at the cross flow gap between adjacent blocks due to the merging of the bypass flow into the main coolant channel flow. In the Flownex results (Figure 69), this pressure drop was found to be 0.18 kPa. The Flownex model therefore exhibits a similar variation in pressure as was found in the experiments and the numerical models of Tak et al. (2014).

6.6.4 Effect of bypass gap and size

The effect of bypass gap and bypass gap size was evaluated on a $1/6^{th}$ assembly model of a PMR200 discussed in section 5.2.5.1.1 and 6.6.1. A comparative bypass gap size study was done similar to those performed by Sato et al. (2010) and Johnson and Sato (2010) discussed in section 2.1.1.1.

The bypass gap sizes that were considered are 0, 3 and 5mm with a mass flow rate of 0.2017 kg/s as given Table 25. In the Flownex model this was done at a pressure of 7 MPa and an inlet pressure of 490 ℃. Figure 71 shows the predicted radial temperature distribution at the bottom of the sixth fuel block in the assembly for different bypass gap sizes. The fuel, graphite and coolant temperatures represent the temperature at the centre of the representative fuel compact for each CV. Temperatures shown were taken along the centreline (indicated by line BD in Figure 32) of the bottom increment of the bottom fuel block assembly. The fuel temperatures were taken at the centre of the fuel compact. The bypass gap sizes were assumed to be uniform along the length of the fuel blocks. Table 25 shows a summary of the input parameters and results for the bypass gap size study.

It can be observed from Figure 71 and Table 25 that the wider the bypass gap, the higher the fuel, graphite and coolant temperatures. The increase in fuel temperatures is due to the reduced cooling by the coolant channels as a result of the loss of coolant to the bypass gaps. Within the fuel block (or a section of the block), the temperature increases from the centre of the fuel block

towards the outside or bypass gap until the bypass cooling takes effect. The decrease in temperature due to bypass cooling becomes more pronounced with increasing gap size. At the edge of the block closer to the bypass gap (line BD in Figure 32), the drop in the fuel temperature is most prominent for the 5 mm bypass gap and lesser for the 3 mm bypass gap. Helium exit temperature was found to be 987.5 ℃ for all cases in this model. This is the fully mixed temperature of the combined coolant channel and bypass gap flows at the outlet. For the case with no bypass gap flow, the fuel, graphite and coolant temperatures were constant through the radial length of the 1/6th section. There was however a slight increase in the gradient towards the edge of the block even though this was not expected.

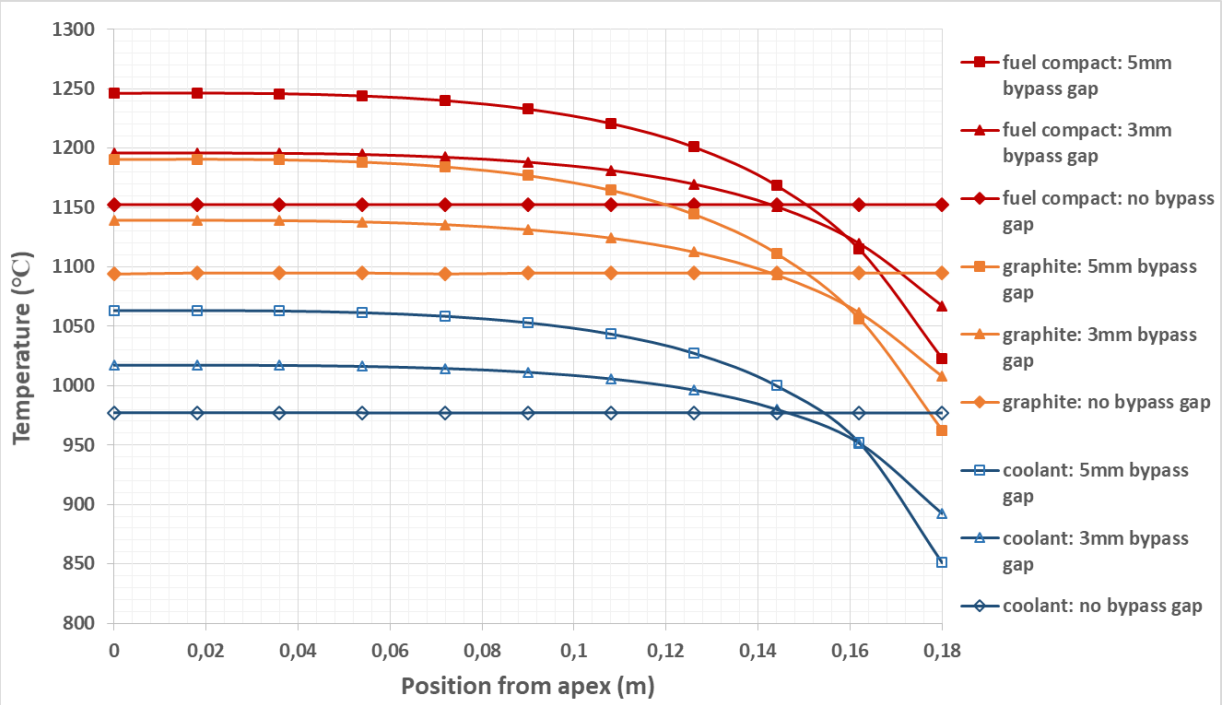

Figure 71: Temperature distribution along the centreline of hotspot plane of a 1/6th assembly for different bypass gap widths

Table 25: Summary of inputs and results for the effect of bypass gap size study

Parameter (unit)	Value		
Gap width (mm)	0	3	5
Assembly mass flow rate (kg/s)	0.2017	0.2017	0.2017
Gap flow fraction (%)	-	8.8	16.96
Gap outlet temperature (℃)	-	727.7	678.4
Max fuel compact temperature (℃)	1152.5	1196	1246.4
Max graphite temperature	1095.9	1139.3	1190.7
Max coolant channel temperature (℃)	980.7	1017.3	1063.3
Bulk outlet temperature (℃)	987.49	987.49	987.49

The maximum fuel compact temperature increased from 1152.5℃ (no bypass gap case) to 1246.4 ℃ for the 5 mm gap case. The increase in the maximum fuel compact temperature is

3.8% and 8.1% for the 3 mm and 5 mm bypass gaps, respectively. The associated increase in the maximum temperature of graphite is 4.1% and 8.7% for the 3 mm and 5 mm bypass gaps, respectively. A similar increase was observed for the maximum coolant temperature where an increase of 4.1 % and 8.8 % was respectively noted for the 3 mm and 5 mm bypass gap sizes.

The maximum temperature difference in the fuel compact along line AB (Figure 32) is 8.2 ℃ for the case where there was no bypass gap, 128.7 ℃ for the 3mm bypass gap case and 223.5℃ for the 5 mm bypass gap case. In the graphite the maximum temperature difference was 131.4 ℃ and 228.1 ℃ for the, 3 mm and 5 mm bypass gap cases, respectively. For the coolant, the maximum temperature differences are 125 ℃ and 212.4 ℃ for the 3 and 5 mm bypass gap sizes, respectively.

These Flownex results for the bypass gap size study cannot be directly compared to those obtained by Sato et al. (2010) and Johnson and Sato (2012) (see section 2.2.1.1) because of differences in the main design and operating parameters. Despite this fact, the difference in the maximum temperature increases in the graphite compare well. The maximum temperature differences in the graphite along line BD (Figure 32) were found to be 125 and 200 ℃ for the 3 and 5 mm bypass gaps from the models by Sato et al. (2010) and 125 and 212.4 ℃ for the 3 and 5 mm bypass gaps in the Flownex model, respectively.

The following points were observed from the bypass gap size study:

- The bypass gap flow diverts a percentage of the coolant and therefore the cooling effect in the main coolant channels decreases. The presence of a bypass gap provides a significant cooling effect near the edge of the block of the prismatic block thus a temperature drop will be observed in this area.
- The maximum coolant channel, graphite and fuel temperature are significantly increased with the increase in gap width.
- The gap outlet temperature decreases with increasing bypass gap size as the mass flow rate through the bypass increases.
- The amount of convection heat transferred increased as the size of the gap increased

6.6.5 Coolant channel blockage in a 1/6th fuel assembly

In this section some of the work of Lee et al. (2014) discussed in section 2.2.2 that was done on a 1/12th fuel column using CORONA, was repeated in Flownex to investigate the effect of channel blockage accidents on fuel temperatures. In CORONA, the coolant channels were

modelled explicitly and the layout of the coolant channels in 1/12th fuel block is shown by the blue circles in Figure 72. The coolant channels in which the blockage was simulated are listed in Table 26.

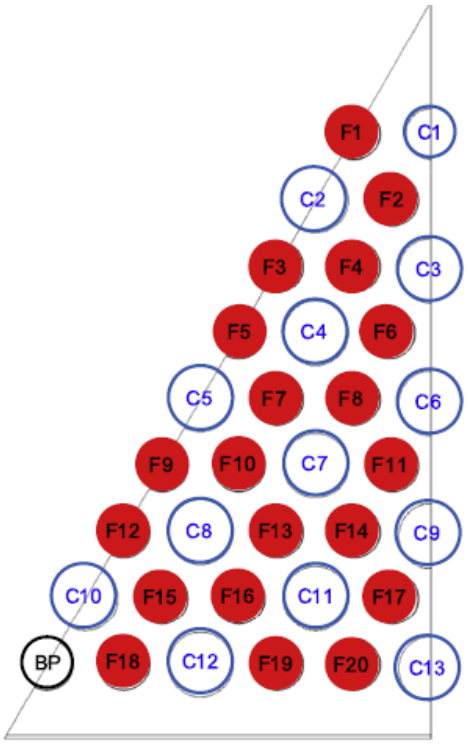

Figure 72: 1/12th fuel assembly and channel layout to identify blockage location (Lee, et al., 2014)

Table 26: Four tested cases for verification of the CORONA model under a coolant channel blockage (Lee, et al., 2014)

Case	Blockage location
Case A	No blockage
Case B	Blockage at C7
Case C	Blockage at C4 and C7
Case D	Blockage at C3, C4 and C7

The coolant channels are modelled implicitly so there is a representative coolant channel for each of the control volumes. The exact location of the coolant channels will therefore not exactly match the real model and the blocked channel might be slightly smaller or bigger than the actual size of a single coolant channel (i.e. 1.59 cm). The simulations were done in Flownex to replicate the cases listed in Table 26.

To model a coolant channel blockage in Flownex, a flow resistance element was introduced at the top of each block and connected by a node to the respective representative coolant channels chosen for each case. The inputs to the flow resistance element include flow resistance behaviour, flow admittance, discretization scheme option, volume, percentage opening and

heat input option. The flow admittance scaling factor was set to 1000 and the opening operation input set to zero.

For case B, which is blockage of channel C7 in Figure 72, the representative coolant channels for CVs 28, 30, 33 and 35 (shown by the orange blocks in Figure 74) were blocked in the Flownex model. The total representative coolant channel number in these two CVs amounts to 1.17 coolant channels.

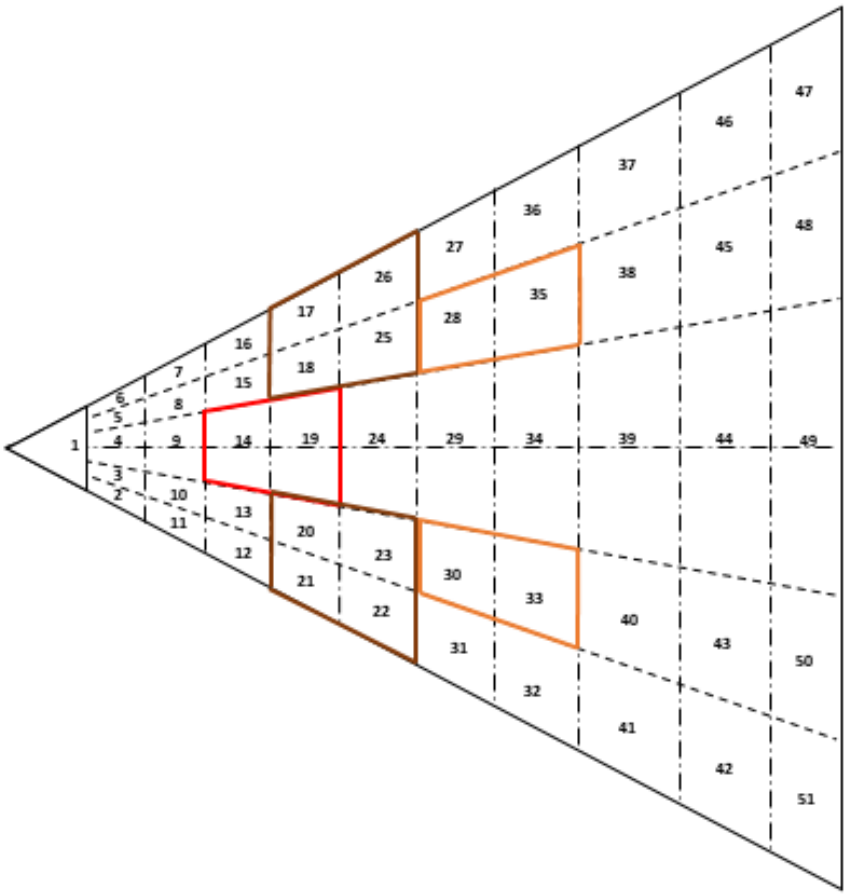

Figure 73: CV schematic for a 11x5 grid indicating CVs with blocked coolant channels

For case C, which is blockage of channels C4 and C7 in Figure 72, CVs 17, 18, 20, 21, 22, 23, 25, 26, 28, 30, 33 and 35 (shown by brown and orange blocks in Figure 73) were blocked in the Flownex model. The total representative coolant channel number for CVs 20, 21, 22 and 22 amounts to 1.22 coolant channels. The total representative coolant channel number for case C CVs is 2.39 coolant channels.

For case D, which is blockage of channels C3, C4 and C7 in Figure 72, CVs 14, 19, 17,18, 20, 21, 22, 23, 25, 26, 28, 30, 33 and 35 (marked by the red, brown and orange blocks in Figure 79) were blocked in the Flownex model. The total representative coolant channel number for

CVs 14 and 19 is 0.63 coolant channels. The total representative coolant channel number for case D control volumes is 3.02 coolant channels.

The results for the axial variation of the predicted fuel temperature taken at the centre of the fuel compacts where the maximum temperature occurs, for the four test cases of coolant channel blockage in Table 26 are shown in Figure 74 to Figure 77. Figure 74 (a) to Figure 77 (a) show Flownex results and CORONA results are displayed in Figure 74 (b) to Figure 77 (b). The CORONA results were verified using results obtained by using the commercial CFD code CFX (ANSYS Inc., 2018) (Lee, et al., 2014). The CORONA results given were also taken at the centre of the fuel compact where the maximum temperature occurs but no information is given on the position of the fuel compact with the highest temperature. It should be noted that in the CORONA model, the non-fuel regions above and below the fuel compacts in each block (i.e. graphite plugs) and the graphite seats were included but not in the Flownex model. The CORONA results will then show a constant temperature at the top and bottom of the fuel assembly. The constant temperature sections at the top and bottom of the CORONA results are probably also due to reflector blocks at the top and bottom. In Flownex the reflector blocks were not modelled. The graphite plugs and non-fuel regions also have an influence particularly between the blocks.

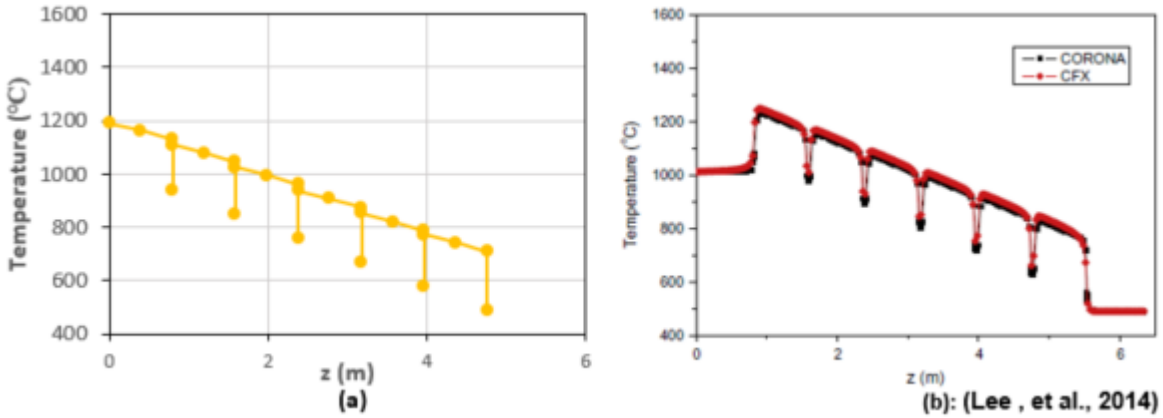

Figure 74: Fuel compact temperature under coolant channel blockage case A

It can be observed that for the base case, case A with no coolant channel blockage, the Flownex results (Figure 74 (a)) are comparable to the CORONA results. The maximum and minimum fuel compact temperatures were found to be 1194.7 ℃ and 727.6 ℃, at the bottom and top of the fuel assembly, respectively.

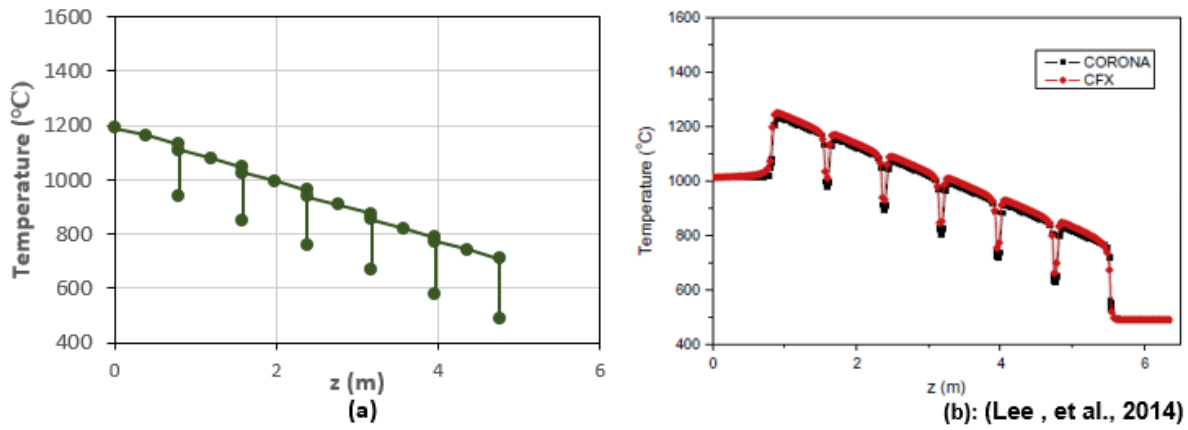

Figure 75: Fuel compact temperature under coolant channel blockage case B

For case B where channel C7 was blocked, the maximum and minimum fuel compact temperatures predicted from Flownex were found to be 1215.5 ℃ and 749.5 ℃, respectively. This shows an increase of 1.7% from case A. These results are still comparable to the CORONA results shown in Figure 75 (b).

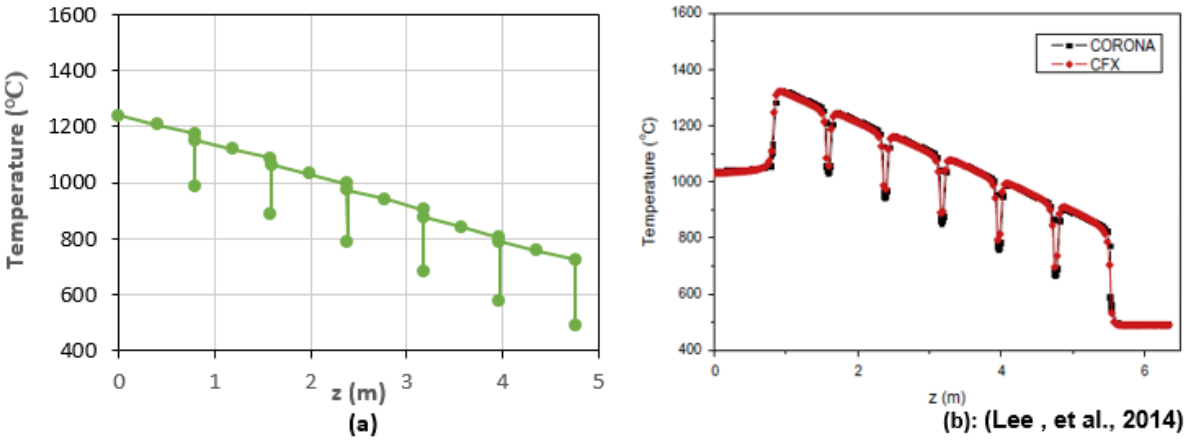

Figure 76: Fuel compact temperature under coolant channel blockage case C

For case C where channel C4 and C7 were blocked, the maximum and minimum fuel compact temperatures predicted from Flownex were found to be 1258.2 ℃ and 764.3 ℃, respectively. This shows an increase of 5% in the fuel compact temperatures from case A. The CORONA results in Figure 76 (b) show the maximum fuel compact temperature to be above 1300 ℃.

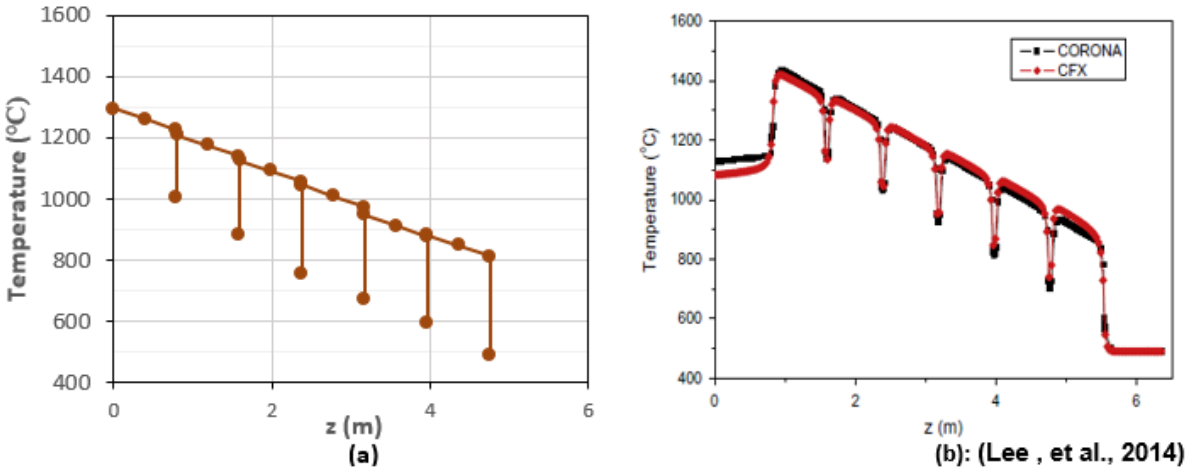

Figure 77: Fuel compact temperature under coolant channel blockage case D

In case D where channels C3 C4 and C7 were blocked, the maximum and minimum fuel compact temperatures predicted from Flownex were found to be 1310.4 ℃ and 838.9 ℃, respectively. This shows an increase of about 9.7% in the fuel compact temperatures from case A. The CORONA results in Figure 78 (b) show the maximum fuel compact temperature to be above 1400 ℃.

It appears that the extent to which Flownex underestimates the fuel compact temperatures becomes more apparent as the number of blocked coolant channels increases. These results show one of the shortcomings of the fuel rod and coolant channel re-distribution over the area of a block. In the actual fuel block one coolant channel is typically surrounded by six fuel rods and the area around the fuel handling hole and the outer edge of the fuel block contains no fuel rods and coolant holes. However, in the Flownex model the coolant channels and the fuel rods were uniformly distributed over the entire cross-sectional area of a fuel block. CORONA fuel temperatures refer to individual fuel rods whereas Flownex refers to a representative fuel rod within a respective control volume. It should also be noted that individual coolant channel blocking in Flownex is not possible but only the sections of coolant channels within a control volume can be blocked.

In this case, Flownex cannot predict local detail but only a trend to show that the fuel compact temperature will increase in case of a coolant channel blockage.

6.6.6 Coolant channel blockage in a fuel block

As discussed in section 2.2.2, Cioni et al. (2006) did a study on multi-coolant channel blockage on a central fuel assembly surrounded by six other fuel assemblies. They found that the coolant channels blockage results in a fuel temperature increase within the affected block but the

increase is only confined to the assembly with the plugged coolant channels. The effect of this increase in temperature on the surrounding assemblies was found to be insignificant.

In this section then, the effect of blocked coolant channels was investigated within a single fuel block as was it assumed that the surrounding blocks will not be affected. This will enable the user to see the effect of the blocked coolant channels in the tangential heat transfer. Therefore in this study the blocked coolant channels were assumed to occur in one of the segments of a standard fuel block shown in Figure 78 by numbers one to six. The blocked coolant channels were assumed to be in segment 1. In this study, fewer coolant channels were blocked compared to the study done by Cioni et al. (2006) where 24 were blocked as shown in Figure 29.

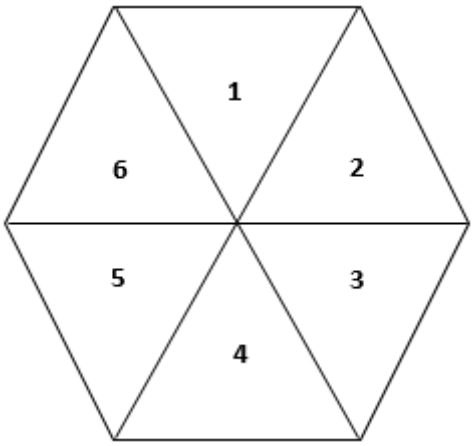

Figure 78: Schematic indicating segment numbering for a fuel block

The Flownex model used for this simulation is shown in Figure 46 but with the flow resistance element added to the coolant channels in the affected CV of segment 1. The simulation was first done under normal operating conditions without the coolant channel blockage. The temperatures at the centre of the fuel compacts and coolant temperatures for one of the segments shown in Table 27 and Table 28 are for normal operating conditions and will therefore serve as reference state. The nominal temperature distribution in the fuel compacts and coolant channels is mirrored in all the six segments because of symmetry.

Table 27: Fuel temperatures in a fuel block without coolant channel blocking

Node number	Fuel compact centre temperature (°C)										
1		757.6	757.5	757.4	757.1	756.5	755.3	752.9	747.9	737.4	716.6
2		757.6	757.5	757.5	757.2	756.8	755.8	753.8	749.3	738.8	712.4
3	757.8	759.6	757.6	757.5	757.3	756.9	756.0	754.2	749.9	739.3	710.9
4		757.6	757.5	757.5	757.2	756.8	755.8	753.8	749.3	738.8	712.4
5		757.6	757.5	757.4	757.1	756.5	755.3	752.9	747.9	737.4	716.6

Table 28: Coolant temperatures in a fuel block without coolant channel blocking

Node number	Coolant temperature (°C)											Byp (°C)
1		566.7	566.7	566.7	566.6	566.4	565.9	565.0	563.0	558.6	546..1	501.3
2		566.8	566.7	566.7	566.6	566.5	566.1	657.3	563.6	559.3	544.4	533.9
3	566.8	566.7	566.7	566.7	566.6	566.5	566.2	565.5	563.9	559.5	543.8	565.5
4		566.8	566.7	566.7	566.6	566.5	566.1	657.3	563.6	559.3	544.4	
5		566.7	566.7	566.7	566.6	566.4	565.9	565.0	563.0	558.6	546.1	

The CVs in segment 1 of Figure 78 in which the coolant channel blockage was simulated are within region indicated by the red lines in Figure 79. Therefore the blocked coolant channels are in CVs 7 to 41 and this works out to a total of 12.6 coolant channels. The results of fuel compact and coolant temperatures after the coolant channels blockage incident are shown in Table 29 and Table 30.

The effect of coolant channel blockage on fuel compact temperatures in the first segment can be seen when one compares the temperatures in Table 27 and Table 29. From the reference case in Table 27, the maximum fuel compact temperature was 759.6 °C (circled in red) and was found to lie on the centreline of the 1/6th fuel block (CV 39 in Figure 79) but closer to the centre of the block. With the blockage being dominantly in the centre of segment 1 (Figure 78), the maximum fuel compact temperature then shifts towards the centre of the segment (CV 29 in Figure 79) and increased to 1068.1 °C (circled in red in Table 29). There is therefore a 40.6% increase in the maximum fuel compact temperature for the segment and 41.2% increase for CV 29. With respect to the surrounding segments in the block (segments 2 to 6 in Figure 78), it can be seen from Table 29 that symmetry within the block was still maintained. The fuel compact temperature at the centre of the fuel block is 789.7 °C and is common to all segments. The segments that would still see a significant increase in fuel compact temperatures are those closest to segment 1 (i.e. segments 2 and 6). The effect on segment 4, which is the furthest from segment 1, would then be less pronounced. These results cannot be directly compared to the case modelled by Cioni et al. (2006) because of different main core parameters and the difference in the number of coolant channels that are blocked.

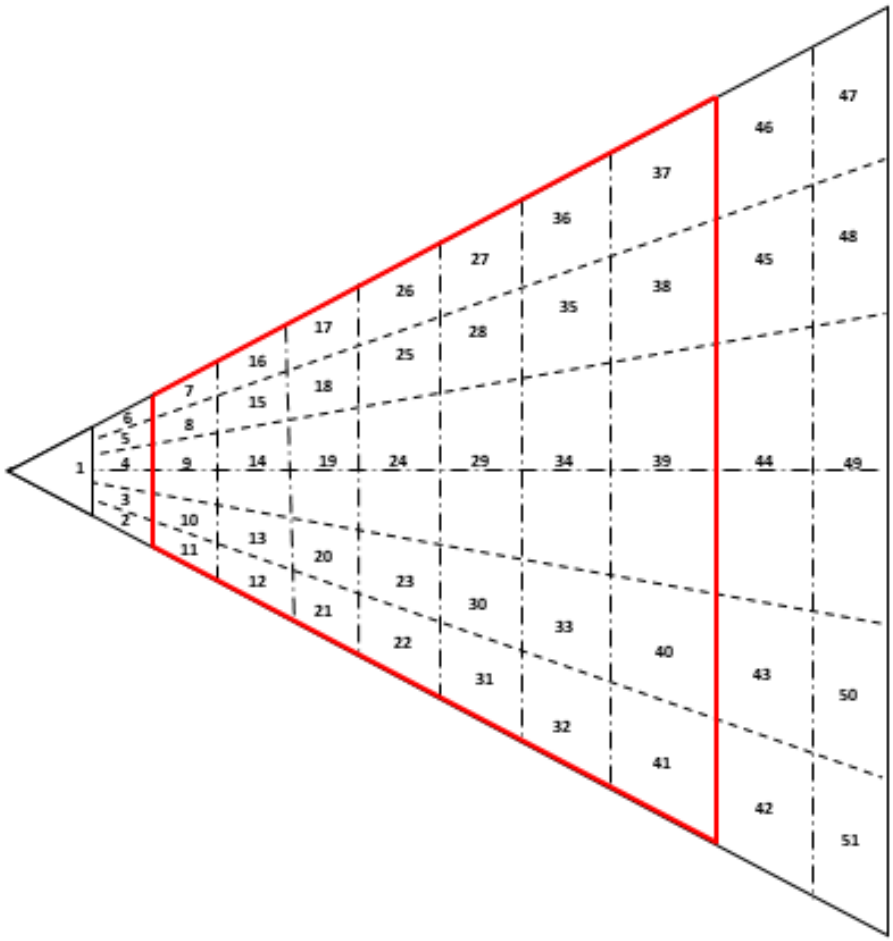

Figure 79: Schematic indicating blocked coolant channel section

Table 30 shows coolant temperatures taken at the bottom of the standard fuel block after a coolant blockage incident. The bypass flow temperature at the bottom of each segment is shown in the last column. It can be seen that the coolant temperature in the radial nodes 3 to 9, which include control volumes 7 to 41 in Figure 74, is the same at 531.5 ℃ since the coolant channels in these control volumes are blocked. For the other control volumes in segment 1 that did not have blocked coolant channels (i.e. control volumes 1 to 6 and control volumes 42 to 51 in Figure 79), an increase in coolant temperature was seen. The coolant channels in control volumes 1 to 6 and control volume 42 to 51 in Figure 79 are the only heat sink for the first segment in this case hence the increase in temperature. Maximum coolant temperatures of 631.6 ℃ occur in segment 2 and segment 6 in control volumes 22 and 26 on the edge closest to the first segment. This is an 11.5% increase from the coolant temperature reference value in control volumes 22 and 26. The bypass flow temperature increased by maximum of 16.6 ℃ from the reference value in segment 1.

Table 29: Fuel compact temperatures in a fuel block with coolant channel blocking in the first segment

Node number	1	2	3	4	5	6	7	8	9	10	11
Fuel compact centre temperature (°C)											
1st segment											
1		818.8	852.5	880.5	900.8	911.6	910.2	892.9	853.4	784.6	739.0
2		834.3	896.0	947.9	989.3	1017.4	1027.8	1011.2	950.8	809.3	740.7
3	789.7	840.2	911.6	971.9	1020.3	1054.2	1068.1	1051.5	983.3	817.5	740.6
4		834.3	896.0	947.9	989.3	1017.4	1027.6	1011.2	950.8	809.3	740.7
5		818.8	852.5	880.5	900.8	911.6	910.2	892.9	853.4	784.6	739.0
2nd segment											
1		818.8	852.5	880.5	900.8	911.6	910.2	892.9	853.4	784.6	739.0
2		800.7	811.6	819.6	823.4	822.4	815.8	802.6	781.4	751.3	715.7
3	789.7	788.1	786.8	784.9	781.9	777.6	771.5	763.2	751.8	734.9	704.6
4		781.1	773.6	767.4	762.1	757.3	752.5	747.1	739.7	727.5	701.7
5		777.9	767.7	759.7	753.7	748.9	744.9	740.4	734.2	723.4	703.2
3rd segment											
1		777.9	767.7	759.7	753.7	748.9	744.9	740.4	734.2	723.5	703.2
2		775.4	763.6	754.3	749.0	744.9	741.8	738.6	733.6	723.4	697.7
3	789.7	774.2	761.6	752.6	746.8	743.0	740.4	737.7	733.3	723.3	695.8
4		774.0	761.3	752.1	746.2	742.4	739.7	737.0	732.5	722.5	696.9
5		774.6	762.0	752.8	746.5	742.4	739.4	736.2	731.1	721.0	700.8
4th segment											
1		774.6	762.0	752.8	752.8	742.4	739.4	736.2	731.1	721.0	700.8
2		773.7	760.7	751.6	751.6	745.6	741.9	736.8	732.4	722.4	696.8
3	789.7	773.3	760.2	751.1	745.3	745.3	741.8	737.0	732.9	772.9	695.4
4		773.7	760.7	751.6	745.6	745.6	741.9	736.8	732.4	7722.4	696.8
5		774.6	762.0	752.8	746.5	742.4	739.4	736.2	731.1	721.0	700.8
5th segment											
1		774.6	762.0	752.8	746.5	742.4	739.4	736.2	731.1	721.0	700.8
2		774.0	761.3	752.1	746.2	742.4	739.7	737.0	732.5	722.5	696.9
3	789.7	774.2	761.6	752.6	746.8	743.0	740.4	737.7	733.3	723.3	695.8
4		775.4	763.6	754.9	749.0	744.9	741.8	738.6	733.6	723.4	697.7
5		777.9	767.7	759.7	753.7	748.9	744.9	740.4	734.2	723.4	703.2
6th segment											
1		777.9	767.7	759.7	753.7	748.9	744.9	740.4	734.2	723.4	703.2
2		781.1	773.6	767.4	762.1	757.3	752.5	747.1	739.7	727.5	701.7
3	789.7	788.1	786.8	784.9	781.9	777.6	771.5	763.2	751.8	734.9	704.6
4		800.7	811.6	819.6	823.4	822.4	815.8	802.6	781.4	715.3	715.7
5		818.8	852.5	880.5	900.8	911.6	910.2	892.9	853.4	784.6	739.0

Table 30: Coolant temperatures in a fuel block with coolant channel blocking in the first segment

Node number	1	2	3	4	5	6	7	8	9	10	11	
	Coolant temperature (°C)											Byp (°C)
1st segment												
1		598.7	531.5	531.5	531.5	531.5	531.5	531.5	531.5	578.7	558.7	*503.8*
2		603.9	531.5	531.5	531.5	531.5	531.5	531.5	531.5	578.4	552.6	*543.7*
3	578.2	600.7	531.5	531.5	531.5	531.5	531.5	531.5	531.5	589.6	551.8	*582.1*
4		604.1	531.5	531.5	531.5	531.5	531.5	531.5	531.5	578.4	552.6	
5		599.3	531.5	531.5	531.5	531.5	531.5	531.5	531.5	578.7	558.7	
2nd segment												
1		590.2	605.8	618.1	626.9	631.6	631.1	623.5	606.1	575.5	551.5	*501.5*
2		582.4	586.9	590.2	591.6	591.1	588.3	582.9	574.3	562.0	543.2	*534.8*
3	578.2	577.1	576.3	575.4	574.1	572.4	569.9	566.9	562.5	555.8	539.4	*566.8*
4		574.3	570.9	568.4	566.3	564.5	562.7	560.8	558.1	553.2	538.6	
5		573.0	568.8	565.5	563.2	561.4	559.9	558.4	556.0	551.6	539.5	
3rd segment												
1		573.0	568.8	565.5	563.2	561.4	559.9	558.4	556.0	551.6	539.4	*500.7*
2		572.1	567.1	563.7	561.5	560.0	558.9	5578	555.9	551.8	537.4	*531.4*
3	578.2	571.5	566.4	562.9	560.7	559.4	558.5	557.6	555.9	551.9	536.7	*560.7*
4		571.6	566.3	562.7	560.5	559.2	558.3	557.3	555.7	551.6	537.2	
5		571.8	566.7	563.0	560.7	559.2	558.2	557.0	555.1	550.9	538.7	
4th segment												
1		571.8	566.7	563.0	560.7	559.2	558.2	557.0	555.1	550.9	538.7	*500.7*
2		571.4	566.1	562.5	560.3	559.0	558.2	557.3	555.6	551.6	537.2	*531.3*
3	578.2	571.3	565.9	562.3	560.2	558.9	558.1	557.4	555.8	551.8	536.6	*560.5*
4		571.4	566.1	562.5	560.3	559.0	558.2	557.3	555.6	551.6	537.2	
5		571.8	566.7	563.0	560.7	559.2	558.2	557.0	555.0	550.9	538.7	
5th segment												
1		571.8	566.7	563.0	560.7	559.2	558.2	557.0	555.1	550.9	538.7	*500.7*
2		571.6	566.3	562.7	560.5	559.2	558.3	557.3	555.7	551.6	537.2	*531.4*
3	578.2	571.5	566.4	562.9	560.7	559.4	558.5	557.6	555.9	551.9	536.7	*560.7*
4		572.1	567.1	563.7	561.5	560.0	558.9	557.8	555.9	551.8	537.4	
5		573.0	568.8	565.5	563.2	561.4	559.9	558.4	556.0	551.6	539.4	
6th segment												
1		573.0	568.8	565.5	563.2	561.4	559.9	558.4	556.0	551.6	539.5	*501.5*
2		574.3	570.9	568.4	566.4	564.5	562.7	560.8	558.1	553.2	538.6	*534.8*
3	578.2	577.1	576.3	575.4	574.1	572.4	569.9	566.9	562.5	555.8	539.4	*566.8*
4		582.6	587.0	590.2	591.6	591.1	588.3	582.9	574.3	562.0	543.2	
5		590.8	605.8	618.0	626.9	631.6	631.1	623.5	606.1	575.5	551.5	

6.6.7 Pressurised Loss of Forced Cooling Transient

Pressurised loss of forced cooling (PLOFC) happens when a forced cooling becomes unavailable due to mechanical failure or loss of power to the blower or circulator and the mass flow drops significantly in a short space of time. In this scenario, the coolant is assumed to remain in the primary circuit as the pressure boundary of the system remains intact, thus

rendering natural convection as a much more important phenomenon. The reactor is also assumed to shut down as soon as a PLOFC is initiated. The thermal power of reactor will then decrease to decay heat level.

The transients that could be performed in the Flownex models developed so far account for the cases where the pressure and / or mass flow rate are reduced (but not to atmospheric or zero). Although this demonstrates that the models have a transient capability, the question arises as to what plant condition these relate to. The way in which the power is applied to the nodes i.e. value distributed over all the fuel nodes (a very large number), it would be a tremendous challenge to simulate a case where the power varies with time (i.e. a DLOFC with decay heat). A $1/6^{th}$ fuel block discretized to 11x5 CVs will contain approximately 560 nodes to which the individual power values are applied.

In this section, a pressurised loss of cooling transient is simulated in a $1/6^{th}$ fuel assembly that is assumed to be adjacent to the side reflector and will therefore have no influence on other assemblies. This is thus a limited case. The radial layout of the reactor elements and the radii for the PMR200 are shown in Figure 80. The radial geometry of the Flownex model from the fuel assembly at the edge of the core extends to the stagnant air volume outside the RPV. The convection coefficient on the surface of the RPV was taken as a combination of convection and radiation.

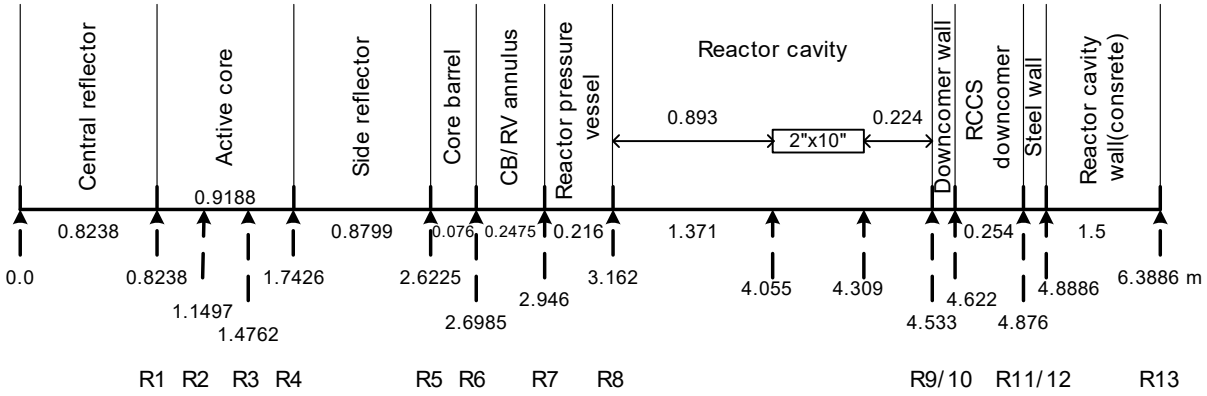

Figure 80: Reactor elements radial layout

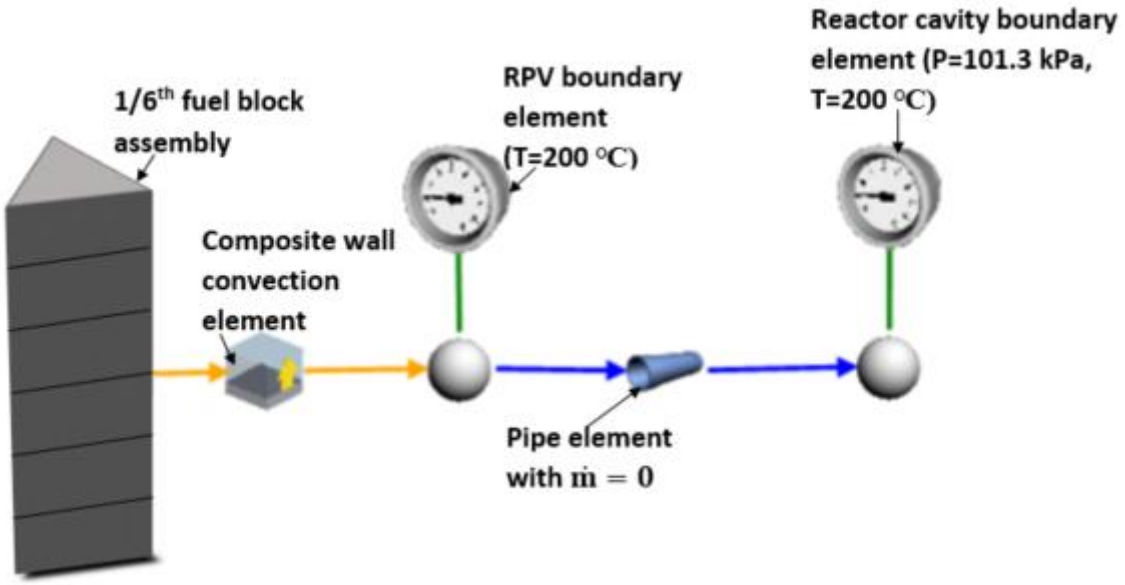

Figure 81: Schematic representing the PLOFC model in Flownex

To simplify the problem, an equivalent thermal circuit used for a series composite wall shown in Figure 82 was implemented. This heat transfer coefficient was used for the composite wall convection element shown in Figure 81.The RCCS is not modelled, but radiation heat transfer from the RPV to the ultimate heat sink (RCCS) through the outside air (assumed stagnant) is accounted for. The thermophysical properties assumed for this problem are shown in Table 31.

Table 31: Thermophysical properties

Material	Conductivity (W/m.K)
Side reflector	30
Core barrel	35
CB/RPV annulus	0.3
RPV	35
Reactor cavity	3.5

Convection on the surface of the RPV accounts for 20% off all the heat transfer in this problem. The convection coefficient on the surface of the RPV was assumed to be 3.5 W/m^2.K. So the convection coefficient was multiplied five times to get the total heat transfer. The heat transfer coefficient was taken as a combination of convection and radiation and was approximated using equation (6-6).

$$h_{cavity} = 3.5 + 5 \times 3.5 = 21 \quad (6\text{-}6)$$

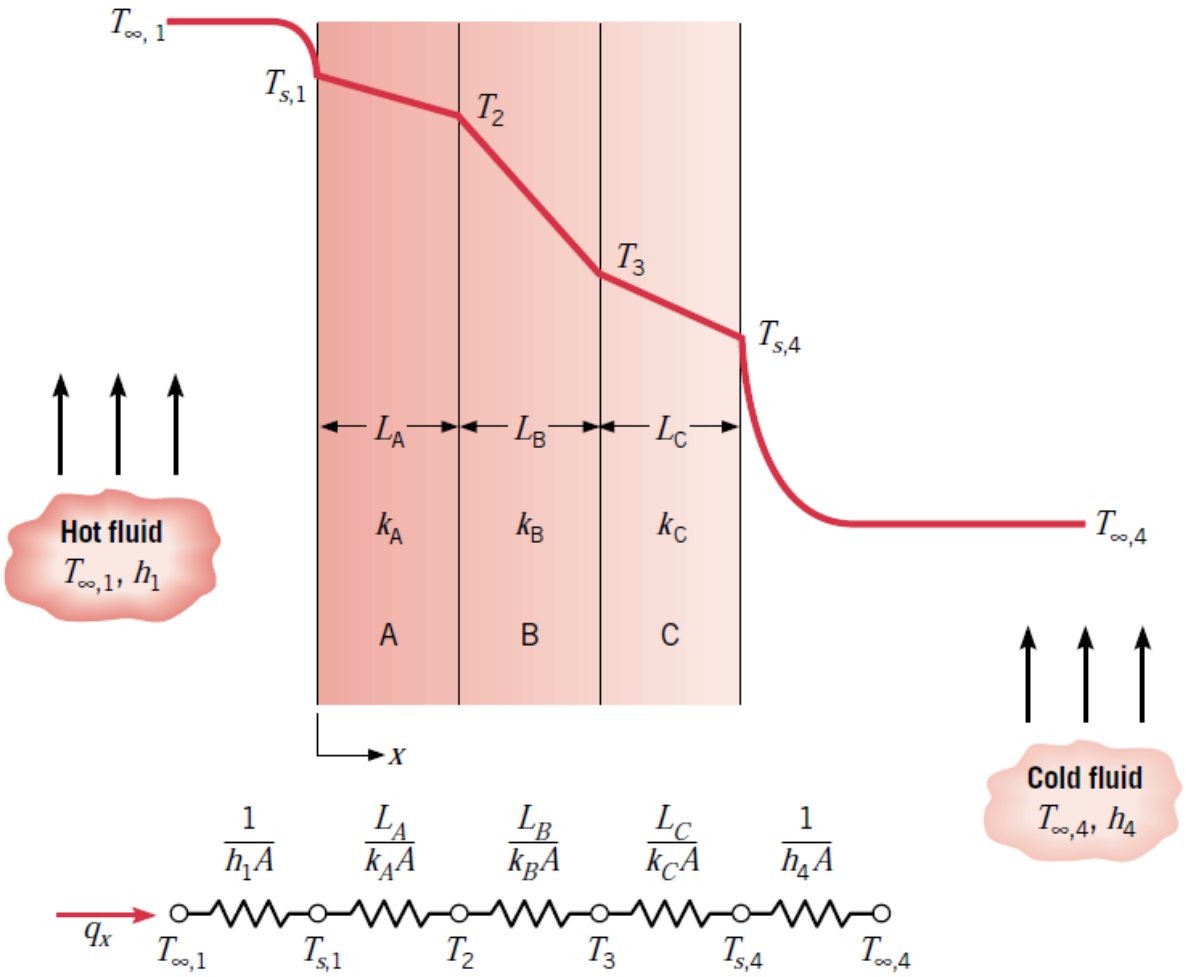

Figure 82: Equivalent thermal circuit for a series composite wall (Incopera, et al., 2007)

A composite wall heat transfer coefficient was calculated for conduction through the side reflector, core barrel (CB), annulus gap, RPV and reactor cavity using equation (6-7).

$$\text{Overall heat transfer coefficient, } U = \frac{1}{R_{tot} A} = \frac{1}{\left[\left(\frac{L_{sr}}{k_{sr}}\right)+\left(\frac{L_{CB}}{k_{CB}}\right)+\left(\frac{L_{Hegap}}{k_{He\ gap}}\right)+\left(\frac{L_{RPV}}{k_{RPV}}\right)+\left(\frac{1}{h_{cavity}}\right)\right]} \quad (6\text{-}7)$$

$$U = \frac{1}{\left[\left(\frac{0.8799}{30}\right)+\left(\frac{0.076}{35}\right)+\left(\frac{0.2475}{0.3}\right)+\left(\frac{0.216}{35}\right)+\left(\frac{1}{21}\right)\right]}$$

$$U = 1.098$$

The loss of flow transient was simulated on a 1/6th assembly fuel block model. The assembly was initially maintained at steady state conditions at inlet temperature of 490 °C, system pressure of 7 MPa, power density 27.16 MW/m^3 and mass flow rate 1.207 kg/s in the coolant

channels. The system pressure was kept constant while the power density and mass flow rate were then reduced under the conditions stated in equation (6-8) and (6-9).

The decay heat of a reactor that has operated for an infinite number of hours and at a steady state power after shutdown can be estimated by equation (6-8) and (6-9) (Kugeler & Schulten, 1989).

$$P_N(t) = P_0 A(t^{-a} - (t + t_0)^{-a}) \quad (6\text{-}8)$$

$$\frac{P_N(t)}{P_0} = A(t^{-a} - (t + t_0)^{-a}) \quad (6\text{-}9)$$

where:

$\frac{P_N(t)}{P_0}$ = the normalised power emanating from the fission products at time t after shutdown

t = time after shutdown (s)

t_0 = reactor operation time (s)

The coefficients to be used for equation (6-8) and (6-9) are given Table 32.

Table 32: Coefficients for the power function (Kugeler & Schulten, 1989)

Time interval (s)	A	a
$10^{-1} < t < 10$	0.0603	0.0639
$10 < t < 150$	0.0766	0.181
$150 < t < 4 \times 10^6$	0.0603	0.0639

The power ratio can be estimated using the graph in Figure 83.

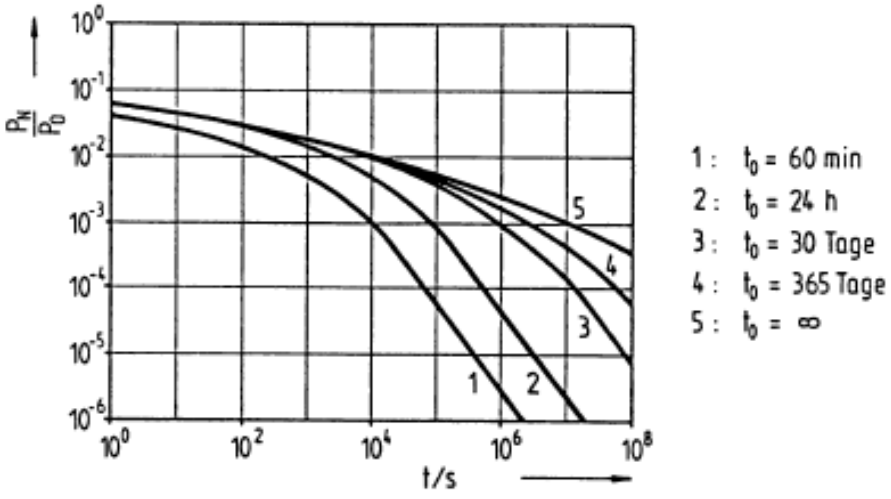

Figure 83: The ratio of the fission product decay power to the reactor operating power as a function of time t after shutdown (Kugeler & Schulten, 1989)

An approximation of the decay power from the fission products assuming a conservative infinite irradiation period is given by equation (6-10).

$$q''' \text{ (decay)} = q_0''' \times 0.0603t^{-0.0639} \quad (6\text{-}10)$$

During a PLOFC event, the helium flow rate is expected to decrease rapidly as the helium flow rate is disrupted. This loss of loss of mass flow would imply a reactor shutdown. So the thermal power in the reactor is a result of decay heat which is transported to the RCCS by conduction and radiation. The decrease of the mass flow rate is expected to be exponential and can be estimated by equations (6-11) and (6-12).

$$\frac{\dot{m}}{\dot{m}_0} = e^{-0.0123t}, \ 0 \leq t \leq 300 \quad (6\text{-}11)$$

$$\frac{\dot{m}}{\dot{m}_0} = -5.6 \times 10^{-7}t + 2.5 \times 10^{-2}, \ t \geq 300 \quad (6\text{-}12)$$

Where $\dot{m}_0 = 7\%$ of the original $\dot{m}$ steady state value

Figure 83 shows the change in temperature through the fuel rod centre and the graphite for the bottom block of the assembly during the PLOFC transient.

The fuel and graphite temperatures are shown in Figure 84. The fuel compact temperatures drop at the onset of the transient while the graphite temperature rises. After the first 15 minutes, the graphite and fuel compact values tend to move closer together to reach a common value of about 1164 ℃ at the bottom of the assembly and 1106 ℃ at the top of the last assembly block after about 20 hours. This is purely an arbitrary "numerical experiment" therefore no direct comparison with other similar studies can be made. It was only done to demonstrate the capability of the Flownex model to simulate transient conditions. The normal operation steady state value is 1195.2 ℃ for the fuel compact.

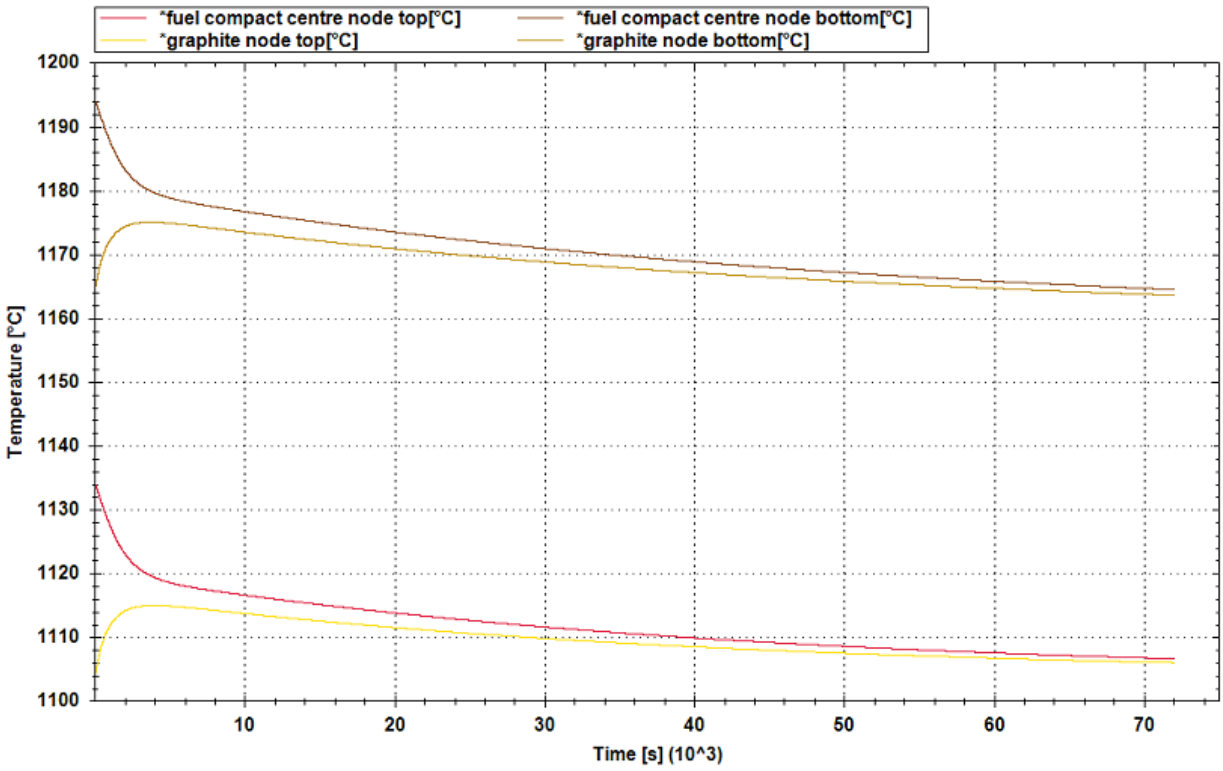

Figure 84: PLOFC temperature results for fuel

6.6.8 Comparison of actual fuel block layout versus Flownex layout

In this section a comparison between the distribution of coolant channels and the fuel compacts in the Flownex model and actual distribution in the standard fuel block is made. To demonstrate this, a 1/6th of a standard fuel block with eleven radial nodes and ten increments as shown in Figure 85 is considered. The first node is at the apex of the 1/6th and eleventh node at the outer edge. As a first approximation, it was assumed that the diameter of all the coolant channels is 1.59 cm including the coolant channel holes around the centre handling hole which are 1.27 cm in the actual fuel block. For the fuel compacts, a diameter of 1.27 cm was used.

The number of increments is shown on the left (numbers 1 to 10 in black in Figure 85) and the number of the rows where the actual fuel compacts or coolant channels are present are shown on the right (numbers 1 to 9 in red in Figure 85). It can be observed that in the first increment (at the apex) there are no coolant channels or fuel compacts.

The radial distance between the rows was calculated in order to get the total radial length. The position of the coolant channel and fuel compact centres, top and bottom were calculated for each layer and are shown in Table 33 for the coolant channels and Table 35 for the fuel compact. These positions were then used to calculate the number or fraction of coolant channels or fuel compacts that fit within a specific increment. As the areas of some of the coolant channels and

fuel compacts do not lie within one increment, fractional areas were calculated in each of the increments. The coolant channel or fuel rod density in an increment was calculated by dividing the number of coolant channels or fuel compacts in that increment by the area of the increment. The values for the number of coolant channels or fuel compacts for each increment and densities are shown in Table 34 and Table 36. It can be observed here that the densities are exactly the same for all increments in the Flownex calculation but differ in the actual fuel block.

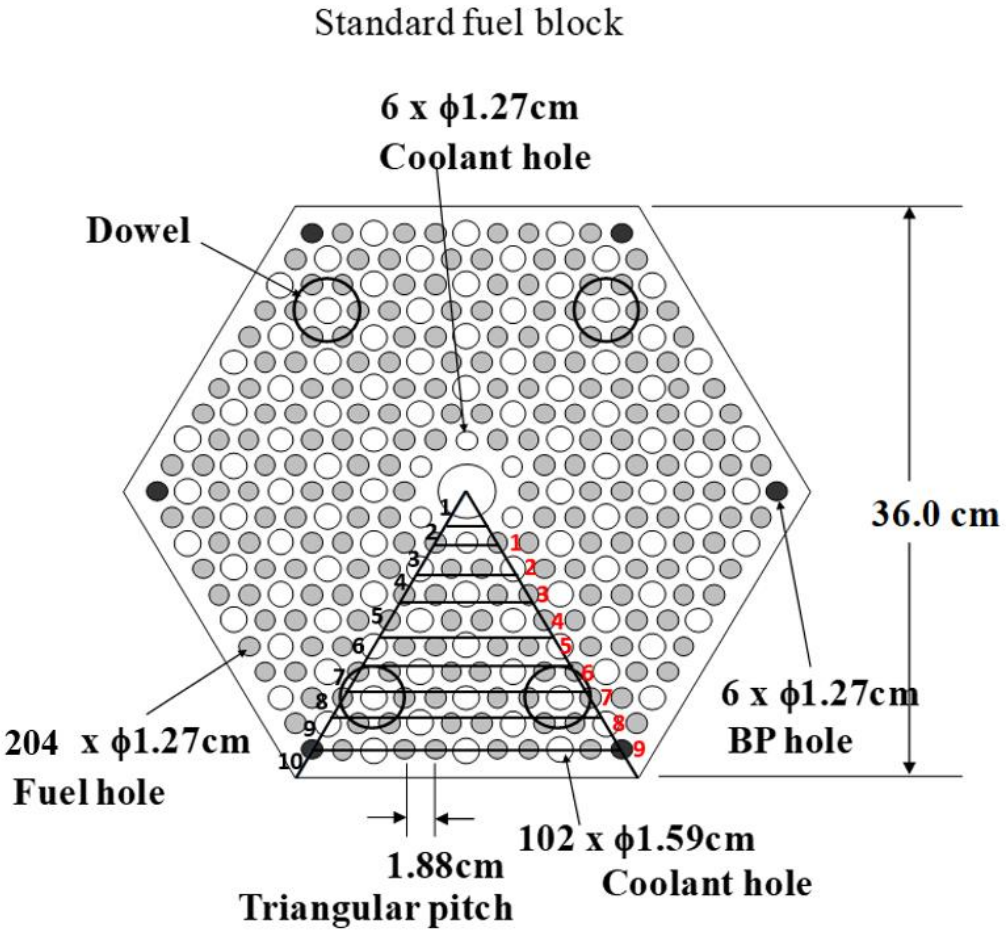

Figure 85: Schematic showing radial increments in a fuel block

Table 33: Positions of coolant channels per increment in the actual fuel block

Layer	Position		
	centre	bottom	top
0	0	0	0.024613
1	0.032563	0.024613	0.040513
2	0.048844	0.040894	0.056794
3	0.065125	0.057175	0.073075
4	0.081406	0.073456	0.089356
5	0.097688	0.089738	0.105638
6	0.113969	0.106019	0.121919
7	0.130250	0.122300	0.138200
8	0.146531	0.138581	0.154481
9	0.162813	0.154863	0.170763

Table 34: Number of coolant channels per Flownex increment compared to the actual number in the fuel block

Actual fuel block increments			Flownex increments		
Increment	**#coolant channels**	**Channel density**	**Increment**	**#coolant channels**	**Coolant channel density**
1	0	0	1	0.18	962.2504
2	0.766428	1365.733	2	0.54	962.2504
3	1.025983	1096.947	3	0.9	962.2504
4	1.178353	899.8972	4	1.26	962.2504
5	2.032816	1207.456	5	1.62	962.2504
6	2.140032	1040.023	6	1.98	962.2504
7	2.386314	981.2956	7	2.34	962.2504
8	3.22433	1149.116	8	2.7	962.2504
9	3.550829	1116.597	9	3.06	962.2504
10	1.694916	476.8811	10	3.42	962.2504

Table 35: Positions of fuel compacts per increment in the actual fuel block

Layer	Position		
	centre	**bottom**	**top**
1	0	0	0.026213
2	0.032563	0.026213	0.038913
3	0.048844	0.042494	0.055194
4	0.065125	0.058775	0.071475
5	0.081406	0.075056	0.087756
6	0.097688	0.091338	0.104038
7	0.113969	0.107619	0.120319
8	0.13025	0.1239	0.1366
9	0.146531	0.140181	0.152881

Table 36: Number of fuel rods per Flownex increment compared to the actual number in the fuel block

Actual fuel block increments			Flownex increments		
Increment	**# fuel rods**	**fuel rod density**	**Increment**	**# fuel rods**	**fuel rod density**
1	0	0	1	0.34	1817.58418
2	0.714146	1272.56969	2	1.02	1817.58418
3	2.190805	2342.33693	3	1.7	1817.58418
4	2.095049	1599.96934	4	2.38	1817.58418
5	3.00	1781.94528	5	3.06	1817.58418
6	4.034974	1960.93692	6	3.74	1817.58418
7	5.422147	2229.68507	7	4.42	1817.58418
8	6.061463	2160.2391	8	5.1	1817.58418
9	7.205086	2265.71792	9	5.78	1817.58418
10	3.276331	921.82780	10	6.46	1817.58418

In the actual fuel block it can be observed that there are no fuel rods at the centre of the block as opposed to the uniform distribution in Flownex that allocates 0.34 of a fuel rod. In the middle of the block though, the number of fuel rods assumed by Flownex is in some areas less than the number of fuel rods in the actual block. At the edge of the block (increment 10), the Flownex model assumes almost double the number of fuel rods as in the actual fuel block. A

similar observation can be made with coolant channels. This is expected to have an effect on the distribution of the power density within the block when comparing Flownex and CORONA results. It is supposed to be evident in the CORONA result around the edges and centre of the block where in the actual block these regions will not have any fuel rods. This is further demonstrated in the calculation in Appendix C.

6.6.9 Summary

In this chapter, a few selected validation and verification the results for selected cases in Flownex were simulated and the results compared to other Flownex results, STAR-CCM+ and also CORONA results where applicable. For the single fuel unit cell, 2-D integrated prismatic fuel block, 3-D integrated prismatic fuel block and fuel block assemblies, Flownex results were found to be in good agreement with the results from other codes. The cross flow, bypass gap size effect seemed to agree with trends reported in literature. Coolant channel blockage simulation was used to demonstrate tangential conduction within the standard fuel block and it was concluded that Flownex can model this phenomenon. However, when the coolant channel blockage was applied to the $1/6^{th}$ assembly fuel block assembly and the results compared to those obtained from CORONA, the short-comings of the coolant channel model in Flownex became apparent.

7 CONCLUSIONS AND FUTURE WORK

From the literature studied, it was apparent that there is quite a number of existing approaches that can be adopted for modelling heat transfer in prismatic block reactors. In this study, a philosophical development of a Flownex network based model of a prismatic block was demonstrated. This methodology was then applied to segments and segment assemblies of the PMR200 standard fuel block.

This study presented the conceptual formulation of a model to simulate the thermal-fluid phenomena of the HTR block. It was shown that a network of elements could be used to construct a comprehensive multi-dimensional network model that can be used as a building block for the analysis of the temperature distribution for a standard fuel block and assembly. The network approach can be used to reasonably predict temperature distributions within a prismatic fuel block. It has been shown that Flownex is capable of simulating the complex models dictated by the prismatic block type core elements. The level of detail for models can vary depending on project needs at a particular time. For integrated system analyses, it is possible to extract data from the more complex models to be used to develop the necessary simplified or reduced order models.

The results obtained from the Flownex models developed in this study agree very well with fairly detailed models developed in CORONA and CFD models that deal with more comprehensive models based on the conservation equations.

7.1 Summary of Work

7.1.1 Temperature distribution through a single fuel rod

To show the adequacy of the fuel compact/ rod discretization used in Flownex, a single fuel rod with surrounding graphite was modelled in Flownex and compared to models with varying mesh sizes created in CORONA. The Flownex discretization was shown to be sufficient for the current project.

7.1.2 1/6th fuel block

The unit cell method was implemented to the control volumes of a 1/6th of a fuel block with varying discretization in the axial and tangential directions. In this model the bypass gap and the cross flow gap were not modelled. This was done to establish grid independence of the models. Even though all the models did not vary much (within 1 °C), it was found that the 11 x5x3 grid was sufficient for the purposes of this project. The 11x5x3 3-D integrated fuel block

Flownex model results were then compared with results obtained from the 2-D integrated fuel block Flownex model created by Sambureni (2015) and the 3-D model from STAR-CCM+. The results were found to be comparable for the three models with the comparison done at the middle line probe inserted halfway through the height of the fuel block for the STAR-CCM+ model. The average exit temperature of the helium was found to be 542.98 ℃ for the 2-D integrated block Flownex model, 542.94 ℃ for the STAR-CCM+ model and 542.55 ℃ for the 3-D integrated block Flownex model. The maximum fuel surface temperature along the centreline was predicted to be 604.4 ℃ from the 2-D integrated block Flownex model, 602.5 ℃ for the 3-D integrated block Flownex model, fuel centre temperature of 609.7 ℃ for the STAR-CCM+ and 607.8 ℃ for the 3-D integrated block Flownex model. The 11x5x3 grid was then implemented in all the subsequent Flownex models up to and including the fuel block assembly models.

7.1.3 1/6th fuel block assembly with leakage flows

A 1/6th six standard fuel block model which includes all cross flow and bypass leakage gaps was then created in Flownex. The results of this model were compared with results obtained from a six full standard fuel block model created in CORONA. The Flownex results were in good agreement to the CORONA results. The difference in the maximum fuel temperatures between the two codes is about 0.53 ºC and the average coolant outlet temperatures were comparable, with 1.4 ºC difference. This assembly was also used to simulate pressurised loss of forced cooling incident and coolant channel blockage accidents.

7.1.4 Fuel block

A complete fuel block model with bypass flow was constructed from the 1/6th model and the radial, axial and tangential temperature distributions were plotted. The temperature distributions for the fuel compact centre, graphite block and coolant channel flow were obtained. In this model, the coated particle discretization and temperature distribution can still be included if there is a need. This model was also used to simulate coolant channel blockage accidents.

7.1.5 Whole fuel block assembly

It was discovered that only three blocks can be stacked in Flownex to form an assembly due to memory and GUI limitations. It was also decided to exclude the discretization in the coated fuel particles to reduce the load on the GUI and memory. A three-fuel block assembly model including bypass and cross flow was constructed from the full fuel block model and the radial, axial and tangential temperature distributions were plotted. The effect of bypass gap size was

investigated. Three bypass gap sizes that were simulated were 0, 3 and 5 mm. It was observed that the bigger the bypass gap size, the higher the fuel temperatures. The axial and radial temperature distributions were plotted and compared to CORONA results for a similar fuel block assembly.

7.2 Concluding Remarks

The following conclusions were drawn from this study:

- It was shown that a collection of network elements could be used to construct a comprehensive multi-dimensional network model that can be used as a building block for the analysis of the temperature distribution for a fuel assembly. The network approach can be used to reasonably predict temperature distributions within a prismatic fuel block.
- The Flownex model was able to provide the coated fuel particle layers, graphite and coolant temperature distributions for each control volume in the fuel block. The results of the Flownex model were compared with those obtained from CORONA and were found to be in good agreement. Current results provide confidence in the ability for Flownex to solve the fundamental conservation and heat transfer relations as applied to the prismatic block core.
- It was discovered that only three blocks can be stacked in Flownex to form an assembly due to memory and GUI limitations.
- The maximum fuel, graphite and coolant channel temperatures were significantly increased with the increase in gap width.
- The gap outlet temperature decreases with increasing bypass gap width as more convection heat transfer from the fuel block to the leaked coolant occurs.
- With the channel blockage incident, the axial, radial and tangential heat transfer within the block and the coolant flow redistribution were demonstrated.

7.3 Recommendations for Future Work

A great deal of effort has been made to develop a comprehensive philosophy and methodology for the development of network models for prismatic HTR core components, however, more work still need to be done to enable thermal-fluid whole-core analyses using Flownex. As mentioned in section 1.5, the models developed did not include all the core components and did not span the full height of the core. Therefore reduced order models that can reasonably

predict temperature distribution within the core still need to be developed and relevant transient analyses still need to be performed to allow for whole-core applications:

- Development of a full-fuel block element/component with limited input and result that can be used as a building block for HTR core models.
- From this, a model that shows the top view of the reactor core can be built
- The model should allow the user to connect leak flow paths with adjacent assemblies.
- Establish how an assembly block component can be used to build a whole HTR core model.
- As an alternative model for a prismatic block core, a prismatic block modelled as a porous medium should be incorporated into Flownex.
- Variable bypass gap studies.
- Control rod block or reserve shutdown block model.
- Permanent side reflectors models.
- Core support structures models.
- The development of whole-core models is currently made difficult by the level of detail the current models have and therefore model and component reduction is essential to alleviate issues that create problems for visualisation of the network models on the Flownex graphic user interface and memory and computational time issues.
- Once the whole-core models have been developed, modelling of the phenomena such as core thermal behaviour under natural circulation conditions, in particular the upward and downward natural circulation within the core itself can be demonstrated.
- A full verification and validation of all models including quantifying uncertainties associated with the results given in this study is still to be done.
- Channel blockage incident can only be modelled for a fraction of a coolant channel or group of coolant channels since the Flownex model uses representative coolant channel approach. If Flownex can model the coolant channels explicitly then this problem can be avoided.
- M-Tech Industrial Pty (Ltd) could look into building a prismatic block element similar to the PBMR element that will hide the network from the GUI and therefore reduce memory concerns.
- Automatic grid generation so that the model can be easier to implement.

- Flownex models that demonstrate the effect of distributing the fuel rods evenly in the fuel versus actual distribution can be created and the results compared to CORONA results.

BIBLIOGRAPHY

ANSYS Inc., 2018. *ANSYS.* [Online] Available at: https://www.ansys.com/ [Accessed 15 September 2018].

Cengel, Y. A., Turner, R. H. & Cimbala, J. M., 2008. *Fundamentals of Thermal-Fluid Sciences.* Third ed. Singapore: McGraw-Hill.

Chung, T. J., 2002. *Computational Fluid Dynamics,* Cambridge: Cambridge University Press.

Cioni, O., Marchand, M., Geffraye, G. & Ducros, F., 2006. 3D Thermal-Hydraulic Calculations of a Modular block-type HTR core. *Nuclear Engineering and Design,* 236(2006), p. 565–573.

Clifford, I. D., 2013. *A hybrid coarse and fine mesh solution method for prismatic high temperature gas-cooled reactor thermal-fluid analysis,* Pennsylvania: Pennsylvania State University.

Du Toit, C. G. & Rousseau, P. G., 2012. Modeling the Flow and Heat Transfer in a Packed Bed High Temperature Gas-cooled Reactor in the Context of a Systems CFD Approach. *Journal of Heat Transfer,* 134(3).

Emslie, F. N., 2005. *Flownex analysis of high temperature test reactor thermo-hydraulic benchmarks,* Potchefstroom, South Africa: North-West University.

General Atomics, 1992. *Preliminary Safety Information Document for the Standard MHTGR,* Idaho: Stone & Webster Engineering Corp.

General Atomics, 1996. *GT-MHR conceptual design description report, Part I,* California: Nuclear Regulatory Commission.

Generation IV International Forum, 2014. *GIF annual report.* [Online] Available at: https://www.gen-4.org/gif/jcms/c_59461/generation-iv-systems [Accessed 15 January 2015].

Generation IV International Forum, 2015. *Generation IV Systems.* [Online] Available at: https://www.gen-4.org/gif/jcms/c_59461/generation-iv-systems [Accessed 15 January 2015].

Greyvenstein , G. P. & Van Antwerpen, H. J., 2004. *A Finite Volume-based Network Method for the Prediction of Heat, Mass and Momentum Transfer in a Pebble Bed Reactor.* Beijing, 2nd International Topical Meeting on HIGH TEMPERATURE REACTOR TECHNOLOGY.

Greyvenstein, G. P., 2002. An Implicit Method for the Analysis of Transient Flows in Pipe Networks. *International Journal for Numerical Methodds in Engineering*, 53(5), pp. 1127-1143.

Greyvenstein, G. P. & Laurie, D. P., 1994. A Segregated CFD Approach to Pipe Network Analysis. *International Journal for Numerical Methods in Engineering*, 37(1994), pp. 3685-3705.

Greyvenstein, G. P., Van Antwerpen, H. J. & Rousseau, P. G., 2004. The system CFD approach applied to a pebble bed reactor. *International Journal of Nuclear Energy Science and Technology*, 1(1), pp. 44-60.

Groehn, H. G., 1982. Estimate of cross flow in high temperature gas-cooled reactor fuel blocks. *Nuclear Technology*, 56(2), pp. 392-400.

Huning, A. J., 2014. *A Steady State Thermal Hydraulic Analysis Method for Prismatic Gas Reactors*, Atlanta: Georgia Institute of Technology.

Incopera, F. P., DeWett, D. P., Bergman, T. L. & Lavine, A. S., 2007. *Fundamentals of Heat and Mass Transfer*. 6th ed. New York: John Wiley & Sons, Inc..

International Atomic Energy Agency, 2010. *High Temperature Gas Cooled Reactor Fuels and Materials*, Vienna: IAEA.

International Atomic Energy Agency, November, 2003. *Evaluation of high temperature gas cooled reactor performance: Benchmark analysis related to initial testing of the HTTR and HTR-10*, Vienna, Austria: IAEA.

Jensen, S. E. & Nonbol, E., 1998. *Description of the Magnox Type of Gas cooled Reactor (MAGNOX)*, Roskilde, Denmark: Riso National Laboratory.

Johnson, R. W. & Sato, H., 2012. *Bypass flow computations using a one-twelfth symmetric sector for normal operation in a 350 MWth prismatic VHTR.* Prague, Czech Republic, Proceedings of HTR 2010.

Johnson, R. W. & Sato, H., 2012. Bypass flow computations using a one-twelfth symmetric sector for normal operation in a 350 MWth prismatic VHTR. *Nuclear Engineering and Design*, 251(2012), pp. 84-91.

Kaburaki, H. & Takizuka, T., 1987. Effect of crossflow on flow distribution in HTGR core column. *Journal of Nuclear Science and Technology*, pp. 516-525.

Kim, M. H. & Lim, H. S., 2011. Evaluation of the influence of bypass flow gap distribution on the core hot spot in a prismatic VHTR core. *Nuclear Engineering and Design,* 241(2011), p. 3076– 3085.

Koster, A., Matzner, H. D. & Nichols, D. R., 2003. PBMR design for the future. *Nuclear Engineering and Design,* 222(2003), pp. 231-245.

Krieth, F. & Bohn, M. S., 2000. *Principles of Heat Transfer.* 6th edition ed. s.l.:CL-Engineering.

Kugeler, K. & Schulten, R., 1989. *Hochtemperaturreatortechnik.* Berlin: Springer-Verlag.

Lamarsh, J. R. & Baratta , A. J., 2001. *Introduction to Nuclear Engineering.* Third ed. New Jersey: Prentice Hall.

Lee, J. H., Cho, H. K. & Park, G. C., 2016 (a). Development of the loss coefficient correlation for cross flow between graphite fuel blocks in the core of prismatic very high temperature reactor-PMR200. *Nuclear Engineering and Design,* 307(2016), pp. 106-118.

Lee, S. N., 2015. *Progress on the Verification and Validation of CORONA Code [personal correspondence]*. Cape Town: KAERI-NWU 6th workshop / follow-up meeting.

Lee, S. N., Tak, N. I. & Kim, M. H., 2016 (b). Fuel Temperature prediction using variable bypass gap size in the prismatic VHTR. *Nuclear Engineering and Design,* 300(2016), pp. 578-590.

Lee, S. N., Tak, N. I., Kim, M. H. & Noh, J. M., 2014. Thermal analysis of prismatic gas-cooled reactor core under coolant channel blockage accidents. *Annals of Nuclear Energy,* 71(2014), pp. 11-22.

Lim, H. S., 2005. *Transient Multicomponent Mixture Analysis for Air Ingress Phenomena in a High-Temperaature Gas-Cooled Reactor (HTGR),* Daejeon: Korea Advanced Institute of Science and Technology (KAIST).

Lim, H. S., 2015. *GAMMA+ 1.0 Volume I: User's Manual, , KAERI/TR-6167/2015,* Daejeon: Korea Atomic Energy Research Institute.

MacDonald, P. E., 2003. *NGNP Preliminary Point Design – Results of the Initial Neutronics and Thermal-Hydraulic Assessments,* Idaho: Idaho National Engineering and Environmental Laboratory.

Matzner, D., 2004. *PBMR project status and the way ahead.* Beijing, 2nd International Topical Meeting on HIGH TEMPERATURE REACTOR TECHNOLOGY.

McEligot, D. M., Magee, P. M. & Leppert, G., 1965. Effect of Large Temeprature Gradient on Convective Heat Transfer: The Downstream Region. *Journal of Heat Transfer,* Volume 87, pp. 67-76.

McEligot, D. M. et al., 2006. *Investigation of Fundamental Thermal-Hydraulic Phenomena in Advanced Gas-cooled Reactors,* Idaho Falls: Idaho National Laboratory.

McKeen, T., 2010. *Nuclear Energy Materials and Reactors - Advanced Gas Cooled Reactors.* Paris, France, [http://www.eolss.net]: Encyclopedia of Life Support Ssytems.

Methnani, M. & Kupitz, J., 2004. *Status of high temperature gas-cooled reactor technology.* Trieste, Italy, Workshop on Nuclear Reaction Data and Nuclear Reactors: Physics, Design and Safety.

M-Tech Industrial, 2016 (b). *Flownex Theory manual,* Potchefstroom: M-Tech Industrial Pty (Ltd).

M-Tech Industrial, 2017. *Flownex Library manual Version 8.8.0.3186,* Potchefstroom: M-Tech Industrial Pty (Ltd).

Nonbol, E., 1996. *Description of the Advanced Gas Cooled Type of Reactor (AGR),* Roskilde, Denmark: Riso National Laboratory.

Nuclear Safety Standards Commission (KTA), 1981. *Reactor Core Design of High-Temperature Gas-Cooled Reactors, Part 3: Loss of Pressure through Friction in Pebble Bed Cores,* Salzgitter: Geschäftsstelle des Kerntechnischen Ausschusses.

Olivier, J. C., 2005. *Network modelling of transient heat exchanger performance,* Potchefstroom, North-West: Potchefstroom University for Christian Higher Education.

Ortensi, J. et al., 2010. *Deterministic Modeling of the High Temperature Test Reactor,* Idaho Falls: Idaho National Laboratory.

Patankar, S. V. & Spalding, D. B., 1972. A Calculation Procedure for Heat, Mass and Momentum Transfer in Three-dimensional Parabolic Flows. *International Journal of Heat and Mass Transfer*, 15(10), pp. 1787-1806.

PBMR, 2010. *PBMR Annual Report,* Pretoria: The Ux Consulting Company, LLC (UxC).

Rousseau, P. G. & Greyvenstein , G. P., 2002 (a). *One-Dimensional Reactor model for the Integrated Simulation of the PBMR Power Plant.* Kruger Park, 1st International Conference on Heat Transfer, Fluid Mechanics and Thermodynamics.

Rousseau, P. G. & Greyvenstein, G. P., 2002 (b). *Modelling of HTTR in Flownet.* Petten, The Netherlands, 1st International Topical Meeting on High Temperature Reactor Technology (HTR).

Sambureni, P., 2015. *Thermal fluid model for a prismatic block in a gas-cooled reactor using FLOWNEX,* Potchefstroom, South Africa: North-West University.

Sato, H., Johnson, R. & Schultz, R., 2010. Computational fluid dynamic analysis of core bypass flow phenomena in a prismatic VHTR. *Annals of Nuclear Energy*, 37(2010), p. 1172–1185.

Schultz, R. R., 2008. *Meeting the thermal-hydraulic analysis needs for advanced gas reactor systems.* Washington DC, USA, Proceedings of the 4th International Topical Meeting on High Temperature Reactor Technology.

Sousa, R. V. et al., 2013. *A preliminary neutronic evaluation of the high temperature gas-cooled test reactor HTR-10 using the scale 6.0 code.* Rio de Janeiro, Brazil, 2013 International Nuclear Stlantic Conference - INAC 2013.

Stainsby, R., Worsley, M., Dawson, F. & Grief, A., 2009. *Investigation of Local Heat Transfer Phenomena in a Prismatic Modular Reactor Core,* Toronto: AMEC NSS Limited.

Strydom, G., Bostelmann, F. & Yoon, S. J., 2015. *Results for phase I of the IAEA Coordinated Research Program on HTGR Uncertainties INL/EXT-14-32944 rev 1,* Idaho Falls, Idaho: Idaho National Laboratory.

Takizuka, . T., 2005. Reactor Technology Development under the HTTR Project. *Progress in Nuclear Energy*, 47(1-4), pp. 283-291.

Tak, N. I., Kim, M. H. & Lee, W. J., 2008. Numerical Investigation of a heat transfer within the prismatic fuel assembly of a very high temperature reactor. *Annals of Nuclear Energy,* Volume 35, pp. 1892-1899.

Tak, N. I., Kim, M. H., Lim, H. S. & Noh, J. M., 2012. A practical method for whole-core thermal analysis of a prismatic gas-cooled reactor. *Nuclear Technology,* Volume 177, pp. 352-365.

Tak, N. I. et al., 2014. Development of a core thermo-fluid analysis code for prismatic gas cooled reactors. *Nuclear Engineering and Technology,* 46(5), pp. 641-654.

Tak, N. I. & Lim, H. S., 2014. *Introduction to GAMMA+,* Daejeon: Korea Atomic Energy Research Institute.

Travis, B. W. & El-Genk, M. S., 2013. Numerical Simulation and Turbulent Convection Heat Transfer Correlation for Coolant Channels in a Very-High-Temperature Reactor. *Heat Transfer Engineering,* 34(1), pp. 1-14.

Travis, B. W. & El-Genk, M. S., 2013. Thermal-hydraulics analyses for 1/6 prismatic VHTR core and fuel element with and without bypass flow. *Energy Conversion and Management,* Volume 67, pp. 325-341.

Tung, Y. H., Ferng, Y. M., Johnson, R. W. & Chieng, C. C., 2016. Transient LOFA computations for a VHTR using one-twelfth core flow models. *Nuclear Engineering and Design,* 201(2016), pp. 89-100.

Van Antwerpen, H. J., 2007. *Modelling a pebble bed High Temperature Gas-Cooled Reactor using a system-CFD approach,* Potchefstroom: North-West University.

Van der Merwe, J. J., 2003. *Simulation of heat and momentum transfer in the high temperature test reactor,* Potchefstroom, South Africa: North-West University.

Versteeg, H. K. & Malalasekera, W., 2007. *An Introduction to Computational Fluid Dynamics: The Finite Volume Method.* Second ed. London: Prentice Hall.

Walter, A., Schultz, A. & Lonhert, G., 2004. *Comparison of Two Models for a Pebble Bed Modular Reactor Core Coupled to a Brayton Cycle.* Beijing, 2nd International Topical Meeting on High Temeprature Reactor Technology.

World Nuclear Association, 2018. *World Nuclear Association.* [Online] Available at: http://www.world-nuclear.org/information-library/country-profiles/countries-g-n/japan-nuclear-power.aspx [Accessed 15 November 2018].

Yang, M. et al., 2013. Denoising method of X-ray phase contrast DR image for TRISO- coated fuel particles. *Particuology,* 11(6), pp. 695-702.

Yoon , S. J. & Strydom, G., 2014. *Comparison of Homogeneous and Heterogeneous CFD Fuel Models for Phase I of the IAEA CRP on Uncertainties Benchmark.* Charlotte, USA, Proceedings of ICAPP 2014.

Yoon, S. J., Lee, J. H., Kim, M. H. & Park, G. C., 2012. The effects of crossflow gap and axial bypass gap distribution on the flow characteristics in the prismatic VHTR core. *Nuclear Engineering and Design,* 250(2012), pp. 465-479.

Zhang, Z. et al., 2016. The Shandong Shidao Bay 200 MWe High-Temperature Gas-Cooled Reactor Pebble-Bed Module (HTR-PM) Demonstration Power Plant: An Engineering and Technological Innovation. *Engineering,* 2(2016), pp. 112-118.

APPENDICES

APPENDIX A

Material properties for Flownex models

Table 37 lists some of the parameters that were obtained from KAERI and used to create a fuel block model in Flownex.

Table 37: Parameters used to simulate 1/6th fuel block in Flownex

Inlet temperature (°C)	490
Inlet Pressure (MPa)	7
Number of standard coolant channels	18
Number of fuel rods	34
Diameter of coolant channels (cm)	1.59
Area of coolant channel (cm^2)	1.99
Area of 1/6th segment (cm^2)	187.1
Height of a block (cm)	79.3
Total heat input (MW)	0.0866
Bypass gap width (mm)	2
Mass flow rate (kg/s)	0.20116

Material properties used in this study are indicated in Table 38 to Table 45 (Lee, 2015).

Table 38: Helium properties

Material Property	Value
Density (kg/m^3)	3.3931
Thermal conductivity (W/m.K)	0.36
Specific heat, (J/kg.K)	5197.6
Dynamic viscosity (Pa.s)	4.6x10^{-5}

Table 39: Graphite H451 properties

Temperature [K]	Cp [J/(kg.K)]
2.94e02	1.00e02
9.7e02	1.00e02
Temperature [K]	k [W/(m.K)]
255.6	28.97
811.1	28.97
950	29.97
1088.9	32.28
1227.8	34.58
1366.7	36.89
1505.6	39.19
1644.4	41.5
1922.2	41.5
3000	41.5

Table 40: Fuel compact properties

Temperature [K]	Cp [J/(kg.K)]	Temperature [K]	k [W/(m.K)]
2.56e02	1.39e03	2.56e02	4.86e00
5.33e02	1.39e03	3.94e02	5.36e00
6.72e02	1.74e03	5.33e02	5.86e00
8.11e02	1.90e03	6.72e02	6.36e00
9.50e02	1.99e03	8.11e02	6.85e00
1.09e03	2.05e03	9.50e02	7.35e00
1.23e03	2.08e03	1.09e03	7.85e00
1.37e03	2.11e03	1.23e03	8.35e00
1.51e03	2.14e03	1.37e03	8.85e00
1.64e03	2.16e03	1.51e03	9.35e00
1.78e03	2.18e03	1.64e03	9.85e00
1.9e03	2.19e03	1.78e03	1.03e01
2.06e03	2.21e03	1.92e03	1.08e01
2.20e03	2.23e03	2.06e03	1.13e01
3.00e03	2.23e03	2.20e03	1.18e01
		3.00e03	1.18e01

Table 41: B_4C properties

Temperature [K]	Cp [J/(kg.K)]
2.94e02	1.00e02
9.73e02	1.00e02
Temperature [K]	**K [W/(m.K)]**
273.15	32.57
293.15	32.57
373.15	28.97
473.15	25.22
673.15	19.88
873.15	16.8
1073.15	15.25
1273.15	14.5
2000	14.5

Table 42: UO_2 properties

Temperature [K]	k [W/(m.K)]
0.0	3.81
1.00e03	3.81
1.20e03	3.46
1.40e03	2.77
1.60e03	2.60
1.80e03	2.42
2.00e03	2.25
3.00e03	2.25
9.00e03	2.25

Table 43: Buffer layer properties

Temperature [K]	k [W/(m.K)]
0.0	2.3
3.50e02	2.3
3.90e02	1.88
4.90e02	1.68
6.00e02	1.48
7.30e02	1.35
8.30e02	1.30
3.00e03	1.30
9.00e03	1.30

Table 44: SiC properties

Temperature [K]	k [W/(m.K)]
0.0	1.99e01
7.73e02	1.99e01
1.17e03	1.83e01
1.37e03	1.79e01
1.57e03	1.78e01
3.00e03	1.78e01
9.00e03	1.78e01

Table 45: PyC properties

Temperature [K]	k [W/(m.K)]
0.0	9.20
3.50e02	9.20
3.90e02	7.5
4.90e02	6.70
6.00e02	5.90
7.30e02	5.40
8.30e02	5.20
3.00e03	5.20
9.00e03	5.20

Parameters of coated fuel particle used in this thesis work and fuel compact are listed in Table 46 and Table 47.

Table 46: Coated fuel particle parameters (Strydom, et al., 2015)

TRISO Fuel Particle Parameter	Dimension (cm)
Fuel kernel radius	2.125E-02
Porous carbon buffer layer outer radius	3.125E-02
Inner PyC outer radius	3.525E-02
SiC outer radius	3.875E-02
Outer PyC outer radius	4.275E-02

Table 47: Fuel compact dimensions (Strydom, et al., 2015)

Parameter	Dimension (cm)
Fuel compact outer radius	0.6225
Fuel/helium gap outer radius	0.6350
Unit cell pitch	1.8796
Fuel compact height	4.9280

APPENDIX B

Heat transfer in a coated fuel particle

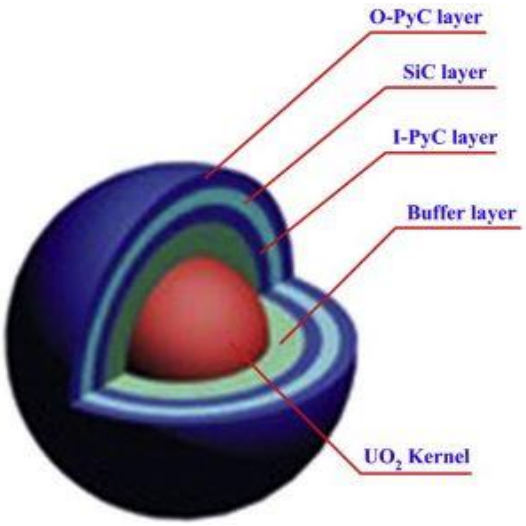

Figure 86: Structure of the TRISO fuel particle (Yang, et al., 2013)

Consider the coated fuel particle shown in Figure 86. The coated fuel particle consists of a fuel kernel with an outer radius of r_k and a thermal conductivity of k_f. The fuel kernel is surrounded by a buffer layer of outer radius r_b and thermal conductivity k_b. The other coatings are of inner and outer pyrolytic carbon and a silicon carbide layer with outer radii of r_{iPyC}, r_{oPyC} and r_{SiC}, respectively and thermal conductivities of k_{iPyC}, k_{oPyC} and k_{SiC}, respectively. Heat is generated uniformly at a rate of $\dot{q}\ \left[\frac{W}{m^3}\right]$ in the fuel kernel. At the centre of the fuel kernel the temperature gradient is $\left|\frac{dT}{dr}\right|_{r=0}$=0 and at the surface of the fuel kernel the temperature is Ts.

The one-dimensional governing differential equation for energy conservation in a sphere can be written in spherical coordinates as:

$$\frac{1}{r^2 \sin\emptyset}\left[\frac{d}{dr}\left(-kr^2 \sin\emptyset \frac{dT}{dr}\right)\right] = q \ \text{ for } \begin{cases} 0 < \emptyset < \pi \\ 0 < \theta < 2\pi \\ r_i < r < r_o \end{cases} \qquad \text{(B-1)}$$

First consider the temperature distribution in the fuel kernel. Assuming the temperatures to be uniform in the azimuthal ($\emptyset$) and tangential (θ) directions, integration in the azimuthal and tangential directions lead to the radial symmetric formulation for the differential equation:

$$4\pi k_f \frac{d}{dr}\left(r^2 \frac{dT}{dr}\right) = -4\pi r^2 \dot{q} \qquad \text{(B-2)}$$

Where: k_f is the thermal conductivity in the fuel kernel

$\dot{q}$ is the heat per unit volume generated in the fuel kernel

r is the radial coordinate

Integrating:

$$4\pi k_f\, r^2 \frac{dT}{dr} = -\frac{4\pi r^3}{3}\dot{q} + C_1 \qquad \text{(B-3)}$$

At r=0, $\frac{dT}{dr}$=0, the fuel kernel maximum temperature at the centre

$\therefore C_1 = 0$

Substituting the result in equation (B-3) and dividing the resulting by r^2 and integrating yields:

$$4\pi k_f \frac{dT}{dr} = -\frac{4\pi r}{3}\dot{q}$$

$$\int 4\pi k_f\, dT = -\int \frac{4\pi r}{3}\dot{q}\; dr$$

$$4\pi k_f\, T(r) = -\frac{4\pi r^2}{6}\dot{q} + C_2 \qquad \text{(B-4)}$$

Assuming that the fuel kernel surface temperature to be:

$$T(r_{kernel}) = T_s$$

Substituting into equation (B-4) then:

$$4\pi k_f\, T_s = -\frac{4\pi r_k^2}{6}\dot{q} + C_2 \qquad \text{(B-5)}$$

$$\therefore C_2 = 4\pi k_f\, T_s + \frac{4\pi r_k^2}{6}\dot{q} = 4\pi\left(k_f\, T_s + \frac{r_k^2}{6}\dot{q}\right) \qquad \text{(B-6)}$$

Substituting equation (B-6) into equation (B-4) and rearranging gives:

$$4\pi k_f\, T(r) = -\frac{4\pi r^2}{6}\dot{q} + 4\pi\left(k_f\, T_s + \frac{r_k^2}{6}\dot{q}\right) = \frac{4\pi}{6}\dot{q}\left(-r^2 + r_k^2\right) + 4\pi k_f\, T_s \qquad \text{(B-7)}$$

Let us assume that the temperature at the centre of the fuel kernel is given by:

At r=0, $T(0) = T_k$

$$4\pi k_f\, T_k = \frac{4\pi}{6}\dot{q}\, r_k^2 + 4\pi k_f\, T_s \qquad \text{(B-8)}$$

Multiplying the first term on the RHS of equation (5-8) by $\frac{r_k}{r_k}$ we get:

$$\frac{4\pi}{6}\dot{q}\,r_k^2 \times \frac{r_k}{r_k} = \frac{4\pi\dot{q}\,r_k^3}{6r_k} = \frac{4\pi\dot{q}\,r_k^3}{3(2r_k)} \tag{B-9}$$

Where the heat input into the fuel kernel $Q = \frac{4\pi r_k^3}{3}\dot{q}$,

Therefore equation (B-9) becomes, $\frac{Q}{2r_k}$

Substitute into equation (B-8) then we get:

$$4\pi k_f\,T_k = \frac{Q}{2r_k} + 4\pi k_f\,T_s$$

$$T_k = \frac{Q}{2r_k(4\pi k_f)} + \frac{4\pi k_f\,T_s}{4\pi k_f}$$

$$T_{kernel} = \frac{Q}{8\pi r_k k_f} + T_s$$

$$\therefore \Delta T_{kernel} = \frac{Q}{8\pi r_k k_f} \tag{B-10}$$

Now consider the temperature distribution in the first coating layer (the buffer layer) ($r_k < r < r_b$) . The differential equation that describes the temperature distribution in the radial direction is given as:

$$4\pi k_b \frac{d}{dr}\left(r^2 \frac{dT}{dr}\right) = 0 \tag{B-11}$$

Integrating equation (B-11) gives:

$$4\pi k_b \left(r^2 \frac{dT}{dr}\right) = C_3$$

Heat flux at $r = r_k$ is given by:

$$4\pi k_b \left|r^2 \frac{dT}{dr}\right|_{r=r_k} = -\frac{4\pi r_k^3}{3}\dot{q} = -Q$$

$$\frac{dT}{dr} = \frac{-Q}{4\pi k_b r_k^2}$$

Integrating gives:

$$\int dT = \int \frac{-Q}{4\pi k_b r_k^2}\,dr$$

$$T(r) = \frac{Q}{4\pi k_b}\left(\frac{1}{r}\right) + C_4 \tag{B-12}$$

If $T(r_0) = T_\infty$ then $T_\infty = \frac{Q}{4\pi k_b}\left(\frac{1}{r_0}\right) + C_4$

$$C_4 = T_\infty - \frac{Q}{4\pi k_b}\left(\frac{1}{r_0}\right)$$

Substituting back into equation (B-12) and rearranging gives the final expression for the temperature distribution each fuel particle coating:

$$T(r) = \frac{Q}{4\pi k_b}\left(\frac{1}{r}\right) + T_\infty - \frac{Q}{4\pi k_b}\left(\frac{1}{r_0}\right) = T_\infty + \frac{Q}{4\pi k_b}\left(\frac{1}{r} - \frac{1}{r_0}\right) \tag{B-13}$$

At $r = r_k$

$$T(r_k) = T_\infty + \frac{Q}{4\pi k_b}\left(\frac{1}{r_k} - \frac{1}{r_0}\right) \tag{B-14}$$

The temperature difference between successive fuel kernel coating layers can then be obtained from equation (B-14) as:

$$\therefore \Delta T_{coating} = \frac{Q}{4\pi k_b}\left(\frac{1}{r_k} - \frac{1}{r_0}\right) \tag{B-15}$$

These equations can therefore be used to obtain the temperature distribution in the coated fuel particle.

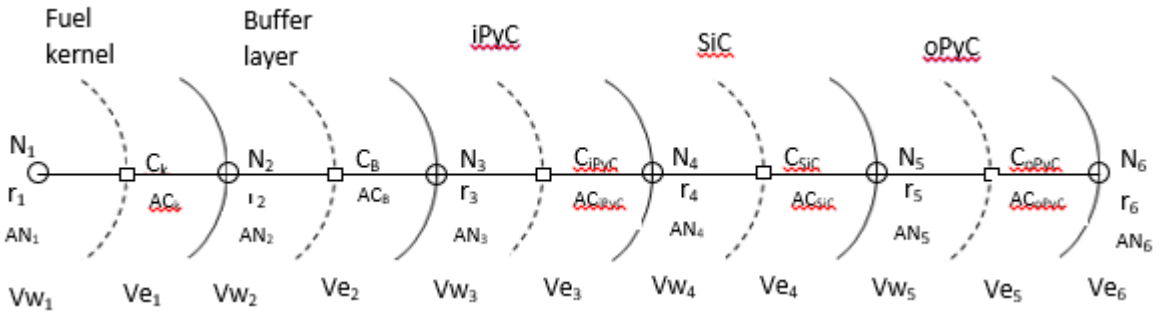

Figure 87: Discretization for coated fuel particle

Consider the discretized coated fuel particle shown Figure 87. Let N_1 to N_6 be the nodal points and C_i be the primitive conduction elements for each layer of the coated fuel particle. The radial positions of the nodal points are r_1 to r_6 with $r_1 = 0$. AN_1 to AN_6 refer to spherical areas associated with the respective nodal points, whilst AC_i are the average spherical areas associated with the respective primitive elements. Ve_1 to Ve_6 are the part of the nodal volumes coming from the primitive element situated to the east (right) of the respective nodal points,

whilst Vw_1 to Vw_6 are the part of the nodal volumes coming from the primitive elements situated to the west (left) of the respective nodal points.

Nodal areas for each coated fuel particle layer are obtained from:

$$AN_i = 4\pi r_i^2$$

Therefore the average primitive element areas are determined from:

$$AC_i = \frac{1}{2}(AN_i + AN_{i+1})$$

For the part of the nodal volume that is on the east of the nodal point, the equation is as follows:

$$Ve_i = \frac{1}{2}(AN_i + AC_i) \cdot \left(\frac{r_{i+1} - r_i}{2}\right)$$

For the part of the nodal volume that is on the west of the nodal point, the equation is as follows:

$$Vw_i = \frac{1}{2}(AC_{i-1} + AN_i) \cdot \left(\frac{r_i - r_{i-1}}{2}\right)$$

APPENDIX C

Distribution of fuel rods in a fuel block

In this section, the calculation for the difference in the distribution of fuel rods and coolant channels in the hexagonal block volume used in Flownex compared to the exact distribution in the actual block is done. The assumptions made for the Flownex model are as follows:

- The fuel and coolant channels are evenly distributed over the surface area of the block
- The length of the fuel rods is the same as the length of the fuel block

If the number of coolant channels obtained for the central CV is converted to the equivalent number for the full fuel block we get 122. However there are only 108 coolant channels in the actual fuel block. Similarly if the number of fuel rods obtained for the central CV is converted to the equivalent number for the full fuel block we get 244. However there are only 204 fuel rods in the actual fuel block. Figure 88 shows the actual distribution of fuel rods, lumped burnable poison rods and coolant channels in the fuel block.

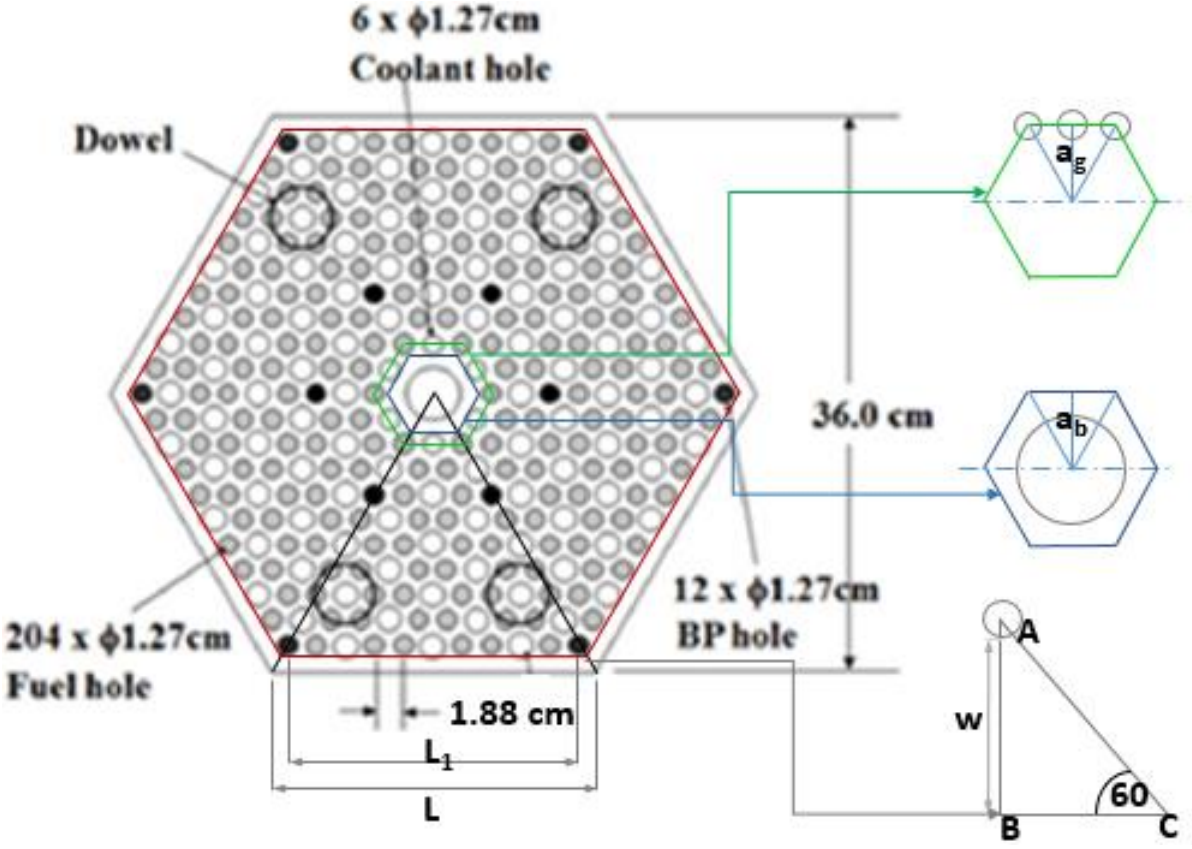

Figure 88: Actual distribution of fuel rods and coolant channels in a fuel block

L is the side of the hexagonal fuel block = $\frac{0.18}{\cos 30} = 0.2078$ m

The pitch between successive fuel rods or coolant channels was given as 1.88 cm and ten cell pitches can be fitted along the side of the hexagon, therefore L_1 = 0.0188x10 = 0.188 m.

To calculate the amount of area of the fuel block that does not contain fuel rods, lumped burnable poison rods and coolant channels (the area outside the red line in Figure 88), triangle ABC shown in Figure 88 can be used.

Length of line BC = $\frac{L-L_1}{2} = \frac{0.2078-0.188}{2} = 0.009923$ m

Length of line AB = BC $\tan 30 = 0.0009923 \times \tan 30 = 0.017187$ m

The diameter of the fuel and burnable poison hole is 1.27 cm

Therefore the width of the outer area without graphite (area outside the red hexagon in Figure 88) is given by: $w = AB - 0.635 = 0.010837$ m.

Area of fuel block = $6 \times \frac{1}{2} \times 0.2078 \times 0.18 = 0.112237$ m^2

Graphite area: $A_{g_{hex_r}} = 0.112237 - 6 \times \frac{1}{2} \times 0.188 \times (0.18 - 0.010837)$

$$= 0.016829 \text{ m}^2$$

Another piece of the fuel block where there are no fuel rods is the area in the middle of the block which is the graphite includes surrounding the fuel handling hole (the area inside the blue inner hexagon in Figure 88).

The sides of the green hexagon can be calculated from the cell pitch size $w_g = 2 \times 0.0188 = 0.0376$ m

The apothem of this hexagon is then:

$a_{green} = \frac{0.0188}{\tan 30} = 0.032563$ m

Given that the diameter of the fuel/coolant hole around the centre of the fuel block is 1.27 cm, the apothem of the graphite area can be calculated as:

$a_{blue} = a_g - \text{radius}_{\text{coolant or fuel hole}} = 0.032563 - 0.00635 = 0.026213$ m

Area of the blue hexagon around fuel handling hole:

$$A_{hex\_b} = \frac{a_{blue} \times \tan 30°}{2} \times a_{blue} \times 12 = 0.00238 \text{ m}^2$$

Total area of region without fuel or coolant holes inside a fuel block:

$$A_{\text{graphite region+fuel handling hole}} = A_{\text{hex}_b} + A_{g_{\text{hex}_r}} = 0.00238 + 0.016829 = 0.019209\ \text{m}^2$$

Each fuel compact has a height of 4.928 cm and 15 fuel compacts are stacked to form a fuel rod.

Therefore the height of a fuel rod is: $h_{fr} = 15 \times 0.04928 = 0.7392$ m and the height of the fuel block is 0.793 m

$$\text{Volume}_{\text{graphite region+fuel handling hole}} = 0.019209 \times 0.793 = 0.015233\ \text{m}^3$$

$$\text{Volume}_{\text{whole block}} 0.112237 \times 0.793 = 0.089004\ \text{m}^3$$

$$\text{Ratio of the volume of the graphite region to the whole block} = \frac{0.015233}{0.089004} = 0.171149$$

$$\text{Percentage Volume}_{\text{fuel and coolant region}} = \frac{0.089004 - 0.015233}{0.089004} \times 100 = 82.9\%$$

Area of the graphite around fuel handling hole:

$$A_{g\_hex\_b} = \frac{a_{blue} \times \tan 30^\circ}{2} \times a_{blue} \times 12 - A_{\text{fuel handling hole}} = 0.00238 - \pi r_{fhh}^2$$

$$0.00238 - \pi \left(\frac{2.2225}{100}\right)^2$$

$$= 0.000828\ \text{m}^2$$

Total graphite only area inside a fuel block:

$$A_{\text{graphite region}} = A_{hex\_b} + A_{g\_hex\_r} = 0.10608\ \text{m}^2$$